

Universidade Estadual Norte Fluminense Darcy Ribeiro – UENF
Programa de Pós-Graduação em Ecologia e Recursos Naturais
Centro de Biociências e Biotecnologia
Laboratório de Ciências Ambientais

**Carbono negro dissolvido no contínuo continente-oceano no rio Paraíba do
Sul**

Jomar Marques da Silva Junior

Orientador: Prof. Dr. Carlos Eduardo de Rezende

Campos dos Goytacazes, 2017

Universidade Estadual Norte Fluminense Darcy Ribeiro – UENF
Programa de Pós-Graduação em Ecologia e Recursos Naturais
Centro de Biociências e Biotecnologia
Laboratório de Ciências Ambientais

**Carbono negro dissolvido no contínuo continente-oceano no rio Paraíba do
Sul**

Jomar Marques da Silva Junior

Tese apresentada ao Centro de Biociências e Biotecnologia da Universidade Estadual do Norte Fluminense, como parte das exigências para a obtenção de título de Mestre em Ecologia e Recursos Naturais.

Orientador: Prof. Dr. Carlos Eduardo de Rezende

Campos dos Goytacazes, 2017

Universidade Estadual Norte Fluminense Darcy Ribeiro – UENF
Programa de Pós-Graduação em Ecologia e Recursos Naturais
Centro de Biociências e Biotecnologia
Laboratório de Ciências Ambientais

Carbono negro dissolvido no contínuo continente-oceano no rio Paraíba do Sul

Tese apresentada ao Centro de Biociências e Biotecnologia da Universidade Estadual do Norte Fluminense, como parte das exigências para a obtenção de título de Mestre em Ecologia e Recursos Naturais.

Aprovada em 3 de abril de 2017.

Comissão examinadora:

Prof. Dr. Marcelo Corrêa Bernardes (Instituto de Geociências – UFF)

Prof. Dr. Luiz Eduardo Oliveira e Cruz de Aragão (INPE)

Prof. Dr. Marcelo Trindade Nascimento (LCA – UENF)

Prof. Dr. Carlos Eduardo de Rezende – Orientador - (LCA- UENF)

“Dedico aos meus pais Jomar Marques da Silva e Maria Rita de Cássia Nogueira Soares e toda a minha família pelo amor, dedicação, confiança, força e apoio ao longo da minha vida. A minha esposa Mylena Coimbra e a nossa Alice Coimbra Marques. Esse trabalho também é dedicado a memória do Sr. Antônio Carlos Oliveira Pessanha (Seu Antônio) por todos os ótimos momentos vividos juntos, sentirei muito sua falta”

Agradecimentos

Ao meu orientador Prof. Carlos Eduardo de Rezende pela orientação, amizade, paciência, risadas e por todos os ensinamentos e pela confiança em meu trabalho ao longo dos 10 anos de convivência.

Ao Dr. Marcelo Gomes de Almeida pelas ajudas nas etapas laboratoriais, pelas importantes discussões e por todos os ensinamentos.

Ao Prof. Dr. Thosten Dittmar e a Dra Jutta Niggemann por todo suporte, ensinamentos e discussões sobre o trabalho, e a todo o seu grupo de pesquisa da Oldenburg University (Dra. Helena Osterhols, Dra. Pamela Rossiel, Dr. Michael Seidel, Dra. Hannelore Waska, Dra. Maren Zark, Dr Gonçalo Gômes, Maren Seibt, Dra. Anika Pohlabein, Beatriz Ortega, Nadine Broda, Maria Del Carmen, Andrea Mentges, Matthias Friebe, Katrin Klapproth, Ina Ulber, Susane Wendeling), no qual fui muito bem recebido e me senti em casa durante o período de um ano.

Ao Dr. Luiz Martinelli pelas discussões e pela revisão do artigo.

Ao Laboratório de Ciências Ambientais da UENF e ao Programa de Pós-Graduação em Ecologia Recursos Naturais.

A CAPES pelo auxílio da bolsa de doutorado. Ao CNPq e ao Programa Ciências Sem Fronteiras (CNPq CSF 400.963/2012-4) pela bolsa de Doutorado Sanduíche na Oldenburg University por um período de um ano.

A Sergej Popove e Teresa Lein e Lena Albers gostaria de agradecer por terem sido minha família alemã, vocês são muito importantes para mim.

Aos amigos Diogo Quitete, Guilherme Schoth, Emilane Lima, Bia Muniz e Tassiana Carvalho por toda ajuda nas coletas e no laboratório. Sem vocês seria impossível a realização deste trabalho.

A Beatriz Araújo por toda amizade e conselhos ao longo desses anos. Marcos Franco por toda amizade e pelas aulas de inglês. Thiago Rangel, Frederico Brito e Bruno Masi pela amizade, risadas, cervejas e por terem feito da **Chinese Republic** um período que nunca irei esquecer “só quem viveu sabe o que foi”. Família não precisa ter conta sanguínea, vocês fazem parte da minha família.

Aos professores do LCA pelo conhecimento que levarei por toda a vida, aos técnicos Alcemir Bueno, Ana Paula Pedrosa, Cristiano Maciel e Arizoli Gobo pelas inúmeras assistências, análises, risadas e amizade.

Aos amigos Bráulio Cherene, Íris Heringer, Pedro Gatts, Roger Carvalho, Bianca Liguori, Flávia Barretto e família por toda amizade, ajuda e conselhos.

Ramon Moraes, Luana Coimbra, Lucas Coimbra, Maria Emília Coimbra, Neiva Coimbra, Marcos Santos Pereira e a todos da família Coimbra.

Enfim agradeço a todas as pessoas que contribuíram no desenvolvimento deste trabalho.

Sumário

Índice de Figuras	VIII
Resumo.....	IX
Abstract.....	X
1 – Introdução.....	1
1.1 – Carbono negro.....	1
1.2 – Métodos de mensuração do carbono negro e a combustão contínua.....	4
1.3 – Produção do carbono negro.....	5
1.4 – Migração do carbono negro no solo.....	6
1.5 – Transporte atmosférico.....	8
1.6 – Transporte fluvial e estuarino.....	9
1.7 – Carbono negro no ambiente marinho.....	15
2 – Justificativa.....	19
3 – Objetivo.....	19
4 – Perguntas.....	20
5 – Resultados.....	21
5.1 – Efeito das mudanças da cobertura vegetal na $\delta^{13}\text{C}$ da matéria orgânica particulada e dissolvida no contínuo continente/oceano do rio Paraíba do Sul. Jomar S.J. Marques, Marcelo G. Almeida, Luiz A. Martinelli, Carlos E. Rezende. (Manuscrito em preparação).....	22
5.2 – Dissolved black carbon in the headwaters-to-ocean continuum of Paraíba do Sul River, Brazil. Jomar S.J. Marques, Thorsten Dittmar, Jutta Niggemann, Marcelo G. Almeida, Gonzalo V. Gomez-Saez, Carlos E. Rezende. Manuscrito publicado na <i>Frontiers Special Issue - From Fires to Oceans: Dynamics of Fire-Derived Organic Matter in Terrestrial and Aquatic Ecosystems (manuscrito)</i>	56
6 – Discussão geral.....	75
7 – Conclusões.....	77
8 – Referências.....	78
9 – Produção durante o doutorado	86

- 9.1 – Microbial and sponge loops modify fish production in phase-shifting coral reefs – ***Environmental Microbiology***.....
- 9.2 - Na extensive reef system at the Amazon River month – ***Science advances***.....
- 9.3 - Regional aerosol emissions contribute to the riverine export of dissolved black carbon. M. W. Jones, T. A. Quine, L. E. O. C. de Aragão, C. E. de Rezende, T. Dittmar, M. Manecki, B. Johnson, J.S.J. Marques. (Manuscrito submetido para o ***Journal of Geophysical Research***).....
- 9.4 - Dissolved black carbon in the headwaters-to-ocean continuum of Paraíba do Sul River, Brazil. Jomar S.J. Marques, Thorsten Dittmar, Jutta Niggemann, Marcelo G. Almeida, Gonzalo V. Gomez-Saez, Carlos E. Rezende. Manuscrito publicado na ***Frontiers Special Issue - From Fires to Oceans: Dynamics of Fire-Derived Organic Matter in Terrestrial and Aquatic Ecosystems***.....

ÍNDECE DE FIGURAS

Figura 1: Quadro descritivo do modelo da formação do CN pela combustão contínua de biomassa vegetal. Adaptado de Hedges <i>et al.</i> , 2000 e Masiello, 2004.....	2
Figura 2: Regiões da “combustão contínua” detectada por cada técnica. Adaptado de Glaser <i>et al.</i> , 1998: Masiello, 2004.....	3
Figura 3: Emissões de CN expresso em toneladas por ano. Imagem de satélite referente ao ano de 1996. Adaptado de Ramanathan and Carmichel, 2008.....	9
Figura 4: Diagrama de Van Krevelen 3D obtido pelos dados da espectrometria de massa de alta resolução em (a) pântano de McDonald e em (b) rio Negro. Adaptado de Kim <i>et al.</i> , 2004.....	11
Figura 5: Série temporal de frequência de queimada, descarga de água e concentração de CND. Adaptado de Dittmar <i>et al.</i> , 2012.....	12
Figura 6: Correlação entre a concentração de COD e o CND de rios ao redor do globo terrestre. Adaptado de Jeffé <i>et al.</i> , 2013.....	13
Figura 7: Distribuição do CN em (A) porcentagem em relação a distância da foz e em (B) concentração em relação a salinidade. Adaptado de Manino and Harvey, 2004.....	14
Figura 8: Modelo de mistura com o $\delta^{13}\text{C}$ e as concentrações de CND. Adaptado de Dittmar <i>et al.</i> , 2012a.....	15
Figura 9: Distribuição de compostos aromáticos policíclicos totais na MOD entre a África do Sul e a Antártica. Adaptado de Dittmar and Paeng, 2009.....	17
Figura 10: Foto-degradação do CN dissolvido da Água Profunda do Atlântico Norte, em (A) concentração em nM e em (B) % em relação a MOD. Adaptado de Stubbins <i>et al.</i> , 2012b.....	18
Figura 11: Modelo da foto-degradação das frações mais condensadas do CN nas águas superficiais do oceano. Adaptado de Masiello and Louchouart, 2013.....	18

RESUMO

Os rios descarregam anualmente 25-28 Tg de matéria orgânica dissolvida pirogênica (ou carbono negro dissolvido, CND) no oceano, o que equivale a cerca de 10% de todo o fluxo continente-oceano do carbono negro dissolvido. O objetivo do trabalho é identificar as fontes e os principais processos que afetam o transporte do CND pelo rio Paraíba do Sul (RPS). Como modelo fluvial, escolhemos o continuum continente/oceano do RPS, o único sistema fluvial que possui série temporal de fluxo de CND disponível. A bacia de drenagem do RPS era coberta originalmente por mata Atlântica (plantas tipo C3), que foi quase completamente destruído por corte e queimadas. Como resultado, grandes quantidades de carvão derivado de madeira ainda existem estocado nos solos. Atualmente, a maior parte da bacia é coberta por pasto (67%) e existem extensivas plantações de cana (plantas tipo C4). As amostras de água foram coletadas em 24 pontos ao longo do rio, 14 pontos nos principais tributários e em 21 pontos ao longo do gradiente de salinidade no estuário e até 35 km de distância da costa. O CND foi determinado a nível molecular, como ácidos benzenopolicarboxílicos (BPCAs). A composição isotópica do carbono ($\delta^{13}\text{C}$) foi determinada no carbono orgânico dissolvido (COD) extraído pela extração de fase sólida ($\delta^{13}\text{C}$ -COD-SPE) para distinguir as fontes C3 e C4. Nossos resultados mostram claramente uma relação entre a hidrologia e as concentrações de CND no RPS, com as maiores concentrações de CND na estação chuvosa e menores concentrações na estação seca. Essa relação indica que CND é principalmente mobilizado dos horizontes superiores do solo durante fortes chuvas. A relação estatisticamente significativa entre o $\delta^{13}\text{C}$ -SPE-COD e as concentrações de CND indicam que a maior parte do CND transportado pelo RPS foi originado de plantas C3 (floresta), por exemplo, a partir de eventos históricos de queimadas da mata Atlântica. Um simples modelo de mistura pode reproduzir as concentrações observadas dentro do continuum continente/oceano. Assim, no sistema fluvial e no estuário, as concentrações de CND se comportaram conservativamente.

ABSTRACT

Rivers annually carry 25-28 Tg of pyrogenic dissolved organic matter (or dissolved black carbon, DBC) into the ocean, which is equivalent to about 10% of the entire land-ocean flux of dissolved organic carbon. Objective of this study was to identify the main processes behind the release and turnover of DBC on a riverine catchment scale. As model system we chose the land to ocean continuum of Paraíba do Sul River (Brazil), the only river system for which long-term DBC flux data exist. The catchment was originally covered by Atlantic rain forest (mainly C3 plants) which was almost completely destroyed over the past centuries by slash-and-burn. As a result, large amounts of wood-derived charcoal reside in the soils. Today, fire-managed pasture and sugar cane (both dominated by C4 plants) cover most of the catchment. Water samples were collected at 24 sites along the main channel of the river, at 14 sites of the main tributaries and at 21 sites along the salinity gradient in the estuary and up to 35 km offshore. Sampling was performed in the wet seasons of 2013 and 2014, and the dry season of 2013. DBC was determined on a molecular level as benzenepolycarboxylic acids after nitric acid oxidation. Stable carbon isotopes ($\delta^{13}\text{C}$) were determined in solid phase extractable dissolved organic carbon (SPE-DOC) to distinguish C4 and C3 sources. Our results clearly show a relationship between hydrology and DBC concentrations in the river, with highest DBC concentrations in the wet season and lowest in the dry season. This relationship indicates that DBC is mainly mobilized from the upper soil horizons during heavy rainfalls. A significant correlation between DBC concentrations and $\delta^{13}\text{C}$ -SPE-DOC indicated that most of DBC in the river system originates from C3 plants, i.e. from the historic burning event of the Atlantic rain forest. A simple mixing model could largely reproduce the observed concentrations within the catchment and the land to ocean continuum. Thus, within the river system and estuary, DBC concentrations behaved mainly conservatively.

1 - Introdução


1.1 – Carbono Negro

As queimadas são comuns em ambientes naturais e em terras manejadas, causando modificações na qualidade e quantidade da matéria orgânica dos solos (MOS) (Forbes et al., 2006). O carbono negro (CN) é uma forma recalcitrante de carbono que não reage facilmente com o oxigênio para formar CO₂ (Masiello, 2004). Este composto é o produto da queima incompleta de biomassa vegetal e combustíveis fósseis e representa um significativo sumidouro no ciclo global do carbono (Andreae & Crutzen, 1997; Hedges et al., 2000; Masiello, 2004). O carbono negro no ambiente ocorre em numerosas formas, variando de tecidos vegetais parcialmente carbonizados a partículas de cinzas que são formadas durante a combustão (Allen-King et al., 2002). A produção anual das diversas formas de carbono negro no ambiente foi calculada em cerca de 50 e 160 Tg, dos quais 80% é atribuída como resultado da queima de vegetação (Kuhlbusch, 1998; Nguyen et al., 2004). Em contra partida, emissões anuais de carbono negro na forma de aerossóis originados na queima de combustíveis fósseis, variam entre 12 e 24 Tg (Nguyen et al., 2004).

Devido a sua natureza recalcitrante, o carbono negro pode ser acumulado nos solos e sedimentos. Além disso, esta forma de carbono não é facilmente sequestrada para outros reservatórios. Por isso possui um longo tempo de residência que pode variar de 10² a 10⁴ anos no solo e de 40 horas na atmosfera (Andreae & Crutzen, 1997; Forbes et al., 2006). Adicionado a isso, o carbono negro estocado no solo pode atingir rios, regiões costeiras e o oceano profundo por meio do escoamento superficial e da descarga fluvial, onde este composto pode estar nas formas dissolvidas e particuladas. O carbono negro pode afetar o transporte e destino de outros poluentes orgânicos, o ciclo global do carbono e a disponibilidade química e biológica do carbono orgânico do solo (Bucheli & Gustafsson, 2002; Allen-King et al., 2002; Nguyen et al., 2004).

De acordo com Hedges et al., (2000) o CN é um “contínuo” de produtos da combustão variando de biomassa levemente carbonizada, que mantém as estruturas das plantas, até a fuligem altamente condensada e refratária sem nenhum resquício de estrutura de plantas. A Figura 1 apresenta o modelo da combustão contínua com seus espectros e propriedades. Todas as frações dos espectros são dominadas por

estruturas aromáticas. A aromaticidade aumenta com o incremento da temperatura e o tempo de exposição ao fogo. Em experimentos realizados por Baldock and Smernik, (2002), utilizando a técnica de ressonância magnética nuclear, foi demonstrado que pinos de madeira queimados por longos períodos, perdem os sinais de intensidade associados à celulose. E por outro lado, ganham sinais de intensidades nos grupamentos arila, associados a estruturas aromáticas.



Características	Biomassa levemente carbonizada	Biomassa carbonizada	Carvão vegetal	Cinza	Grafite
Tamanho	mm ou maior		mm a micrômetro	micrômetro	
Estrutura de plantas	abundante	presença significativa	pouco	ausência	
Reservatório inicial	solos		solos e atmosfera		
Alcance	metros	metros a quilômetros		quilômetros	
(O/C) _a	0,8	0,6	0,4	0,2	0

Figura 1: Quadro descritivo do modelo de formação do CN pela combustão contínua de biomassa vegetal. A razão atômica (O/C)_a quanto mais próxima de zero o valor, menos reativo é o composto. Adaptado de Hedges et al., 2000 e Masiello, 2004.

Existem muitos métodos capazes de detectar diferentes partes do “contínuo” em diferentes matrizes ambientais, tais como atmosfera, água, sedimento e solos, que geram resultados desiguais para amostras de mesma matriz (Hammes et al., 2007; Schneider et al., 2011). Como consequência, os dados obtidos por essas diferentes metodologias e também de diferentes matrizes são difíceis de serem comparados. A Figura 2 apresenta as regiões da “combustão contínua” detectada por cada método.

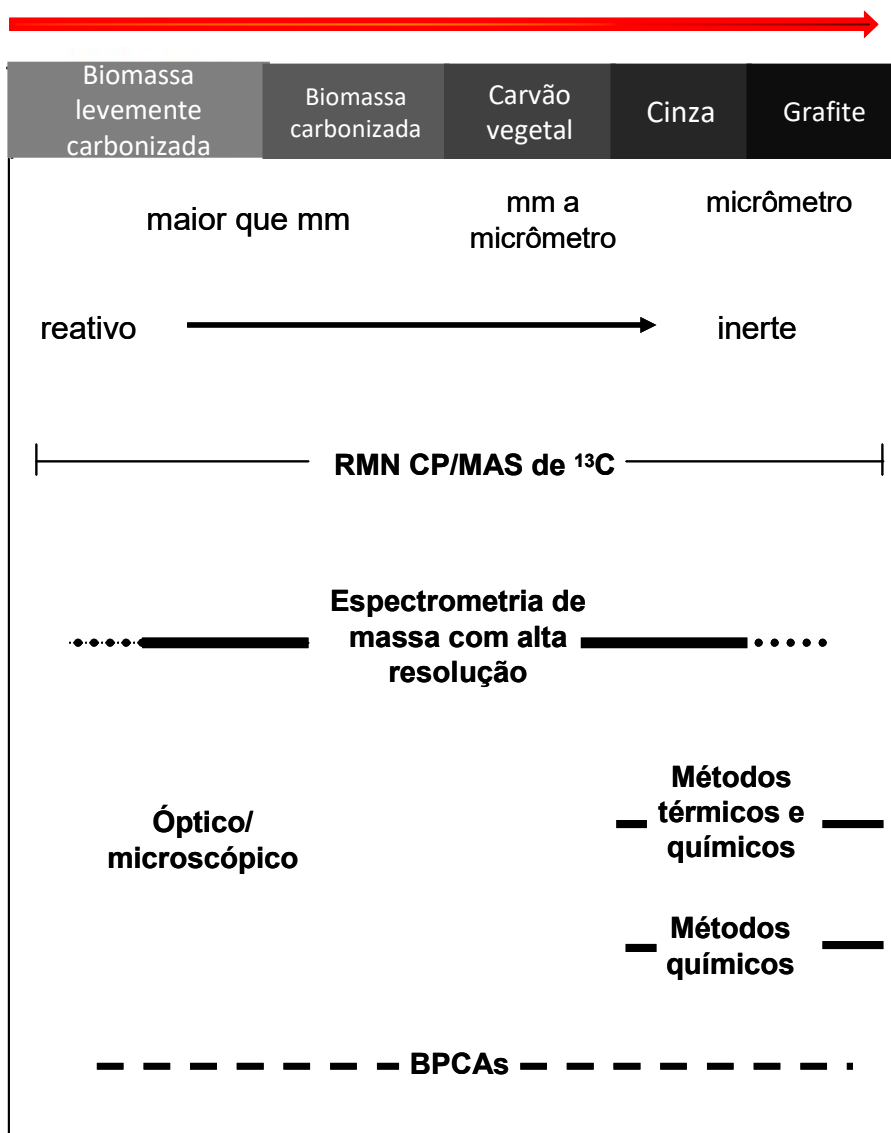


Figura 2: Regiões da “combustão contínua” detectada por cada técnica. Adaptado de Glaser et al., 1998; Masiello, 2004.

Uma maneira de se comparar resultados gerados por diferentes metodologias e matrizes ambientais é a utilização da porcentagem de CN em relação ao conteúdo de CO. Estudos têm observado variadas porcentagens de carbono negro em relação ao total de carbono orgânico em diferentes ecossistemas. No golfo de Maine, localizado na costa Nordeste da América do Norte, estes valores variaram entre 3 e 6% (Gustafsson & Gschewend, 1998). Em regiões profundas do Oceano Atlântico próximo à costa da África as porcentagens de carbono negro observadas foram superiores a 50% (Verardo & Riddiman, 1996). No ambiente terrestre, a camada superficial de solos da Savana Tropical de Zimbábue com sucessivos

eventos de queimadas, apresentou valores variando entre 2 a 8% (Bird et al., 1999). Em solos com intensa atividade agrícola na América do Norte as porcentagens foram superiores a 30% (Skemstad et al., 2002).

Algumas das variações naturais na porcentagem de carbono negro em relação ao carbono orgânico do solo (CN/COS) ocorrem por processos naturais. A atividade agrícola pode aumentar a exposição do carbono orgânico do solo em condições de decomposição e com isso promover um enriquecimento preferencial das frações refratárias dentre estas, o carbono negro (Skemstad et al., 2002; Maciello, 2004). Entretanto, uma significativa fração das aparentes variações naturais de carbono negro em solos e sedimentos está relacionada com as incertezas nas metodologias. Parte destas incertezas é devido a falta de informação a respeito da região do contínuo em que a metodologia utilizada atua. Um trabalho utilizou diferentes metodologias na quantificação do carbono negro em um material de referência de matriz poeira urbana (NIST SRM1649a), identificou uma porcentagem de carbono orgânico na forma de carbono negro variando de 7 a 50%, e mostrando um fator da ordem de 10 nas diferenças dependendo da metodologia usada (Currie et al., 2002). Neste sentido, a compreensão dos dados de carbono negro, envolve pelo menos em parte, de que região do contínuo do CN os diferentes métodos atuam (Maciello, 2004). Os resultados de porcentagem de carbono negro pelo carbono orgânico (Corg) variaram em função do ambiente, método utilizado e a matriz. Como mencionado acima, a variabilidade causada pela metodologia utilizada torna difícil a comparação de dados de diferentes ambientes se a metodologia utilizada não for a mesma.

1.2 - Métodos de mensuração do carbono negro e a combustão contínua

As técnicas de mensuração do carbono negro são divididas em seis classes, sendo elas: microscópica (Clark and Patterson, 1997), óptica (Clarke et al., 1987), térmica (Cachier et al., 1989; Gustafsson et al., 1997), química (Verardo, 1997; Wolbach and Anders, 1989), espectroscopia (Skjemstad et al., 1999) e marcadores moleculares (Glaser et al., 1998; Elias, 2001; Dittmar et al., 2008). Alguns estudos utilizam uma ou mais técnicas. A técnica microscópica conta o número de pedaços de carvão visíveis utilizando o microscópio óptico. A técnica óptica mensura a concentração de carbono negro de uma amostra pela interação de um feixe de luz

sob a amostra e fornece informações importantes para o entendimento sobre o impacto do carbono negro na forma de aerossóis na atmosfera. O método térmico determina o carbono negro remanescente após a oxidação por aquecimento e o método químico mensura o carbono negro remanescente após a extração química. A técnica espectroscópica atua nas bandas do infravermelho características dos produtos da combustão com base nas forças ou frequências dessas bandas após a remoção oxidativa de compostos orgânicos não alterados termicamente. O método dos marcadores moleculares determina a concentração de classes de compostos derivados do carbono negro e utiliza estas informações para calcular a concentração do carbono negro.

Assim, é importante destacar que cada técnica mensura uma região dentro do contínuo do CN. A técnica microscópica de contagem detecta somente pequenas partículas de carvão na amostra sólida e não atua nas frações cinza e grafite do espectro da combustão contínua. Os métodos térmicos e químicos oxidam as partículas menos refratárias que o carvão, detectando o carbono negro nas frações cinza e grafite do contínuo (Gelinas et al., 2001a). Os métodos espectroscópio e de marcadores moleculares identificam as assinaturas químicas dos compostos termicamente modificados, e por isso, possui uma ampla faixa de atuação nas frações que compõem o contínuo (Glaser et al., 1998; Simoneit, 2002).

A Figura 2, expressa uma extrapolação sugerida por Glaser et al., (1998) e Masiello, (2004), que mostra em qual região da combustão contínua cada um dos métodos atua. A mesma figura ajuda a explicar contradições na comparação dos dados de carbono negro obtidos com diferentes metodologias. Por exemplo, a comparação de dados mensurados pela técnica microscópica (detecta carvão) com dados obtidos pela técnica térmica (detecta cinza) gera informações deturpadas, pois as técnicas atuam em diferentes espectros da combustão contínua. Devido ao fato da técnica dos ácidos poli-carboxílicos (BPCAs) atuarem em todas as faixas do continuum e de também serem a única metodologia quantitativa, essa técnica foi utilizada no presente estudo.

1.3- Produção de carbono negro

Os primeiros autores a calcular a produção global de CN foram Seiler e Crutzen (1980). Dados demográficos e de uso da terra foram utilizados e foi estimado que a produção fosse de 500 – 1700 Tg.ano⁻¹. No entanto, essas

estimativas foram consideradas muito elevadas e mais tarde, Crutzen e Andreae (1990), propuseram que a produção global era de 200 e 600 Tg.ano⁻¹. Segundo os mesmos autores, essa taxa de produção de CN poderia reduzir a liberação líquida de CO₂ na atmosfera pelo desmatamento de 2 a 18%. Essa redução pode ser a fração perdida do carbono no balanço global com influência antrópica. Determinações experimentais do CN em resíduos de pós-fogo em diversos biomas estimaram que a produção fosse de 76 e 241 Tg.ano⁻¹ (Kuhlbusch e Crutzen, 1995). Em um trabalho seguinte, Kuhlbusch et al., (1996), calcularam a produção de 44 e 194 Tg.ano⁻¹, nos resíduos pós fogo em savanas da África e Venezuela. Um trabalho realizado em florestas boreais no Canadá estimou que de 1 a 7% da biomassa queimada foi convertida a CN, com a produção de CN na ordem de 7 a 17 Tg.ano⁻¹ de CN na forma de carvão e de 2 a 2,5 Tg.ano⁻¹ de CN na forma de aerossol. Os mesmos autores levantaram a hipótese de que nessas estimativas não é levado em consideração a degradação microbiana e as reações inorgânicas do CN. Estudos realizados na Amazônia mostraram uma produção de 4,3±5,9 t.ha⁻¹ de CN, com 2,9 e 7,8% de biomassa convertida em carvão e 0,8 e 5,3% convertido em cinzas (Fearnside et al., 2001). Assim, as estimativas são muito altas e apresentam uma margem de erro elevada quando se comparam com as determinações de CN nos solos (Preston and Schmidt, 2006). Em solos ricos em carbono orgânico do Sudeste da Ásia foram encontrados de 3 a 7% de CN (oxidação por dicromato) na MOS (Rumpel et al., 2006). Em um trabalho realizado na Europa Central, foram observados de 4 a 45% de CN (foto-oxidação por ultravioleta) na MOS (Schmidt et al., 2002). Glaser & Amelung, (2003) utilizando ácidos benzeno-policarboxílicos observaram de 4 a 18% de CN na MOS em solos de pradaria nativas da América do Norte. Neste sentido, assumindo que as estimativas atuais de produção global do CN são confiáveis, e que o transporte de CN do continente para o oceano é menor que a taxa de produção, uma quantidade significativa de CN parece ser degradada no ambiente. Essa degradação é a principal responsável pelas discrepâncias nas estimativas globais de produção de CN no ambiente.

1.4 – Migração do carbono negro no solo

Um assunto muito discutido sobre a migração do CN nos solos é a sua decomposição. Na literatura, o CN é considerado uma fração refratária da MOS

devido a sua estrutura química ser rica em anéis aromáticos que dificulta a decomposição microbiana (Glaser et al., 2001; Krull and Skjemstad, 2002; Forbes et al., 2006). Segundo esses autores, o CN apresenta grande resistência a uma ampla gama de agentes oxidantes; preserva-se por longos períodos em registros geológicos; está presente em profundas camadas dos solos; e seu tempo de residência excede 1000 anos. Evidências do longo tempo de residência do CN são baseadas em trabalhos que utilizaram a $\Delta^{14}\text{C}$ em solos (Schmidt et al., 2002; Gavin et al., 2003) e sedimentos marinhos (Masiello et al., 2002). Em contrapartida, Hamer et al., (2004) observaram através do fluxo de CO_2 , que de 0,3 a 0,8% do CN foi mineralizado em um período de 60 dias na temperatura de 20°C em uma mistura de areia livre de carbono orgânico e carvão produzido em laboratório. Neste mesmo trabalho, foi observado que uma fonte lábil de matéria orgânica (MO) (glicose marcada com ^{14}C) aumenta para 1,2% a massa de CN mineralizado nas mesmas condições anteriores. Isso indica que a MO lábil do solo pode acelerar a decomposição do CN. Estudos indicam que o tempo de residência do CN pode variar de <50 a 10^7 anos (Zimmerman, 2010; Bird et al., 2012). Isto mostra que a MO lábil do solo pode favorecer a decomposição do CN no solo.

Atualmente acredita-se que apesar do CN ser um composto resistente a degradação (biológica ou química), o mesmo possui uma fração mais suscetível a decomposição no ambiente (Forbes et al., 2006). Isso depende da temperatura de formação, do material de origem e das propriedades do solo (Baldock and Smernik, 2002; Nguyen et al., 2010). A foto-oxidação e a decomposição biológica são os principais mecanismos da degradação do CN, embora a erosão e a dissolução do CN dentro das camadas do solo sejam também uma explicação para as perdas do mesmo (Czimezik et al., 2003; Ding et al., 2013). A degradação de materiais carbonizados no solo resulta na produção de ácidos carboxílicos, que com isso aumentam a solubilidade do CN e promovem a translocação do CN para a fase dissolvida (Dittmar et al., 2012a; Ding et al., 2013). Apesar do mecanismo da dissolução não ser conhecido, esse processo pode ser o principal mecanismo de migração do carbono negro dissolvido (CND) para os corpos hídricos. A existência de CND nos ambientes fluvial e marinho confirma a importância da dissolução na migração do CN no solo e entre o continente e o oceano.

1.5 – Transporte atmosférico

Após um evento de queimada, grandes quantidades de CN na forma de aerossóis são produzidos e lançados na atmosfera. Os aerossóis produzidos por queimadas desempenham um importante papel na química atmosférica e estão relacionados diretamente com a qualidade do ar e com as mudanças globais como efeito estufa (Jacobson, 2001; Lee et al., 2005). Segundo Johnson et al., (2005), o CN na forma de aerossóis pode permanecer na atmosfera de 6 dias a meses. Com exceção das queimadas naturais em florestas, todas as outras emissões de CN são antropogênicas (Hitzenberger and Tohno, 2001). A maior parte do CN na atmosfera atualmente é originada pela queima de combustíveis fósseis. Neste contexto, as cidades são consideradas fontes pontuais de CN na forma de aerossóis, enquanto, as queimadas antropogênicas são consideradas fontes difusas. Como exemplos podemos citar: a pluma de fumaça originada na Sibéria em 2003 que afetou a qualidade do ar na Coreia (Lee et al., 2005); queimadas em florestas do Canadá que foram associadas com o aumento das concentrações de CO₂ e CN nos Estados Unidos (Wotawa and Trainer, 2000); o CN produzido nos trópicos que pode alcançar à Antártica (Wolf and Cachier, 1998). Além disso, o aumento do CN na forma de aerossóis tem diminuído o volume das monções na Índia devido ao aumento da temperatura na baixa-troposfera, dificultando com isso a formação das nuvens (Meehl et al., 2008). O trabalho de Preston e Schmidt, (2006), estimou que de 1 a 7% da biomassa queimada em florestas boreais da Austrália foi convertida em CN, com a produção de 7 e 17 TgCN.ano⁻¹ na forma de resíduos nos solos e 2 e 2,5 Tg.CN.ano⁻¹ na forma de aerossóis.

Estudos sobre o transporte atmosférico do CN baseados na formação de nuvens marrons (***brown clouds***) mostraram uma grande distribuição do CN pelo transporte atmosférico. As nuvens marrons são compostas por numerosos tipos de aerossóis, incluindo o CN, mas também sulfatos, nitratos, poeira entre outros componentes. O CN é removido da atmosfera pela chuva e neve (Ramanathan and Carmichel, 2008). Observações de campo em conjunto com imagens de satélite mostraram uma ampla distribuição das nuvens marrons ao redor do globo terrestre (Figura 3), com o sul da África e da Ásia se destacando como as principais fontes de CN na forma de aerossóis para a atmosfera (Ramanathan and Carmichel, 2008). Como mostrado na Figura 3, o CN produzido no Sul da África pode ser depositado

no Oceano Atlântico, assim como, o CN produzido no Sul da Ásia pode ser depositado no Oceano Índico e Pacífico (Ramanathan and Carmichel, 2008).

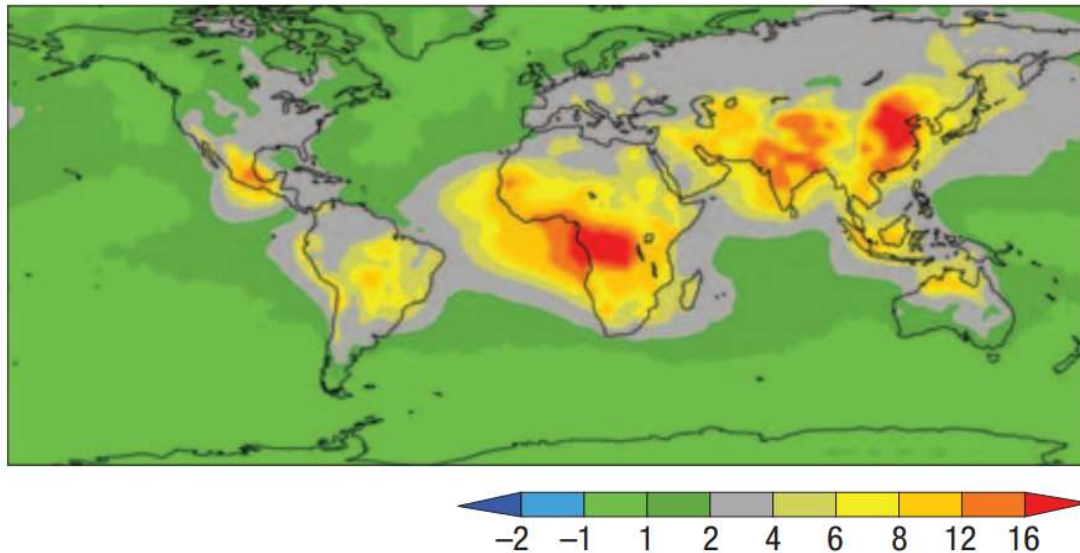


Figura 3: Emissões de CN expresso em toneladas por ano. Imagem de satélite referente ao ano de 1996. Adaptado de Ramanathan and Carmichel, 2008.

Outra forma de entrada do CN para o ambiente marinho por meio da atmosfera seria pela neve depositada em geleiras. Stubbins et al., (2012a), caracterizaram a matéria orgânica dissolvida de neve e ambientes aquáticos da geleira de Mendenhall, Alaska, USA. Neste estudo os autores observaram baixas concentrações de lignina na neve, indicando que a MO não foi originada em florestas. Em contra partida, a MO é empobrecida em ^{14}C , que indica como origem combustível fósseis. Adicionado a isso, por meio das análises do espectrômetro de massa de ultra-resolução foram identificados produtos de combustão encontrados em aerossóis antropogênicos. Esses achados reforçam a ideia da ampla distribuição do CN pelo transporte atmosférico sob a forma de aerossóis e mostram que o derretimento das geleiras pode aumentar a entrada de CN além dos níveis dos oceanos.

1.6 – Transporte Fluvial e estuarino

Após um evento de queimada, o solo é o principal compartimento responsável pelo acúmulo do CN. Além disso, a frequência de queimadas pode desempenhar um

importante papel na característica da MOS e na acumulação de CN nos solos (Ding et al., 2013). Aproximadamente de 5 a 20% de todo carbono orgânico sedimentado no oceano pode estar na forma de CN (Masiello and Druffel, 1998). O CN tem sido considerado como um composto altamente refratário e estável no ambiente. No entanto, as taxas de produção atuais superam as estimativas de decomposição. Desse modo, haveria mais CN que MO nos solos (Masiello, 2004; Schmidt, 2004). Este paradoxo indica que a erosão é uma possível via de perda de CN do solo. Um estudo realizado no rio Santa Clara na Califórnia observou que a porcentagem de CN em relação ao carbono orgânico particulado (COP) variou de 8 a 17% na estação chuvosa. Em contrapartida, na estação seca o CN não foi determinado no material particulado do rio (Masiello and Druffel, 2001). Os autores atribuíram que o CN é originado no solo e durante a estação chuvosa carregado para o rio Santa Clara pelo escoamento superficial, formando um material particulado em suspensão enriquecido em CN nesta estação. Mitra et al., (2002) calcularam o fluxo de CN para o Golfo do México sendo da ordem de 5×10^{-4} Pg C, contribuindo com 5% de todo CN de origem terrestre encontrado no ambiente marinho. Os dados supracitados indicam que a erosão atua na migração do CN na forma particulada dos solos para os corpos hídricos. Outra forma de migração seria a dissolução do CN nos solos. Segundo Hockaday et al., (2007), durante anos de ataque microbiológico ao CN alguns átomos de oxigênio podem ser inseridos formando ácidos carboxílicos, que por sua vez aumentam a solubilidade do CN na fração dissolvida no solo. Apesar do mecanismo da dissolução não ser conhecido, a existência do CN_D em rios e no oceano foi confirmada e quantificada (Kim et al., 2004; Dittmar et al., 2012b; Ding et al., 2013).

A existência de moléculas de CN na MOD foi confirmada por Kim et al., (2004). Neste estudo foi utilizada a espectrometria de massa de alta resolução na identificação de moléculas derivadas do CN_D em amostras do pântano de McDonalds (EUA) e do rio Negro (Brasil). Com os resultados da composição elemental foram calculadas as razões H/C e O/C. Esses dados foram usados para a construção do diagrama de Van Krevelen 3D (Figura 4). No diagrama das amostras do pântano de McDonalds (Figura 4a), as maiores intensidades foram observadas na região esperada para moléculas de lignina. Em contrapartida, no diagrama das amostras do rio Negro (Figura 4b), houve uma distribuição bimodal, com uma região similar a do pântano de McDonald e outra região que indica que essas moléculas

são deficientes em hidrogênio (baixa razão H/C). Essa deficiência em hidrogênio indica que esses compostos fazem parte do carbono negro dissolvido.

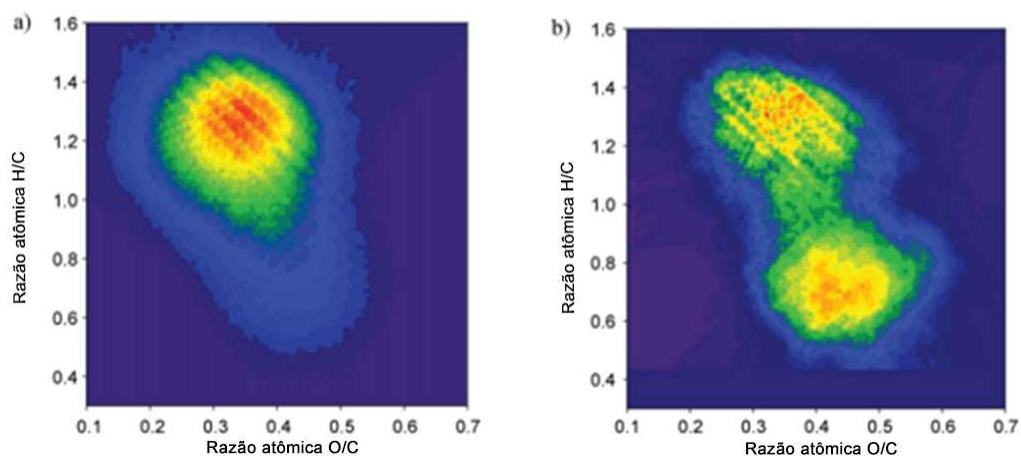


Figura 4: Diagrama de Van Krevelen 3D obtido pelos dados da espectrometria de massa de alta resolução em (a) pântano de McDonald e em (b) rio Negro. As intensidades relativas do sinal aumentam na ordem, roxo, azul, verde, amarelo e vermelho. Adaptado de Kim et al., 2004.

Dittmar et al., (2012b) observou que o carbono negro dissolvido transportado pelo rio Paraíba do Sul foi de 3 a 16 vezes maior do que o produzido pelas fontes existentes na bacia de drenagem atualmente, como por exemplo, queimadas de plantações de cana de açúcar e em pastagens, além do CN oriundo da queima de combustíveis fósseis. Neste estudo, foi analisada uma série temporal de 1997 até 2008, e na estação chuvosa as concentrações foram de até $29 \mu\text{mol C.L}^{-1}$. Por outro lado, na estação de seca as concentrações foram menores e algumas abaixo do limite de detecção de $0,2 \mu\text{mol.C.L}^{-1}$ (Figura 5). As maiores concentrações apresentaram um comportamento inverso aos eventos de queimadas. Assim, os autores descartaram a deposição atmosférica e atribuíram que durante a estação chuvosa ocorre uma entrada de água do solo com altas concentrações de COD e CND. Nos últimos 200 anos grandes quantidades de carbono negro foram produzidos na bacia de drenagem do rio Paraíba do Sul durante a derrubada da Mata Atlântica para criação de área de agricultura. Neste estudo foi estimado que o rio Paraíba do Sul transporta de $2,300$ a $3,100\text{T.ano}^{-1}$ de CND para o oceano.

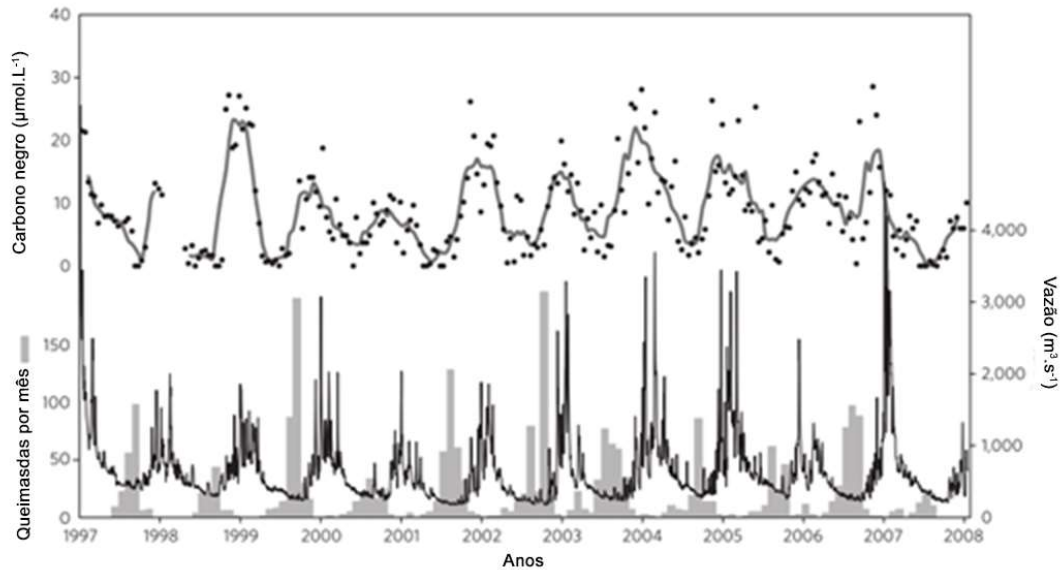


Figura 5: Série temporal de freqüência de queimada, descarga de água e concentração de CND. Adaptado de Dittmar et al., 2012b.

Uma questão importante na migração do CN nos solos é a sua requeima. O impacto da queima de biomassa na qualidade e quantidade da MOS são variados (Hamer et al., 2004). Neste sentido, a freqüência de queimadas poderia desempenhar um papel importante na característica da MOS, na acumulação e disponibilidade do CN. Ding et al., (2013), não observaram relação entre a freqüência de queimadas e as concentrações de CND. Entretanto, foi observada uma forte relação entre o COD e o CND, sugerindo que o mecanismo de mobilização do COD e do CND é acoplado. O mesmo padrão foi observado por Jeffé et al., (2013), em escala global de diversos rios e ecossistemas úmidos ao redor do globo terrestre. Neste estudo os autores também observaram uma forte ligação entre as concentrações do COD com as do CND (Figura 6). Os autores destacaram a participação do COD no processo de translocação física do CND pelo solo e foi estimado que cerca de 26,5 milhões de toneladas métricas (MMT = 10^{12} gramas) de CND entram nos oceanos todos os anos. Esse valor é quase da mesma ordem de grandeza que a estimativa de produção mundial de 40 a 250 MMT.ano⁻¹ de CN originado na queima de biomassa (Kuhlbusch et al., 1996).

Ainda segundo Jeffé et al., (2013), o COD é um importante suporte ambiental, atuando no estoque e transferência de CN. As contínuas perturbações antropogênicas nas bacias de drenagem (queimadas e agricultura) e os impactos das mudanças globais no clima (derretimento das geleiras polares) podem provocar

um aumento na exportação de COD do continente para os oceanos, e provavelmente o fluxo de CND aumente na mesma proporção.

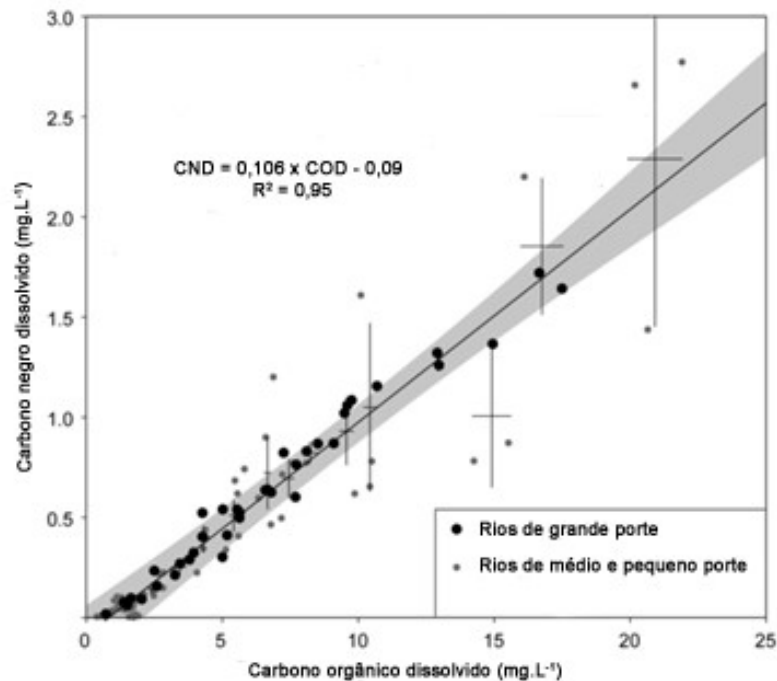


Figura 6: Correlação entre a concentração de COD e o CND de rios ao redor do globo terrestre. Adaptado de Jeffé et al., 2013.

A transferência de CN de origem terrestre para o ambiente marinho através dos estuários é controlada pela vazão fluvial (Dittmar et al., 2012a; Jeffé et al., 2013). Os rios e os estuários são responsáveis pelo aporte de grandes quantidades de materiais orgânicos terrestres que são transferidos para o sistema marinho (Keil et al., 1997; Rezende et al., 2010), representando algo em torno de 1 a 2% da produtividade primária terrestre anual (Hedges e Keil, 1995). O transporte pelas marés, juntamente com os fluxos fluviais, representa uma das mais importantes fontes de MO terrestre para as áreas costeiras adjacentes, servindo de base alimentar para diversos tipos de peixes e invertebrados de grande importância econômica (Dittmar et al., 2006). Neste sentido, a região estuarina e os ecossistemas costeiros como, manguezais e marismas atuam como fonte de CN para o oceano. Manino and Harvey, (2004) investigaram o transporte continente-

oceanos de CN na forma coloidal de baixo peso molecular ($1\text{kDa} < \text{Ø} < 30\text{kDa}$) no rio Delaware e na baía de Chesapeake. As concentrações de CN variaram de 45 a $1038\mu\text{g.L}^{-1}$ e a porcentagem de CN em relação a COD variaram de 4,6 a 72%. Tanto as concentrações quanto as porcentagens apresentaram correlação inversa com a salinidade (Figura 7 B). Isso indica que o CN foi originado no continente e o estuário de Delaware e a baía de Chesapeake são importantes fontes de CN para o ambiente marinho. Os autores atribuíram as maiores concentrações e porcentagens de CN na região de maior turbidez devido à proximidade desta região com o Porto de Delaware, maior porto de água doce do mundo (Figura 7A). Nesta região ocorre uma grande ressuspensão de sedimentos devido a penetração da cunha salina e circulação interna resultando na ressuspensão do CN depositado no sedimento e, além disso, é uma região altamente industrializada e com intenso fluxo de navios que poderiam gerar o CN encontrado na fração coloidal.

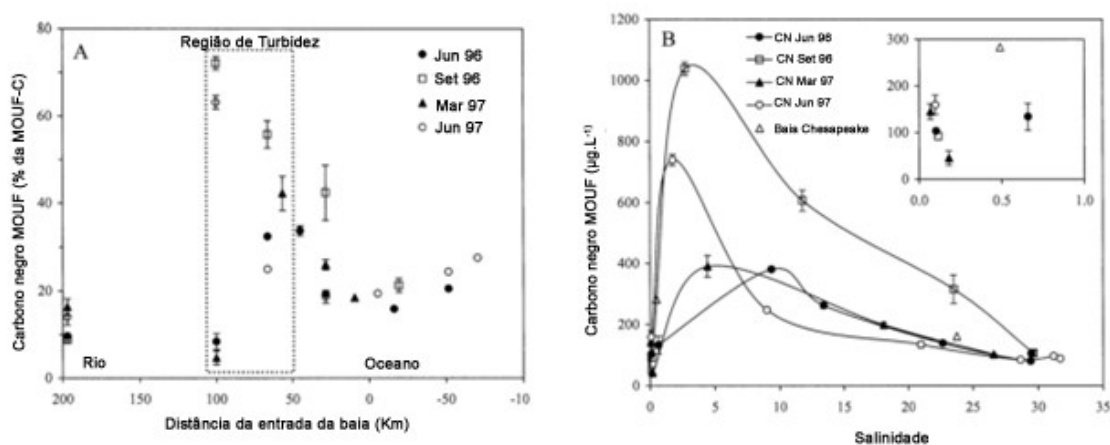


Figura 7: Distribuição do CN em (A) porcentagem em relação a distância da foz e em (B) concentração em relação a salinidade. Adaptado de Manino and Harvey, 2004.

O maior volume de escoamento de água nos continentes ocorre na zona entremarés, com inundações, lavagem e drenagem pela maré de grandes áreas com vegetação em geral mais que uma vez por dia (Dittmar et al., 2012a). A exportação de materiais terrestres pelas marés é tão eficiente que em muitas zonas costeiras, o fluxo de MO das áreas entremarés vegetadas excede o fluxo fluvial (Dittmar et al., 2001). Com o objetivo de identificar a contribuição dos “**salt**

marshes” na dinâmica de exportação de CND Dittmar et al., (2012a) também observaram uma forte relação entre o COD e o CND. Neste estudo, em conjunto com as concentrações de CND foi utilizado a composição isotópica do carbono para se inferir sobre a fonte do CND, sendo considerado três “**end-members**”. O modelo de mistura mostrou que a maior contribuição de CND seria a água intersticial dos “**salt marshes**” (Figura 8). Os autores destacaram a participação da água intersticial na exportação do CND que pode ser distribuído em grandes escalas no ambiente marinho.

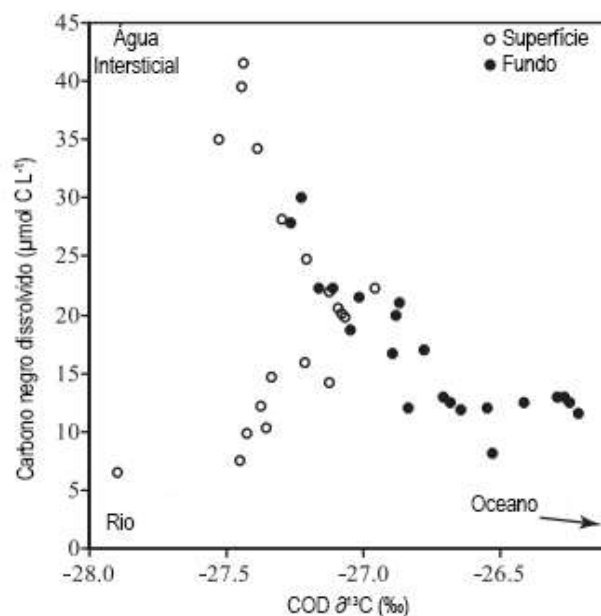


Figura 8: Modelo de mistura com o $\delta^{13}\text{C}$ e as concentrações de CND. Adaptado de Dittmar *et al.*, 2012a.

1.7 - O carbono negro no ambiente marinho

A matéria orgânica dissolvida (MOD) desempenha um importante papel nos processos biogeoquímicos como no fornecimento de energia para a fauna microbiana e atua no transporte de carbono e outros nutrientes e elementos traços do continente para o oceano. O estoque de MOD nos oceanos representa um dos maiores estoques mundiais de carbono, com aproximadamente 700PgC. Esse valor corresponde ao carbono encontrado nos organismos vivos no planeta (Hansell, 2002; Stubbins et al., 2012b). Dentre o total da MOD, o CN dissolvido representa

uma importante fração em relação a outros compostos. Dittmar e Paeng, (2009), encontraram concentrações de CN dissolvido variando entre 600 a 810 nM.C.L⁻¹ com o CN representando 2% do total da MOD em um transecto realizado entre a Antártica e a África do Sul. Em contrapartida, fenóis derivados da lignina, marcadores de MOD terrestre, compreendem <0,1% do total da MOD marinha (Opsahl and Benner, 1998; Hernes and Benner, 2006), aminoácidos hidrolisáveis < 1,9% e polissacarídeos < 0,6% (Kaizer and Benner, 2009). O CN dissolvido foi encontrado em massas d'água profundas da zona abissal, levando a ser sugerida uma fonte de CN no oceano profundo, possivelmente associado ao aquecimento das fontes hidrotermais (Dittmar e Koch, 2006). Masiello e Druffel, (1998), encontraram a porcentagem média de CN em perfis de sedimento variando entre 15 ± 2% no Nordeste do Pacífico (220 km da costa da Califórnia) e 21 ± 6% no Oceano Antártico (500 km das ilhas Antípodas, Nova Zelândia). Neste estudo, as áreas estudadas foram escolhidas pela pressuposição que não existiria influência fluvial e o CN seria originado da queima de combustíveis fósseis e atingiriam o ambiente marinho pelo transporte atmosférico. No entanto, a datação do CN com ¹⁴C revelou que o CN não é originado pela queima de combustíveis fósseis, pois é um carbono recente. Os autores consideraram que o CN poderia ser de origem terrestre e transportado pela fração dissolvida para regiões remotas no Oceano.

Dittmar (2008), investigou a origem do CN no norte do golfo do México, utilizando os ácidos benzeno-policarboxílicos (BPCAs) e observou que as concentrações dos BPCAs apresentaram uma relação inversa com a salinidade. Na baía de Apalachee a concentração de BPCA correspondeu a 2,9% da MO. Na quebra da plataforma continental (80km da costa) a concentração correspondeu a 1,2% da MO. A maior porcentagem do CN na baía de Apalachee indica que o CN é originado no continente. Esses dados mostram que o CN pode ser transportado para longas distâncias no ambiente marinho pela MOD. Em um estudo feito entre a costa da África do Sul e a Antártica Dittmar e Paeng, (2009), observaram que as concentrações de compostos aromáticos policíclicos totais apresentaram uma distribuição homogênea na coluna d'água (Figura 8). Neste estudo, a porcentagem do CN em relação à MOD foi de 2%, e as concentrações variaram entre 600 a 800nM.C.L⁻¹ de BPCA. As maiores concentrações de BPCA próximo a costa da África do Sul, indicam a origem continental do CN devido à descarga de rios e aporte de aerossóis nas regiões costeiras. Estes dados mostram que o CN na forma

dissolvida é distribuído no oceano pelas massas d' água, alcançando regiões mais remotas. A descoberta de concentrações similares de CN dissolvido no oceano profundo indica que o CN é uma molécula recalcitrante (Dittmar e Paeng, 2009).

Stubbins et al., (2010), observaram que em 57 dias todo o CN identificado pelo espectrômetro de massa de alta resolução no rio Congo foi perdido após uma simulação de irradiação da luz solar. Esses resultados assim como a fotoreatividade de outros compostos dissolvidos condensados (Stubbins et al., 2008; Spencer et al., 2009), mostram que a foto-oxidação pode ser um significativo sumidouro do CN dissolvido em águas naturais (Stubbins et al., 2012b). Stubbins et al., (2012b) observou que as concentrações de CN dissolvido em uma das principais massas de água profunda do Oceano (Água Profunda do Atlântico Norte) diminuíram de $1044\text{nM}\pm 164\text{nM}$ para $55\pm 15\text{nM}$ após 28 dias de simulação de irradiação da luz solar (Figura 9A). A porcentagem de CN também apresentou um decréscimo significativo, indo de 2,1% antes da irradiação para 0,2% após (Figura 9B). Masiello e Louchouart, (2013), sugerem que a fração mais refratária (mais condensada) do CN após sua entrada no oceano é foto-oxidada nas águas superficiais, levando a uma acumulação das frações menos condensadas no oceano profundo (Figura 10).

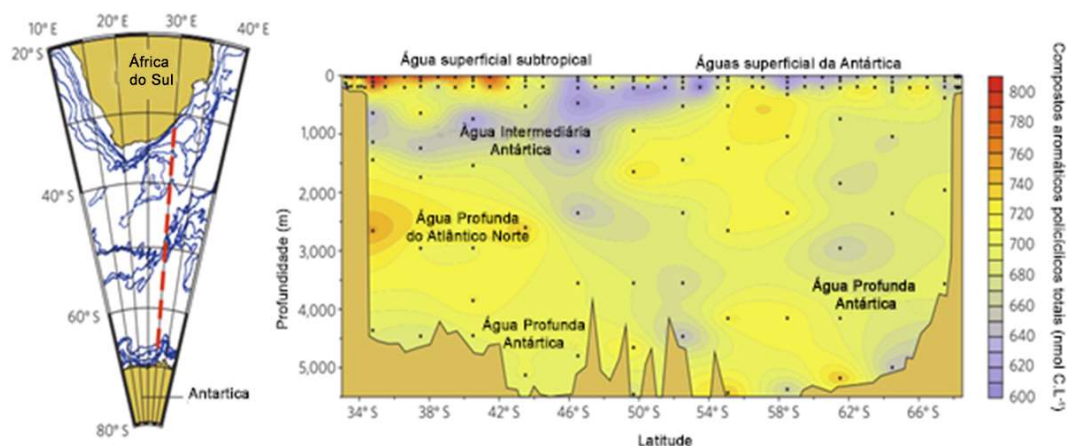


Figura 9: Distribuição de compostos aromáticos policíclicos totais na MOD entre a África do Sul e a Antártica. Adaptado de Dittmar and Paeng, 2009.

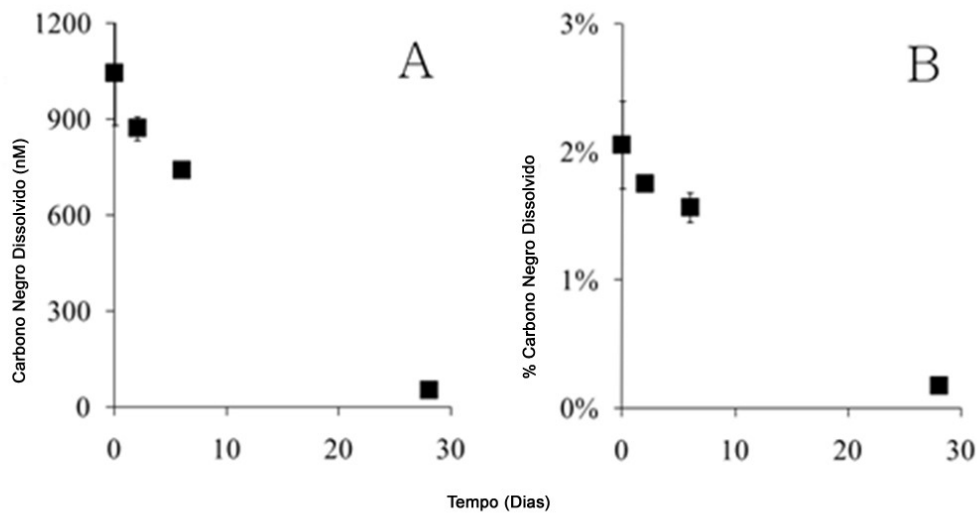


Figura 10: Foto-degradação do CN dissolvido da Água Profunda do Atlântico Norte, em (A) concentração em nM e em (B) % em relação a MOD. Adaptado de Stubbins et al., 2012b.

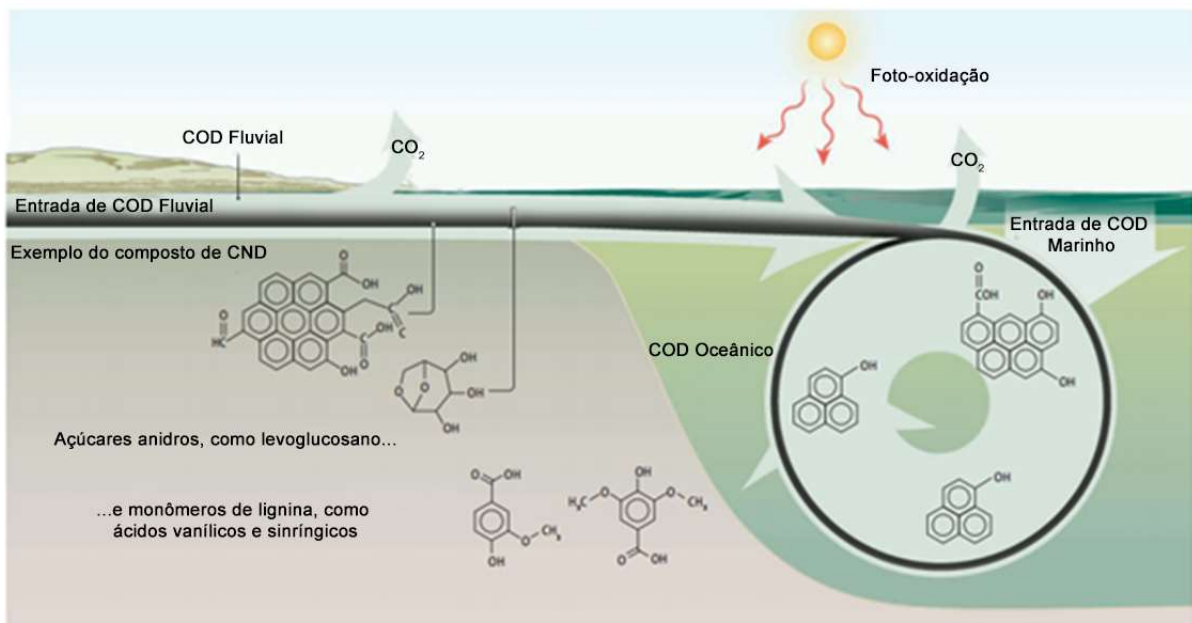


Figura 11: Modelo da foto-degradação das frações mais condensadas do CN nas águas superficiais do oceano. Adaptado de Masiello and Louchouart, 2013.

2 - Justificativa

No oceano profundo, cerca de 2% da MOD está na forma de carbono negro. Estudos indicam que o aporte continental via estuários seria a principal fonte de CND para o ambiente marinho, mas, no entanto esses dados são escassos na literatura. Neste sentido, o rio Paraíba do Sul foi escolhido como modelo de contínuo continente/oceano, pois é o único rio em escala global que possui uma série temporal de fluxo de CND disponível (Dittmar et al., 2012a). Além disso, na derrubada da Mata Atlântica foram utilizadas queimadas como forma de limpeza dos campos. Com isso uma grande quantidade de carvão foi gerada e o mesmo permanece estocado nos solos ainda nos dias de hoje.

Atualmente, a maior parte da bacia de drenagem é coberta por gramíneas onde as queimadas são utilizadas como forma de limpeza dos campos e na pré-colheita (pasto e cana de açúcar respectivamente). Assim, para identificar o tipo de vegetação a partir da qual o CND foi produzido, a composição isotópica do carbono ($\delta^{13}\text{C}$) se apresenta como uma ferramenta poderosa. A mesma abordagem foi utilizada por Dittmar et al., (2012b) onde foi identificado que a água intersticial do sedimento era a principal fonte de CND para um canal de maré em um “*salt marsh*” no norte do Golf do México.

3 – Objetivo

O objetivo do presente estudo foi identificar as fontes e os principais processos que afetam o transporte do carbono negro dissolvido e também identificar o efeito da mudança da cobertura vegetal na composição isotópica do carbono da matéria orgânica no contínuo continente/oceano do rio Paraíba do Sul.

4 – Perguntas

- A mudança da cobertura vegetal tem alterado a qualidade do carbono orgânico transportado pelo RPS?
- Em um estudo anterior, os autores mostraram que desmatamento da vegetação de Mata Atlântica seria o principal responsável pela a maior parte

do CND transportado pelo RPS. Assim, é possível utilizar a composição isotópica do carbono orgânico como traçador de fontes de carbono negro dissolvido?

- A hidrologia desempenha um importante papel na migração do CND dos solos para os corpos hídricos?
- A foto-oxidação é um processo que atua na remoção do CND principalmente na estação seca, quando ocorre maior penetração da radiação solar na coluna d' água?

5 – Resultados

Os resultados desta tese serão apresentados na forma de artigo científico a seguir:

5.1 – Efeito das mudanças da cobertura vegetal na $\delta^{13}\text{C}$ da matéria orgânica dissolvida e particulada no contínuo continente/oceano do rio Paraíba do Sul.

Jomar S.J. Marques, Marcelo G. Almeida, Luiz Antônio Martinelli e Carlos E. Rezende.

(Manuscrito em preparação)

5.2 - Dissolved black carbon in the headwaters-to-ocean continuum of Paraíba do Sul River, Brazil. Jomar S.J. Marques, Thorsten Dittmar, Jutta Niggemann, Marcelo G. Almeida, Gonzalo V. Gomez-Saez, Carlos E. Rezende. (***Manuscrito publicado na Frontiers Special Issue - From Fires to Oceans: Dynamics of Fire-Derived Organic Matter in Terrestrial and Aquatic Ecosystems***).

Efeito das mudanças da cobertura vegetal na $\delta^{13}\text{C}$ da matéria orgânica no contínuo continente/oceano do rio Paraíba do Sul.

Jomar S.J. Marques¹, Marcelo G. Almeida¹, Luiz Antônio Martinelli² Matthew W. Jones³ e Carlos Eduardo de Rezende¹

¹Research Group for Aquatic Ecosystem Biogeochemistry, Laboratório de Ciências Ambientais, Centro de Biociências e Biotecnologia Universidade Estadual do Norte Fluminense, Campos dos Goytacazes, Rio de Janeiro, Brazil.

²Laboratório de Ecologia Isotópica, Centro de Energia Nuclear na Agricultura, Universidade de São Paulo, Av. Centenário, Piracicaba, São Paulo

³University of Exeter, United Kingdom.

Resumo

O rio Paraíba do Sul (RPS) é um importante rio da região sudeste, banhando os estados de São Paulo, Minas Gerais e Rio de Janeiro. Este rio é responsável pelo abastecimento de mais de 14 milhões de habitantes. Apesar de sua importância, nos últimos 200 anos a bacia de drenagem do RPS sofreu um intenso processo de mudança de sua cobertura vegetal original de Mata Atlântica. Atualmente, apenas 8% da bacia é coberta por Mata Atlântica, e está restrita a pequenos fragmentos isolados uns dos outros, enquanto 74% da bacia é coberta principalmente por gramíneas como pasto e próximo a região estuarina existem extensivas plantações de cana de açúcar. A composição isotópica permite o monitoramento de mudanças nos ecossistemas e promove ligações específicas entre ecologia, uso da terra e processos biogeoquímicos. Este estudo tem como objetivo identificar as principais fontes de matéria orgânica particulada (COP) e dissolvida (COD) transportada pelo rio Paraíba do Sul, em diferentes períodos sazonais (chuvoso e seco). As amostras foram coletadas nos períodos chuvosos (2013 e 2014) e período seco (2013). As amostras de água foram coletadas ao longo do RPS (24 amostras), nos principais tributários (14 amostras) e na região estuarina e costeira (24 amostras), seguindo o gradiente de condutividade elétrica. A fração majoritária no transporte do carbono orgânico foi a fração dissolvida variando de 40 a 95%. Os valores do $\delta^{13}\text{C}$ no COP variaram de -27,2‰ a -21,1, enquanto no COD a variação foi de -29,0 a -20,0‰. Os valores da razão (C/N) variaram de 6 a 41. A $\delta^{13}\text{C}$ foi mais leve em ambas as cheias no COP e COD. O valor médio do $\delta^{13}\text{C}$ na cheia de 2013 no RPS e no estuário aproxima-se a valores de solo de mata atlântica e das espécies de manguezal, respectivamente, indicando a contribuição de material alóctone na coluna d' água, carregado pela lavagem dos solos da bacia de drenagem durante a estação chuvosa. Os valores do $\delta^{13}\text{C}$ nos pontos mais externos do ambiente marinho indicam a presença de material de origem terrestre, devido à alta vazão. A jusante do rio, os valores do $\delta^{13}\text{C}$ exibiram enriquecimento do ^{13}C em ambos os períodos, refletindo a influência da substituição da vegetação original de mata atlântica por pastagem e cana de açúcar, que possuem valores do $\delta^{13}\text{C}$ mais pesados. Em síntese, a MOD transportada pelo RPS é composta de múltiplas fontes (mistura de vegetais vasculares C3 e C4 e também produção autóctone), mostrando que o uso da terra na bacia de drenagem promove uma mudança qualitativa e quantitativa na MOD transportada pelo RPS.

Palavras chaves: matéria orgânica, composição elementar e isotópica, rio Paraíba do Sul, mudança da cobertura vegetal.

Introdução

O aporte fluvial das formas orgânicas e inorgânicas de carbono nas regiões costeiras é um importante componente do balanço global do carbono (Hedges, 1992; Benner, 2004). Os rios promovem uma ligação direta entre os componentes terrestre e marinho do ciclo do carbono (Seidel et al., 2015). Os pequenos rios tropicais podem transportar 50 % do total de carbono de origem terrestre que é descarregado no oceano (Lyons et al., 2002). No entanto, a exportação do carbono terrestre por esses rios, parece ser diretamente ligada com a hidrologia (Alin et al., 2008; Hatten et al., 2010). Assim, a escassez de informação sobre as características da matéria orgânica (MO) e também sobre a exportação em rios tropicais de pequeno e médio porte para o oceano é, portanto, uma lacuna importante na compreensão das relações continente/oceano nos ciclos biogeoquímicos (Moyer et al., 2013).

Os rios de pequeno e médio porte transportam grandes quantidades de MO originada nos solos (Cole e Caraco, 2001; Smith et al., 2001). Neste contexto, suas bacias de drenagens e estuários são locais de intenso processamento da MO (Moyer et al., 2013). Esses processos internos influenciam na quantidade, composição e reatividade da MO descarregada na região costeira. Em adição, as mudanças na cobertura vegetal e as modificações humanas na paisagem alteram intensamente a quantidade e a qualidade da MO terrestre que é exportada para o oceano (Houghton et al., 2000; Lu et al., 2014). A geoquímica da matéria orgânica no ambiente requer informações sobre a composição elementar (C/N)_a e isotópica ($\delta^{13}\text{C}$) (Countway et al., 2007).

A razão (C/N)_a é considerada uma importante ferramenta na discriminação do grau de degradação da MO e acoplada a $\delta^{13}\text{C}$ fornece informações sobre suas fontes (Rumolo et al., 2011). Plantas terrestres possuem elevados níveis de polímeros aromáticos como lignina e tanino que proporcionam valores da razão (C/N)_a acima de 15. Em contrapartida, o fitoplâncton possui maiores concentrações de lipídeos e proteínas entre seus constituintes, proporcionando assim valores da (C/N)_a na faixa de 5 a 10 (Rumolo et al., 2011). A investigação sobre as alterações da matéria orgânica fornece informações importantes para o entendimento dos processos biogeoquímicos que ocorrem em ambientes naturais (McCallister *et al.*, 2006). A composição isotópica permite o monitoramento das mudanças nos

ecossistemas e promove ligações específicas entre ecologia, uso da terra e processos biogeoquímicos (McCallister *et al.*, 2006; Fry, 2006 Bouillon *et al.*, 2008; Prasad & Ramanathan, 2009). A composição isotópica tem sido aplicada em regiões tropicais em estudos sobre a ciclagem da matéria orgânica do solo (MOS), onde florestas (plantas com fotossíntese tipo C3) foram substituídas por gramíneas (plantas com fotossíntese tipo C4) (Rossi *et al.*, 2013). A mudança da cobertura vegetal é um problema grave no Brasil e como exemplo de ecossistema afetado pode se destacar a Mata Atlântica. A bacia de drenagem do rio Paraíba do Sul (RPS) foi originalmente coberta por Mata Atlântica (plantas do tipo C3) que foi quase que completamente destruídas ao longo dos séculos passados existindo apenas 8% da vegetação original nos dias de hoje. Atualmente, a maior parte da bacia de drenagem é coberta por pastagens (74%), e na porção inferior existe extensivas plantações de cana-de-açúcar, plantas do tipo C4 (Ribeiro *et al.*, 2009). O conhecimento de como o uso antropogênico da terra pode alterar o ciclo do carbono no ambiente aquático ainda é bastante limitado (Lu *et al.*, 2013). Neste contexto, o uso da composição elementar e isotópica na caracterização das principais fontes de MO transportada pelo RPS para a região costeira se mostra de extrema importância no entendimento do impacto causado pela mudança da cobertura vegetal.

Objetivo

O objetivo do estudo é identificar como a mudança da cobertura vegetal, de Mata Atlântica (C3) e, para pasto e cana de açúcar (C4) têm afetado a biogeoquímica da matéria orgânica (MO) particulada e dissolvida transportada pelo rio Paraíba do Sul.

Material e métodos

Área de estudo

A bacia do rio Paraíba do Sul está localizada na região Sudeste do Brasil. Esta apresenta uma área de drenagem de aproximadamente 55.400 km² ocupando os estados de São Paulo, Minas Gerais e Rio de Janeiro e está localizada entre as latitudes 20°26' e 23°28'S e longitudes 41°00' e 46°30'W (Ovalle *et al.*, 2013). A cabeceira do RPS é formada pela confluência dos rios Paraibuna e Paraitinga. O

RPS possui uma extensão de 1.145 km. A bacia do RPS pode ser dividida em três macro setores (Fig 1a.): (1) Setor bacia superior com uma área de 7.300 km², onde o rio desce de uma altitude de cerca de 1800 m para 600 m através de vales estreitos e incorporados esculpidos em rochas cristalinas; (2) Setor bacia média com uma área de 27.500 km² e altitude média de 510 m, nesta área estão localizados a maioria das indústrias; (3) Setor bacia inferior com uma área de 22.500 km² que é ocupado principalmente por planície costeira com inúmeros meandros ribeirinhos e ilha.

A bacia do RPS é altamente urbanizada e industrializada, com uma população de cerca cinco milhões de habitantes. O RPS é responsável pelo abastecimento hídrico de uma população superior a 14 milhões de habitantes. Na cidade de Barra do Piraí, cerca de 160m³s⁻¹ são desviadas do RPS para o uso na cidade do Rio de Janeiro. Na bacia do RPS existem cerca de 6.000 fazendas e 8.500 diferentes tipos de indústrias (Ovalle et al., 2013). A produção industrial é especialmente, de aço, produtos químicos, alimentos e papel. Estas indústrias estão concentradas na bacia do setor médio e superior e nas sub-bacias dos rios Pomba e Paraibuna (Ovalle et al., 2013). No setor inferior da bacia, a agricultura extensiva é a principal atividade, especialmente a produção de cana-de-açúcar. Além disso, quarenta e sete diferentes reservatórios e represas hidrelétricas com diferentes tamanhos também são encontrados em toda a bacia (Ovalle et al., 2013).

O estuário do rio Paraíba do Sul está localizado na planície costeira formada pelo delta do RPS no Norte do Estado do Rio de Janeiro, perto da cidade de São João da Barra. A zona estuarina é dividida em dois setores fisiograficamente diferentes: (1) O canal principal, que é a maior fonte de água doce para a região costeira; (2) O canal secundário com o fluxo do rio reduzido, permitindo a entrada mais frequente da água do mar (especialmente na estação seca). Nos arredores do estuário há 8 km² de manguezais. As espécies dominantes são *Rhizophora mangle*, *Avicennia germinans* e *Laguncularia racemosa*. A região estuarina da RPS passou por um intenso processo de erosão devido à redução do fluxo fluvial (Bernini et al., 2010). No período de dezembro a fevereiro observa-se a estação chuvosa com grandes vazões podendo chegar a valores de 4.384 m³/s. No período de junho a agosto tem-se a estação seca, onde se observa vazões mínimas de 181 m³/s (ANA, 2006; Almeida, et al, 2007).

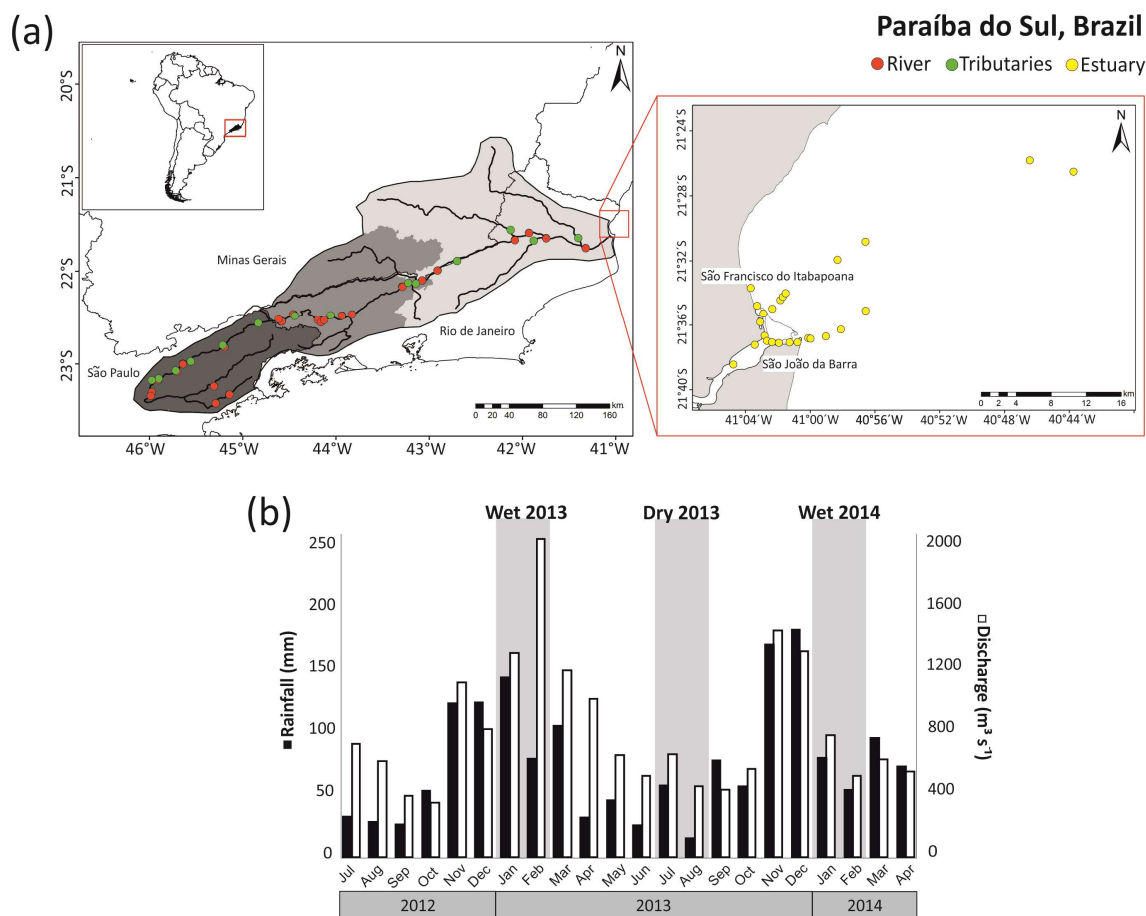


Fig. 1: (a) Mapa mostrando a bacia de drenagem do RPS e as estações de amostragem no RPS (vermelho), tirbutários (verde) e estuário (amarelo); (b) vazão (branco) e precipitação (preto) do RPS entre os anos de 2012 a 2014, as faixas cinza indicam os períodos de amostragem (cheia de 2013, seca de 2013 e cheia de 2014).

Amostragem

As amostras dos rios, estuário e marinhas foram coletadas durante a estação de cheia em janeiro e fevereiro de 2013 e 2014 (média do fluxo fluvial: $1875\text{m}^3\text{s}^{-1}$ e $719\text{m}^3\text{s}^{-1}$, respectivamente) e durante a estação de seca em julho e agosto de 2013 (média de fluxo fluvial: $478\text{m}^3\text{s}^{-1}$) (Fig. 1). As amostras de água superficiais (3L água doce e 10 litros água marinha) foram coletadas com garrafas limpas previamente (HCl 10%) em 24 estações ao longo do canal principal do RPS (Fig. 1a em vermelho), e 14 estações nos principais tributários (Fig. 1a verde). Na região estuarina/marinha foram coletadas 24 estações na cheia de 2013 e 21 na seca de 2013 e cheia de 2014, seguindo um gradiente de condutividade elétrica até 35 km da costa (Fig. 1a amarelo). As amostras do RPS e tributários foram coletadas sobre

pontes com auxílio de corda e balde, enquanto as estuarinas e marinhas foram coletadas com uma traineira.

Isolamento do carbono orgânico particulado

Para o isolamento do COP, de 3 – 8L das amostras foram filtradas com filtros GF/F (Whatman 0,7 μ m), previamente descontaminados em mufla (400° 4h). Os filtros foram pesados antes e após a filtração, com as concentrações de MPS sendo obtidas por gravimétrica.

Isolamento do carbono orgânico dissolvido

Logo após a filtração, as amostras foram acidificadas com HCl (32%, p.a.) até pH 2 e em seguida o COD foi isolado das amostras de água pela técnica de extração de fase sólida (Dittmar, 2008). As amostras filtradas foram passadas por gravidade nos cartuchos de extração de fase sólida (1g PPL, Agilent). Os cartuchos foram dessalinizados com solução 0,01 mol⁻¹ de HCl, secos em fluxo de N₂ e eluídos com 8 mL de metanol (grau HPLC). A eficácia da extração do COD foi determinada para cada amostra depois de evaporação de uma alíquota do extrato de metanol até *secura*. Em seguida, o carbono orgânico foi dissolvido em água ultrapura a pH 2, e determinado as concentrações de COD nesta solução. A razão entre as concentrações de COD extraído e total é considerada a eficiência de extração. Em média, entre todas as amostras (n = 177), 45% (\pm SE 13%) de DOC foi recuperado pela SPE.

Carbono orgânico dissolvido

As concentrações de COD foram medidas usando um instrumento de elevada temperatura de combustão (Shimadzu TOC 5000), com cinco padrões de calibrações na mesma escala das amostras. Todos os valores de COD reportados aqui são referentes à média entre três réplicas com o coeficiente de variação menor que 5%. Entre as amostras foram rodados brancos com nenhum valor detectável de COD. O limite de detecção analítico foi de 5 μ m.

Composição elementar e isotópica

A determinação do COP foi realizada a partir dos filtros secos. Já a determinação da composição elementar e isotópica do COD foi realizado em 800 a

1600 µL do extrato de metanol com a matéria orgânica dissolvida que foi previamente estocado em recipiente de vidro calcinado e evaporado até secar sob fluxo de N₂. Este volume foi seco e dissolvido em 50 µL de metanol. Em seguida, esse volume foi lentamente adicionado em recipiente de estanho e seco a 60° por 24 horas. A composição elementar (C e N) e a composição isotópica (δ¹³C e δ¹⁵N) foram determinadas pelo analisador CHNS-O acoplado a um espectrômetro de massa (**Thermo Fisher Scientific**). A razão do isótopo estável de carbono é expressa como δ¹³C relativo ao padrão Pee Dee Belemnite (PDB) enquanto o do nitrogênio é em relação ao valor atmosférico.

Modelo de mistura isotópico de duas fontes

Para estimar a contribuição de MO derivada de plantas do tipo C4 no RPS e tributários, foi utilizado o modelo de mistura de duas fontes (equação 1, Martinelli et al., 2002).

$$C4(\%) = \frac{\delta^{13}C_{amostra} - \delta^{13}C_{C3\ solo}}{\delta^{13}C_{C4\ solo} - \delta^{13}C_{C3\ solo}} \times 100 \quad (1)$$

onde δ¹³C_{amostra} é a composição isotópica do COP e ou COD em uma dada amostra, δ¹³C_{C3 solo} é a composição isotópica de um solo de floresta (-29‰) coletado no Parque Nacional da Serra do Mar e o δ¹³C_{C4 solo} é a composição isotópica do solo de uma área coberta por pastagem (-15‰). Nesse modelo, é assumido que existem apenas duas fontes principais de MOD. Outras fontes, como o esgoto e ou a produção autóctone podem introduzir uma pequena incerteza ao modelo.

Resultados

As concentrações de COP variaram entre 17 a 1009 µmol.L⁻¹ no RPS enquanto as concentrações de COD variaram de 168 e 894 µmol.L⁻¹, com a estação chuvosa de 2013 apresentando os maiores valores para ambos (Teste t-student, p<0,01, Tabela 1). Os valores tanto do COD e do COP na cheia de 2013 aumentaram ao longo do curso do rio, devido a um deslocamento de massa, causado pela chuva. O coeficiente de variação espacial ao longo do RPS na estação chuvosa de 2013 para o COD e COP foi de 243% e 160% respectivamente.

Nos tributários as concentrações de COP variaram entre 7 a 1306 $\mu\text{mol.L}^{-1}$ e as de COD variaram entre 143 e 1381 $\mu\text{mol.L}^{-1}$. As concentrações foram similares nas estações de cheia e diferentes entre as estações de cheia e a de seca (Teste t-student, $p < 0,01$, Tabela 2), com as maiores concentrações nas estações chuvosas. Na região estuarina as concentrações de COP variaram entre 3 a 500 $\mu\text{mol.L}^{-1}$ enquanto as concentrações de COD variaram entre 72 a 529 $\mu\text{mol.L}^{-1}$, com a estação de chuvosa de 2013 apresentando as maiores concentrações (Teste t-student $p < 0,01$, Tab. 3). As concentrações de COP e COD apresentaram um declínio em relação ao aumento da condutividade elétrica (Fig. 3 e 4).

No RPS os valores da (C/N)_a da fração particulada variaram entre 6 a 20 enquanto na fração dissolvida a variação foi de 14 e 42 (Tab.1). Nos tributários a variação foi de 5 a 35 na fração particulada e 8 a 41 na fração dissolvida (Tab.2). No estuário os valores da (C/N)_a variaram entre 6 a 13 na fração particulada e de 13 a 26 na fração dissolvida (Tab. 3). Os valores da composição isotópica ($\delta^{13}\text{C}$) na fração particulada variaram entre -27,2 a -21,1‰, enquanto na fração dissolvida a variação foi de -29,0 a -23,5‰ no RPS (Tab.1). Nos tributários a $\delta^{13}\text{C}$ da fração particulada variou de -25,9 a -21,8‰, enquanto na fração dissolvida a variação foi de -28,0 a -21,3‰ (Tab. 2). Na região estuarina os valores da $\delta^{13}\text{C}$ variaram de -26,7 a -17,8‰ na fração particulada e de -25,7 a -20,0‰ na dissolvida (Tab. 3). De modo geral, a $\delta^{13}\text{C}$ foi empobrecida no ^{13}C nas estações chuvosa em comparação com a estação de seca tanto nos ambientes de água doce quanto marinho. A $\delta^{13}\text{C}$ também apresentou um enriquecimento no sentido cabeceira para a região estuarina, assim como, ao longo do gradiente de condutividade elétrica (Fig. 3).

Tabela 1: Distância da foz, área da bacia referente ao ponto de coleta coberta por plantas C4, concentrações de COD, COP, valores de $\delta^{13}\text{C}$ e (C/N)_a nos pontos ao longo do RPS nas estações sazonais amostradas.

Local	estação	Distância	C4*	COD	$\delta^{13}\text{C}_{\text{COD}}$	(C/N) _{aCOD}	COP	$\delta^{13}\text{C}_{\text{COP}}$	(C/N) _{aCOP}
RPS		km	%	$\mu\text{mol.L}^{-1}$	‰		$\mu\text{mol.L}^{-1}$	‰	
Paraibuna Floresta	Cheia 2013			373	-29.0	25	110	-25.6	10
	Seca 2013	986	25	345	-27.4	36	82	-23.8	20
	Cheia 2014			256	-28.8	27	31	-26.4	8
Paraibuna Pasto	Cheia 2013			571	-28.8	27	297	-26.9	10
	Seca 2013	952	21	326	-28.0	36	475	-25.0	12
	Cheia 2014			260	-28.6	27	38	-26.1	10
Paraitinga	Cheia 2013			439	-25.5	15	1009	-24.6	8
	Seca 2013	970	71	303	-24.2	31	503	-22.8	17
	Cheia 2014			293	-26.0	27	147	-24.5	10
Jacareí I	Cheia 2013			277	-27.2	19	114	-24.8	7
	Seca 2013	787	55	290	-25.5	38	84	-24.4	10
	Cheia 2014			354	-26.4	42	85	-25.1	9
Jacareí II	Cheia 2013			269	-27.0	23	84	-24.4	8
	Seca 2013	779	55	282	-25.4	33	52	-24.5	10
	Cheia 2014			365	-27.6	30	61	-25.1	8
S.J. Campos	Cheia 2013			310	-27.0	14	168	-25.4	10
	Seca 2013	752	54	266	-24.9	36	171	-24.0	13
	Cheia 2014			386	-25.5	33	184	-23.5	9
Caçapava	Cheia 2013			442	-26.3	18	122	-23.6	8
	Seca 2013	711	54	281	-24.0	26	133	-24.6	13
	Cheia 2014			333	-26.6	21	104	-24.2	7
Taubaté	Cheia 2013			401	-25.7	24	208	-24.4	8
	Seca 2013	686	55	278	-24.2	30	81	-24.4	10
	Cheia 2014			375	-25.3	28	118	-24.3	9
Guaratinguetá	Cheia 2013			406	-26.0	17	264	-24.5	9
	Seca 2013	614	56	286	-24.3	29	241	-24.4	10
	Cheia 2014			401	-26.0	19	147	-23.4	9
Queluz	Cheia 2013			645	-24.8	21	266	-23.5	9
	Seca 2013	540	56	294	-24.2	28	67	-23.8	9
	Cheia 2014			347	-26.1	19	141	-23.4	13
Itatiaia	Cheia 2013			565	-26.0	18	207	-22.7	7
	Seca 2013	520	56	259	-24.6	26	136	-21.1	7
	Cheia 2014			287	-24.8	27	90	-22.0	6
Resende	Cheia 2013			531	-25.3	22	152	-24.8	8
	Seca 2013	487	56	312	-24.8	27	41	-23.0	7
	Cheia 2014			310	-24.3	26	88	-23.3	15
Barra Mansa	Cheia 2013			534	-25.2	22	285	-24.2	7
	Seca 2013	435	56	261	-25.0	26	36	-23.6	8
	Cheia 2014			303	-24.5	26	66	-23.7	10

* dados obtidos do programa MapBiomias: <http://mapbiomas.org/#>

Tabela 1: Continuação

Local	estação	Distância	C4*	COD	$\delta^{13}\text{C}_{\text{COD}}$	(C/N) _{aCOD}	COP	$\delta^{13}\text{C}_{\text{COP}}$	(C/N) _{aCOP}
RPS		km	%	$\mu\text{mol.L}^{-1}$	‰		$\mu\text{mol.L}^{-1}$	‰	
Volta Redonda I	Cheia 2013			723	-24.5	23	921	-23.1	10
	Seca 2013	427	56	271	-24.4	27	43	-23.7	7
	Cheia 2014			290	-24.6	25	106	-23.3	11
Volta Redonda II	Cheia 2013			701	-25.1	24	321	-23.1	10
	Seca 2013	414	54	231	-24.8	24	68	-22.5	8
	Cheia 2014			290	-24.3	25	109	-23.7	14
Barra do Pirai	Cheia 2013			643	-24.8	19	545	-23.0	11
	Seca 2013	381	56	285	-24.2	24	47	-23.4	9
	Cheia 2014			250	-24.4	24	17	-23.8	11
Paraíba do Sul	Cheia 2013			731	-24.5	21	506	-23.8	11
	Seca 2013	294	58	281	-23.5	28	104	-23.9	13
	Cheia 2014			316	-24.4	25	98	-23.8	12
Três Rios	Cheia 2013			694	-24.8	18	447	-23.8	11
	Seca 2013	286	58	295	-23.9	27	88	-24.1	13
	Cheia 2014			310	-24.8	24	53	-23.8	11
Sapucaia	Cheia 2013			583	-25.5	17	409	-23.7	10
	Seca 2013	239	60	227	-23.5	22	52	-25.1	10
	Cheia 2014			292	-24.8	27	41	-25.3	8
Além Paraíba	Cheia 2013			459	-25.3	22	496	-23.7	11
	Seca 2013	213	61	218	-24.3	22	32	-25.5	10
	Cheia 2014			267	-24.5	30	32	-24.5	8
Itaocara	Cheia 2013			894	-25.7	15	337	-23.8	9
	Seca 2013	138	63	205	-24.4	24	44	-23.4	8
	Cheia 2014			222	-24.1	26	62	-23.9	10
Cambuci	Cheia 2013			530	-25.7	14	608	-27.2	12
	Seca 2013	118	67	182	-24.5	23	37	-24.7	9
	Cheia 2014			243	-25.4	24	77	-23.9	10
São Fidélis	Cheia 2013			384	-25.8	14	585	-24.1	12
	Seca 2013	91	67	216	-24.4	23	32	-24.8	8
	Cheia 2014			251	-25.2	17	65	-24.6	10
Campos	Cheia 2013			396	-25.5	22	479	-24.0	12
	Seca 2013	40	69	168	-24.2	23	51	-24.3	10
	Cheia 2014			315	-24.5	24	102	-25.2	9

* dados obtidos do programa MapBiomias: <http://mapbiomas.org/#>

Tabela 2: Distância da foz, área da bacia referente ao ponto de coleta coberta por plantas C4, concentrações de COD, COP, valores de $\delta^{13}\text{C}$ e (C/N)_a nos pontos ao longo dos tributários nas estações sazonais amostradas.

Local	estação	Distância	C4*	COD	$\delta^{13}\text{C}_{\text{COD}}$	(C/N) _a _{COD}	COP	$\delta^{13}\text{C}_{\text{COP}}$	(C/N) _a _{COP}
Tributários		km	%	$\mu\text{mol.L}^{-1}$	‰		$\mu\text{mol.L}^{-1}$	‰	
rio Jaguari	Cheia 2013			308	-25.9	16	470	-25.9	11
	Seca 2013	763	52	198	-25.2	24	133	-24.3	11
	Cheia 2014			202	-25.4	24	49	-23.2	5
rio Buquira	Cheia 2013			258	-26.0	15	1039	-24.0	8
	Seca 2013	750	48	170	-25.9	25	192	-23.6	11
	Cheia 2014			458	-23.4	28	1256	-23.2	9
ribeirão Caçapava	Cheia 2013			333	-24.5	16	628	-21.8	7
	Seca 2013	709	62	333	-24.9	29	59	-22.5	11
	Cheia 2014			319	-24.5	26	530	-25.1	14
ribeirão Taubaté	Cheia 2013			575	-25.5	19	150	-23.9	8
	Seca 2013	673	32	380	-23.2	26	179	-25.6	7
	Cheia 2014			432	-26.8	10	263	-23.0	7
ribeirão Guaratinguetá	Cheia 2013			326	-24.7	15	131	-24.2	10
	Seca 2013	616	63	219	-24.0	29	142	-23.9	9
	Cheia 2014			227	-24.5	28	105	-23.1	10
rio Claro	Cheia 2013			735	-25.6	14	243	-24.1	11
	Seca 2013	547	30	279	-24.8	29	71	-24.4	8
	Cheia 2014			308	-25.2	27	117	-22.8	9
rio Alambari	Cheia 2013			700	-27.4	15	146	-25.1	7
	Seca 2013	586	31	266	-25.9	24	278	-22.2	9
	Cheia 2014			240	-26.2	25	258	-23.6	10
rio Minhocas	Cheia 2013			1122	-24.3	15	470	-23.5	10
	Seca 2013	334	58	281	-23.5	26	7	-24.4	9
	Cheia 2014			244	-24.1	21	50	-23.3	9
rio Piabanha	Cheia 2013			560	-28.0	9	246	-25.0	12
	Seca 2013	275	57	208	-26.8	20	107	-24.5	13
	Cheia 2014			222	-26.1	22	134	-24.2	10
rio Calçado	Cheia 2013			281	-26.6	9	120	-24.4	10
	Seca 2013	262	81	127	-24.9	23	67	-24.9	13
	Cheia 2014			194	-24.8	26	59	-27.0	9
rio Pirapetinga	Cheia 2013			966	-24.2	14	1306	-23.6	35
	Seca 2013	177	80	1126	-21.3	41	333	-20.3	13
	Cheia 2014			1381	-23.5	27	411	-23.0	9
rio Pomba	Cheia 2013			459	-25.3	12	62	-25.4	8
	Seca 2013	163	82	143	-24.6	20	30	-24.8	9
	Cheia 2014			229	-24.6	27	104	-24.5	11
rio Dois Rios	Cheia 2013			824	-27.1	8	98	-25.0	10
	Seca 2013	108	67	147	-25.3	18	64	-24.6	11
	Cheia 2014			229	-24.2	27	113	-24.7	13
rio Muriaé	Cheia 2013			181	-24.7	13	24	-25.1	8
	Seca 2013	66	82	211	-23.0	19	33	-23.2	10
	Cheia 2014			240	-24.2	27	161	-23.5	8

* dados obtidos do programa MapBiomas: <http://mapbiomas.org/#>

Tabela 3: Condutividade elétrica, concentrações de COD, COP, valores de $\delta^{13}\text{C}$, e (C/N)_a nos pontos do gradiente de condutividade elétrica do estuário nas estações sazonais amostradas.

Local	estação	Condutividade	COD	$\delta^{13}\text{C}_{\text{COD}}$	(C/N) _a _{COD}	COP	$\delta^{13}\text{C}_{\text{COP}}$	(C/N) _a _{COP}
Estuário		($\mu\text{S}\cdot\text{cm}^{-1}$)	($\mu\text{mol}\cdot\text{L}^{-1}$)	(‰)		($\mu\text{mol}\cdot\text{L}^{-1}$)	(‰)	
#1	Cheia 2013	58	529	-25.7	16	192	-24.0	11
	Seca 2013	84	158	-22.5	19	171	-19.4	7
#2	Cheia 2014	62	189	-24.8	25	81	-24.1	8
	Cheia 2013	59	511	-25.1	22	169	-24.6	10
	Seca 2013	76	182	-22.7	20	157	-19.0	8
#3	Cheia 2014	65	152	-24.6	25	63	-24.0	6
	Cheia 2013	59	335	-25.7	15	165	-24.8	11
	Seca 2013	2790	194	-22.5	23	120	-24.8	6
#4	Cheia 2014	71	187	-24.6	25	53	-24.0	6
	Cheia 2013	159	441	-24.6	20	95	-26.7	10
	Seca 2013	1238	174	-23.1	18	163	-19.3	8
#5	Cheia 2014	235	173	-24.7	25	81	-24.1	6
	Cheia 2013	5070	414	-24.7	19	305	-26.5	7
	Seca 2013	8200	167	-22.4	20	102	-21.0	6
#6	Cheia 2014	3600	199	-24.5	25	75	-23.5	7
	Cheia 2013	1801	393	-24.8	19	322	-22.8	8
	Seca 2013	9330	180	-22.5	19	121	-20.9	6
#7	Cheia 2014	25500	155	-23.7	24	92	-24.0	6
	Cheia 2013	83	334	-25.6	17	500	-23.5	13
	Seca 2013	74	161	-22.5	21	216	-19.4	9
#8	Cheia 2014	17780	216	-24.0	25	105	-20.2	7
	Cheia 2013	56	485	-25.7	14	458	-23.7	12
	Seca 2013	74	174	-22.9	20	205	-19.9	9
#9	Cheia 2014	71	174	-24.5	26	44	-23.0	8
	Cheia 2013	57	481	-25.6	17	190	-24.6	12
	Seca 2013	80	165	-22.9	20	178	-19.2	8
#10	Cheia 2014	86	162	-24.5	25	35	-21.9	7
	Cheia 2013	63	393	-25.7	13	541	-23.4	12
	Seca 2013	88	167	-22.8	20	114	-19.4	7
#11	Cheia 2014	702	169	-24.8	19	41	-22.2	6
	Cheia 2013	60	519	-25.4	20	491	-23.4	13
	Seca 2013	108	169	-22.9	20	136	-19.5	7
#12	Cheia 2014	10510	168	-24.5	25	53	-21.5	8
	Cheia 2013	62	363	-25.4	18	210	-23.9	12
	Seca 2013	173	170	-22.7	18	119	-19.4	6
#13	Cheia 2014	25600	329	-24.5	26	35	-21.7	7
	Cheia 2013	3710	245	-25.3	19	63	-24.1	9
	Seca 2013	638	175	-22.0	22	189	-18.9	7
#14	Cheia 2014	10800	202	-24.3	16	257	-22.5	11
	Cheia 2013	20000	215	-24.8	17	90	-19.3	10
	Seca 2013	3810	174	-21.3	25	193	-19.3	7
#15	Cheia 2014	22900	123	-25.8	12	113	-17.8	8
	Cheia 2013	37000	218	-23.7	15	92	-19.6	9
	Seca 2013	23400	143	-21.1	20	63	-22.2	8
	Cheia 2014	33500	164	-23.8	23	33	-19.0	9

Tabela 3: Continuação

Local	estação	Condutividade	COD	$\delta^{13}\text{C}_{\text{COD}}$	(C/N) _{aCOD}	COP	$\delta^{13}\text{C}_{\text{COP}}$	(C/N) _{aCOP}
Estuário		($\mu\text{S.cm}^{-1}$)	($\mu\text{mol.L}^{-1}$)	(‰)		($\mu\text{mol.L}^{-1}$)	(‰)	
#16	Cheia 2013	48400	108	-24.0	14	41	-20.1	11
	Seca 2013	36700	134	-21.1	19	65	-18.2	6
	Cheia 2014	40900	137	-22.8	24	115	-17.9	11
#17	Cheia 2013	50800	75	-25.0	17	7	-22.7	2
	Seca 2013	45800	115	-20.5	18	55	-18.8	7
	Cheia 2014	48000	102	-22.3	26	20	-22.6	9
#18	Cheia 2013	50900	74	-24.9	25	6	-24.2	6
	Seca 2013	51000	88	-20.0	18	7	-18.9	7
	Cheia 2014	48200	148	-22.3	26	3	-21.5	7
#19	Cheia 2013	50900	72	-23.5	21	6	-23.9	7
	Seca 2013	51000	106	-20.8	17	3	-18.8	7
	Cheia 2014	48200	147	-22.2	25	7	-22.1	9
#20	Cheia 2013	50800	102	-24.5	22	7	-20.3	5
	Seca 2013	49000	99	-20.0	15	73	-18.9	8
	Cheia 2014	47800	94	-22.2	23	114	-22.2	6
#21	Cheia 2013	37500	154	-24.8	16	61	-19.6	10
	Seca 2013	31700	130	-20.8	20	81	-23.1	6
	Cheia 2014	26700	138	-25.6	16	100	-19.9	7
#22	Cheia 2013	20400	195	-25.1	16	64	-21.3	12
	Seca 2013	-	-	-	-	-	-	-
	Cheia 2014	-	-	-	-	-	-	-
#23	Cheia 2013	12590	232	-25.6	22	53	-20.8	8
	Seca 2013							
	Cheia 2014							
#24	Cheia 2013	3370	191	-25.8	19	164	-23.7	12
	Seca 2013							
	Cheia 2014							

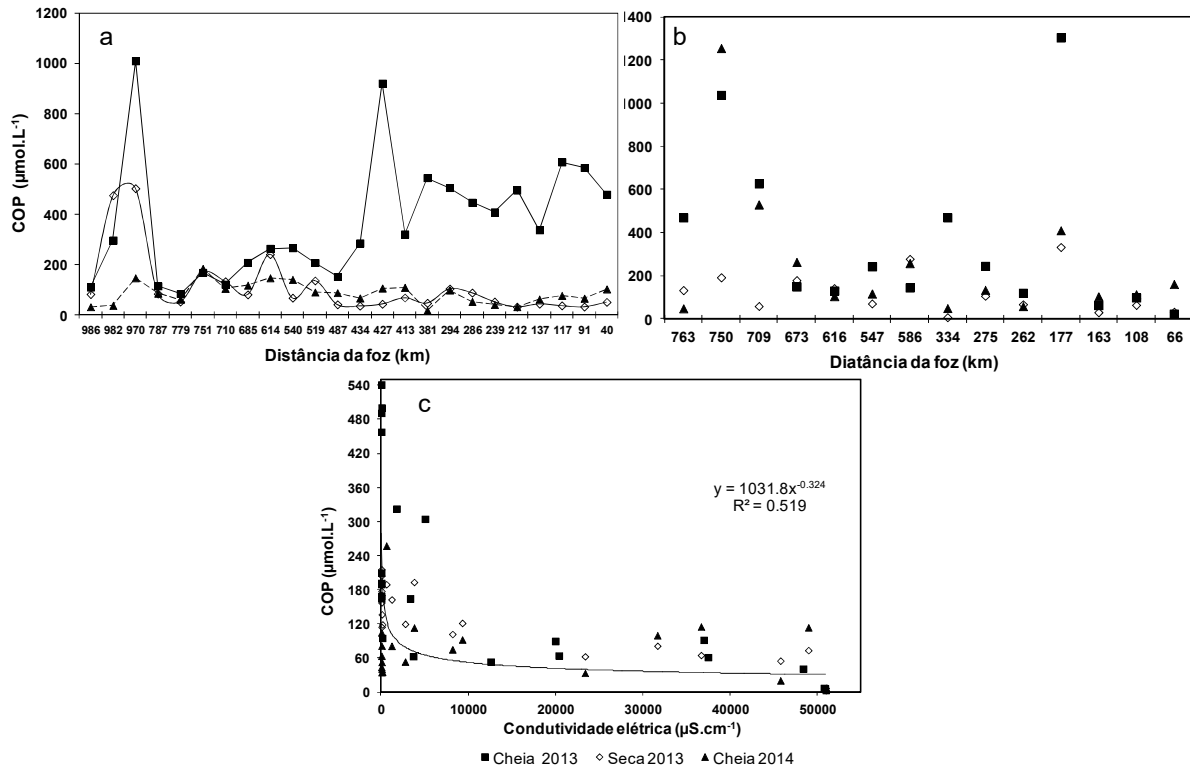


Fig. 3: Concentração do COP ao longo do RPS (a), nos tributários (b) em relação à distância da foz e no estuário em relação ao gradiente de condutividade elétrica (c).

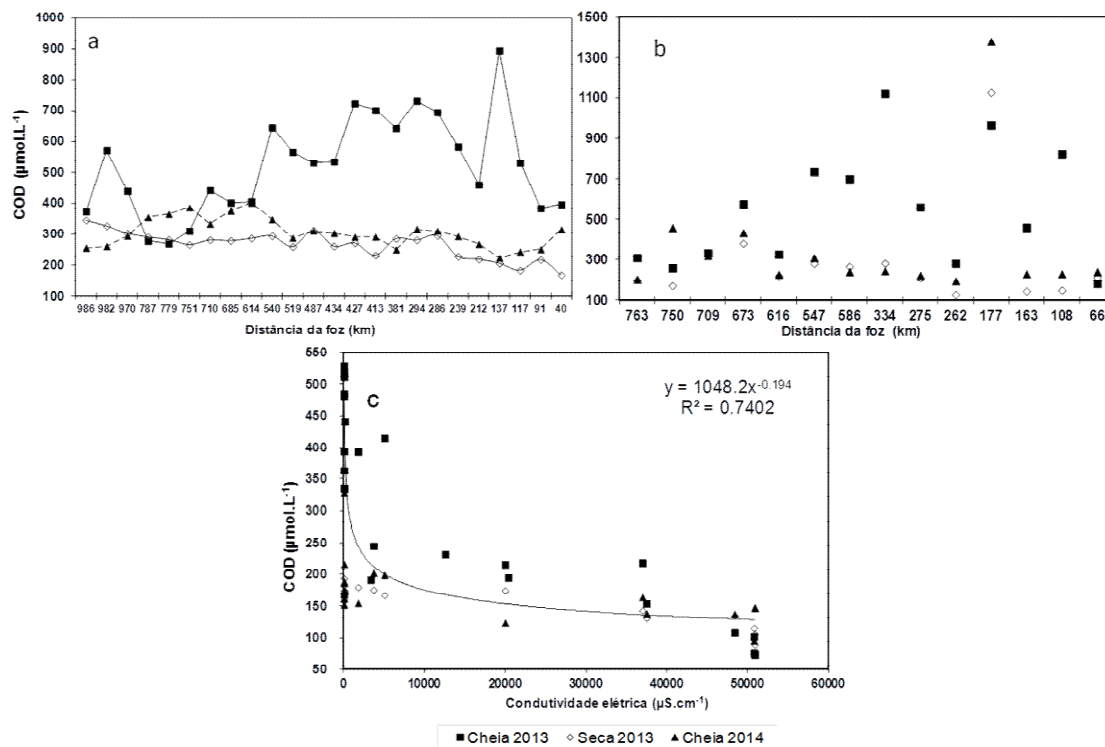


Fig. 4: Concentração do COD ao longo do RPS (a), nos tributários (b) em relação à distância da foz e no estuário em relação ao gradiente de condutividade elétrica (c).

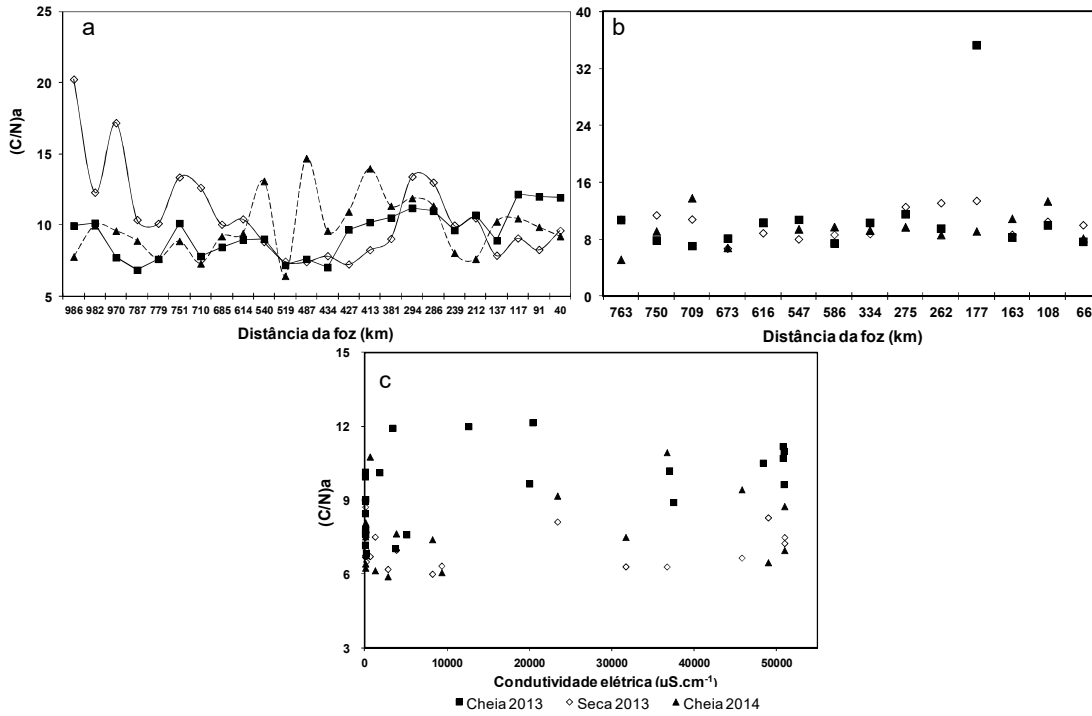


Fig.5: Distribuição dos valores da (C/N)a do COP ao longo do RPS (a), nos tributários (b) em relação à distância da foz e no estuário em relação ao gradiente de condutividade elétrica (c).

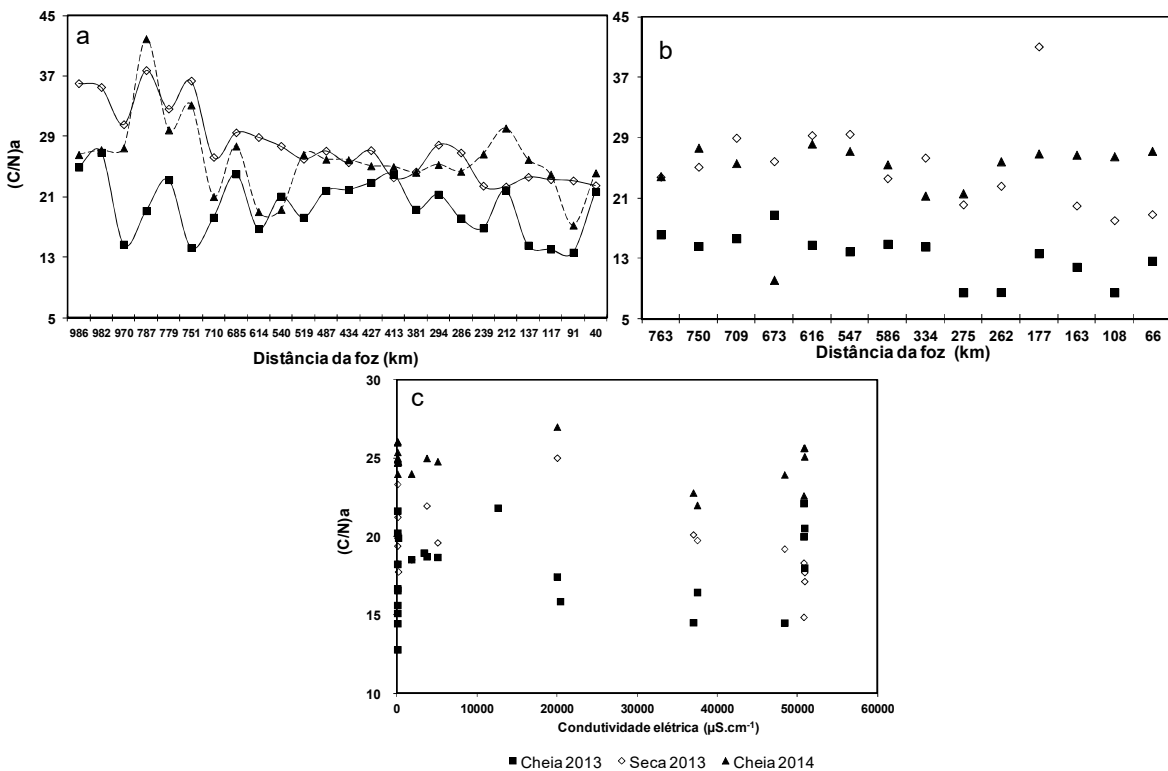


Fig.6: Distribuição dos valores da (C/N)a do COD ao longo do RPS (a), nos tributários (b) em relação à distância da foz e no estuário em relação ao gradiente de condutividade elétrica (c).

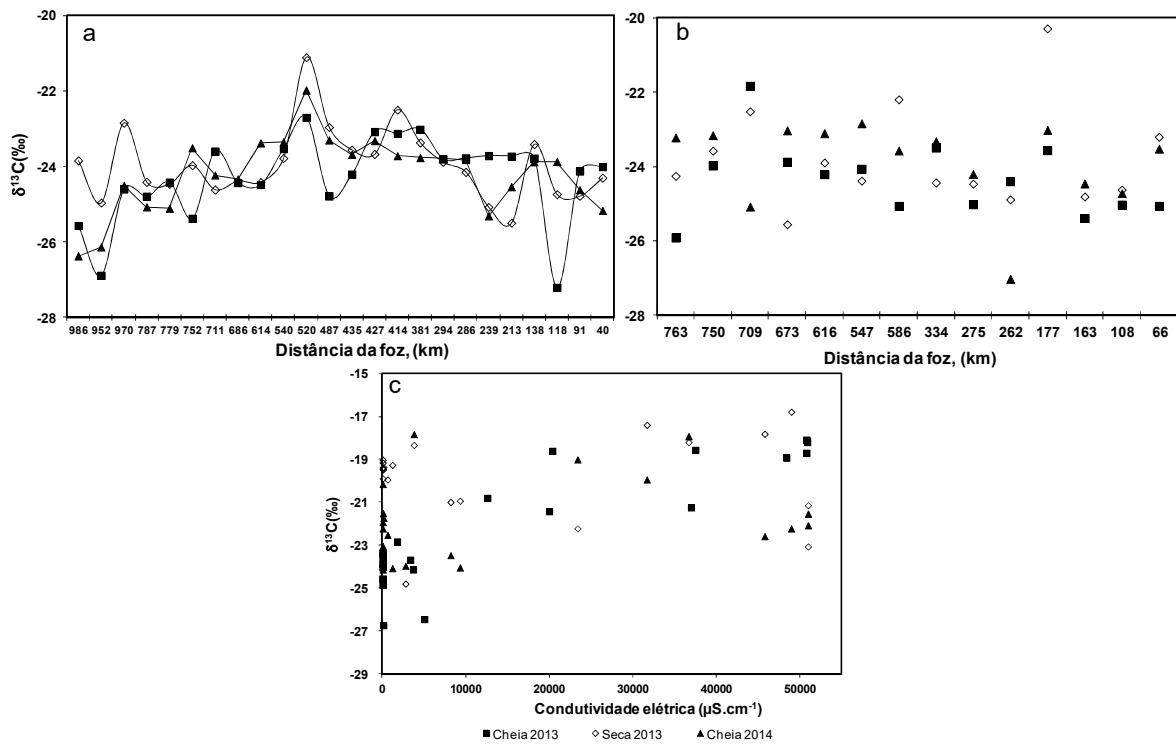


Fig.7: Distribuição dos valores da $\delta^{13}\text{C}$ do COP ao longo do RPS (a), nos tributários (b) em relação à distância da foz e no estuário em relação ao gradiente de condutividade elétrica (c).

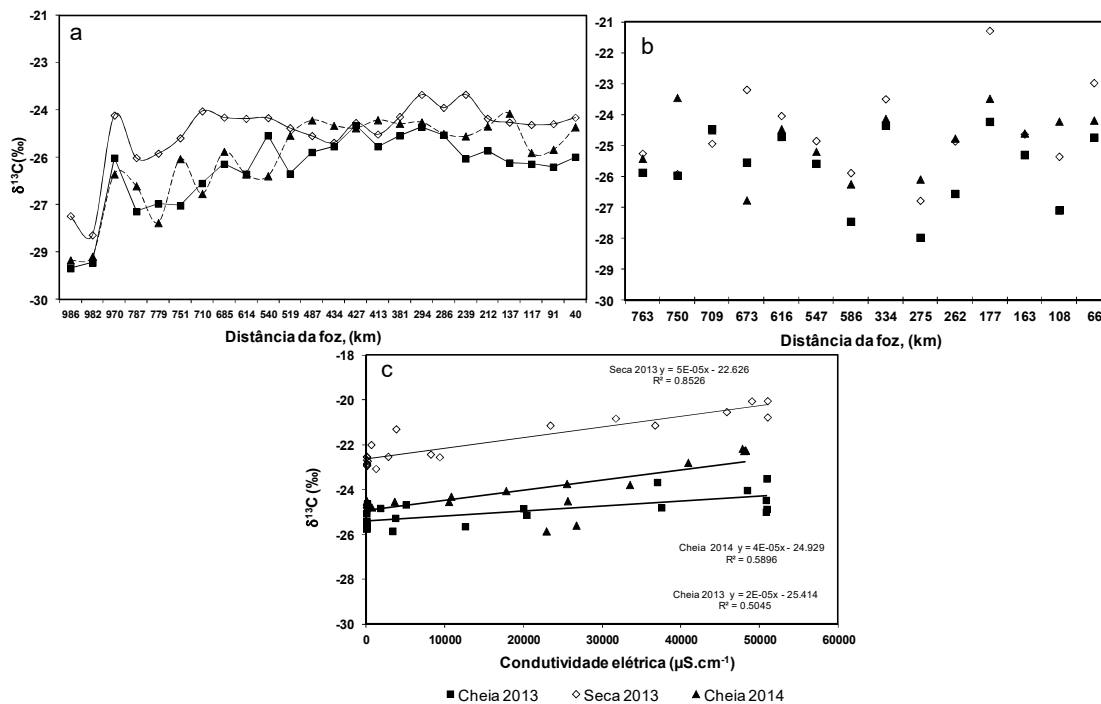


Fig.8: Distribuição dos valores da $\delta^{13}\text{C}$ do COD ao longo do RPS (a), nos tributários (b) em relação à distância da foz e no estuário em relação ao gradiente de condutividade elétrica (c).

Discussão

Variação espacial e sazonal do COP e COD.

As concentrações do COP e COD no RPS e nos tributários apresentaram uma alta variação espacial e temporal. A variabilidade das concentrações de COP e COD nos rios é impulsionada por numerosas interações entre processos biológicos, químicos, geológicos e hidrológicos (Moyer et al., 2013), sendo comum em rios de médio a grande porte (Ward et al., 2015). Em adição, as flutuações das concentrações do COP e COD podem ocorrer devido a processos como entrada do solo, dessorção do COP na coluna d' água e degradação microbiana (Lu et al., 2013). A variação sazonal das concentrações de COP e COD foi devido à intensidade das chuvas durante as estações sazonais. Na estação de cheia de 2013 onde foram observadas as maiores concentrações de COP e COD, a quantidade de chuva que era esperada para todo o mês de Janeiro, ocorreu em poucos dias. Assim, houve um intenso processo de lixiviação nos solos da bacia de drenagem, com a entrada do MO oriundo da lavagem do solo e também da lixiviação da serapilheira fresca. Estudos anteriores têm observado que grandes quantidades de COP e COD alóctone são carregados dos solos e da serapilheira para os corpos hídricos durante eventos de alta precipitação (Royer e David, 2005; Lu et al., 2013; Moyer et al., 2012). O mesmo padrão foi observado nos tributários na cheia de 2013 (Tab. 2 e Fig. 2b e 3b).

Em comparação com os principais grandes rios mundiais, a faixa de concentração de COP observada no RPS e tributários (7 a 1306 $\mu\text{mol.L}^{-1}$) é maior que a faixa observada na porção inferior do rio Amazonas (22 a 241 $\mu\text{mol.L}^{-1}$) (Ward et al., 2015). Por outro lado, as maiores concentrações de COD observadas na cheia de 2013 no RPS (600 a 894 $\mu\text{mol.L}^{-1}$ respectivamente) estão na mesma faixa que as do rio Congo no mesmo período sazonal (508 a 898 $\mu\text{mol.L}^{-1}$) (Spencer et al., 2012). No entanto, nas estações com baixo volume de chuva as concentrações de COD variaram entre 168 a 401 $\mu\text{mol.L}^{-1}$ no RPS na mesma faixa de variação que as concentrações observadas em um rio de pequeno porte de Porto Rico (rio Loco) 113 a 444 $\mu\text{mol.L}^{-1}$ (Moyer, et al, 2013). As concentrações de COP e COD dos tributários apresentaram a mesma tendência que as do RPS, com as maiores concentrações na cheia de 2013 e menores nas demais (Fig. 2b e 3b), com destaque para o rio

Pirapetinga que em todas as amostragens apresentou concentrações elevadas de COD e de COP (Tab. 2). Em relação à distribuição do Corg (COP + COD), a fração dissolvida foi a majoritária no transporte do CO, especialmente na estação de cheia de 2014 onde de 65 % a 95% do CO transportado pelo RPS estava na forma dissolvida, mesma faixa observada por Spencer et al., (2012) no rio Congo. Os tributários apresentaram a mesma tendência que o RPS (Tab. 1 e 2).

No estuário as concentrações de COP e COD da estação chuvosa de 2013 apresentaram um comportamento não conservativo, com um significativo declínio das concentrações com o aumento da condutividade elétrica (Fig. 3c e 4c) onde o COD variou de 519 $\mu\text{mol.L}^{-1}$ no início do estuário a 74 $\mu\text{mol.L}^{-1}$ no ponto mais externo (35 km da costa) e o COP variou de 192 a 6 $\mu\text{mol.L}^{-1}$ no mesmo gradiente. O declínio das concentrações do COP e COD indica a atuação de processos de sumidouro do Corg como, por exemplo, degradação microbiana, diluição, floculação e sedimentação (Abril et al., 2002; Cai et al., 2012). Por outro lado, nas estações de seca de 2013 e cheia de 2014 o COD apresentou um comportamento conservativo, variando de 194 a 88 $\mu\text{mol.L}^{-1}$ na seca e 216 a 94 $\mu\text{mol.L}^{-1}$ na cheia de 2014. Esses comportamentos foram influenciados diretamente pelas concentrações de COP e COD observadas no RPS. A faixa de concentração de COD do estuário é inferior que as observadas na baía de São Luís no norte do Golfo do México 273 a 783 $\mu\text{mol.L}^{-1}$ (Cai et al., 2012). Em contra partida, a faixa de COP observada no estuário do RPS (3 a 500 $\mu\text{mol.L}^{-1}$) foi mais ampla que na mesma baía (67 a 282 $\mu\text{mol.L}^{-1}$). Essas diferenças entre as regiões podem ser atribuído à geomorfologia e também devido à amostragem que no RPS chegou ao meio da plataforma continental, possuindo maior influência marinha.

Variação espacial e sazonal da composição elementar e isotópica

Os valores da (C/N)_a apresentaram uma ampla faixa de variação ao longo do RPS e nos tributários e estuário, tanto para o COP, quanto para o COD (Fig. 5 e 6). Em todas as amostras os valores da (C/N)_a do COP foram menores que os do COD (Tab. 1 e 2). Isso mostra que apesar do MO dissolvida e particulada terem origem predominantemente no solo, processos intrínsecos afetam em diferentes intensidades as formas de carbono orgânico. Os maiores valores da (C/N)_a do COD são devido ao seu maior estágio de degradação, causado por processos físicos

(transporte), químicos e biológicos. Essa tendência também foi observada em outros estudos (Hedges et al., 1994; Masiello and Druffel, 2001; Krusche et al., 2002). Essas diferenças podem ser explicadas pelo modelo cromatográfico de bacia de drenagem formulado por Hedges et al., (1986). Segundo estes autores, apesar da fonte da MO das frações particulada e dissolvida ser a mesma, elas sofrem processos diferentes ao longo do transporte dos solos para os rios. Assim, existiria uma partição da MO nos solos, onde o material adsorvido nas partículas estaria mais protegido da degradação e com isso mais enriquecido em nitrogênio, enquanto o material dissolvido estaria mais disponível a degradação sendo com isso, mais empobrecido em nitrogênio. Tais processos seriam os principais envolvidos na diferença entre os valores da (C/N)_a entre o COP e COD.

Os valores da (C/N)_a foram mais elevados nas épocas com baixo volume de chuva (seca de 2013 e cheia de 2014) variando entre 10 e 42 no COD e no COP os valores foram mais elevados na seca (Fig. 5 e 6). Em contra partida, na cheia de 2013 os valores da (C/N)_a foram inferiores variando de 14 a 27 no COD. No COP em ambas as cheias os valores foram inferiores que os da seca (Fig. 5 e 6). Os menores valores indicam a entrada de compostos ricos em nitrogênio provenientes do intenso processo de lavagem da camada orgânica superficial do solo. Esse mesmo padrão foi observado nos tributários. No estuário, os valores da (C/N)_a apresentaram uma ampla variabilidade não apresentando um padrão destacado com seus valores na mesma faixa que os observados na Big Sur Coast (8 a 25), região costeira da Califórnia (Walker e MacCarthy, 2012).

O uso da composição isotópica como traçador de fontes de MO é possível, pois existe uma marcada diferença entre as duas principais fontes existentes na bacia do RPS. As plantas do tipo C3 (Mata) em regiões tropicais possuem a $\delta^{13}\text{C}$ variando de -32 a -27‰, enquanto plantas do tipo C4 (gramíneas) possuem $\delta^{13}\text{C}$ variando de -16 a -12‰ (Krusche et al., 2002). Em adição, o seu uso na região estuarina permite a identificação de fontes terrestres e marinhas de MO (Cai et al., 2012; Canuel e Hardison, 2016) . Os valores da $\delta^{13}\text{C}$ apresentaram uma ampla variabilidade espacial e sazonal no RPS, tributários e estuário (Fig. 7 e 8 e Tab. 1, 2 e 3). No RPS foi observada uma tendência de enriquecimento da $\delta^{13}\text{C}$ ao longo do curso do rio no COP e no COD (Fig. 7 e 8). Isso é atribuído às mudanças da cobertura vegetal em toda a bacia. Nos dois pontos amostrados no rio Paraibuna, o

COD em todos os períodos sazonais apresentou valores de $\delta^{13}\text{C}$ entre -27,4 a -29,0‰. O COP com exceção da estação de seca no primeiro ponto amostrado neste rio (-23,8‰), os demais valores de $\delta^{13}\text{C}$ variaram de -25,0 a -26,9‰. Os valores de COP e COD neste rio indicam como principal fonte de MO a Mata Atlântica do Parque Nacional da Serra do Mar. Esses valores estão na mesma faixa que os observados por Ward et al., (2015) nos rios Óbidos e Tapajós, região de Floresta Amazônica. Em contra partida, o rio Paraitinga, apresentou a $\delta^{13}\text{C}$ mais pesada em relação ao Paraibuna (Tab.1). Apesar de rio Paraitinga nascer em uma região preservada (Parque Nacional da Serra da Bocaina), esse rio corta regiões onde ocorreu a substituição da mata por gramíneas, o que resultou no enriquecimento da $\delta^{13}\text{C}$ na MO. Após a confluência dos rios formadores do RPS (Paraibuna e Paraitinga), foi observado um enriquecimento de ~2‰ em todos os períodos sazonais ao longo do curso do rio. Esse enriquecimento mostra que a mudança da cobertura vegetal está alterando qualitativamente a composição química da MO transportada pelo RPS. Um estudo realizado no rio Piracicaba (São Paulo) que possui pressões antrópicas semelhantes ao RPS investigou a $\delta^{13}\text{C}$ das frações ultrafiltradas. Neste trabalho foi observado que a $\delta^{13}\text{C}$ das frações ultrafiltradas se tornaram mais enriquecidas nas áreas cobertas por pasto e cana-de-açúcar (Krusche et al., 2002).

Além da variação espacial, os valores de $\delta^{13}\text{C}$ apresentaram uma variação sazonal nos rios e na região estuarina, com valores enriquecidos na estação de seca e em ambas as cheias apresentando valores empobrecidos (Fig. 7 e 8). Esse comportamento da $\delta^{13}\text{C}$ indica que existe uma mudança na fonte da MO entre os períodos sazonais, sendo isso mais destacado no COD. Os valores enriquecidos da $\delta^{13}\text{C}$ na estação de seca mostram uma grande influência das plantas do tipo C4 na MO. É importante destacar que a produção primária é uma importante fonte de MO na estação de seca, devido a maior penetração da radiação solar na coluna d'água. Em adição, a $\delta^{13}\text{C}$ do COP e COD originado pelo fitoplâncton fluvial deveria estar na faixa de -28 a -31‰ (Martinelli et al 1999). No entanto, os valores de $\delta^{13}\text{C}$ do COP e COD nos rios foram mais pesados que a faixa atribuída a MO fitoplânctonica (Fig.8 e 9). Uma possível explicação para isso seria a utilização do CO_2 enriquecido no isótopo ^{13}C proveniente da degradação de detritos de plantas do tipo C4 pelo fitoplâncton. De acordo com Vuorio et al., (2006), a $\delta^{13}\text{C}$ do fitoplâncton é

diretamente dependente da $\delta^{13}\text{C}$ do carbono inorgânico dissolvido. Embora na estação seca o volume de chuva seja reduzido, alguns eventos esporádicos de chuva são observados. Durante esses eventos, quantidades significativas de detritos de plantas do tipo C4 que cobrem a maior parte da bacia podem ser carregadas para os corpos hídricos. Com isso, a decomposição destes detritos libera tanto, MO quanto CO_2 com a $\delta^{13}\text{C}$ enriquecida na coluna d' água e isso estaria promovendo o enriquecimento observado no COP e no COD. Esse fato é reforçado pela $\delta^{13}\text{C}$ observada no COP da represa de Furnas em Itatiaia que a $\delta^{13}\text{C}$ variou de -21.1 a -22.7‰. Neste ponto de amostragem em todos os períodos sazonais, a água apresentou coloração verde, assim como o material retido pelo filtro. Reforçando esses achados, um estudo realizado por Soares et al., (2008) na mesma região mostrou que no período de um ano de amostragem o material particulado em suspensão foi composto de fitoplâncton. Isso é explicado devido às características de uma represa em que ocorre uma mudança em relação ao fluxo de água, mudando de um ambiente lótico para lêntico, isso favorece a deposição do material particulado em suspensão. Assim, a radiação solar pode penetrar na coluna d' água promover o crescimento fitoplanctônico nestes sistemas.

Por outro lado, na cheia os valores empobrecidos da $\delta^{13}\text{C}$ indicam como principal fonte de MO para o RPS plantas do tipo C3. O maior volume de chuva observado nesta estação promove um intenso processo de lixiviação, que carrega grandes quantidades de materiais orgânicos proveniente dos solos (Dalzell et al., 2007). Dentre esses materiais estão os detritos de plantas, MOD contida nos poros dos solos e o carbono orgânico adsorvido nas partículas (Valiela et al., 2013). Apesar da bacia de drenagem do RPS apresentar uma grande área coberta por plantas C4 (74%), em algumas partes, essa substituição é recente e o solo ainda possui MO produzida pela vegetação original adsorvida em suas partículas. A $\delta^{13}\text{C}$ de solos com cana-de-açúcar e pastagem parece ser uma função do tempo de estabelecimento da cultura (Martinelli et al., 2002). A $\delta^{13}\text{C}$ na MO do solo depois de doze anos de cultivo de cana-de-açúcar mudou de -25‰ para -23‰ e depois de 50 anos para -20‰ (Vitorello et al., 1989). Assim, na coluna d' água a MO produzida pela vegetação original adsorvida nas partículas do solo, podem por meio do processo de dessorção migrar da fase particulada para a dissolvida (Ward et al., 2015; Siedel et al., 2015).

Na região estuarina, os valores da $\delta^{13}\text{C}$ apresentaram o mesmo padrão sazonal que o observado no RPS e tributários, com valores enriquecidos na seca e valores empobrecidos na cheia. A mudança de fonte de MO observada no RPS se refletiu na região estuarina. Devido à alta vazão do RPS na cheia de 2013 ($1875 \text{ m}^3 \cdot \text{s}^{-1}$), o COD de origem terrestre com a $\delta^{13}\text{C}$ mais leve foi observada em pontos com elevados valores de condutividade (Fig.8c). Isso mostra que durante elevada vazão o COD com a $\delta^{13}\text{C}$ terrestre chega ao ambiente marinho. Entretanto, na fração particulada nos pontos mais distantes da costa os valores da $\delta^{13}\text{C}$ se tornaram mais pesados, indicando maior influência de COP de origem marinha (Canuel e Hardison, 2016). Por outro lado, na estação seca os valores da $\delta^{13}\text{C}$ apresentaram valores mais pesados, indicando a produtividade autóctone como principal fonte de MO. Na cheia de 2013 os valores da $\delta^{13}\text{C}$ do COD variaram de -25,8 a -23,7‰ em relação ao gradiente de condutividade elétrica. Esses valores são mais enriquecidos que os observados por Seidel et al., (2015) na foz do rio Amazonas (-30,0 a -25,1‰), região dominada por floresta Amazônica e com elevado aporte de MOD terrestre no ambiente marinho. Já em relação ao COP, os valores da $\delta^{13}\text{C}$ variaram entre -26,7 a -19,3‰, com valores mais enriquecidos nos pontos de maior influência marinha. Na cheia de 2014, a variação da $\delta^{13}\text{C}$ do COP e COD foi similar a da cheia de 2013, (Fig.7c e 8c). A variação da $\delta^{13}\text{C}$ do COP e COD de ambas as estações de cheia são da mesma ordem de grandeza que as observadas no estuário de Tana (norte do Quênia) onde a $\delta^{13}\text{C}$ do COP variou de -24,2 a -17,1‰ e o COD de -28,0 a -20,0‰ (Bouillon et al., 2007). Já na estação de seca, a $\delta^{13}\text{C}$ apresentou valores mais enriquecidos, quando comparados com os de ambas às cheias, variando de -24,8 a -18,2‰ no COP e de -23 a -20‰ no COD (Fig.7c e 8c).

O enriquecimento da $\delta^{13}\text{C}$ ao longo do gradiente de condutividade elétrica indica a transição de fontes, com a fonte terrestre apresentando valores mais empobrecidos e na medida em que os valores de condutividade aumentam os valores da $\delta^{13}\text{C}$ se tornam mais enriquecidos devido a influência da MO marinha (Bouillon et al., 2011). Na seca, devido a baixa vazão ($478 \text{ m}^3 \cdot \text{s}^{-1}$) o sistema possui uma baixa capacidade de transporte, com isso o aporte de materiais terrestre no ambiente marinho é reduzido. Em adição, durante a estação seca, ocorre maior entrada de água marinha na porção interna do estuário. Essa situação de menor descarga fluvial favorece a uma elevada produção autóctone, sendo isso mostrado

pelos valores da $\delta^{13}\text{C}$ que indicam como fonte de MOD o fitoplâncton estuarino (Lu et al., 2013). É importante destacar que o RPS é a principal fonte de MO para a região estuarina, e as variações qualitativas e quantitativas na MO neste ambiente estão diretamente ligadas as alterações do uso da terra em sua bacia de drenagem.

A substituição da cobertura vegetal transformou a paisagem da bacia do RPS em um mosaico em que a vegetação predominante é a C4, enquanto a C3 está distribuída em pequenos fragmentos desconectados uns dos outros (Dittmar et al., 2012). Uma forte relação entre a $\delta^{13}\text{C}$ do COD e a porcentagem de plantas C4 que cobre a área drenada por cada ponto de amostragem foi observada no RPS ($r=0,7002$, $p<0,01$, $n=72$, Fig.9, a). Por outro lado, na fração particulada apesar de não ser estatisticamente significativo, foi observado uma tendência de enriquecimento do ^{13}C com o aumento da cobertura por C4 (Fig.9, b). Isso mostra que a substituição da mata por gramíneas promove um enriquecimento no ^{13}C fração dissolvida. O efeito da mudança da cobertura vegetal na $\delta^{13}\text{C}$ foi mais acentuado no COD que corresponde à fração do ciclo rápido do carbono. Esse mesmo padrão foi observado por Bernardes et al., (2004) em estudo na bacia do rio Ji-Paraná, Rondônia. Nesse contexto, foi utilizado o modelo de duas fontes (Martinelli et al., 2002) para identificar a contribuição de MO derivada de plantas do tipo C4 nas frações particulada e dissolvida das amostras do RPS e tributários. No estuário, essa abordagem não foi feita, pois existe uma sobreposição de valores da $\delta^{13}\text{C}$ entre as fontes existentes, tornando esse modelo não adequado para esse ambiente. Reforçando o que foi discutido acima, o modelo mostrou um aumento da porcentagem de plantas do tipo C4 na MO na estação de seca, sendo isso mais destacado no COD (Fig.10 e 11). O modelo mostrou também que a porcentagem de plantas C4 aumenta ao longo do curso do RPS. Os dois pontos localizados no Parque Nacional da Serra do Mar apresentaram as menores porcentagens de plantas C4 no COD, com 6% nas estações de cheia e 16% na seca, enquanto nos pontos do RPS fora do Parque essa porcentagem chegou a até 40% e nos tributários a 55%. Em contra partida, no COP a porcentagem de C4 foi maior que no COD, sendo isso atribuído às áreas de C4 ao entorno do Parque. As variações da MO derivada de plantas do tipo C4 na MO entre os períodos sazonais indica uma mudança da fonte de MO do RPS devido a hidrologia e as mudanças do uso da terra. Como discutido acima, com o passar dos anos a contribuição de plantas C4

tende a aumentar, e a mudança qualitativa ocorrida na MO poderá causar alterações na ciclagem do carbono e na comunidade detrítica que utiliza o Corg como fonte de energia.

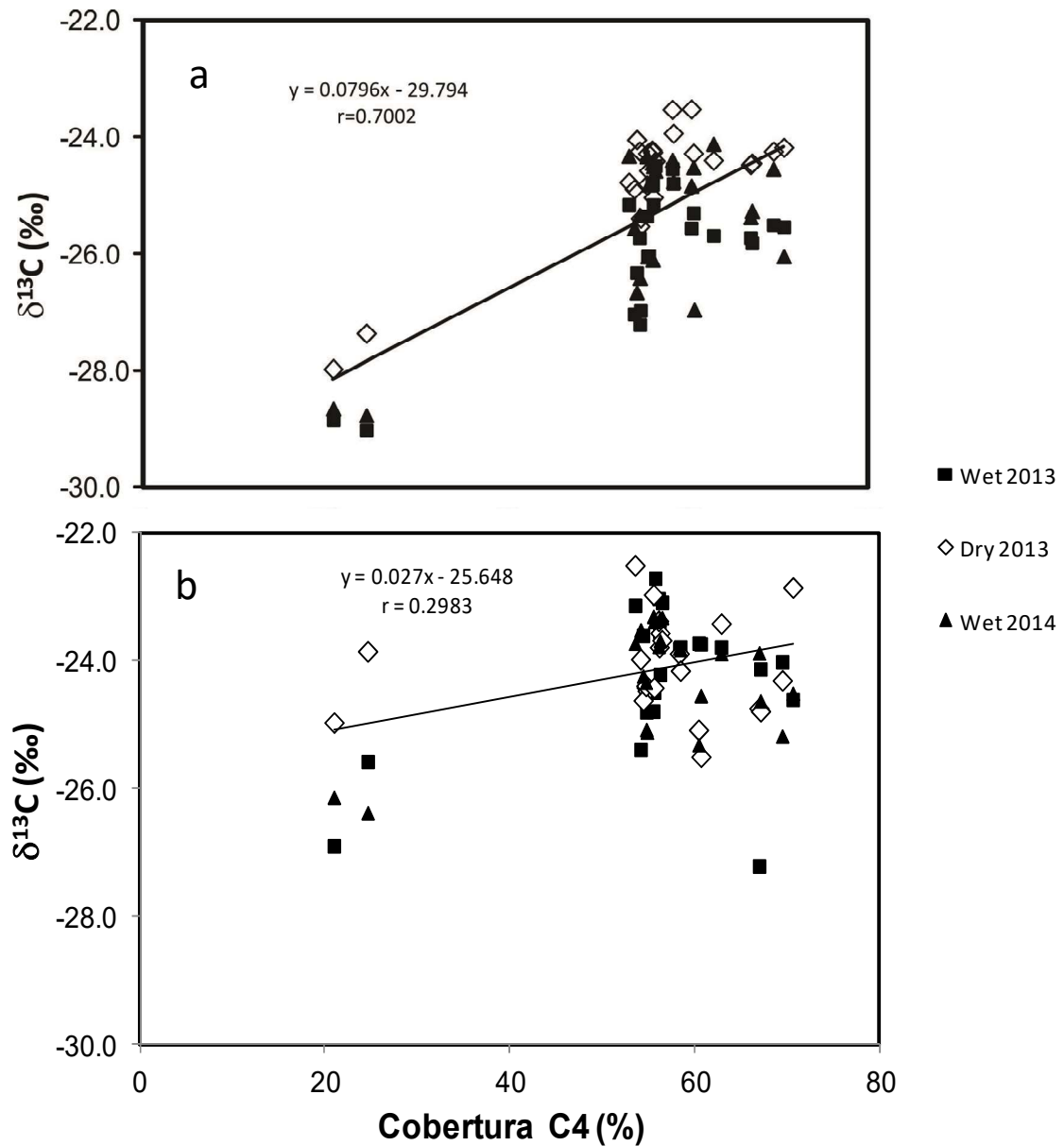


Fig.9: Relação entre os valores de $\delta^{13}\text{C}$ e a porcentagem da cobertura de plantas C4 em cada ponto do RPS em (A) na fração dissolvida e em (B) na fração particulada. Dados cobertura de plantas C4 fonte: <http://mapbiomas.org/#>

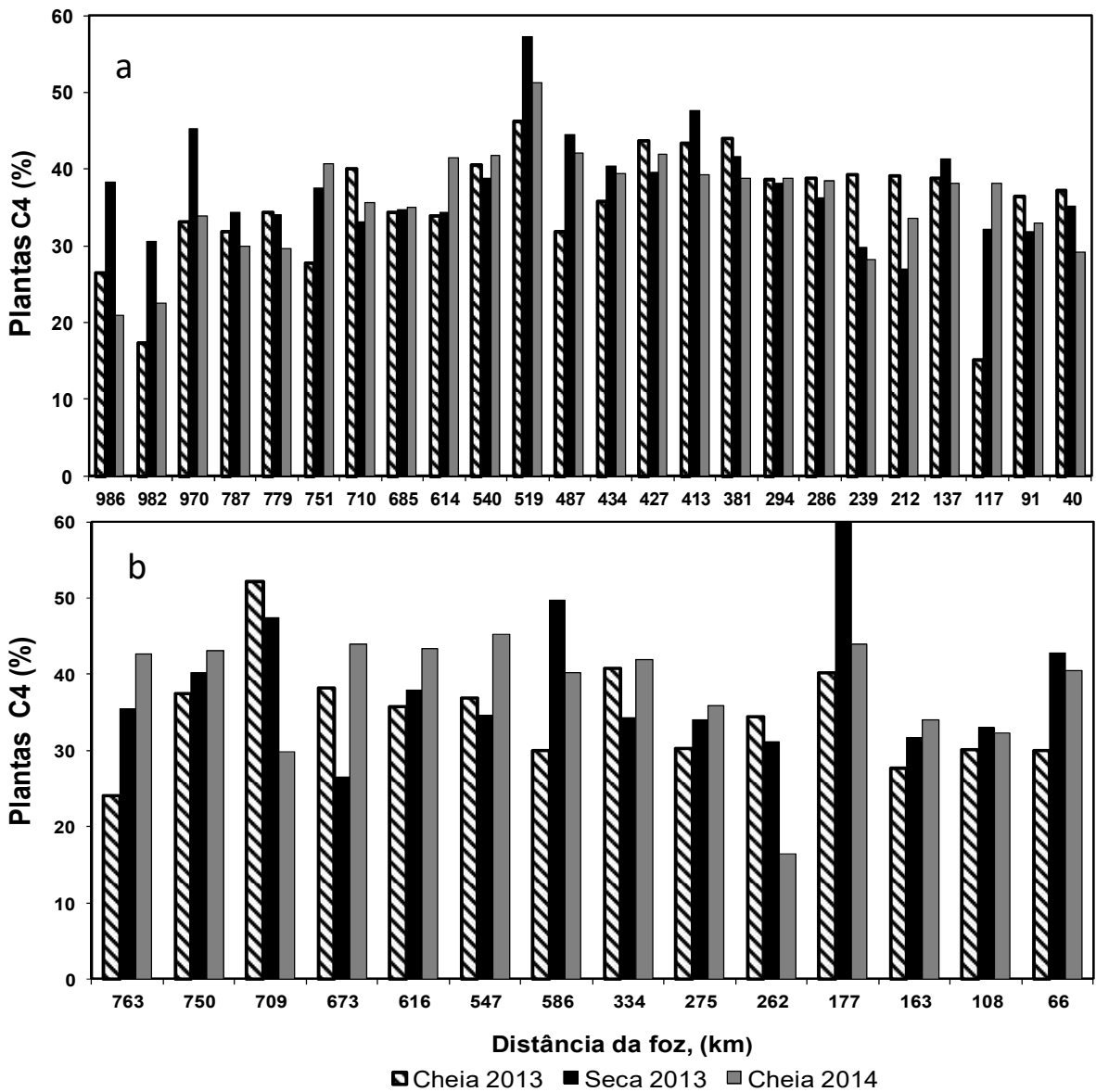


Fig.10: Distribuição da porcentagem de plantas C4 no COP ao longo do RPS a) e nos tributários nos diferentes períodos sazonais amostrados.

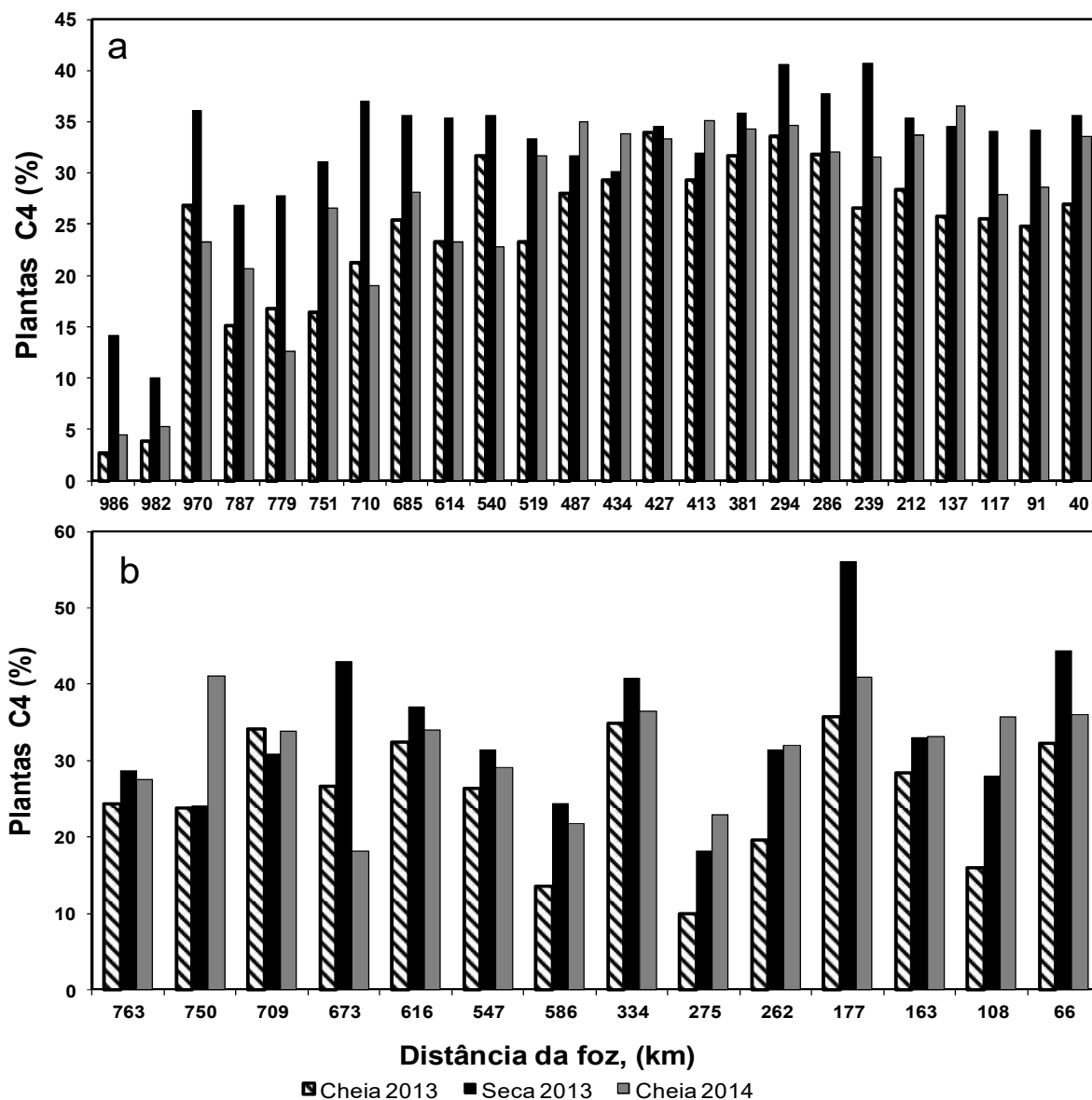


Fig.11: Distribuição da porcentagem de plantas C4 no COD ao longo do RPS a) e nos tributários nos diferentes períodos sazonais amostrados.

Potenciais fontes de material orgânico no RPS, tributários e região estuarina

Os valores da $\delta^{13}\text{C}$ e da (C/N)_a encontrados no presente estudo foram comparados com as possíveis fontes de MO existentes na bacia do RPS (Fig. 12). Os valores de plantas do tipo C3, solo coberto por plantas C3 e solos coberto por plantas C4 existentes na bacia do RPS foram obtidos de Ribas, (2012). Os valores de fitoplâncton como descrito acima foram obtidos do COP coletado na represa de Furnas localizada em Itatiaia. Os valores da $\delta^{13}\text{C}$ marinho foram obtidos de Barros et al., (2010) e os valores da (C/N)_a foram obtidos de Cai et al., (2012).

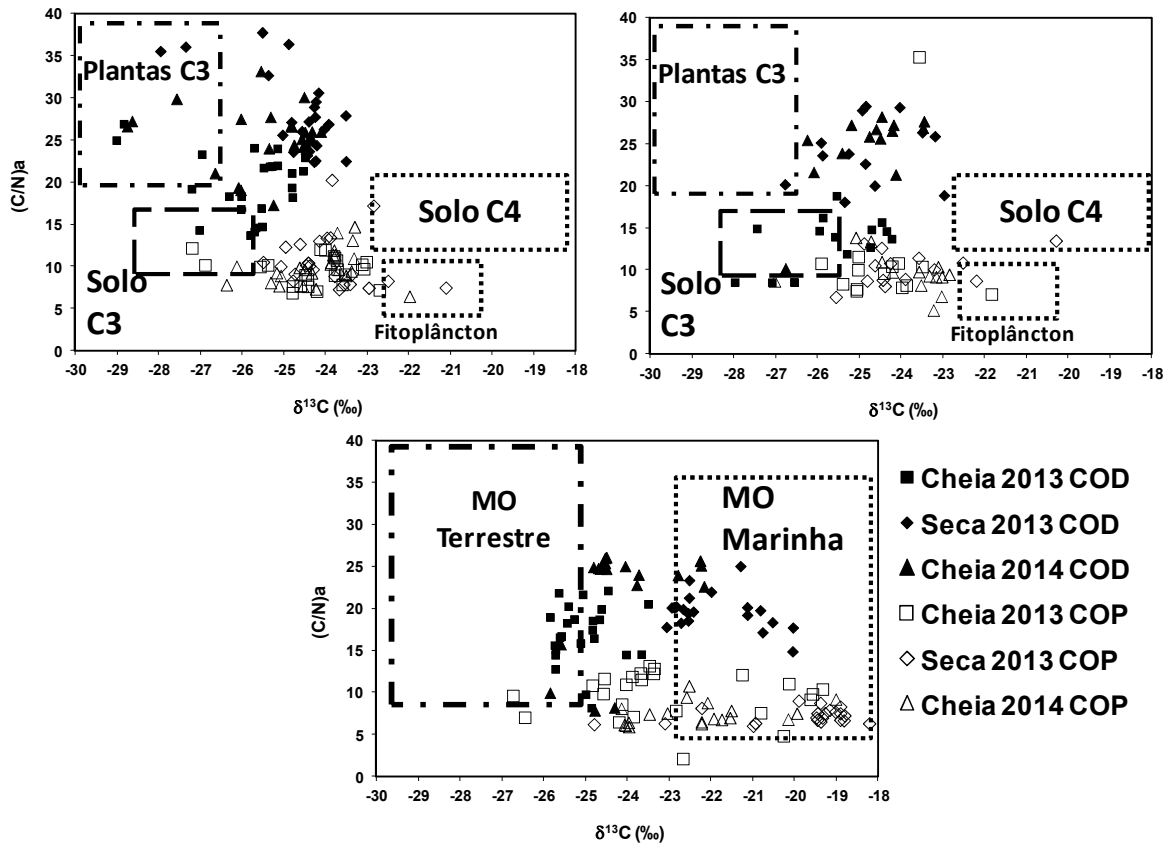


Fig.12: Valores da (C/N)_a e da δ¹³C das frações COP e COD nas amostras e potenciais fontes de MO no RPS em a), nos tributários em b), e na região estuarina em c).

Os valores da (C/N)_a e da δ¹³C nas amostras indicam que a MO transportada pelo RPS, tributários e a exportada pelo estuário é formada por uma mistura de múltiplas fontes. De modo geral, no COP do RPS e tributários parte das amostras apresentaram valores da (C/N)_a e δ¹³C entre os do solo de plantas C3 e do fitoplâncton enquanto no COD na maioria das amostras apresentaram valores próximos aos da vegetação e solo do tipo C3 (Fig. 12a e b). Apesar da bacia do RPS possuir uma ampla cobertura de plantas do tipo C4, em algumas regiões, existem fragmentos de Mata situados próximo ao canal do RPS, podendo a MO produzida nestes locais ser transportada para o rio em eventos de chuva. Em adição, o aporte dos tributários que drenam áreas cobertas por Mata Atlântica também possui uma grande influência nos valores da δ¹³C observados no RPS.

Por outro lado, uma grande parte das amostras da estação de seca, situaram na faixa da $\delta^{13}\text{C}$ entre -25 a -23‰. Esses valores indicam uma mistura entre as fontes C3 e C4. No modelo de duas fontes, a contribuição de C4 nessa faixa de valores da $\delta^{13}\text{C}$ seria de 27 a 40%. A $\delta^{13}\text{C}$ do MO fluvial reflete tipicamente a influência da cobertura vegetal de sua bacia de drenagem (Moyer et al., 2013), deixando claro o efeito da mudança da cobertura vegetal na bacia do RPS na MOD transportada pelo rio e destacando as plantas do tipo C4 como potenciais fontes de MO.

Na região estuarina, os valores da (C/N)_a e $\delta^{13}\text{C}$ foram agrupados como terrestre e como marinho que corresponde a variação da (C/N)_a e da $\delta^{13}\text{C}$ no ambiente estuarino e marinho, respectivamente. As amostras de ambas as estações chuvosas apresentaram valores próximos aos valores terrestres (Fig. 12c). Isso é atribuído ao aporte de materiais orgânicos de origem terrestre no ambiente marinho nos períodos de elevada vazão (Dalzell et al., 2007; Cai et al., 2012). Em contrapartida, as amostras da estação de seca apresentaram valores próximos aos das fontes de MO de origem marinha, com destaque para o COP (Fig. 12c). Isso mostra que durante a baixa vazão, devido ao aporte da água marinha no ambiente estuarino ocorre a importação de MO de origem marinha. Esse comportamento mostra que o estuário do RPS atua tanto como exportador, quanto importador, sendo isso governado pela descarga fluvial. Em adição, no estuário do RPS existe o segundo maior manguezal do estado do Rio de Janeiro (Bernini e Rezende, 2004), um estudo conduzido por Brito, (2014) em um canal de maré, identificou o manguezal do RPS como uma importante fonte de MO para o ambiente estuarino. Embora a vazão exerça um importante papel na dinâmica de importação/exportação de materiais no gradiente continente/oceano, as variações nos valores da (C/N)_a e $\delta^{13}\text{C}$ ao longo do gradiente de condutividade elétrica indicam que a MO estuarina é composta de múltiplas fontes.

Conclusão

Os resultados mostraram uma forte evidência que as pressões antropogênicas ocorrida na bacia de drenagem do RPS se refletem na MO. A mudança da cobertura vegetal de floresta para pasto e cana de açúcar tem causado

uma mudança quantitativa e qualitativa na MO. Essa mudança se mostra tanto sazonalmente, quanto espacialmente. Espacialmente os valores de $\delta^{13}\text{C}$ se tornaram enriquecidos no ^{13}C nas áreas coberta por pastagens e cana de açúcar. Sazonalmente os valores de $\delta^{13}\text{C}$ foram enriquecidos na estação de seca. Nessa mesma estação o modelo de duas fontes mostrou que em alguns pontos a porcentagem de plantas do tipo C4 na MO chegou a 55%. Isso reflete o efeito da mudança da cobertura vegetal na MO presente no RPS e também mostra que a hidrologia possui um importante papel no ciclo do carbono orgânico entre o continente e o oceano. Nas estações de alta vazão, os valores de $\delta^{13}\text{C}$ indicam a existência de COD de origem terrestre nos pontos mais afastados da costa.

Apesar da extensa área coberta por C4 na bacia do RPS, a MOD com a $\delta^{13}\text{C}$ mais leve na cheia sugere que ainda existe estocado no solo MO produzida pela vegetação original. No entanto, de médio a longo prazo essa MO derivada da mata estocada no solo será substituída pela a da vegetação atual, mudando completamente as suas características químicas. Essas mudanças nas características químicas da MO pode altera o ciclo do carbono orgânico entre o continente e o oceano. Além de também causar uma alteração na comunidade microbiana que utiliza a MO como fonte de energia, promovendo com isso uma alteração em toda a teia trófica, devido à diminuição da biodisponibilidade da Morg com o aumento da influência de plantas C4 na Morg.

Referências

- Abril, G., Nogueira, M., Cabeçadas, G., Lemaire, E., Brogueira, M.J. 2002. Behaviour of organic carbon in nine contrasting European estuaries. *Estuarine, Coastal and Shelf Science*, 54, 241-262.
- Agência Nacional das Águas, (2015): (<http://hidroweb.ana.gov.br/>)
- Alin, S.R., Aalto, R., Goñi, M.A., Richey, J.E., Dietrich, W.E. 2008. Biogeochemical characterization of carbon sources in the Strickland and Fly rivers, Papua New Guinea. *Journal of Geophysical Research*, 113, F01S05. doi:10.1029/2006JF000625
- Almeida, M.G; Rezende, C.E; Souza, C.M.M. 2007. Variação temporal, transporte e partição de Hg e carbono orgânico nas frações particulada e dissolvida da

- coluna d'água da bacia inferior do rio Paraíba, RJ, Brasil. *Geoquímica Brasiliensis*, 21, 111-129.
- Barros, G.V., Martinelli, L.A., Novais, T.M.O., Ometto, J.P.H.B., Zuppi, G.M. 2010. Stable isotopes of bulk organic matter to trace carbon and nitrogen dynamics in an estuarine ecosystem in Babitonga Bay (Santa Catarina, Brazil). *Science of the Total Environment*, 408, 2226-2232.
- Benner, R. 2004. What happens to terrestrial organic matter in the ocean? *Marine Chemistry*, 92, 307–310.
- Bernini, E., Rezende, C.E. 2004. Estrutura da vegetação em florestas de mangue do estuário do rio Paraíba do Sul, Estado do Rio de Janeiro, Brasil. *Acta Botanica Brasílica*, 18, 491-502.
- Bouillon, S., Dehairs, F., Schiettecate, L.S., Borges, A.V. 2007. Biogeochemistry of the Tana estuary and delta (northern Kenya). *Limnology and Oceanography*, 52, 46 – 59.
- Bouillon, S., Connolly, R.M., Lee, S.Y. 2008. Organic matter exchange and cycling in mangrove ecosystems: Recent insights from stable isotope studies. *Journal of Sea Research*, 59, 44-58.
- Bouillon, S., Connolly, R.M., Gillikin, D.P. 2011. Use of stable isotopes to understand food webs and ecosystem functioning in estuaries. In: Wolanski, E. and McLusky, D.S (eds.) *Treatise on Estuarine and Coastal Science*, 7, 143 – 173.
- Brito, F.P. Composição e fluxo da matéria orgânica em um canal de maré no ecossistema de manguezal do estuário do rio Paraíba do Sul, Costa Norte do Rio de Janeiro. Dissertação apresentada ao Programa de Pós-Graduação em Ecologia e Recursos Naturais da Universidade Estadual do Norte Fluminense – UENF.p.89.
- Cai, Y., Guo, L., Wang, X., Mojzsis, A., Redalje, D.G. 2012. The source and distribution of the dissolved and particulate organic matter in the Bay of St. Louis, northern Gulf of Mexico. *Estuarine, Coastal and Shelf Science*, 96, 96-14.
- Canuel, E.A. e Hardison, A.K. 2016. Sources, ages, and alterations of organic matter in estuaries. *Annual Review of Marine Science*, 8, 409 – 434.

- Cole, J.J. e Caraco, N.F. 2001. Carbon in catchments: connecting terrestrial carbon losses with aquatic metabolism. *Marine and Freshwater Research*, 52, 101–110.
- Countway, R.E., Canuel, E.A., Dickhut, R.M. 2007. Sources of particulate organic matter in surface waters of the York River, VA estuary. *Organic Geochemistry*, 38, 365-379.
- Dalzell, B.J., Filley, T.R., Harbor, J.H. 2007. The role of hydrology in annual organic carbon loads and terrestrial organic matter export from a midwestern agricultural watershed. *Geochimica et Cosmochimica Acta*, 71, 1448-1462.
- Dittmar, T., Koch, B., Hertkorn, N., Kattner, G. 2008. A simple and efficient method for the solid-phase extraction of dissolved organic matter (SPE-DOM) from seawater. *Limnology and Oceanography Methods*. 6, 230-235. doi: 10.4319/lom.2008.6.230
- Dittmar, T., Rezende, C.E., Manecki, M., Niggemann, J., Ovalle, A.R.C., Stubbis, A., Bernades, M.C. 2012. Continuous flux of dissolved black carbon from a vanished tropical forest biome. *Nature Geoscience*, DOI:10.1038/NNGEO1541.
- Fry, B. 2006. *Stable Isotope Ecology*. Springer, New York, p.390.
- Hatten, J.A., Goñi, M.A., Wheatcroft, R.A. 2010. Chemical characteristics of particulate organic matter from a small, mountainous river system in the Oregon Coast Range, USA. *Biogeochemistry*, doi:10.1007/s10533-010-9529-z
- Hedges, J.I., Clark, W.A., Quay, P.D., Richey, J.E., Devol, A.H., Santos, U.M. 1986. Composition and fluxes of particulate organic material in the Amazon River. *Limnology and Oceanography*, 31, 717-738.
- Hedges, J.I. 1992. Global biogeochemical cycles: progress and problems. *Marine Chemistry*, 39, 67–93.
- Houghton, R.A., Skole, D.L., Nobre, C.A., Hackler, J.L., Lawrence, K.T., Chomentowski, W.H. 2000. Annual fluxes of carbon from deforestation and regrowth in the Brazilian Amazon. *Nature*, 403, 301–304.
- Kruche, A.V., Martinelli, L.A., Victoria, R.L., Bernades, M., Camargo, P.B., Ballester, M.V., Trumbore, S.E. 2002. Compositional of particulate and dissolved organic matter in a disturbed watershed of southeast Brazil (Piracicaba River basin). *Water Research*, 36, 2743-2752.

- Lu, Y.H., Bauer, J.E., Canuel, E.A., Chambers, R.M., Yamashita, Y., Jaffé, R., Barrett, A. 2014. Effects of land use on sources and ages of inorganic and organic carbon in temperate headwater streams. *Biogeochemistry*, doi:10.1007/s10533-014-9965-2
- Lyons, W.B., Nezat, A.C., Carey, A., Hicks, D.M. 2002 Organic carbon fluxes to the ocean from high-standing islands. *The Journal of Geology*, 30, 443–446.
- Martinelli, L.A., Krusche, A.V., Victoria, R.L., Camargo, P.B., Bernardes, M., Ferraz, E.S., Moraes, J., Ballester, M.V. 1999. Effects of sewage on the chemical composition of Piracicaba River, Brazil. *Water Air Soil Pollution*, 110, 67–79.
- Martinelli, L.A., Camargo, P.B., Lara, L.B.L.S., Victoria, R.L., Artoso, P. 2002. Stable carbon and nitrogen isotopic composition of bulk aerosol particles in a C4 plant landscape of southeast Brazil. *Atmospheric Environmental*, 36, 2427-2432.
- McCallister, S.L., Bauer, J.E., Cherrier, J.E., Ducklow, H.W. 2004. Assessing sources and ages of organic matter supporting river and estuarine bacterial production: a multi-isotope ($\Delta^{14}\text{C}$, $\delta^{13}\text{C}$ and $\delta^{15}\text{N}$) approach. *Limnology and Oceanography*, 49, 1687-1702.
- Moyer, R.P., Bauer, J.E., Grotoli, A.G. 2013. Carbon isotope biogeochemistry of tropical small mountainous river, estuarine and coastal systems of Puerto Rico. *Biogeochemistry*, 112, 589-612. Doi: 10.1007/s10533-012-9751-y
- Ovalle, A.R.C., Silva, C.F., Rezende, C.E., Gatts, C.E.N., Suzuki, M.S., Figueiredo, R.O. 2013. Long-term trends in hydrochemistry in the Paraíba do Sul River, southeastern Brazil. *Journal of Hydrology*, 481, 191-203. doi.org/10.1016/j.jhydrol.2012.12.036
- Prasad, M.B.K., Ramanathan, A.L. 2009. Organic matter characterization in a tropical estuarine-mangrove ecosystem of India: Preliminary assessment by stable isotopes and lignin phenols. *Estuarine, Coastal and Shelf Science*, 84, 617-624.
- Ribas, L.M. 2012. Caracterização de fontes de matéria orgânica do estuário do rio Paraíba do Sul, RJ, Brasil. Tese apresentada ao Programa de Pós-Graduação em Ecologia e Recursos Naturais da Universidade Estadual do Norte Fluminense – UENF.p.114.
- Ribeiro, M.C., Metzger, J.P., Martensen, A.C., Ponzoni, F.J., Hirota, M.M. 2009. The Brazilian Atlantic Forest: how much is left, and how the remaining forest

- distributed? Implications for conservation. *Biology Conservation*. 142, 1141–1153. doi.org/10.1016/j.biocon.2009.02.021
- Rossi, C.Q., Pereira, M.G., Loss, A., Gazolla, P.R., Perin, A., Anjos, L.H.C. 2013. Changes in soil C and N distribution assessed by natural $\delta^{13}\text{C}$ and $\delta^{15}\text{N}$ abundance in a chronosequence of sugarcane crops managed with pré-harvest burning in a Cerrado area of Goiás, Brazil. *Agriculture, Ecosystems and Environmental*, 170, 36-44.
- Royer, T.V., David, M.B. 2005. Export of dissolved organic carbon from agricultural streams in Illinois, USA. *Aquatic Sciences*, 67, 465–471.
- Rumolo, P., Barra, M., Gherardi, S., Marsella, E., Sprovieri, M. 2011. Stable isotopes and C/N ratios in marine sediments as a tool for discriminating anthropogenic impact. *Journal of Environmental Monitoring*, 13, 3399-3408.
- Siedel, M., Yager, P.L., Ward, N.D., Carpenter, E.J., Gomes, H.R., Kruske, A.L., Richey, J.E., Dittmar, T., Medeiros, P.M. 2015. Molecular-level changes of dissolved organic matter along the Amazon River-to-ocean continuum. *Marine Chemistry*. doi.org/10.1016/j.marchem.2015.06.019.
- Smith, S.V., Renwick, W.H., Buddemeier, R.W., Crossland, C.J. 2001. Budgets of soil erosion and deposition for sediments and sedimentary organic carbon across the conterminous United States. *Global Biogeochemical Cycles*, 15,697–707.
- Soares, M.C.S., Marinho, M.M., Huszar, V.L.M., Branco, C.W., Azevedo, S.M.F.O. 2008. The effects of water retentation time and watershed features on the limnology of two tropical reservoirs in Brazil. *Lakes & Reservoirs: Research and Management*, 13, 257-269
- Spencer, R.G.M., Hernes, P.J., Aufdenkampe, A.K., Baker, A., Gulliver, P., Stubbins, A., Aiken, G.R., Dyda, R.Y., Butle, K.D., Mwamba, V.L., Mangangu, A.M., Wabakanghanzi, J.N., Six. 2012. An initial investigation into the organic matter biogeochemistry of the Congo River. *Geochimica et Cosmochimica Acta* 84, 614-627.
- Valiela, I., Bartholomew, M., Gilbin, A., Tucker, C., Martinetto, M., Otter, L., Stone, T. 2014. Watershed deforestation and down-estuary transformations alter sources, transport, and export of suspended particles in Panamanian mangroves estuaries. *Ecosustems*, 17, p.96-111. DOI: 10.1007/s10021-013-9709-5.

- Vitorello, V.A., Cerri, C.C., Andreux, F., Feller, C., Victoria, R.L., 1989. Organic matter and natural carbon-13 distribution in forested and cultivated oxisols. *Soil Science Society of America Journal*, 53, 773–778.
- Vuorio, K., Meili, M., Sarvala, J. 2006. Taxon-specific variation in the stable isotopic signatures ($\delta^{13}\text{C}$ and $\delta^{15}\text{N}$) of lake phytoplankton. *Freshwater Biology*, 51, 807-822.
- Walke, B.D. e McCarthy, M.D. 2012. Elemental and isotopic characterization of dissolved and particulate organic matter in a unique California upwelling system: Importance of size and composition in the export of labile material. *Limnology and Oceanography*, 57, 1757-1774. doi:10.4319/lo.2012.57.6.1757
- Ward, N.D., Krusche, A.V., Sawakuchi, H.O., Brito, D.C., Cunha, A.C., Moura, J.M.S., Silva, R., Yager, P.L., Keil, R.G., Richey, J.E. 2015. The compositional evolution of dissolved and particulate organic matter along the lower Amazon River – Óbitos to the ocean. *Marine Chemistry*, 117, 244-256. doi.org/10.1016/j.marchem.2015.06.013.

1 **DISSOLVED BLACK CARBON IN THE HEADWATERS-**
2 **TO-OCEAN CONTINUUM OF PARAÍBA DO SUL RIVER,**
3 **BRAZIL**

4 **Jomar S.J. Marques^{1,2*}, Thorsten Dittmar², Jutta Niggemann², Marcelo G.**
5 **Almeida¹, Gonzalo V. Gomez-Saez², Carlos E. Rezende¹**

6 ¹Research Group for Biogeochemistry of Aquatic Ecosystems, Laboratório de Ciências
7 Ambientais, Centro de Biociências e Biotecnologia Universidade Estadual do Norte
8 Fluminense, Campos dos Goytacazes, Rio de Janeiro, Brazil.

9 ²Research Group for Marine Geochemistry (ICBM – MPI Bridging Group), Institute for
10 Chemistry and Biology of the Marine Environment (ICBM), Carl von Ossietzky
11 University, Oldenburg, Germany.

12 ***Correspondence:**

13 Corresponding Author

14 jomar.uenf@gmail.com

15 **Keywords: headwaters-to-ocean, black carbon, dissolved black carbon, dissolved**
16 **organic carbon, Paraíba do Sul River.**

17
18 **ABSTRACT**

19 Rivers annually carry 25-28 Tg carbon in the form of pyrogenic dissolved organic
20 matter (dissolved black carbon, DBC) into the ocean, which is equivalent to about 10%
21 of the entire riverine land-ocean flux of dissolved organic carbon (DOC). The objective
22 of this study was to identify the main processes behind the release and turnover of DBC
23 on a riverine catchment scale. As a model system, we chose the headwater-to-ocean
24 continuum of Paraíba do Sul River (Brazil), the only river system with long-term DBC
25 flux data available. The catchment was originally covered by Atlantic rain forest
26 (mainly C3 plants) which was almost completely destroyed over the past centuries by
27 slash-and-burn. As a result, large amounts of wood-derived charcoal reside in the soils.
28 Today, fire-managed pasture and sugar cane (both dominated by C4 plants) cover most
29 of the catchment area. Water samples were collected along the river, at the main
30 tributaries, and also along the salinity gradient in the estuary and up to 35 km offshore
31 during three different seasons. DBC was determined on a molecular level as
32 benzenepolycarboxylic acids (BPCAs). Stable carbon isotopes ($\delta^{13}\text{C}$) were determined
33 in solid phase extractable DOC (SPE-DOC) to distinguish C4 and C3 sources. Our
34 results clearly show a relationship between hydrology and DBC concentrations in the
35 river, with highest DBC concentrations and fluxes in the wet season (flux of 770 moles
36 sec^{-1} in 2013 and 59 moles sec^{-1} in 2014) and lowest in the dry season (flux of 27 moles
37 sec^{-1}). This relationship indicates that DBC is mainly mobilized from the upper soil
38 horizons during heavy rainfalls. The relationship between DBC concentrations and
39 $\delta^{13}\text{C}$ -SPE-DOC indicated that most of DBC in the river system originated from C3
40 plants, i.e. from the historic burning event of the Atlantic rain forest. A conservative
41 mixing model could largely reproduce the observed DBC fluxes within the catchment
42 and the land to ocean continuum. Comparably slight deviations from conservative
43 mixing were accompanied by changes in the molecular composition of DBC (i.e. the
44 ratio of benzenepenta- to benzenehexacarboxylic acid) that are indicative for
45 photodegradation of DBC.

46

47

48 1 - INTRODUCTION

49 Forest fires produce airborne combustion products and charred residues on and in the
50 ground (Preston and Schmidt, 2006). Charred materials include a wide range of
51 compounds, from dehydrated sugars formed at low charring temperature to highly-
52 condensed graphite-like material produced at high temperatures, and secondary
53 condensation products like soot (Santín et al., 2016). Also fuel characteristics are
54 important, charcoal from woody and soft plant tissues often have different levels of
55 condensation and oxygen content (Forbes et al., 2006; Schneider et al., 2010; Ding et
56 al., 2014). The entire continuum of charred material is considered pyrogenic organic
57 matter, of which the most condensed fraction is commonly referred to as black carbon
58 (BC) (Forbes et al., 2006).

59
60 Black carbon, which is largely derived from high-temperature woody chars, has
61 received large attention in the literature, because it is more resistant to further biological
62 and chemical degradation than the biomolecular precursors (Forbes et al., 2006). As a
63 consequence, BC is ubiquitous in soils, sediments and aquatic environments (Forbes et
64 al., 2006; Jaffé et al., 2013). Important removal mechanisms of BC from soils are
65 solubilization and subsequent transport in the dissolved phase (Dittmar et al., 2012a)
66 and lateral transport of BC particles in the landscape (Major et al., 2010). During
67 degradation in soils, oxygen atoms can be introduced into condensed aromatic
68 structures of charcoal (Abiven et al., 2011). The resulting carboxylated molecular
69 subunits partially dissolve in water and migrate through the soil as dissolved BC (DBC)
70 (Cheng & Lehman, 2009). There is a significant time lag between wildfire induced BC
71 production, incorporation into soils, and the actual release of DBC to aquatic systems
72 (Dittmar et al., 2012a; Ding et al., 2014). Microbial reworking of charcoal may be
73 required to enhance the translocation of soil BC to DBC (Ding et al., 2014). This
74 translocation process can explain the presence of DBC in dissolved organic matter
75 (DOM) in rivers, estuaries and the ocean (Kim et al., 2004; Mannino & Harvey, 2004;
76 Ziolkowski and Druffel, 2010). Global export of DBC from land to ocean amounts to
77 approximately 27 Tg carbon year⁻¹, which is equivalent to 10% of the entire riverine
78 dissolved organic carbon (DOC) flux (Jaffé et al., 2013). DBC is distributed throughout
79 the ocean and may impact biogeochemical processes on a global scale (Ziolkowski and
80 Druffel, 2010). Even in the most remote basins of the deep ocean, ~2% of DOM
81 contains a heat-induced molecular signature (Dittmar & Koch, 2006; Dittmar & Paeng,
82 2009).

83
84 Very little is known on how DBC behaves in aquatic environments. While there is
85 evidence that DBC is very stable in the deep ocean having conservative, salt-like
86 properties (Dittmar and Paeng, 2009; Ziolkowski and Druffel, 2010), it is very
87 susceptible to UV radiation in sunlit waters (Stubbins et al., 2012). Once exposed to
88 sunlight, most of DBC is lost from seawater (Stubbins et al., 2012) and river water
89 (Riedel et al., 2016). It is unclear what proportion of DBC that is introduced from soils
90 and groundwater into the rivers eventually survives riverine transport from the
91 headwaters to the estuaries and from there into the open ocean. The objective of this
92 study was to fill this gap of knowledge for one of the best studied rivers in this context.
93 Paraíba do Sul River (PSR) in Brazil is the only river system for which long-term DBC
94 flux data are available (Dittmar et al., 2012a). In this river, DBC annual export exceeds
95 by far present BC production rates, and charcoal still residing in the soils after historic
96 forest fires is the most likely source of DBC in the river today. PSR drains an area
97 formerly covered entirely by Brazilian Atlantic Forest. Its original area comprised 1.3

98 million km², but nowadays, only 12-15% of its original extension remains as secondary
99 forest distributed as isolated, disconnected patches (SOS Mata Atlântica e INPE, 2011;
100 Ribeiro et al., 2009; Lira et al., 2012). Deforestation occurred mainly between 1850 and
101 1970 via slash-and-burn (Warren, 1995). Today, 74% of the watershed is covered by
102 fire-managed grassland and, in the area close to the coastal region, fire-managed sugar
103 cane plantations. DBC concentration in PSR fluctuates with seasons, with highest
104 concentrations during wet seasons and lowest ones during dry seasons, excluding direct
105 deposition as a significant source (Dittmar et al., 2012a).

106

107 In this study we tested the hypothesis that due to limited light penetration and bio-
108 recalcitrant properties, DBC is funneled unmodified within the PSR from the
109 headwaters to the estuary and into the open ocean. We focused on the polycyclic
110 aromatic fraction of DBC that can be quantified in natural waters with help of molecular
111 proxies, i.e. benzenepolycarboxylic acids that are released from DBC during nitric acid
112 oxidation (Hammes et al., 2007; Dittmar, 2008). We tested for conservative behavior of
113 DBC in the headwaters-to-ocean continuum in three sampling campaigns, two in the
114 rainy and one in the dry season.

115

116 Furthermore, we searched for chemical evidence that DBC in PSR is indeed mainly
117 released from charcoal produced in historic forest fires and not primarily derived from
118 today's fire management practice, as deduced previously from budget calculations
119 (Dittmar et al., 2012a). We took advantage of the fact that the historic Atlantic forest
120 vegetation was composed mainly of C3 plants, while today's pastures and sugar cane
121 plantations are dominated by plants with the C4 photosynthetic pathway. Both types of
122 plants carry a distinct carbon isotopic signature ($\delta^{13}\text{C}$) in their organic tissue. We
123 determined $\delta^{13}\text{C}$ on bulk SPE-DOM along the headwater-to-ocean continuum, which
124 provided us with information about the main sources of DOM, of which DBC is a
125 significant fraction.

126

127 **2 - Materials and methods**

128 **2.1 - Study area**

129 The PSR watershed occupies an area of 57,300 km² in the states of São Paulo, Minas
130 Gerais and Rio de Janeiro, located between 20°26' and 23°28'S latitude and 41°00' and
131 46°30'W longitude (Ovalle et al., 2013). The headwaters of the PSR are formed by the
132 confluence of the Paraitinga and Paraibuna Rivers. The total length of the river channel
133 is approximately 1150 km. The PSR basin can be divided into three macro-sectors
134 (**Figure 1a**): (1) An upper basin sector with an area of 7,300 km², where the river
135 descends from an altitude of around 1800 m to 600 m through narrow and embedded
136 valleys carved out of crystalline rocks; (2) A middle basin sector with an area of 27,500
137 km² and average elevation of 510 m, this sector is most influenced by industry, meanly
138 for steel, chemicals, food and paper; (3) A lower basin sector with an area of 22,500
139 km² that is mainly occupied by coastal plain with numerous riverine meanders and
140 islands.

141

142 The area within the PSR watershed is highly urbanized and industrialized, with about 5
143 million inhabitants. The PSR is used for supplying drinking water to over 14 million
144 people. Close to Barra do Piraí city, approximately 160 m³ s⁻¹ of water is diverted from
145 PSR for water supply to Rio de Janeiro city. There is a strong seasonality in water
146 discharge in PSR. The high and low water periods range from December to February
147 and from June to August, respectively. Major industrial areas are concentrated in the

148 middle and upper sector basin and in the sub-basins of the Pomba and Paraibuna Rivers
149 (Ovalle et al., 2013). In the lower basin sector, extensive farming prevails, especially
150 sugar cane production. In addition, forty-seven different reservoirs and hydroelectric
151 dams with varying sizes influence the hydrology of the river system throughout the
152 basin (Ovalle et al., 2013). The Paraíba do Sul estuary is located at the coastal plain
153 formed by the PSR delta in the North of Rio de Janeiro state, near São João da Barra
154 city (Souza et al., 2010).

155 156 **2.2 - Sampling**

157 Samples from rivers, estuary and adjacent ocean (**Figure 1a**) were collected during the
158 wet seasons in January 2013 and February 2014. Average fluvial discharge in the lower
159 reaches of PSR (Campos dos Goytacazes) was $1875 \text{ m}^3 \text{ s}^{-1}$ in January 2013 and 719 m^3
160 s^{-1} in February 2014. Sampling in the dry season was done in July and August of 2013,
161 with an average discharge of $478 \text{ m}^3 \text{ s}^{-1}$. The discharges values were estimated using
162 river velocity and cross-sectional area measurements (General Oceanic model 2030
163 current meter). Surface water samples (3 L) were collected in acid rinsed bottles at 24
164 sites along the main channel of the PSR (**Figure 1a**, red symbols) and 14 sites at the
165 PSR tributaries (**Figure 1a**, green symbols). In the estuary and adjacent ocean up to 35
166 km offshore, 24 samples were collected along the salinity gradient in the wet season of
167 2013, and 21 sites during the other campaigns (**Figure 1a**, yellow symbols). The PSR
168 and tributaries were sampled from bridges while the estuary and ocean were sampled
169 from a trawler. All samples were retrieved from the water surface with acid-rinsed
170 buckets. We collected superficial soil samples in the forest and pasture sites (three
171 samples at each site) to constrain the end-members used in the two sources isotopic
172 model as C3 plants (forest site) and C4 plants (pasture site).

173 174 **2.3 - Sample processing**

175 Immediately after sampling, samples were filtered through pre-combusted GF/F filters
176 (Whatman, nominal pore size $0.7 \mu\text{m}$). After filtration, samples were acidified with HCl
177 (32%, analytical grade) to pH 2 and DOM was isolated from the water samples via
178 solid-phase extraction (SPE) (Dittmar et al., 2008). In brief, filtered samples were
179 passed by gravity through solid-phase cartridges (1 g PPL, Agilent). The cartridges
180 were desalted with 0.01 mol L^{-1} HCl, dried with a stream of N_2 , and DOM was eluted
181 with 8 mL of methanol (HPLC grade). The DOC extraction efficiency was determined
182 for each sample by evaporating an aliquot of the methanol extract to dryness, re-
183 dissolving it in ultrapure water at pH 2, and relating the DOC concentration of this
184 solution to that of the original sample. On average among all samples ($n = 177$), 45 %
185 (SE $\pm 13\%$) of DOC was recovered by the SPE. Extraction efficiency did not
186 systematically vary along the river and along the salinity gradient. Soil samples were
187 freeze-dried and the fraction $> 2.0 \text{ mm}$ isolated by sieving.

188 189 **2.4 - Dissolved organic carbon and stable carbon isotope determination**

190 The concentration of DOC in filtered samples was determined by the high-temperature
191 catalytic oxidation method on an automated TOC analyzer (Shimadzu TOC 5000),
192 using five calibration solutions spanning the concentration range of the samples. All
193 DOC data reported are the mean of three replicate injections, for which the coefficient
194 of variance was less than 5 %. Procedural blanks, including the filtration step, were
195 obtained using ultrapure water. These blank samples did not contain any detectable
196 amounts of DOC. The detection limit for DOC was $5 \mu\text{M}$, and the analytical accuracy
197 (relative to the reference material) and precision (replicate injections) were within ± 1

198 μM . The deep sea reference material provided by D. Hansell (University of Miami,
199 USA) was repeatedly analyzed in each run to control accuracy.

200

201 The stable carbon isotope composition of SPE-DOM was determined following an
202 established protocol (Seidel et al., 2015). In brief, an aliquot of 800 – 1600 μL of SPE-
203 DOM extract, corresponding to approximately 20 μg of SPE-DOC, was dried under N_2
204 flux. Then, it was re-dissolved in 50 μL of methanol, transferred into Sn combustion
205 capsules (Elemental) and dried in an oven at 60 $^\circ\text{C}$ for 24 h. Soil samples were weighed
206 (10 mg) in Sn combustion capsules (Elemental). The isotopic composition was analyzed
207 on an elemental analyzer (Flash 2000) coupled to an isotope-ratio mass spectrometer
208 Delta V Advantage (Thermo Scientific, Germany). Stable carbon isotope ratio is
209 expressed as $\delta^{13}\text{C}$ (‰) relative to the Pee Dee Belemnite (PDB) standard reference.

210

211 **2.5 - Dissolved black carbon**

212 The benzenepolycarboxylic acids (BPCAs) method (Dittmar, 2008) was used to
213 quantify the condensed polyaromatic fraction of DBC. This method is the most sensitive
214 and unequivocal method for the determination of BC in fluvial and marine DOM
215 (Dittmar et al., 2012b). Moreover, the proportions of the different detectable BPCAs are
216 indicative of the extent of condensation and size of the polycyclic aromatics. For
217 example, char produced at 1000 $^\circ\text{C}$ is typically highly condensed and BPCAs released
218 by nitric acid oxidation are basically composed of benzenehexacarboxylic acid.
219 Charcoal produced at 200 $^\circ\text{C}$ is characterized by a low number of condensed aromatic
220 rings, and BPCAs are less carboxylated compared to high-temperature chars (Schneider
221 et al., 2010). For BPCAs analysis, 300 – 500 μL of the methanol extracts, corresponding
222 to 1-10 μmol of SPE-DOC, were transferred into 2 mL glass ampoules, evaporated to
223 dryness in an oven at 60 $^\circ\text{C}$ and dissolved in 0.5 mL of concentrated HNO_3 (65%). The
224 ampoules were flame sealed, placed in a stainless-steel pressure bomb and kept for 9 h
225 at 170 $^\circ\text{C}$ in a furnace. After the ampoules had cooled, the HNO_3 was evaporated to
226 dryness in a speed vacuum centrifuge (60 $^\circ\text{C}$, Christ RV2-18). Samples were dissolved
227 in 100 μL of phosphate buffer at pH 7.2 (Na_2HPO_4 and NaH_2PO_4 , each 0.5 mM) and
228 analyzed on an ultrahigh performance liquid chromatography system (Waters Acquity
229 UPLC), equipped with a photodiode array light-absorbance detector. BPCAs were
230 identified in accordance to retention time and absorbance spectra (220 – 380 nm).
231 Quantification was performed using the absorbance signal at 240 nm and an external
232 calibration. The injection volume was 1 μL . BPCA concentrations were converted into
233 DBC concentrations after the equation of Dittmar (2008), with the slight modification
234 outlined in Stubbins et al. (2015), where the most robustly quantified B6CA and B5CA
235 are used for estimating DBC. For the equations we refer to Stubbins et al. (2015).

236

237 **2.6 - Two source isotopic model**

238 To estimate the contribution of C_4 plant derived organic matter to PSR and tributaries
239 DOM, we used a linear two-source mixing model (Martinelli et al., 2002):

$$240 \quad \text{C4}(\%) = \frac{\delta^{13}\text{C}_{\text{sample}} - \delta^{13}\text{C}_{\text{C3 soil}}}{\delta^{13}\text{C}_{\text{C4 soil}} - \delta^{13}\text{C}_{\text{C3 soil}}} \times 100 \quad (1)$$

241

242 where $\delta^{13}\text{C}_{\text{sample}}$ is the isotopic composition of SPE-DOM in a given sample, $\delta^{13}\text{C}_{\text{C3 soil}}$
243 ($-29.4 \pm 0.4\text{‰}$) is the isotopic composition of the forest soil and $\delta^{13}\text{C}_{\text{C4 soil}}$ ($-14.9 \pm 0.3\text{‰}$)
244 is the isotopic composition of the pasture soil. An underlying assumption of our
245 calculations is that there are only two main sources of SPE-DOM. Other sources, like

246 sewage or autochthonous production by algae reduce the accuracy of our calculations.
247 Also isotope fractionation during DOM decomposition is not considered in our model.

248

249 **2.7 - Hydrological and conservative mixing models**

250 Daily water discharge data are available for the lower reach of PSR, at the city of
251 Campos dos Goytacazes. We used electric conductivity as a tracer to backwards
252 calculate the water discharge of the tributaries and at each sampling point of PSR.
253 Electrical conductivity was determined in situ with a WTW portable probe calibrated
254 directly before each measurement. Under the reasonable assumption that electrical
255 conductivity behaves conservatively during mixing, the relative proportion of water
256 discharge of a tributary and the mainstream before and after the effluent was calculated,
257 based on the principles of mass conservation:

258

$$259 Q_{\text{after}} = Q_{\text{before}} + Q_{\text{tributary}} \quad (2)$$

260

$$261 \sigma_{\text{after}} \cdot Q_{\text{after}} = \sigma_{\text{before}} \cdot Q_{\text{before}} + \sigma_{\text{tributary}} \cdot Q_{\text{tributary}} \quad (3)$$

262

263 Q is the water discharge after the tributary (Q_{after}), before the tributary (Q_{before}) and of
264 the tributary ($Q_{\text{tributary}}$); and σ is the electrical conductivity at the respective position. For
265 example, the water discharge in Campos dos Goytacazes (Q_{after}) was $1875 \text{ m}^3 \text{ s}^{-1}$ in
266 January 2013 and σ_{after} at that site was $65 \text{ }\mu\text{S}\cdot\text{cm}^{-1}$. From the electrical conductivity of
267 the next upstream tributary ($\sigma_{\text{tributary}}$; $73 \text{ }\mu\text{S}\cdot\text{cm}^{-1}$) and the river sample before the
268 tributary (σ_{before} ; $59 \text{ }\mu\text{S}\cdot\text{cm}^{-1}$), we calculated a water discharge of $803 \text{ m}^3 \text{ s}^{-1}$ from the
269 tributary and $1071 \text{ m}^3 \text{ s}^{-1}$ from the PSR upstream the tributary. Loss of water (e.g.,
270 through evaporation) and unknown sources of water (e.g., groundwater inputs) are
271 sources of errors in this model.

272

273 As a second step we calculated the respective fluxes of DBC (F_{DBC}) as water discharge
274 multiplied by DBC concentration (c_{DBC}) at each site.

275

$$276 F_{\text{DBC}} = Q \cdot c_{\text{DBC}} \quad (4)$$

277

278 DBC fluxes were then compared to the theoretical DBC fluxes for ideal conservative
279 behavior at each site. Deviations of the measured fluxes from these conservative fluxes
280 indicate additional source and sink terms along the river. Conservative fluxes were
281 calculated on the assumption that DBC behaves like electrical conductivity in the
282 conservative case. Consequently, the theoretical, conservative DBC flux at a given
283 station is the DBC flux of the uppermost station in PSR, plus the additive flux of each
284 tributary upstream of a given station:

285

$$286 F_{\text{DBC, conservative}} = F_{\text{DBC, uppermost station}} + \Sigma F_{\text{DBC, all tributaries upstream}} \quad (5)$$

287

288 The theoretical, conservative DBC concentration ($c_{\text{DBC, conservative}}$) at each station is:

289

$$290 c_{\text{DBC, conservative}} = F_{\text{DBC, conservative}} / Q \quad (6)$$

291

292 Similar calculations were done for the estuary. The proportion of freshwater ($\%_{\text{fresh}}$) and
293 seawater ($\%_{\text{sea}}$) in each estuarine sample was calculated from electrical conductivity.
294 We considered the samples taken in PSR in Campos dos Goytacazes (freshwater) and the

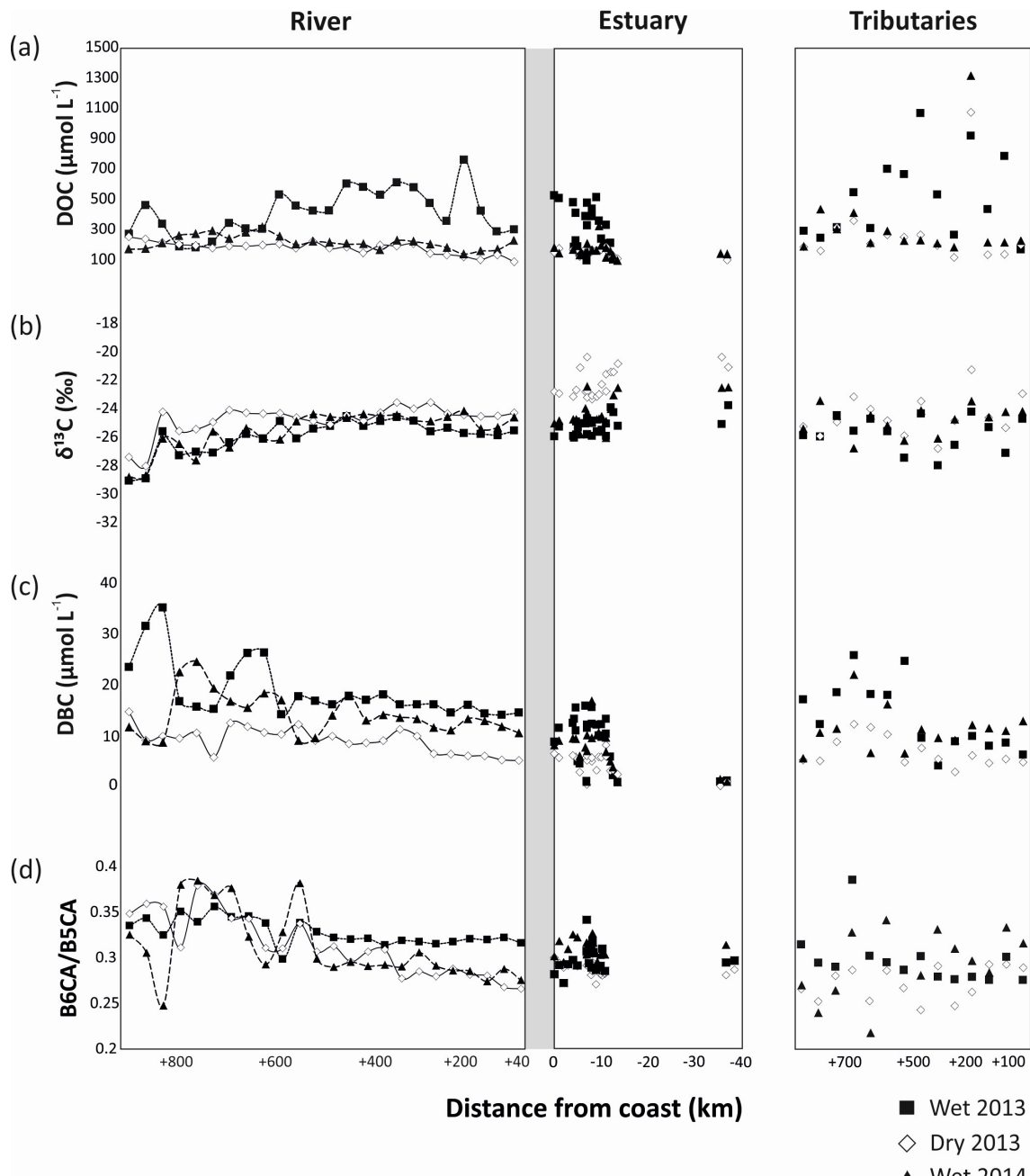
322
323
324
325
326
327
328
329
330
331
332
333
334
335
336
337
338
339
340
341
342
343
344
345
346
347
348
349
350
351
352
353
354
355
356
357
358
359
360
361
362
363
364
365
366
367
368
369
370
371

3 - RESULTS

DOC and DBC concentrations were highly variable between sites and seasons in the main stem of the river, the tributaries and the estuary. The DOC concentration in the PSR system ranged between 168 - 894 $\mu\text{mol L}^{-1}$ in riverine samples, 72 - 529 $\mu\text{mol L}^{-1}$ in estuarine samples and 143 - 1381 $\mu\text{mol L}^{-1}$ in tributaries (**Figure 2a, Table S1, S2 and S3**). Riverine and estuarine DOC concentrations were distinctly higher during the wet season of 2013, while during the dry season of 2013 and the wet season of 2014 DOC concentrations were lower (Student's t-test, $p < 0.01$, **Figure 2a, Table S1, S2 and S3**). In contrast, DOC concentrations in the tributaries were not significantly different between both wet seasons, but differed between wet and dry seasons (Student's t-test, $p < 0.05$, **Figure 2a, Table S1, S2 and S3**). DOC concentrations in the estuary decreased with distance offshore. In all the sampling periods, DOC concentrations slightly deviated from conservative mixing in the river and estuary (**Figure 2a**), but the resulting DBC fluxes were not significantly different from those calculated from the conservative mixing model. The stable carbon isotopic composition ($\delta^{13}\text{C}$) of SPE-DOM ranged between -29.0 ‰ and -23.5 ‰ in the main stem of PSR, and from -28.0‰ to -21.3‰ in the tributaries. In the estuary, $\delta^{13}\text{C}$ increased from a minimum of -25.7 ‰ inshore to -20.0 ‰ in the marine endmember offshore (**Figure 2b, Table S1, S2 and S3**). Riverine and estuarine $\delta^{13}\text{C}$ were more depleted (more negative $\delta^{13}\text{C}$ values) in the wet season of 2013 (Student's t-test, $p < 0.05$, **Figure 2b**), followed by the wet season of 2014 and finally of dry season of 2013 (Student's t-test, $p < 0.05$, **Figure 2b**). The $\delta^{13}\text{C}$ of forest soil sample was -29.4 ± 0.4 ‰ whilst it was -14.9 ± 0.3 ‰ for the pasture soil sample.

DBC concentrations in PSR ranged between 5 - 35 $\mu\text{mol L}^{-1}$, with significantly higher values during the wet season of 2013 compared to the other sampling campaigns (Student's t-test, $p < 0.01$, **Figure 2c, Table S1**). DBC concentrations in the tributaries ranged from 3 - 26 $\mu\text{mol L}^{-1}$, and were similar in both wet seasons, but distinctly different between wet and dry seasons (Student's t-test, $p < 0.01$, **Figure 2c, Table S2**). Estuarine DBC concentrations ranged from 0.3 - 17 $\mu\text{mol L}^{-1}$, strongly decreasing from in- to offshore; they were similar in both wet seasons, and distinctly different between wet and dry seasons (Student's t-test, $p < 0.01$, **Figure 2c, Table S3**). The concentration ratio of benzenhexa- to benzenepentacarboxylic acids (B6CA/B5CA) in PSR ranged between 0.27 - 0.36, in the tributaries between 0.22 - 0.34 and in the estuary between 0.27 - 0.34 (**Figure 2d, Table S1, S2 and S3**), with a decreasing trend from in- to offshore.

372
373
374



375
376
377
378
379
380
381
382
383
384
385
386
387

Figure 2: Spatial distributions of (a) DOC concentrations, (b) $\delta^{13}\text{C}$ of SPE-DOC, (c) DBC concentrations and (d) B6CA/B5CA ratio in the river, estuary and tributaries of Paraíba do Sul during the different sampling seasons.

4 - DISCUSSION

4.1 - The source of DBC

The PSR catchment area was once covered by Atlantic forest. Due to almost complete destruction via the slash-and-burn practice until the mid-1970's large amounts of charcoal had been deposited in the soils of the catchment. DBC is slowly released when charcoal ages in soils (Ding et al., 2013). Simultaneous microbial oxidation of soil

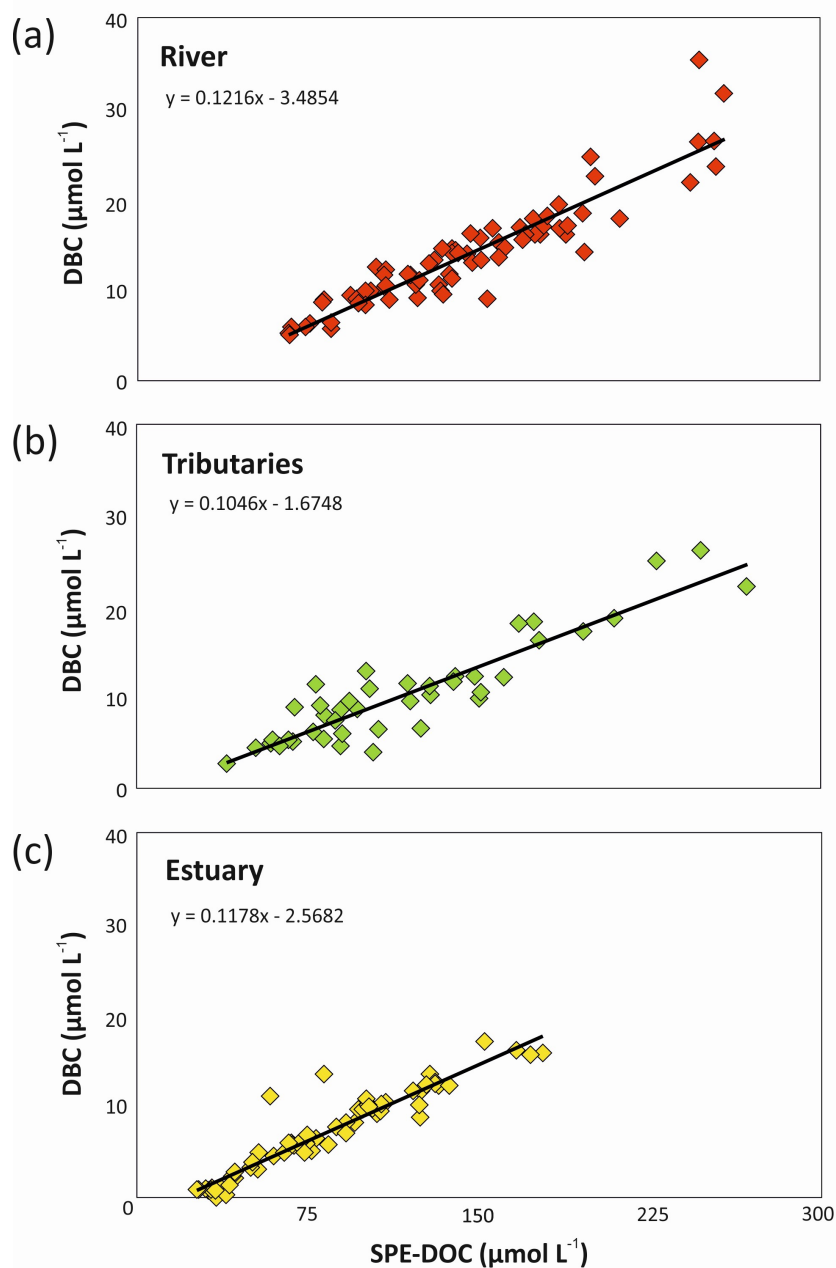
388 organic matter and charcoal likely results in a strong relationship between DOC and
389 DBC concentrations in the rivers draining the area (Ding et al., 2013). Consistent with
390 this concept, statistically significant correlations between DBC and DOC concentrations
391 were observed for PSR, tributaries and estuary (**Figure 3**). Similar relationships were
392 previously found in intertidal systems (Dittmar et al., 2012b), intermittent grassland
393 streams (Ding et al., 2013) and fluvial systems (Dittmar et al., 2012a; Jaffé et al., 2013;
394 Stubbins et al., 2015). In our study, the slope of the resulting regressions indicated that
395 the DOC pool in the river contained 12.2% of DBC, followed by the estuary with 11.8%
396 and the tributaries with 10.5%, which is close to the previously reported global riverine
397 average (Jaffé et al., 2013).

398
399 It was proposed that DBC in PSR is largely derived from historic charcoal deposits in
400 the soils, and only to a minor degree from today's fire-management practice (Dittmar et
401 al. 2012a). The historic forest vegetation was composed mainly of C3 plants, while
402 today's pastures and sugar cane plantations are dominated by C4 plants. DBC
403 concentrations in the river system inversely correlated with the percentage of DOC that
404 was derived from C4 plants (**Figure 4**). The higher the contribution of C3 plants the
405 higher was the concentration of DBC in the river. The relationship between all samples
406 presented a strong negative correlation ($r_s = -0.605$, $p < 0.001$, $n = 114$) indicating that
407 historical fire events from Atlantic Forest represented a more important source of DBC
408 to the river water today than recent burning activities.

409
410 The source of DOC shifted between the seasons and was consistent with DBC
411 concentrations. During the rainy season, DBC concentrations were high, and the DOC
412 was largely derived from historic carbon sources (C3) with more depleted $\delta^{13}\text{C}$ values.
413 In the dry season, DBC concentration was lower and the contribution of today's
414 vegetation (C4) was higher, with $\delta^{13}\text{C}$ values more enriched. The identification of C3 or
415 C4 plants with carbon isotopic composition was possible due the marked differences in
416 $\delta^{13}\text{C}$ values between each kind of plants. C3 plants have $\delta^{13}\text{C}$ values depleted close to -
417 31‰, while C4 plants have $\delta^{13}\text{C}$ values less depleted close to -14‰ (Krusche et al.,
418 2002). This observation is probably a reflection of water flow paths. During the rainy
419 season, upper soil horizons, where most (historic) charcoal deposits are, are flushed.
420 Deeper groundwater that fuels the river during base flow seems to be less influenced by
421 soil-derived DOM. In accordance, in the Amazon Forest, the upper soil horizons (upper
422 60 cm) contain higher amounts of BC and char than deeper horizons (Glaser et al.
423 2001). The char in soil in the Amazon had an apparent radiocarbon age of 1775 ± 325
424 years (Glaser et al. 2001), indicating a long residence time of char in tropical soils. In
425 addition, enhanced in-situ production by algae during the dry season caused by deeper
426 light penetration should be taken into account. Algae are potentially another source of
427 isotopically heavy and DBC-poor DOC to the river. Nevertheless, the historic C3
428 vegetation is apparently the predominant source of bulk DOC and associated DBC to
429 the river system.

430
431
432
433
434
435
436
437

438
439
440



441
442
443
444
445
446
447
448
449
450
451
452
453

Figure 3: Geometric mean regression between SPE-DOC and DBC concentrations in (a) Paraíba do Sul river, (b) tributaries and (c) estuary.

454
 455
 456
 457
 458
 459
 460
 461
 462
 463
 464
 465
 466
 467
 468
 469
 470
 471
 472
 473
 474
 475
 476
 477
 478
 479
 480
 481
 482
 483
 484
 485
 486
 487
 488
 489
 490
 491
 492
 493
 494
 495
 496
 497
 498
 499
 500
 501
 502
 503

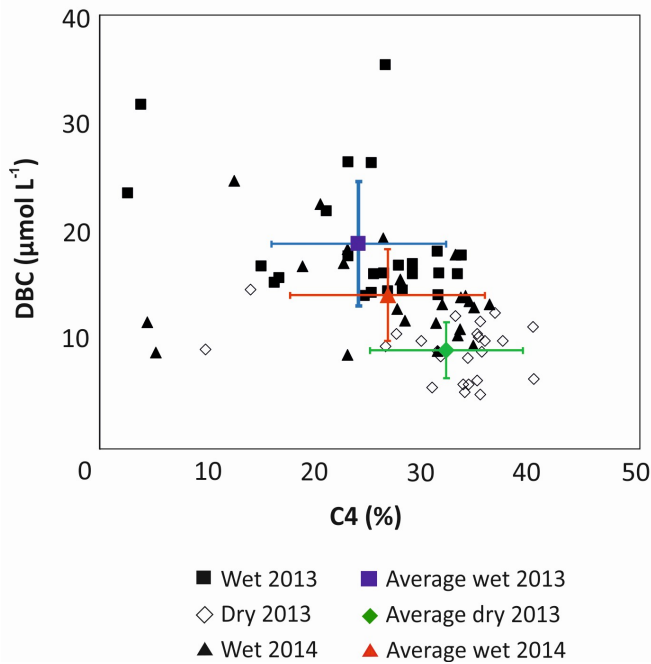


Figure 4: Relationship between the estimated percentage of C4-derived carbon in SPE-DOC (derived from $\delta^{13}\text{C}$) and DBC concentrations in Paraíba do Sul river and tributaries.

4.2 - Processing of DBC in the river-to-ocean continuum

In the headwaters-to-ocean continuum of PSR, the DBC concentrations varied over one order of magnitude. Within the main river, the DBC concentrations matched those reported earlier for PSR in Campos dos Goytacazes (Dittmar et al. 2012a), and are within the range of global rivers (Jaffé et al., 2013) and coastal wetlands (Dittmar et al., 2012b; Ding et al., 2014). The much lower concentrations offshore are consistent with the low DBC concentrations reported for the sea surface in the Gulf of Mexico (Dittmar 2008) and the Southern Indian Ocean (Dittmar and Paeng, 2009).

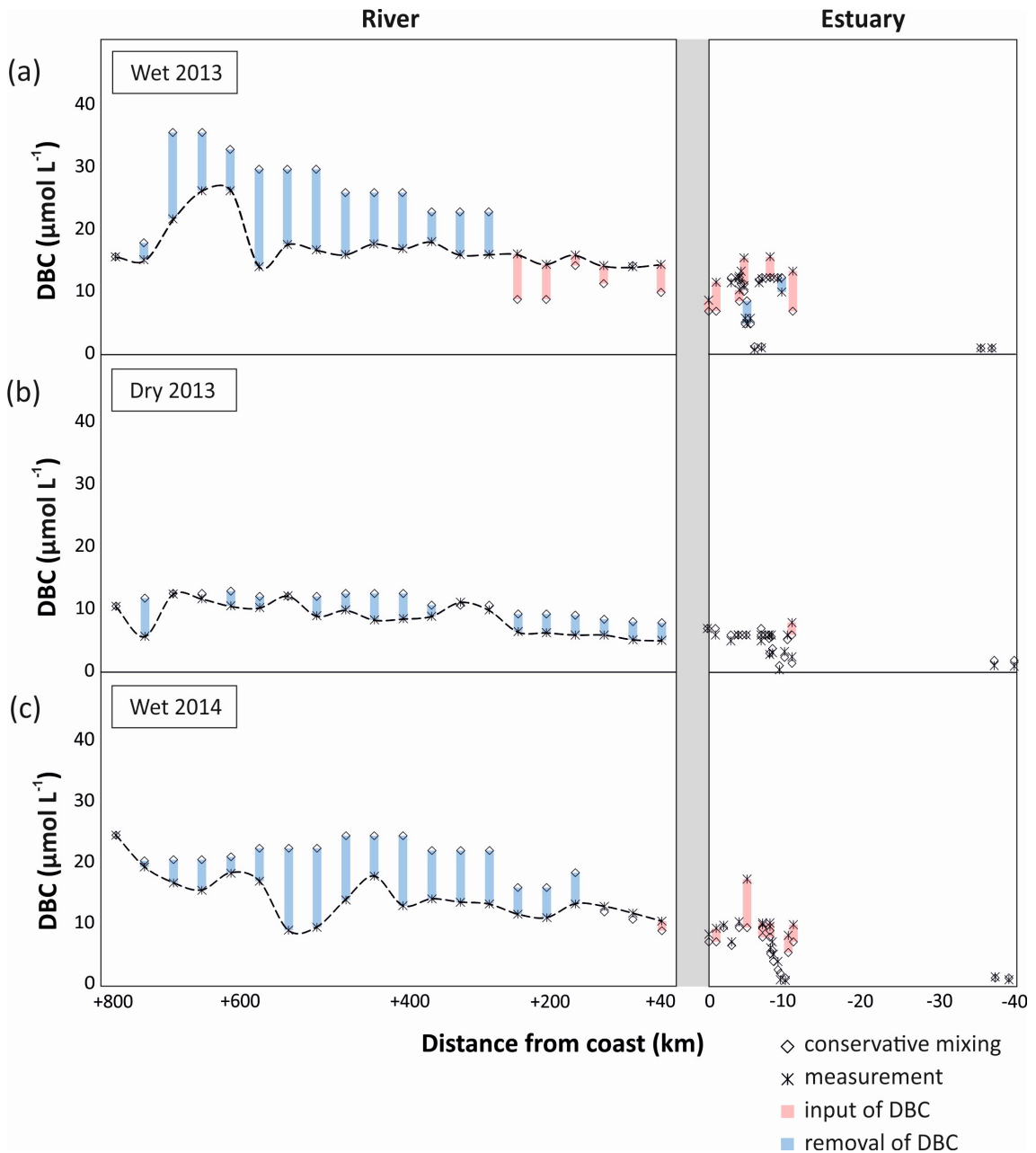
To identify potential sources and sinks along the PSR and estuary we compare the observed trends with those expected from conservative mixing, i.e. a scenario in which DBC has salt-like characteristics in the headwater-to-ocean continuum. In all sampling campaigns a cumulative net-removal of DBC was observed from the headwaters down to the lower reaches of the riverine system (300 km inland, **Figure 5**). This apparent non-conservative behavior of DBC was restricted to few sites and the introduced deviation propagated downstream. An apparent net-removal of DBC persisted all the way to the estuary in the dry season of 2013, but was counteracted or even outbalanced by inputs of DBC in the lower reaches of the river during the wet seasons. In the estuary, a net-input was observed in both rainy seasons; in the dry season, DBC mixed conservatively in the estuary and inner shelf. Overall, the slight deviations of DBC concentration from the conservative mixing model had comparatively little effect on DBC fluxes in the rivers system that were dominated by the large discharge of few tributaries in the lower reaches of PSR (**Figure 6**).

504 In principle, two explanations can be put forward for a non-conservative behavior of
505 DBC in the river-to-ocean continuum. First, unknown sources of water with different
506 DBC to conductivity ratios than the sampled tributaries introduce errors in our mass
507 balance calculations. Deep groundwater is generally poor in DBC (Dittmar et al., 2012a;
508 Stubbins et al., 2015). With increased rainfall, the hydrological pathway also
509 incorporates active soil layers that are rich in organic compounds and charcoal
510 (Guggenberger et al., 2008; Stubbins et al., 2015). At base flow during the dry season,
511 deep groundwater is the main source of water to PSR and the DBC concentrations are
512 consequently lower than during the rainy season when upper soil horizons are flushed
513 (Dittmar et al., 2012a). Lateral input of groundwater into the tributaries is indirectly
514 considered in our mass balance model, but direct inputs of groundwater into the main
515 stem not. Depending on the source of groundwater, these undetected inputs may cause
516 net-inputs from upper soil horizons (rainy seasons) or an apparent net-removal due to
517 dilution with deep groundwater (dry season). Because we observed an overall consistent
518 pattern of net-removal of DBC during wet and dry seasons we consider methodological
519 artifacts as an unlikely reason for the observed net-removal. About 23 to 40% of DBC
520 was lost along the transect from river to estuary during the various seasons.

521
522 DBC consists of condensed organic compounds, and is thus sensible to photooxidation
523 (Stubbins et al., 2008; Spencer et al., 2009). This could be an important sink for DBC in
524 the riverine system, and explain the observed net-removal. One way to assess whether
525 photooxidation indeed occurred is provided by changes of the B6CA/B5CA ratio.
526 Benzenhexacarboxylic acid (B6CA) is indicative of highly condensed aromatics,
527 whereas benzenepolycarboxylic acids with a lower number of carboxylic substitutes are
528 indicative of molecules with a lower number of condensed rings in their core structure
529 (Schneider et al., 2010). Thus, the B6CA/B5CA ratio was proposed as a measure for the
530 degree of condensation of DBC (Stubbins et al., 2012). Highly condensed structures are
531 preferentially degraded by irradiation, and 28 days of exposure to sunlight of North
532 Atlantic Deep Water caused a decrease of B6CA/B5CA from 0.32 to 0.23 (Stubbins et
533 al., 2012). Similarly in our study, apparent loss of DBC was associated with a decrease
534 of B6CA/B5CA (**Figure 2d**). In the dry season of 2013 and the wet season of 2014, the
535 B6CA/B5CA ratio decreased from 0.38 to 0.27 along the river, which is a clear
536 indication for photodegradation. In the wet season of 2013, the change in B6CA/B5CA
537 was not as pronounced, as there was a net-input of DBC in the lower reaches of the
538 river. In the lower reaches of PSR and next to the estuary, there are extensive fire-
539 managed sugar cane plantations located in direct vicinity of the estuary. These areas of
540 sugar cane plantations have been managed since 1538 (Oscar, 1985). It is plausible that
541 lateral inputs from these areas especially during the rainy season caused the observed
542 net-inputs in the corresponding areas. DBC from upper soil horizons has not been
543 exposed to sunlight yet, which is consistent with the relatively high B6CA/B5CA in the
544 respective area and season. Furthermore, during the wet season of 2013, the load of
545 suspended particles in the river was almost one order of magnitude higher than during
546 the other campaigns at station Campos dos Goytacazes (120 mg L^{-1} , compared to 15 mg
547 L^{-1} , unpublished data). Particles shade the water and reduce photodegradation. In
548 addition, DBC may desorb from the particles thereby contributing to the apparent net-
549 input of DBC in the lower reaches of the river during the rainy season of 2013.

550 In the rainy seasons, DBC concentrations were higher than during the dry season. In
551 conjunction with the higher water discharge, DBC fluxes were even more enhanced
552 during the rainy seasons (**Figure 6**). This cumulative effect of higher DBC
553 concentration and higher water discharge was most pronounced during the wet season

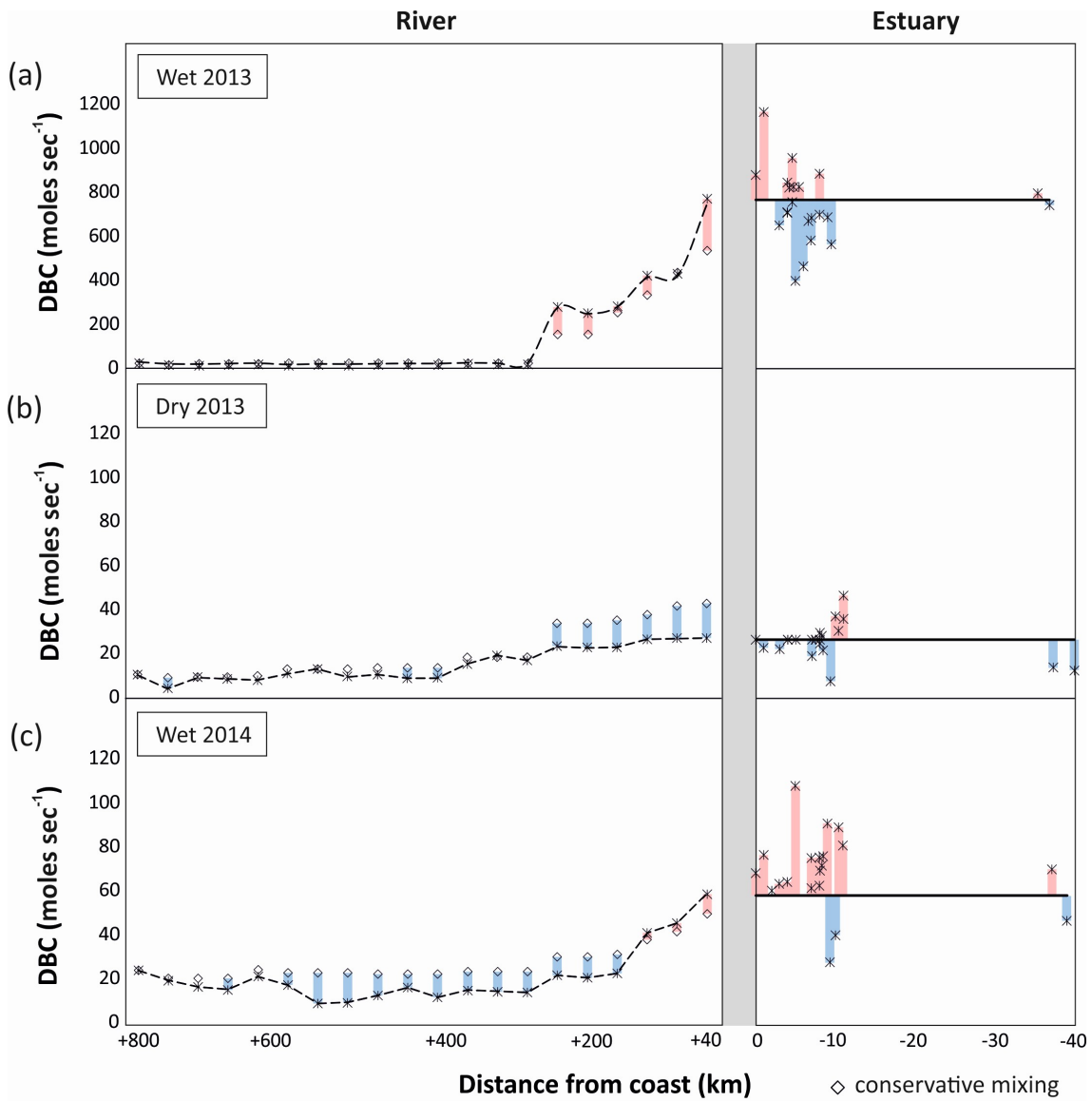
554 of 2013. During this campaign water discharge was more than one order of magnitude
 555 higher at the lowest reaches of PSR compared to the other sampling campaigns,
 556 resulting in correspondingly high fluxes of DBC from the river to the ocean. The flux of
 557 DBC fluctuated in the estuary, but there was no indication for net-removal of DBC.
 558 Fluctuations are likely due to spatial heterogeneity of DBC concentration and local
 559 inputs from resuspended sediments, tidal creeks and groundwater discharge. Overall, it
 560 appears that a large fraction of the DBC survived transport through the estuary and onto
 561 the inner shelf, and possibly over larger scales in the ocean.
 562
 563



564
 565
 566
 567
 568
 569
 570

Figure 5: DBC concentration along the headwaters-to-ocean continuum of Paraíba do Sul (measured concentration and conservative mixing model), indicating potential inputs of DBC (in red; real measurement > conservative mixing model value) and potential sinks of DBC (in blue; conservative mixing model value > real measurement). (a) Wet season 2013, (b) dry season 2013 and (c) wet season 2014.

571
 572
 573
 574
 575
 576
 577
 578
 579



580
 581
 582
 583
 584
 585
 586
 587

Figure 6: Flux of DBC (moles sec⁻¹) in the headwaters-to-ocean continuum of Paraíba do Sul system, indicating potential inputs of DBC (in red; real measurement > conservative mixing model value) and potential sinks of DBC (in blue; conservative mixing model value > real measurement), for the different sampled seasons: (a) Wet season 2013, (b) dry season 2013 and (c) wet season 2014. Note different scales for DBC fluxes.

588
589
590
591
592
593
594
595
596
597
598
599
600
601
602
603
604
605
606
607
608
609
610
611
612
613
614
615
616
617
618
619
620
621
622
623
624
625
626
627
628
629
630
631
632
633
634
635
636
637

5 - CONCLUSIONS

This study presents the first data about the DBC spatial and seasonal behavior in a tropical basin. As model system, we chose the Paraíba do Sul system (Brazil), the only river system for which long-term DBC flux data exist. Our study indicates that hydrology plays an important role in DBC dissolution and migration, with highest DBC concentrations in the wet season and lowest in the dry season. This relationship suggests that DBC is mainly mobilized from the upper soil horizons during heavy rainfalls. Therefore, lateral transport to the ocean seems to be an important removal mechanism for BC in soils. A direct relationship between DOC and DBC concentrations was observed, indicating fire-altered carbon as an intrinsic component of the DOC pool. The similarities in the mechanisms of DOC and DBC stabilization and loss, suggested that DOC may contribute to the mobilization of soil BC to the aquatic systems. In addition, a statistically significant relationship between DBC and $\delta^{13}\text{C-SPE-DOC}$ is consistent with previous literature suggestion (Dittmar et al., 2012a), that DBC in the PSR system is derived from aged charcoal, produced during the Atlantic forest destruction and historically accumulated in soils. Future studies should be directed towards compound-specific carbon isotope analysis on BPCAs to unambiguously confirm the source and age of DBC.

A simple mixing model could largely reproduce the observed DBC fluxes within the catchment and the headwaters-to-ocean continuum. Photooxidation likely removed some DBC along the course of the river-to-ocean-continuum. High water discharge and increased DBC concentrations had a cumulative effect on DBC flux during the rainy seasons. We found no evidence for net DBC removal in the estuary or inner shelf, thus large-scale transport in the ocean is likely. Anticipated temperature increase and changes in the water cycle may result in an increase of fire frequency. As global climate change effects promote extreme dry and wet seasons, the DBC export may increase proportionally and alter the size of the refractory DOM pool in the deep ocean.

AUTHOR CONTRIBUTIONS

All authors contributed to the design of the study. JM and MA analyzed samples for stable carbon isotopic composition. JM and JN analyzed samples for dissolved black carbon. TD, CER and JM conducted modeling studies. All authors contributed to the writing of the manuscript.

FUNDING

INCT-TMCOcean on the Continent-Ocean Materials Transfer (CNPq: 573.601/08-9). Prof. C.E. Rezende received financial support from CNPq (506.750/2013-2) and FAPERJ (E-26/111.616/2011 and E-26/201.188/2014). The Science without Border (CNPq CSF 400.963/2012-4) provided financial support for Jomar Marques da Silva Jr (JM) 1 year in a sandwich program at the University of Oldenburg; Dr. Marcelo Gomes de Almeida (MA) 1 year of Post Doctor position in Environmental Sciences Laboratory (UENF) and Prof. Thorsten Dittmar (TD) 3 months as a Visiting Professor at Universidade Estadual do Norte Fluminense.

638 **ACKNOWLEDGMENTS**

639 The authors are grateful to the *Laboratório de Ciências Ambientais* of the *Centro de*
640 *Biociências e Biotecnologia* at the *Universidade Estadual do Norte Fluminense* and the
641 University of Oldenburg Research Group for Marine Geochemistry (ICBM - MPI
642 Bridging Group), Institute for Chemistry and Biology of the Marine Environment
643 (ICBM) for the use of its facilities. We thank Thiago Rangel, Diogo Quitete for
644 sampling assistance and I. Ulber and M. Friebe for assistance in the lab.

645
646 **REFERENCES**

- 647 Abiven, S., Hengartner, P., Scheider, M.P.W., Singh, N., Schmidt, M.W.I. (2011).
648 Pyrogenic carbon soluble fraction is larger and more aromatic in aged charcoal
649 than in fresh charcoal. *Soil Biol. Biochem.* 43, 1615-1617.
650 doi.org/10.1016/j.soilbio.2011.03.027.
- 651 Agência Nacional das Águas, (2015): (<http://hidroweb.ana.gov.br/>)
652 Comitê de integração da Bacia hidrográfica do rio Paraíba do Sul, (2006). Available in:
653 Hyperlink <http://www.ceivap.org.br/downloads/PSR-010-R0.pdf>.
- 654 Cheng, C.H., & Lehmann, J. (2009). Ageing of black carbon along a temperature
655 gradient. *Chemosphere.* 75, 1021–
656 1027, doi:10.1016/j.chemosphere.2009.01.045 Dittmar, T., & Koch, B. P. (2006).
657 Thermogenic organic matter dissolved in the abyssal ocean, *Mar. Chem.* 102,
658 208–217. doi.org/10.1016/j.marchem.2006.04.003
- 659 Dittmar, T., Koch, B., Hertkorn, N., Kattner, G. (2008). A simple and efficient method
660 for the solid-phase extraction of dissolved organic matter (SPE-DOM) from
661 seawater. *Limnol. Oceanogr. Methods.* 6, p.230-235. doi: 10.4319/lom.2008.6.230
- 662 Dittmar, T. (2008). The molecular level determination of black carbon in marine
663 dissolved organic matter. *Org. Geochem.* 39, 396-407. doi:
664 10.1016/j.orggeochem.2008.01.015
- 665 Dittmar, T., & Paeng, J. (2009). A heat-induced molecular signature in marine dissolved
666 organic matter. *Nat. Geosci.* 2, 175–179. doi: 10.1038/ngeo440
- 667 Dittmar, T., Rezende, C.E., Manecki, M., Niggemann, J., Ovalle, A.R.C., Stubbis, A., et
668 al. (2012a). Continuous flux of dissolved black carbon from a vanished tropical
669 forest biome. *Nat. Geosci.* 5, 618 – 622. doi:10.1038/ngeo1541.
- 670 Dittmar, T., Paeng, J., Gihring, T.M., Suryaputra, I.G.N.A., Huettel, M. (2012b).
671 Discharge of dissolved black carbon from a fire-affected intertidal system. *Limnol.*
672 *Oceanogr.* 57, 1171-1181. doi: 10.4319/lo.2012.57.4.1171
- 673 Ding, Y., Yamashita, Y., Dodds, W.K., Jaffé, R. (2013). Dissolved black carbon in
674 grassland streams: Is there an effect of recent fire history? *Chemosphere.* 90,
675 2557-2562. doi.org/10.1016/j.chemosphere.2012.10.098
- 676 Ding, Y., Cawley, K.M., Cunha, C.N., Jaffé, R. (2014). Environmental dynamics of
677 dissolved black carbon in wetlands. *Biogeochemistry.* 119, 259-273.
678 doi.org/10.1016/j.chemosphere.2012.10.098
- 679 Ferreira, M.P., Alves, D.S., Shimabukuro, Y.E. (2015). Forest dynamics and land-use
680 transitions in the Brazilian Atlantic Forest: the case of sugarcane expansion. *Reg.*
681 *Env. Change.* 15, 365-377. doi: 10.1007/s10113-014-0652-6
- 682 Forbes, M.S., Raison, R.J., Skjemstad, J.O. (2006). Formation, transformation and
683 transport of black carbon (charcoal) in terrestrial and aquatic ecosystems. *Sci.*
684 *Total Envir.* 370, 190-206. doi: 10.1029/97WR01881
- 685 Fundação SOS Mata Atlântica and Instituto Nacional de Pesquisas Espaciais. 2011.
686 Atlas dos remanescentes florestais da Mata Atlântica, período 2008–2010.

- 687 Glaser, B., Haumaier, L., Guggenberger, G., Zech, W. (2001). The ‘‘Terra Preta’’
688 phenomenon: a model for sustainable agriculture in the humid tropics.
689 *Naturwissenschaften*. 88, 37- 41. DOI 10.1007/s001140000193
- 690 Guggenberger, G., Rodionov, A., Shibistova, O., Grabe, M., Kasansky, O., Fuchs, H., et
691 al. (2008). Storage and mobility of black carbon in permafrost soils on the forest
692 tundra ecotone in Northern Siberia. *Glob. Change Biol.* 14, 1397-1381. doi:
693 10.1111/j.1365-2486.2008.01568.x
- 694 Hammes, K., Schmidt, M.W.I., Smernik, R.J., Currie, L.A.; Ball, W.P., Nguyen, T.H.,
695 et al. (2007). Comparison of quantification methods to measure fire-derived
696 (black/elemental) carbon in soils and sediments using reference materials from
697 soil, water, sediment and the atmosphere. *Global Biogeochem. Cy.* 21,
698 doi:10.1029/2006GB002914.
- 699 Jaff e, R., Ding, Y., Niggemann, J., V ah atalo, A.V., Stubbins, A., Spencer, R.G.M., et al.
700 (2013). Global charcoal mobilization from soils via dissolution and riverine
701 transport to the oceans. *Science*. 340, 345-347. doi: 10.1126/science.1231476
- 702 Kim, S., Kaplan, L.A., Benner, R., Hatcher, P.G. (2004). Hydrogen-deficient molecules
703 in natural riverine water sample – evidence for existence of black carbon in DOM.
704 *Mar Chem.* 92, 225-234. doi.org/10.1016/j.marchem.2004.06.042
- 705 Kruche, A.V., Martinelli, L.A., Victoria, R.L., Bernades, M.C., Camargo, P.B.,
706 Ballester, M.V., et al. (2002). Compositional of particulate and dissolved organic
707 matter in a disturbed watershed of southeast Brazil (Piracicaba River basin). *Water*
708 *Res*, 36, 2743-2753. doi.org/10.1016/S0043-1354(01)00495-X
- 709 Lira, P.K., Tambosi, L.R., Ewers, R.M., Metzger, J.P. (2012). Land-use and land-cover
710 change in Atlantic Forest landscapes. *Forest Ecol. Manag.* 15, 80–89.
711 doi.org/10.1016/j.foreco.2012.05.008
- 712 Major, J., Lehmann, J., Rondon, M., Goodale, C. (2010). Fate of soil-applied black
713 carbon: Downward migration, leaching and soil respiration. *Glob. Change Biol.*
714 16, 1366–1379. doi: 10.1111/j.1365-2486.2009.02044.x
- 715 Manino, A., Harvey, H.R. (2004). Black carbon in estuarine and coastal ocean dissolved
716 organic matter. *Limnol. Oceanogr.* 49, 735– 740. doi: 10.4319/lo.2004.49.3.0735
- 717 Martinelli, L.A., Camargo, P.B., Lara, L.B.L.S., Victoria, R.L., Artaxo, P. (2002).
718 Stable carbon and nitrogen isotopic composition of bulk aerosol particles in a C4
719 landscape of southeast Brazil. *Atmos. Environ.* 36, 2427-2432.
720 doi.org/10.1016/S1352-2310(01)00454-X
- 721 Oscar, J. Escravid o & engenhos: Campos, S o Jo o da Barra, Maca e e S o Fid elis. Rio
722 de Janeiro, Achiame (1985). 260p.
- 723 Ovalle, A.R.C., Silva, C.F., Rezende, C.E., Gatts, C.E.N., Suzuki, M.S., Figueiredo,
724 R.O. (2013). Long-term trends in hydrochemistry in the Para iba do Sul River,
725 southeastern Brazil. *J. Hydrol.* 481, 191-203.
726 doi.org/10.1016/j.jhydrol.2012.12.036
- 727 Preston, C.M., & Schmidt, M.W.I. (2006). Black (pyrogenic) carbon in boreal forests: a
728 synthesis of current Knowledge and uncertainties. *Biogeosciences Discussions*.
729 European Geosciences Union, 3, 211-271. <hal-00297763>
- 730 Ribeiro, M.C., Metzger, J.P., Martensen, A.C., Ponzoni, F.J., Hirota, M.M. (2009). The
731 Brazilian Atlantic Forest: how much is left, and how the remaining forest
732 distributed? Implications for conservation. *Biol. Conserv.* 142, 1141–1153.
733 doi.org/10.1016/j.biocon.2009.02.021
- 734 Riedel, T., Zark, M., V ah atalo, A. V., Niggemann, J., Spencer, R. G. M., Hernes, P. J.,
735 et al. (2016) Molecular signatures of biogeochemical transformations in dissolved

736 organic matter from ten World Rivers. *Front. Earth Sci.* doi:
737 10.3389/feart.2016.00085.

738 Santín, C., Doerr, S.H., Kane, E.S., Masiello, C.A., Ohlson, M., Rosa, J.M., et al.
739 (2016). Towards a global assessment of pyrogenic carbon from vegetations fires.
740 *Glob Change Biol.* DOI: 10.1111/gcb.12985

741 Schneider, M.P.W., Hilf, M., Vogt, U.F., Schmidt, M.W.I. (2010). The benzene
742 polycarboxylic acid (BPCA) pattern of wood pyrolyzed between 200 degrees C
743 and 1000 degrees C. *Org. Geochem.* 41, 1082-1088.
744 doi.org/10.1016/j.orggeochem.2010.07.001

745 Siedel, M., Yager, P.L., Ward, N.D., Carpenter, E.J., Gomes, H.R., Kruske, A.L., et al.
746 (2015). Molecular-level changes of dissolved organic matter along the Amazon
747 River-to-ocean continuum. *Mar. Chem.* doi.org/10.1016/j.marchem.2015.06.019.

748 Souza, T.A., Godoy, J.M., Godoy, M.L.D.P., Moreira, I., Carvalho, Z.L., Salomão,
749 M.S.M.B., et al. (2010). Use of multitracers of the study of water mixing in the
750 Paraíba do Sul River estuary. *J. Environ Radioactiv.* 101, 564-570.
751 doi.org/10.1016/j.jenvrad.2009.11.001

752 Spencer, R. G. M., Stubbins, A., Hernes, P. J., Baker, A., Mopper, K., Aufdenkampe, A.
753 K., et al. (2009). Photochemical degradation of dissolved organic matter and
754 dissolved lignin phenols from the Congo River. *J. Geophys. Res.* 114, G03010,
755 doi:10.1029/2009JG000968.

756 Stubbins, A., Hubbard, V., Uher, G., Aiken, G., Law, C. S., Upstill-Goddard, R. C., and
757 Mopper, K. (2008). Relating carbon monoxide photoproduction to dissolved organic
758 matter functionality. *Environ. Sci. Technol.* 42, 3271-3276. doi: 10.1021/es703014q

759 Stubbins, A., Niggemann, J., Dittmar, T. (2012). Photo-lability of deep ocean dissolved
760 black carbon. *Biogeosciences.* 9, 1661 – 1670. doi: 10.5194/bg-9-1661-2012

761 Stubbins, A., Spencer, R.G.M., Mann, P.J., Holmes, R.M., McClelland, J.W.,
762 Niggemann, J., Dittmar, T. (2015) Utilizing colored dissolved organic matter to
763 derive dissolved black carbon export by arctic rivers. *Front. Earth Sci.* 3:63,
764 doi:10.3389/feart.2015.00063.

765 Warren, D. Broadax and Firebrand. The destruction of the Brazilian Atlantic forest.
766 Univ. California Press. (1995). 504 p.

767 Ziolkowski, L.A., & Druffel, E.R.M. 2010. Aged black carbon identified in marine
768 dissolved organic carbon. *Geophys. Res. Lett.* 37:L16601. doi:10.1029/2010GL043963.

769

770

6 – Discussão geral

A bacia de drenagem do rio Paraíba do Sul vem sofrendo inúmeras modificações antropogênicas. Dentre essas modificações, podemos destacar a mudança do uso da terra, que com suas consequências promoveu efeitos negativos na ciclagem da matéria orgânica. A substituição da vegetação original de Mata Atlântica que cobria toda a bacia de drenagem do RPS por gramíneas que atualmente cobrem a maior parte da bacia. Essa substituição causou uma mudança na fonte de matéria orgânica na calha fluvial do RPS e também nos tributários, assim como na matéria orgânica exportada pelo estuário para a região costeira. O efeito dessa substituição foi observado nos dados da composição isotópica do carbono. A $\delta^{13}\text{C}$ apresentou uma grande variabilidade espacial e sazonal, espacialmente com a MO apresentando um enriquecimento da $\delta^{13}\text{C}$ ao longo do percurso do rio. Sazonalmente a $\delta^{13}\text{C}$ apresentou valores mais leves nos períodos chuvosos e valores mais pesados no período seco, mostrando um dos efeitos negativos da mudança de fontes entre os períodos sazonais. Isso foi reforçado por meio do uso do modelo de duas fontes (Martinelli *et al.*, 2002), onde foi observado incremento da porcentagem de gramíneas na MO durante a estação seca. A mudança da fonte de MO poderá acarretar em mudanças na comunidade microbiana e com isso essa mudança pode ser amplificada por toda teia trófica. Outro fato importante a ser destacado, foi o modo que essas mudanças na paisagem foram realizadas. Na década de 1850 as queimadas foram usadas em um massivo processo de desmatamento que se intensificou nos anos seguintes, em 1973 existia menos que 15% de mata. Como consequência do uso de queimadas, grandes quantidades de carvão foram produzidas e estocadas nos solos. Nos dias atuais, as queimadas ainda são usadas na como forma de limpeza dos pastos e também acontecem nos fragmentos de mata. O desafio do presente estudo foi identificar a fonte do dissolvido transportado e exportado pelo RPS.

Os resultados obtidos neste estudo mostram que existe uma forte relação entre as concentrações do carbono negro e a hidrologia. No período de cheia, ocorre uma forte mobilização do CND oriundo dos horizontes superficiais do solo com subsequente entrada do mesmo nos ambientes hídricos. Isso é mostrado claramente pela sazonalidade, onde as maiores concentrações de CND são

observadas nas estações chuvosas e as menores concentrações nas estações seca. A distribuição do carbono negro ao longo do continuum continente/oceano apresentou um comportamento não conservativo, mostrando que existe um desbalanço entre entrada e saída do CN ao longo do contínuo. Dentre os processos de remoção do CN podemos destacar a foto-oxidação, visto que nas estações sazonais onde a luz solar pode penetrar na coluna d' água (seca 2013 e cheia de 2014), em conjunto com a remoção do CND da coluna d' água os valores da razão B6CA/B5CA diminuíram ao longo do contínuo. Indicando uma degradação preferencial no B6CA que é mais sensível a foto-oxidação (Stubbins et al., 2008; Spencer et al., 2009)

Embora a razão B6CA/B5CA indique a foto-oxidação como um importante processo de remoção do CND da coluna d' água, não podemos esquecer que nas estações de seca, a água do lençol freático atua como a importante fonte de água para a calha fluvial. Devido à baixa concentração de CND na água do lençol freático (Dittmar et al., 2012a), pode está ocorrendo em conjunto com a foto-oxidação a diluição do CND fluvial. Em contrapartida, a diferença entre os valores reais e os valores do modelo de mistura na cheia de 2013, provavelmente foi devido à diluição promovida pela grande quantidade de chuva ocorrida neste período. Isso é reforçado com a baixa variação dos valores da razão B6CA/B5CA ao longo do contínuo (Stubbins et al., 2012).

A forte relação entre as concentrações de CND e o COD derivado das plantas C3 é um indicativo que a maior parte do CND transportado pelo RPS pode possuir como principal fonte a matéria orgânica originada da Mata Atlântica. Esse fato reforça que o histórico de queimadas ocorrido na bacia possui um peso maior que as queimadas atuais. Isso mostra que o CND presente nos sistemas hídricos provavelmente é derivado de carvão historicamente acumulado nos solos da bacia de drenagem, como mostrado por Ding et al., (2013), em um estudo realizado na reserva biológica de Konza Prairie (USA), as concentrações do CND não apresentaram relação com a frequência de queimadas atuais. A estrutura química do CN possui é rica em anéis aromáticos, isso promove uma resistência a uma ampla gama de agentes oxidantes. Um trabalho realizado por Schmidt et al., (2002) em chernossolo na Europa Central, foi observado pequenas partículas oriundas da queima de biomassa no horizonte A

constituindo de 15 a 45% da matéria orgânica do solo. Por meio da datação com o $\Delta^{14}\text{C}$, foi observado que o CN possuía milênios de idade (~5040 anos de radiocarbono). As informações supracitadas suportam a tese de que antes de se torna solúvel em água, o CN passa por um longo tempo estocado no solo, onde após diversos ataques microbiológicos, uma fração do CN se torna solúvel. Esses fatos reforçam que o CND encontrado no RPS e tributários foi originado na derrubada da Mata Atlântica. Em adição, os resultados obtidos pelo modelo inverso proposto por Jones et al., (2016, submetido) corrobora com os dados do presente estudo, apontando o carvão estocado nos solos como principal fonte de CND em todos os períodos sazonais. Especialmente nos períodos de cheia, a proporção de carvão, aerossóis queimadas e aerossóis combustíveis fósseis chegou a 85:15:0 na cheia e seca de 2013 e na cheia de 2014 essa proporção chegou a 95:5:0.

A forte relação entre o COD e o CND indica que o mecanismo de mobilização de ambos é mais importante que os eventos de queimadas atuais. Isso mostra que o COD é um importante suporte ambiental, e atua no estoque e na transferência do CND para o ambiente marinho. No futuro, o CN produzido atualmente poderá incorporado no COD e ser mobilizado e transportado para o oceano. Nesse sentido, o aumento das perturbações antrópicas nas bacias drenagem (queimadas e agricultura) e também os impactos causados pelas mudanças globais no clima (aumento da temperatura e derretimentos das geleiras polares) podem provocar um aumento na exportação de COD e CND para os oceanos na mesma proporção. A mobilização do CND dos solos e sua aparente recalcitrância no oceano profundo sugerem que um aumento da produção do CN pode aumentar a proporção da matéria orgânica dissolvida refratária no oceano profundo em longo prazo.

7 - Conclusões

O presente estudo apresenta indícios sobre os efeitos da mudança da cobertura vegetal. Com o uso da composição elementar e isotópica foi possível observar que a mudança do uso da terra tem causado uma alteração qualitativa na composição da MO particulada e dissolvida. Através do modelo de duas fontes foi observado que na estação seca um aumento da porcentagem de MO derivada de plantas do tipo C4. Embora a maior parte da bacia do RPS seja coberta gramíneas,

os valores da $\delta^{13}\text{C}$ indica que a MO é formada por uma mistura entre a vegetação dominante do passado e a atual.

O trabalho mostra os primeiros dados sobre a distribuição espacial e sazonal do CND em uma bacia tropical. O modelo de mistura mostrou que no contínuo continente/oceano o CND apresentou um comportamento não conservativo. As maiores concentrações de CND foram observadas na cheia, enquanto as menores concentrações na seca. Isso indica que a hidrologia desempenha um importante papel na dissolução e migração do CND dos solos. Essa relação sugere que o CND é principalmente mobilizado dos horizontes superficiais dos solos durante os pesados eventos de chuva. Assim, o transporte lateral seria uma importante entrada do CND nos oceanos via estuários.

O declínio dos valores da razão B6CA/B5CA nos períodos sazonais onde houve um volume reduzido de chuva indica a foto-oxidação como um importante processo de remoção do CND do contínuo. Embora devemos ressaltar que a água do lençol freático pode promover uma diluição do CND na calha fluvial.

A relação inversa estatisticamente significativa entre as concentrações do CND e a porcentagem de MO derivada de plantas C4 indica que é possível o uso desta ferramenta como traçador de fontes do CND. A mesma relação mostra que a maior parte do CND transportado pelo RPS foi originada no passado na derrubada da Mata Atlântica. Esse fato reforça que o histórico de queimadas é mais importante que os eventos atuais.

8 – Referências

Allen-King, R.M.; Grathwohl, P.; Ball, W.P. 2002. New modeling paradigms for the sorption of hydrophobic organic chemicals to heterogeneous carbonaceous matter in soils, sediments and rocks. *Advances in Water Resources*, vol.25, 985-1016.

- Andreae, M.O.; Crutzen, P.J. 1997. Atmospheric aerosols: Biogeochemical sources and role in atmospheric chemistry. *Science*, vol. 276, p. 1052-1058.
- Baldock, J.A.; Smernik, R.J. 2002. Chemical composition and bioavailability of thermally altered *Pinus resinosa* (Red pine) wood. *Organic Geochemistry*; vol.33, p.1093–10109.
- Bird, M.I., Moyo, C., Veenedaal, E., Lloyd, J., Frost, P. 1999. Stability of elemental carbon in a savanna soil. *Global Biogeochemical Cycles*, 13, 923-932.
- Bird, M.I.; Ascough, P.L. 2012. Isotopes in pyrogenic carbon: A review. *Organic Geochemistry*, vol.42, p.1529-1539.
- Bucheli, T.D., Gustafsson, O., 2000. Quantification of the soot–water distribution coefficient of PAHs provides mechanistic basis for enhanced sorption observations. *Environmental Science and Technology*, vol.34, 5144–5151.
- Clark, J.S., Patterson, W.A.I., 1997. Background and local charcoal in sediments: scales of fire evidence in the paleorecord. In: Clark, J.S., Cachier Goldammer, J.G., Stocks, B. (Eds.), *Sediment Records of Biomass Burning and Global Change*. Springer-Verlag, Berlin, pp. 23 – 48.
- Clarke, A.D.; Noone, K.J.; Heintzenberg, J.; Warrens, S.G.; Covert, D.S. 1987. Aerosol light absorption measurement techniques: analysis and intercomparisons. *Atmospheric Environment*, vol.21, 1455 – 1465.
- Currie, L.A., Benner, B.A.; Kessler, J.D.; Klinedinst, D.B.; Klouda, G.A.; Marolf, J.V.; Slater, J.F.; Wise, S.A.; Cachier, H.; Cary, R.; Chow, J.C.; Watson, J.; Hedges, J.I.; Prentice, K.M.; Kirchstetter, T.W.; Novakow, T.; Puxbaum, H.; Schmid, K. 2002. A critical evaluation of interlaboratory data on total, elemental, and isotopic carbon in the carbonaceous particle reference material, NIST SRM 1649a. *Journal of Research of the National Institute of Standards and Technology*, vol.107, 279 – 298.
- Crutzen, P. J. and M. O. Andreae 1990, Biomass burning in the tropics: impact on atmospheric chemistry and biogeochemical cycles, *Science*, vol.250, p.1669–1678.
- Czimczik, C.I.; Preston, C.M.; Schmidt, M.W.I.; Schulze, E. 2003. How surface fire in Siberian Scots pine forests affects soil organic carbon in the forest floor: Stocks, molecular structure, and conversion to black carbon (charcoal). *Global Biogeochemical Cycles*, vol.17, p.201–2014.

- Ding, Y.; Yamashita, Y.; Dodds, W.K.; Jaffé, R. 2013. Dissolved black carbon in grassland streams: Is there an effect of recent fire history? *Chemosphere*, vol.90, p.2557 – 2562.
- Dittmar, T.; Lara, R.J.; Kattner, G. 2001. River or mangrove? Tracing major organic matter sources in tropical Brazilian coastal water. *Marine Chemistry*, vol.73, p.253-271.
- Dittmar, T.; Koch, B. P. 2006. Thermogenic organic matter dissolved in the abyssal ocean, *Marine Chemistry*, vol.102, p.208–217.
- Dittmar, T. 2008. The molecular level determination of black carbon in marine dissolved organic matter. *Organic Geochemistry*, vol.39, p.396 – 407.
- Dittmar, T.; Paeng, J. 2009. A heat-induced molecular signature in marine dissolved organic matter. *Nature Geoscience*, vol.2, p.175–179.
- Dittmar, T.; Paeng, J.; Gihring, T.M.; Suryaputra, I,G.N.A.; Huettel, M. Discharge of dissolved black carbon from a fire-affected intertidal system. 2012a. *Limnology and Oceanography*, vol.57, p.1171-1181.
- Dittmar, T.; Rezende, C.E.; Manecki, M.; Niggemann, J.; Ovalle, A.R.C.; Stubbis, A.; Bernades, M.C. 2012b. Continuous flux of dissolved black carbon from a vanished tropical forest biome. *Nature Geoscience*, DOI:10.1038/NCEO1541.
- Elias, V.O., 2001. Evaluating Levoglucan as an indicator of biomass burning in Carajas, Amazonia: a comparison to the charcoal record. *Geochimica Cosmochimica Acta*, vol.65, 267 – 272.
- Fearnside, P.M.; Graça, P.M.L.A.; Rodrigues, F.J.A. 2001. Burning of Amazonian rainforests: burning efficiency and charcoal formation in forest cleared for cattle pasture near Manaus, Brazil. *Forest Ecology and Management*, vol.28, p.146:115.
- Forbes, M.S.; Raison, R.J.; Skjemstad, J.O. 2006. Formation, transformation and transport of black carbon (charcoal) in terrestrial and aquatic ecosystems. *Science and Total Environmental*, vol. 370, p.190-206.
- Gavin, D.G.; Brubaker, L.B.; Lertzman, K.P. 2003. Holocene fire history of a coastal temperate rain forest based on soil charcoal radiocarbon dates. *Ecology*, vol.84, p.186–201.
- Gélinas, Y.; Baldock, J.A.; Hedges, J.I. 2001a. Demineralization of marine and freshwater sediments for CP/MAS ¹³C NMR analysis. *Organic Geochemistry*, vol.32, p.677–693.

- Glaser, B., Haumaier, L., Guggenberger, G., Zech, W., 1998. Black carbon in soils: the use of benzenecarboxylic acids as specific markers. *Organic Geochemistry*, vol.29, 811 – 819.
- Glaser B, Haumaier L, Guggenberger G, Zech W. 2001. The 'Terra Preta' phenomenon: a model for sustainable agriculture in the humid tropics. *Naturwissenschaften*, vol.88, p.37–41.
- Glaser, B.; Amelung, W. 2003. Pyrogenic carbon in native grassland soils along climosequence in North America. *Global Biogeochemical Cycles*, vol.17, p.1-8.
- Gustafsson, O., Haghseta, F., Chan, C., MacFarlane, J., Gschwend, P.M., 1997. Quantification of the dilute sedimentary soot phase: implications for PAH speciation and bioavailability. *Environmental Science and Technology*, vol.31, 203 – 209.
- Gustafsson, O., Gschwend, P.M., 1998. The flux of black carbon to surface sediments on the New England continental shelf. *Geochimica et Cosmochimica Acta*, vol. 62, 465 – 472
- Hamer, U.; Marschner, B.; Brodowski, S.; Amelung, W., 2004. Interactive priming of black carbon and glucose mineralization. *Organic Geochemistry*, vol.35, p.823–830.
- Hammes, K.; Schmidt, M.W.I.; Smernik, R.J.; Currie, L.A.; Ball, W.P.; Nguyen, T.H.; Louchouart, P.; Houel, S.; Gustafsson, O.; Elmquist, M.; Cornelissen, G.; Skjemstad, J.O.; Masiello, C.A.; Song, J.; Peng, P.; Mitra, S.; Dunn, J.C.; Hatcher, P.G.; Hockaday, W.C.; Smith, D.M.; Hartkopf-Froeder, C.; Boehmer, A.; Luer, B.; Huebert, B.J.; Amelung, W.; Brodowski, S.; Huang, L.; Zhang, W.; Gschwend, P.M.; Flores-Cervantes, D.X.; Largeau, C.; Rouzaud, J.N.; Rumpel, C.; Guggenberger, G.; Kaiser, K.; Rodionov, A.; Gonzalez-Vila, F.J.; Gonzalez-Perez, J.A.; de la Rosa, J.M.; Manning, D.A.C.; Lopez-Capel, E.; Ding, L. 2007. Comparison of quantification methods to measure fire-derived (black/elemental) carbon in soils and sediments using reference materials from soil, water, sediment and the atmosphere. *Global Biogeochemical Cycles*, vol.21, doi:10.1029/2006GB002914.
- Hansell, D. A. 2002. DOC in the Global Ocean Carbon Cycle, in: *Biogeochemistry of Marine Dissolved Organic Matter*, Academic Press, Boston, USA, 685–715.
- Hedges, J.I., Keil, R.G., 1995. Sedimentary organic matter preservation: an assessment and speculative synthesis. *Marine Chemistry* 49, p.81-115.

- Hedges, J.I.; Eglinton, G.; Hatcher, P.G.; Kirchman, D.L.; Arnosti, C.; Derenne, S.; Evershed, R.P.; Kogel-Knabner, I.; de Leeuw, J.W.; Littke, R.; Michaelis, W.; Rullkotter, J. 2000. The molecularly-uncharacterized component of nonliving organic matter in natural environments. *Organic Geochemistry*, vol.31, p.945-958.
- Hernes, P. J.; Benner, R.2006. Terrigenous organic matter sources and reactivity in the North Atlantic Ocean and a comparison to the Arctic and Pacific Oceans, *Marine Chemistry*, vol.100, pp.66–79.
- Hitzenberger, R., Tohno, S. 2001. Comparison of black carbon (BC) aerosols in two urban areas – concentrations and size distributions. *Atmospheric Environmental*, 35, 2153 – 2167.
- Hockaday, W.C.; Grannas, A.M.; Kim, S.; Hatcher, P.G. 2007. The transformation and mobility of charcoal in a fire-impacted watershed. *Geochimica et Cosmochimica Acta*, vol.71, p.3432-3445.
- Jacobson, M.Z. 2001. Strong radiative heating due to the mixing state of black carbon in atmospheric aerosols. *Nature*, vol.409, p.965 – 967.
- Jaffé, R.; Ding, Y.; Niggemann, J.; Vähätalo, A.V.; Stubbins, A.; Spencer, R.G.M.; Campbell, J.; Dittmar, T. 2013. Global charcoal mobilization from soils via dissolution and riverine transport to the oceans. *Science*, vol.340, p.345-347.
- Johnson, K.S.; Zuberi, B.; Molina, L.T.; Molina, M.J.; Iedema, M.J.; Cowin, J.P.; Gaspar, D.J.; Wang, C.; Laskin, A. 2005. Processing of soot in an urban environment: case study from the Mexico City Metropolitan Area. *Atmospheric Chemistry and Physics*, vol.5, p.3033 – 3043.
- Kaiser, K.; Benner, R. 2009. Biochemical composition and size distribution of organic matter at the Pacific and Atlantic times-series stations. *Marine Chemistry*, vol.113, p.63–77, doi:10.1016/j.marchem.2008.12.004.
- Keil, R.G., Mayer, L.M., Quay, P.D., Richey, J.E., Hedges, J.I., 1997. Loss of organic matter from riverine particles in deltas. *Geochimica et Cosmochimica Acta* 61, p.1507e1511
- Kim, S.; Kaplan, L.A.; Benner, R.; Hatcher, P.G. 2004. Hydrogen-deficient molecules in natural riverine water sample – evidence for existence of black carbon in DOM. *Marine Chemistry*, vol.92, 225-234.

- Krull, E.S.; Skjemstad, J.O. 2002. $\delta^{13}\text{C}$ and $\delta^{15}\text{N}$ profiles in ^{14}C -dated Oxisol and Vertisols as a function of soil chemistry and mineralogy. *Geoderma*, vol.1890, p.1–29.
- Kuhlbusch, T. A. J.; Crutzen, P. J. 1995. Toward a global estimate of black carbon in residues of vegetation fires representing a sink of atmospheric CO_2 and a source of O_2 . *Global Biogeochem. Cycles*, vol.9, p.491–501.
- Kuhlbusch, T. A. J.; Cachier, O. H.; Goldammer, J. G.; Lacaux, J.P.; Shea, R.; Crutzen, P. J. 1996. Black carbon formation by savanna fires: Measurements and implications for the global carbon cycle, *Journal of Geophysical Research*, vol.101, p.651–665.
- Kuhlbusch, T.A.J., 1998. Black carbon and the carbon cycle. *Science*, vol. 280, p.1903–1904.
- Lee, K.L.; Kim, J.E.; Kim, Y.J.; Kim, J.; Hoyningen-Huence, W. 2005. Impact of the smoke aerosol from Russian forest fires on the atmospheric environment over Korea during May 2003. *Atmospheric Environment*, vol.19, p. 85 – 99.
- Manino, A.; Harvey, H.R. 2004. Black carbon in estuarine and coastal ocean dissolved organic matter. *Limnology and Oceanography*, vol.49, p.735– 740.
- Masiello, C.A.; Druffel, E.R.M. 1998. Black carbon in deep-sea sediments. *Science*, vol.280, p.1911–1913.
- Masiello, C.A.; Druffel, E.R.M. 2001. Carbon isotope geochemistry of the Santa Clara River. *Global Biogeochemical Cycles*, vol.15, p.407 – 416.
- Masiello, C.A.; Druffel, E.R.M.; Currie, L.A., 2002. Radiocarbon measurements of black carbon in aerosols and ocean sediments. *Geochimica et Cosmochimica Acta*, vol.66, 1025 – 1036.
- Masiello, C.A. 2004. New directions in black carbon organic geochemistry. *Marine Chemistry*, vol. 92, p.201-213.
- Masiello, C.A., Louchouart, P. 2013. Fire in the Ocean. *Science*, doi: 10.1126/science.1237688.
- Meehl, G.A.; Arblaster, J.M.; Collins, W. 2008. Effects of black carbon on the Indian monsoon. *Journal of Climate*, vol.21, p.2869 – 2882.
- Mitra, S.; Bianchi, T.S.; Mckee, B.A.; Sutula, M. 2002. Black carbon from the Mississippi river: quantities, source and potential implications for the global carbon cycle. *Environmental Science and Technology*, vol.36, p.2296-2302.

- Nguyen, T.H., Brown, R.A., Ball, W.P., 2004. An evaluation of thermal resistance as a measure of black carbon content in diesel soot, wood char, and sediment. *Organic Geochemistry* vol.35, 217 – 234.
- Nguyen, B.T.; Lehmann, J.; Hockaday, W.; Josph, S.; Masiello, C.E. 2010. Temperature Sensitivity of Black Carbon Decomposition and Oxidation. *Environmental Science and Technology*, vol.44, p.3324-3331.
- Opsahl, S. ;Benner, R. 1998. Photochemical reactivity of dissolved lignin in river and ocean waters, *Limnology and Oceanography*, vol.43, p.1297– 1304.
- Preston, C.M.; Schmidt, M.W.I. 2006. Black (pyrogenic) carbon in boreal forests: a synthesis of current Knowledge and uncertainties. *Biogeosciences Discussions*, Vol.3, p.211-271.
- Ramanathan, V.; Carmichael, G. 2008. Global and regional climate changes due to black carbon. *Nature Geoscience*, vol.1, p.221-227.
- Rezende, C.E.; Pfeiffer, W.C.; Martinelli, L.A.; Tsamakis, E.; Hedges, J.I.; Keil, R.G. 2010. Lignin phenols used to infer organic matter sources to Sepetiba Bay – RJ, Brasil. *Estuarine, Coastal and Shelf Science*, vol.87, p.479-486.
- Rumpel, C; Alexis, M.; Chabbi, A.; Chaplot, V.; Rasse, D.P.; Valentin, C.; Mariotti, A. 2006. Black carbon contribution to soil organic matter composition in Tropical tropical sloping land under slash and burn agriculture. *Geoderma*, vol.130, p.35–46.
- Schmidt, M.W.I; Skjemstad, J.O; Jäger, C. 2002. Carbon isotope geochemistry and nanomorphology of soil black carbon: Black chernozemic soils in central Europe originate from ancient biomass burning. *Global Biogeochemical Cycles*, vol.16, p.71 – 77.
- Schmidt, M.W.I. 2004. Carbon budget in the black. *Nature*, vol.427,p.305-307.
- Schneider, M.P.W.; Smittenberg, R.H.; Dittmar, T.; Schmidt, M.W.I. 2011. Comparison of gas with liquid chromatography for the determination of benzenepolycarboxylic acids as molecular tracers of black carbon. *Organic Geochemistry*, vol.42, p.275-282.
- Seiler, W.; Crutzen, P.J.; 1980. Estimates of gross and net fluxes of carbon between the biosphere and the atmosphere from biomass burning. *Climatic Change*, vol.2, p.207–247.
- Skjemstad, J.O., Taylor, J.A., Smernik, R.J., 1999. Estimation of charcoal (char) in soils. *Communications in Soil Science and Plant Analysis*, vol.30, 2289 – 2298.

- Skjemstad, J.O.; Reicosky, D.C.; Wilts, A.R.; McGowan, J.A. 2002. Charcoal carbon in U.S. agricultural soils. *Soil Science Society of America*, vol.66, p.1249-1255.
- Spencer, R. G. M.; Stubbins, A.; Hernes, P. J.; Baker, A.; Mopper, K.; Aufdenkampe, A. K.; Dyda, R. Y.; Mwamba, V. L.; Mangangu, A. M.; Wabakanghanzi, J. N.; Six, J. 2009. Photochemical degradation of dissolved organic matter and dissolved lignin phenols from the Congo River, *Journal of Geophysical Research*. Vol.114, G03010, doi:10.1029/2009JG000968.
- Stubbins, A., Hubbard, V., Uher, G., Aiken, G., Law, C. S., UpstillGoddard, R. C., and Mopper, K. 2008. Relating carbon monoxide photoproduction to dissolved organic matter functionality. *Environmental Science & Technology*, vol.42, p.3271–3276.
- Stubbins, A.; Spencer, R. G. M.; Chen, H., Hatcher, P. G.; Mopper, K., Hernes, P. J.; Mwamba, V. L., Mangangu, A. M.; Wabakanghanzi, J. N.; Six, J. 2010. Illuminated darkness: molecular signatures of Congo River dissolved organic matter and its photochemical alteration as revealed by ultrahigh precision mass spectrometry, *Limnology and Oceanography*, vol.55, 1467–1477.
- Stubbins, A.; Hood, E.; Raymond, P.A.; Aiken, G.R.; Sleighter, R.L.; Hernes, P.J.; Butman, D.; Hatcher, P.G.; Striegl, R.G.; Schuster, P.; Adbulla, H.A.N.; Vermilyea, A.W.; Scott, D.T.; Spencer, R.G.M. 2012a. Anthropogenic aerosols as a source of ancient dissolved organic matter in glaciers. *Nature Geoscience*, vol.5, p. 198 – 201.
- Stubbins, A.; Niggemman, J.; Dittmar, T. 2012b. Photo-lability of deep ocean dissolved black carbon. *Biogeosciences*, vol.9, p.1661 – 1670.
- Verardo, D.J., Ruddiman, W.F., 1996. Late Pleistocene charcoal in tropical Atlantic deep-sea sediments: climatic and geochemical significance. *Geology*, vol.24, 855 – 857.
- Verardo, D.J., 1997. Charcoal analysis in marine sediments. *Limnology and Oceanography*, vol.42, 192 – 197.
- Wolbach, W.S., Anders, E., 1989. Elemental carbon in sediments: determination and isotopic analysis in the presence of kerogen. *Geochimica et Cosmochimica Acta*, vol. 53, 1637 – 1647.
- Wolff, E.W.; Cachier, H. Concentrations and seasonal cycle of black carbon in aerosol at a coastal Antarctic station. *Journal of Geophysical Research: Atmospheres*, vol.103, p.1984 – 2012.

Wotawa, G.; Trainer, M. 2000. The influence of Canadian forest fires on pollutant concentrations in the United States. *Science*, vol.288, p.324 – 328.

Zimmerman, A. R. 2010. Abiotic and Microbial Oxidation of Laboratory-Produced Black Carbon (Biochar). *Environmental Science and Technology*, vol. 44, p.1295–1301.

9 – Produção durante o doutorado

9.1 – Microbial and sponge loops modify fish production in phase-shifting coral reefs – Environmental Microbiology

9.2 - Na extensive reef system at the Amazon River mouth – Science advances

9.3 – Dissolved black carbon in the headwaters-to-Ocean continuum of Paraíba do Sul River, Brazil – Frontiers in Earth Science

9.4 – Regional aerosol emissions contribute to the riverine export of dissolved black carbon

Microbial and sponge loops modify fish production in phase-shifting coral reefs

Cynthia B. Silveira,¹ Arthur W. Silva-Lima,¹
Ronaldo B. Francini-Filho,² Jomar S.M. Marques,³
Marcelo G. Almeida,³ Cristiane C. Thompson,¹
Carlos E. Rezende,³ Rodolfo Paranhos,¹
Rodrigo L. Moura,¹ Paulo S. Salomon¹ and
Fabiano L. Thompson^{1*}

¹*Instituto de Biologia, Universidade Federal do Rio de Janeiro, Rio de Janeiro, Brasil.*

²*Departamento de Engenharia e Meio Ambiente, Universidade Federal da Paraíba, Paraíba, Brasil.*

³*Laboratório de Ciências Ambientais, Universidade Estadual Norte Fluminense, Rio de Janeiro, Brasil.*

Summary

Shifts from coral to algae dominance of coral reefs have been correlated to fish biomass loss and increased microbial metabolism. Here we investigated reef benthic and planktonic primary production, benthic dissolved organic carbon (DOC) release and bacterial growth efficiency in the Abrolhos Bank, South Atlantic. Benthic DOC release rates are higher while water column bacterial growth efficiency is lower at impacted reefs. A trophic model based on the benthic and planktonic primary production was able to predict the observed relative fish biomass in healthy reefs. In contrast, in impacted reefs, the observed omnivorous fish biomass is higher, while that of the herbivorous/coralivorous fish is lower than predicted by the primary production-based model. Incorporating recycling of benthic-derived carbon in the model through microbial and sponge loops explains the difference and predicts the relative fish biomass in both reef types. Increased benthic carbon release rates and bacterial carbon metabolism, but decreased bacterial growth efficiency could lead to carbon losses through respiration and account for the uncoupling of benthic and fish production in phase-shifting reefs. Carbon recycling by microbial

and sponge loops seems to promote an increase of small-bodied fish productivity in phase-shifting coral reefs.

Introduction

The high productivity of coral reef systems is a paradox, given their location in oligotrophic tropical waters (Odum and Odum, 1955; Gordon, 1971; Hatcher, 1988; Jantzen *et al.*, 2013). This high productivity is mainly a result of benthic primary production (performed by fleshy macroalgae, turf algae, zooxanthellate corals and epiphytic microphytes) and is sustained by complex interactions between system components that contribute to efficient nutrient recycling (Hatcher, 1990). Inputs of allochthonous organic carbon as plankton and detritus can also contribute to total net organic carbon input in reef flats experiencing unidirectional water flow (Alldredge *et al.*, 2013). Finally, benthic-pelagic coupling among the many trophic compartments is fundamental for maintaining high productivity levels (Wild *et al.*, 2004; Lesser, 2006). Carbon recycling pathways might, therefore, also play a central role in sustaining high productivity in coral reef complex trophic webs. In the microbial loop, energy stored as dissolved organic carbon (DOC) is utilized by microbes, and converted to particulate organic carbon (POC) as assimilated microbial biomass, which is thereby made available for higher trophic levels (Azam and Malfatti, 2007). Recently, another DOC recycling pathway, the so-called sponge loop, was proposed for coral reefs and other benthic environments (de Goeij *et al.*, 2013). Analogous to the microbial loop, sponges consume DOC and produce, via rapid cell shedding, large amounts of detritus, which is taken up by detritivorous organisms (De Goeij *et al.*, 2009; Alexander *et al.*, 2014).

Eutrophication, overfishing and climate change are driving the shift from coral-dominated to algae-dominated reefs all over the world (Hughes *et al.*, 2007; Sandin *et al.*, 2008; Bruce *et al.*, 2012). The loss of fish biomass and abundance, particularly of apex predators, is accompanied by shifts in benthic cover because of impaired top-down control and cascading effects on the benthic community (Jackson *et al.*, 2001; Friedlander and Demartini, 2002; Mumby *et al.*, 2006). Impaired herbivorous control leads to the increase in algae growth and the release of algal-derived dissolved compounds (Haas

Received 9 June, 2014; revised 17 March, 2015; accepted 17 March, 2015. *For correspondence. E-mail fabianothompson1@gmail.com; Tel. +55 21 39386567; Fax +55 21 39386567. Author Contributions: Study Design: FLT, CBS; Data Collection: CBS, AWSL, RBFF, JSM, TR, RLM; Analyses: CBS, RP, RBFF, MGA, CR, PSS, FLT; Manuscript Writing: CBS and FLT wrote the manuscript and all authors contributed substantially to revisions.

et al., 2011; Roff and Mumby, 2012). This, in turn, enhances microbial activity at the coral–algae interface causing the mortality of corals and further algae growth (Smith *et al.*, 2006). Positive feedbacks of algae dominance and coral loss are therefore established (Barott *et al.*, 2011; Barott and Rohwer, 2012). Chemical cues released by algae repulse coral and fish juveniles (Dixon *et al.*, 2014), and DOC released by coral and distinct algal functional groups differentially stimulate planktonic microbial metabolism (Haas *et al.*, 2011; 2013; Nelson *et al.*, 2013). However, the role of benthic productivity and DOC recycling for higher trophic levels in the context of phase-shifting reefs has never been addressed.

While most studies concerning coral reefs focus on Caribbean and Pacific reefs, South Atlantic reefs are far less investigated, although they are key environments regarding biodiversity. They show high endemism levels (approximately 25% in fish and 50% in corals) concentrated in a small reef area (5% of West Atlantic reefs) regardless of their low richness (Moura, 2002). The Abrolhos Bank, an extension of the eastern Brazilian continental shelf (approximately 46 000 km²), comprises the largest and richest reefs of the South Atlantic, with at least 20 species of corals, including six that are endemic to Brazil (Leão *et al.*, 2003). The Abrolhos region sustains intensive fisheries that significantly affect the reef community (Francini-Filho and de Moura, 2008; Francini-Filho and Moura, 2008) and is currently experiencing an expansion of activities, such as oil/gas mining, dredging/shipping and shrimp farming. High levels of inorganic nutrients were correlated to higher macroalgae cover and also higher pelagic chlorophyll *a* concentration in these reefs (Costa *et al.*, 2008). However, no significant differences in nutrient concentrations and chlorophyll *a* were found among coastal and offshore reefs in the Abrolhos Bank (Bruce *et al.*, 2012). In contrast with other reef systems worldwide, the Abrolhos reefs thrive in chlorophyll- and nutrient-rich waters, which are at least 10-fold higher in nitrogen and phosphorous than the suggested eutrophication threshold concentration (Bruce *et al.*, 2012).

Elucidation of the energy fluxes within coral reef trophic webs is a key step for unveiling the impacts of anthropogenic activity and global changes on coral reef ecosystems. Low biomass and abundance of large herbivorous reef fish was recorded in macroalgae-dominated, low coral cover reefs in Abrolhos (Francini-Filho and de Moura, 2008). However, the outcome of changes in benthic primary production and carbon recycling on higher trophic levels is still unclear. Here we investigated changes in the planktonic and benthic productivity in the context of reef phase-shifting and the role of benthic–pelagic coupling for carbon recycling through microbial utilization of benthic-derived DOC.

We performed a broad sampling strategy, covering approximately 800 km², through different coral reef and rocky shore areas along the Abrolhos Bank experiencing different levels of natural and human-induced impacts. These included coastal reefs subject to terrigenous influence, offshore reefs, and reefs located inside both well-enforced (since 1983) and non-enforced marine protected areas (MPAs). We estimated the contribution of the main benthic primary producers (turf algae, fleshy algae, scleractinian corals and zoanthids) and that of phytoplankton to reef primary production. The effect of primary productivity changes on fish biomass production was then estimated by building a trophic web model that incorporates the microbial and sponge loops. This is the first study to integrate primary production, DOC release, and carbon recycling by bacterial and sponge loops to make predictions about the productivity of fish communities on coral reefs. We show contrasting microbial carbon metabolism in algae- and coral-dominated reefs, and enhanced biomass production of small-bodied, omnivorous and invertivorous fish through benthic DOC recycling in algae-dominated reefs.

Results

Primary planktonic production

One-way analysis of variance (ANOVA) showed no significant difference in inorganic nutrient concentrations among the reef areas, tested by clustering together sites within the same reef (Supporting Information Table S1). Chlorophyll *a* concentrations did not differ among the sites of each reef area for each time point according to one-way ANOVA (Fig. 1A). Sites were therefore grouped into reef areas for subsequent analysis (Fig. 1B). Parcel dos Abrolhos (PAB) reefs, located inside a well-enforced MPA (Figure S1), presented the highest chlorophyll *a* concentration. No significant difference was detected among Parcel das Paredes, Sebastião Gomes, Timbebas and Archipelago. Phytoplankton net primary production derived from chlorophyll *a* and irradiance made a significantly greater contribution to the total primary production in PAB reefs, with an average contribution of 16%, compared with 4% in the other reef areas (Table 1). DOC concentrations showed no significant difference among sites at different times (Fig. 1C) or among reef areas using grouped sites (Fig. 1D). Prokaryotic cell abundances showed no clear tendency of increase or decrease (Fig. 1E) and no significant difference among sites (Fig. 1F). Prokaryotic cells were discriminated as autotrophs and heterotrophs (Supporting Information Fig. S3A), showing a remarkable dominance of heterotrophs in all studied sites, comprising 80–90% of the total prokaryotic community. The fractions of heterotrophic prokaryotic cells with high nucleic acid content and with low nucleic acid content were close to

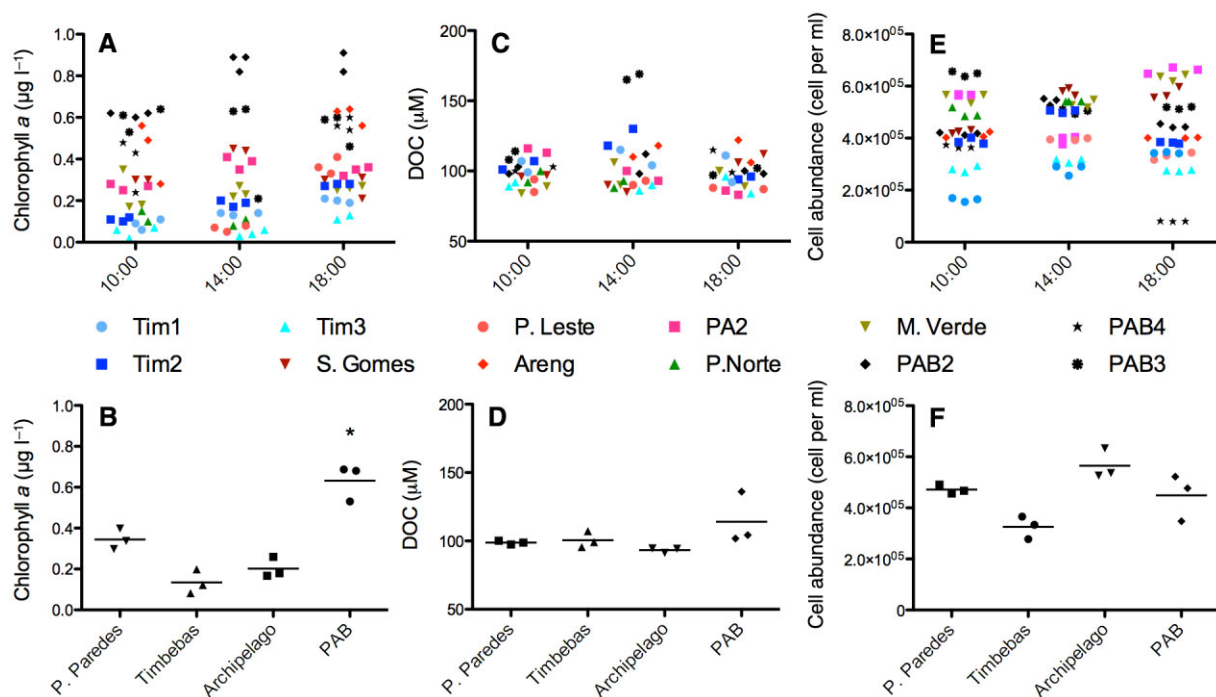


Fig. 1. Abrolhos Bank planktonic productivity parameters. Chlorophyll *a* (A and B), DOC concentration (C and D) and prokaryotic cell abundance (E and F) at different times of the day (A, C and E) and for different reefs (B, D and F). Reef sites are shown in A, C and D; $n = 3$ for each time point in each reef ($n = 9$ for each reef in total); reef areas are shown in B, D and F, where reef sites were grouped according to its area and each point in the graph is a time point ($n = 36$ for Parcel das Paredes, $n = 27$ for Timbebas, $n = 18$ for Archipelago and $n = 27$ for PAB).

50% in all the studied reefs, indicating an actively reproducing prokaryotic community (Supporting Information Fig. S3B). The abundance of planktonic heterotrophic prokaryotes showed a significant positive correlation ($r^2 = 0.08$, $P = 0.0063$) with the phytoplankton biomass derived from chlorophyll *a* concentration (Fig. 2A). Additionally, the variation in chlorophyll *a* concentration between two time points within a day had a positive correlation to the variation in heterotrophic prokaryotes abundance during the same time period (Fig. 2B).

Benthic production

Gross photosynthetic production ranged from 269 mg C m⁻² h⁻¹ for crustose coralline algae (CCA) to 589 mg C m⁻² h⁻¹ for *Dyctiopteris plagiogramma*, a fleshy macroalgae, and was within the range observed for reef organisms and communities previously studied (Table 2). Corals and macroalgae showed the highest gross photosynthetic activity, followed by *Palythoa caribaeorum* (a zoanthid), turf algae and CCA. When corrected for benthic surface cover, turf and fleshy algae were the main primary producers per square meter. Reefs with the highest benthic production were Pedra de Leste and Mato Verde (Table 1), with 71 to 388 mgC m⁻² h⁻¹ and 66 to 383 mgC m⁻² h⁻¹ respectively. Benthic net primary pro-

duction ranged from 24.8 to 379.7 mgC m⁻² h⁻¹ in PAB reefs. Benthic production corresponded to the largest fraction of total reef primary production, ranging from 82.0% in PAB4 to 98.3% in Pedra de Leste, and averaging $95 \pm 4.8\%$ (SD) for Abrolhos.

Corals and phytoplankton contributed to a larger fraction of primary production per square meter in PAB reefs (up to 51 and 16 mgC m⁻² h⁻¹, representing 8% and 17.9% of total production, respectively) compared with Parcel das Paredes (up to 23 and 4.7 mgC m⁻² h⁻¹, representing 3.3% and 4.5%, respectively). In contrast, macroalgae contributed to a larger fraction of the primary production in Parcel das Paredes (25.4%) while contributing to only 0.6% of the production in PAB.

Benthic DOC release and bacterial growth

Incubation bottles with benthic organisms showed a significant increase in DOC concentration compared with the ambient seawater concentration (Table 3, values corrected for controls). Higher DOC release rates were found for fleshy macroalgae, 274 and 806 µmolC dm⁻² h⁻¹ (± 80 and ± 205 , SE) for P. Norte and P. Leste respectively. *Mussismilia braziliensis*, a scleractinian coral, and *P. caribaeorum* presented similar DOC release rates within the same reef site. However, release rates of corals

Table 1. Minimum and maximum estimated biomass and net primary production (NPP) of planktonic and benthic compartments and fish biomass in Abrolhos reefs.

Site	Phytoplankton biomass (mg C m ⁻²) ^a	Phytoplankton NPP (g C m ⁻² year ⁻¹) ^a	Heterotrophic bacterioplankton biomass (mg C m ⁻²) ^b	Benthic biomass (g C m ⁻²) ^c	Benthic NPP (g C m ⁻² year ⁻¹) ^c	Fish biomass (g C m ⁻²) ^d
S. Gomes	15–175	6.9–24.9	26.2–27.6	16.5–108.9	202.6–1515.6	0.68–0.97
Arengueira	16–190	7.6–27.1	30.1–31.7	14.9–90.7	126.1–1437.6	2.80–3.94
PA2	34–405	16.1–57.8	25.6–26.9	9.9–75.0	170.8–1362.2	3.22–4.54
P. Leste	9–110	4.4–15.8	16.0–16.8	29.8–179.4	314.5–1705.9	1.08–1.52
Tim 1	10–124	4.9–17.7	21.9–23.1	7.4–62.3	163.5–1308.5	6.48–9.13
Tim 2	17–202	8.0–28.7	43.6–45.9	13.3–91.1	171.0–1708.2	3.49–4.92
Tim 3	5–68	2.7–9.7	29.8–31.4	13.0–85.0	144.0–1508.0	9.73–13.90
P. Norte	8–97	3.8–13.8	41.6–43.8	6.9–56.4	142.7–1505.7	10.07–14.17
M. Verde	14–163	6.4–23.2	36.8–38.7	17.8–124.3	290.8–1683.0	13.06–18.39
PAB 2	85–995	39.6–141.8	53.0–55.8	11.2–94.3	248.1–1665.4	9.49–13.36
PAB 3	57–672	20.6–73.7	67.2–70.7	8.4–62.7	127.7–1274.3	7.04–9.92
PAB 4	57–667	26.6–95.3	30.9–32.5	16.3–94.1	108.8–1653.9	15.80–22.31
Abrolhos	29–337	13.4–48.1	35.2–37.1	14.1–94.7	184.2–1527.4	6.92–9.74

a. Based on chlorophyll *a* concentrations, *n* = 9 for each reef.

b. Based on bacterial abundance, *n* = 9 for each reef.

c. Based on FSIII quantum yield (*n* = 42 to 125 for each organism) and photoquadrats (*n* = 10 for each organism; Francini-Filho *et al.*, 2013).

d. Based on fish counts (*n* = 10 for each reef; Francini-Filho and de Moura, 2008).

and zoanths were significantly higher at P. Leste ($P = 0.0486$). Although fleshy macroalgae DOC release was higher than the other benthic organisms, a negative correlation between DOC concentrations in the ambient water column and algae cover was observed (Fig. 3A). An increase in bacterial abundance was observed for all treatments compared with controls; however, bacterial cell yield was significantly higher on the fleshy macroalgae-derived DOC at both P. Norte and P. Leste (5 and 17×10^5 cell per $l^{-1} h^{-1}$, respectively), and on zoanthid DOC at P. Leste (1×10^5 cell per $l^{-1} h^{-1}$) (Table 3). Bacterial oxygen demand was highest for fleshy algae treatments, although all three treatments were significantly higher than the controls. Bacterial growth efficiency (BGE, i.e. the ratio of bacterial biomass carbon to bacterial carbon demand) displayed a distinct pattern between the two reef sites. At P. Leste, BGE was higher for macroalgae incubations, while corals and zoanths exhibited no significant difference in comparison with the controls. At P. Norte, in contrast, all three treatments showed significantly lower BGE compared with the controls. No

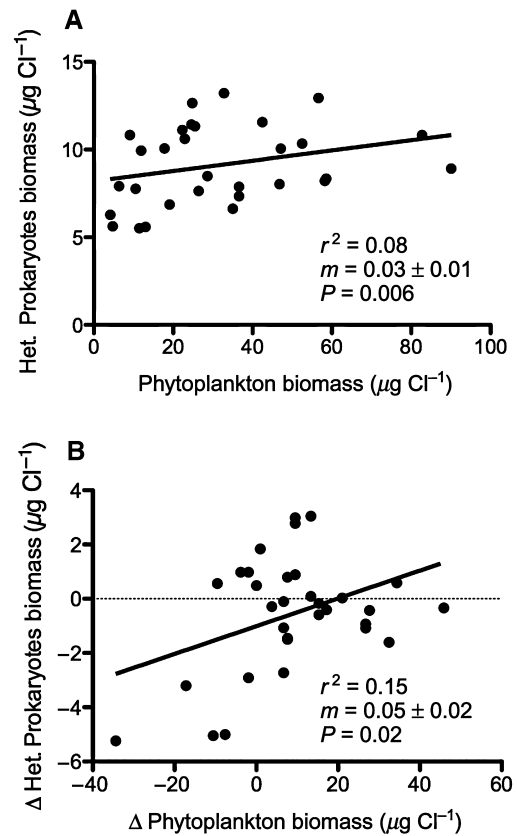


Fig. 2. Phytoplankton and bacterioplankton coupling. Correlation between phytoplankton biomass and bacterioplankton biomass (A) and the change of phytoplankton biomass and bacterioplankton biomass throughout the day (B) at all sites surveyed.

Table 2. Net primary production.

Organism/site	Primary production	Reference
Gross production (mg C m ⁻² h ⁻¹)		
<i>Orbicella annularis</i> (<i>Montastrea annularis</i>)	400	Patterson <i>et al.</i> , 1991
<i>Palythoa</i> sp.	1500	Tun <i>et al.</i> , 1997
Turf algae	360–930	Rogers and Salesky, 1981
CCA	230–430	Wanders, 1976
<i>Mussismilia braziliensis</i>	510	This study
<i>Palythoa caribaeorum</i>	507	This study
<i>Dictyopteris plagiogramma</i>	589	This study
Turf algae	381	This study
CCA	269	This study
Net community production (mmol C m ⁻² day ⁻¹)		
Marshall Islands	0–720	Smith and Marsh, 1973
Guam	320	Marsh, 1974
Great Barrier Reef	192–198	Kinsey and Davies, 1979; Barnes and Devereux, 1984
Moorea	0–288	Allredge <i>et al.</i> , 2013
Abrolhos	0–250	This study

Primary production for individual benthic species and reef communities (planktonic included, but considered as a minor fraction) measured by changes in oxygen concentration (previous research) and estimated by PAM fluorometry (this research).

significant correlation was found between the reef water column bacterial abundance and the algae cover (Fig. 3B).

Trophic web model

The protected reefs of PAB and the highly impacted coastal reefs of Parcel das Paredes showed remarkably distinct trends of carbon transfer through the trophic web (Supporting Information Fig. S5). Although the range of omnivorous and herbivorous/corallivorous fish biomass production was similar for both reefs, the observed fish biomass in Parcel das Paredes differed from that estimated by the model. In contrast, in PAB reefs the observed relative fish biomass in each trophic group was proportional to the carbon production for each trophic group predicted by the model (Supporting Information Table S3) (Francini-Filho and de Moura, 2008). Of all fish trophic groups, the largest net production was observed for herbivorous/corallivorous fish (2–15 mg C m⁻² h⁻¹), which feed directly on benthic primary producers, such as corals, CCA and fleshy macroalgae. These comprise mainly the parrotfishes *Scarus trispinosus*, which dominate the fish assemblages in the Abrolhos Bank (Francini-Filho and de Moura, 2008). This coupling of fish and benthic primary production was not observed for Parcel das Paredes. A higher proportion of herbivorous/corallivorous fish production (59.7–71.9% of total fish production) was predicted as a result of the enhanced primary production because of high algae cover. However, the actual biomass of these fish is much lower (47.5%, Supporting Information Table S3). Omnivorous fish showed the opposite trend, with the observed biomass (~30%) exceeding the fraction theoretically supported by primary production in the primary production-

derived model (18–22%). From the production rates calculated for PAB reefs (considering these as no-take areas), and considering that apart from fishing activities the turnover rates in both reefs are equal, we could expect 11.5 g C m⁻² of total fish biomass in Parcel das Paredes, much more than the observed biomass of 2.3 g C m⁻².

The role of microbial and sponge loops in the channeling of benthic-derived carbon to higher trophic levels was then implemented in the primary production and carbon recycling-based model (Fig. 4). The gap between fish production predicted by the model and the actual biomass was remarkably decreased in Parcel das Paredes reefs when using the second model (Supporting Information Table S3). Relative net production of herbivorous/corallivorous fish decreased to 2–12 mg C m⁻² h⁻¹ (49% of fish production), while omnivorous production increased to 1.6–1.8 mg C m⁻² h⁻¹ (approximately 36% of total fish production) in Parcel das Paredes, approaching the observed relative biomass of these two compartments (47.52% and 30% for herbivorous/corallivorous and omnivorous respectively). Although the model with microbial and sponge loops fits both reef areas, larger changes were observed in Parcel das Paredes reefs in comparison with the primary production-based model as result of the high fleshy macroalgae and turf algae cover in these sites, as well as the higher DOC release rates of the benthic organisms.

Discussion

Phytoplankton production in Abrolhos was approximately 20 times higher than the production of reefs in other oceanic regions (Odum and Odum, 1955; Hatcher, 1990; Allredge *et al.*, 2013). Primary planktonic production

Table 3. DOC release rates by benthic organisms, bacterial cell yield, oxygen demand and bacterial growth efficiency in incubation bottles.

Organism	Site	DOC release ($\mu\text{molC dm}^{-2} \text{h}^{-1}$)			Bacterial cell yield ($10^5 \text{ cell per l}^{-1} \text{h}^{-1}$)			Bacterial oxygen demand ($\mu\text{mol l}^{-1} \text{h}^{-1}$)			Bacterial growth efficiency		
		Average	t-test (P)	Tukey	Average	t-test (P)	Tukey	Average	t-test (P)	Tukey	Average	t-test (P)	Tukey
Algae	P. Norte	274.15 ± 80.0	0.0098	A	5.06 ± 1.51	0.0261	A	13.3 ± 1.38	< 0.0001	A	0.06 ± 0.01	0.0388	ns
	P. Leste	806.63 ± 205.82	0.0086	A	16.8 ± 2.75	0.0015	A	17.4 ± 1.27	< 0.0001	A	0.14 ± 0.01	0.008	A
	P. Norte	28.03 ± 6.89	0.0038	B	1.01 ± 0.37	0.8366	B	5.80 ± 1.34	0.0054	B	0.03 ± 0.02	0.0331	ns
Coral	P. Leste	68.30 ± 18.43	0.0027	B	3.15 ± 1.28	0.0588	B	9.73 ± 2.03	0.0055	B	0.05 ± 0.02	0.5124	B
	P. Norte	28.06 ± 7.07	0.0008	B	1.43 ± 0.32	0.6877	B	7.96 ± 1.76	0.0043	AB	0.03 ± 0.01	0.0321	ns
Zoanthid	P. Leste	77.52 ± 1.70	0.0098	B	1.00 ± 0.04	< 0.0001	B	3.11 ± 0.49	0.0022	C	0.05 ± 0.01	0.1574	B
	P. Norte	0.17 ± 0.17	-	-	0.45 ± 0.42	-	-	0.09 ± 0.15	-	-	0.57 ± 0.28	-	-
Control	P. Norte	0.15 ± 0.03	-	-	0.13 ± 0.02	-	-	0.54 ± 0.10	-	-	0.04 ± 0.01	-	-

Two-tailed t-test P values are reported for comparisons of each treatment to controls, bold indicates significant differences. Tukey's tests are reported comparing means among treatments within the same reef (different letters indicate a significant difference, $n = 4$; Average is shown followed by standard error).

accounted for 1.9–12.2% of total net production in Abrolhos, except for PAB reefs, where planktonic production accounted for 17.9%, a large fraction of the total production. The high planktonic primary production observed at Abrolhos reefs can be considered the result of high nutrient and light availability and limited water circulation. High proportion of genes associated with autotrophy has been found in the microbial plankton of healthy, coral-dominated reefs, in contrast to a high proportion of heterotrophic metabolism genes in impacted reefs (Dinsdale *et al.*, 2008; Bruce *et al.*, 2012). Altogether, these data suggest that planktonic autotrophic metabolism is a proxy of healthy reef systems. Whether this is a global trend in healthy reefs needs to be tested in coral reefs from distinct geographical areas.

Although the sampled area comprises reefs experiencing distinct levels of continental runoff influence and management regimes, nutrients concentrations showed no significant difference among reef areas. Therefore, we cannot attribute changes in the productivity within Abrolhos reefs to human driven-eutrophication (Gruner *et al.*, 2008). This is discordant to previous observations, in which coral reefs extensively subjected to human activities usually show higher nutrient concentrations (Dinsdale

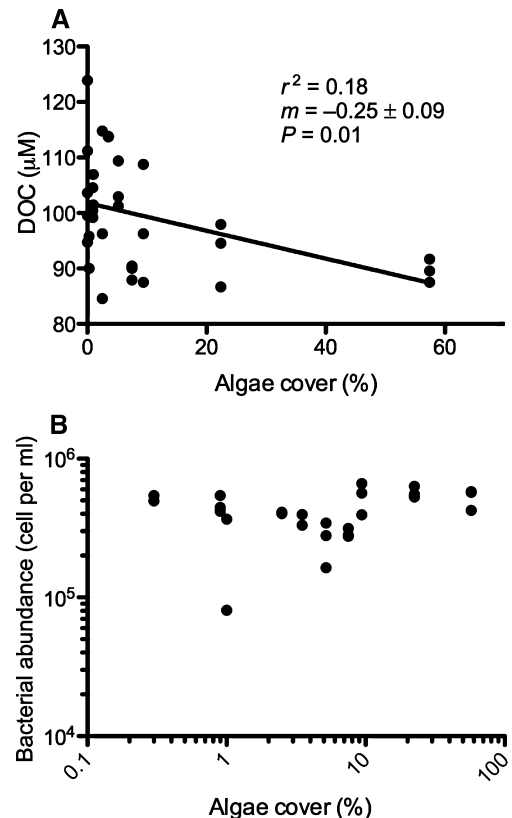


Fig. 3. Algae cover, DOC and bacterial abundance. Correlation between the algae cover and the water column DOC concentrations (A) and the bacterial abundance (B).

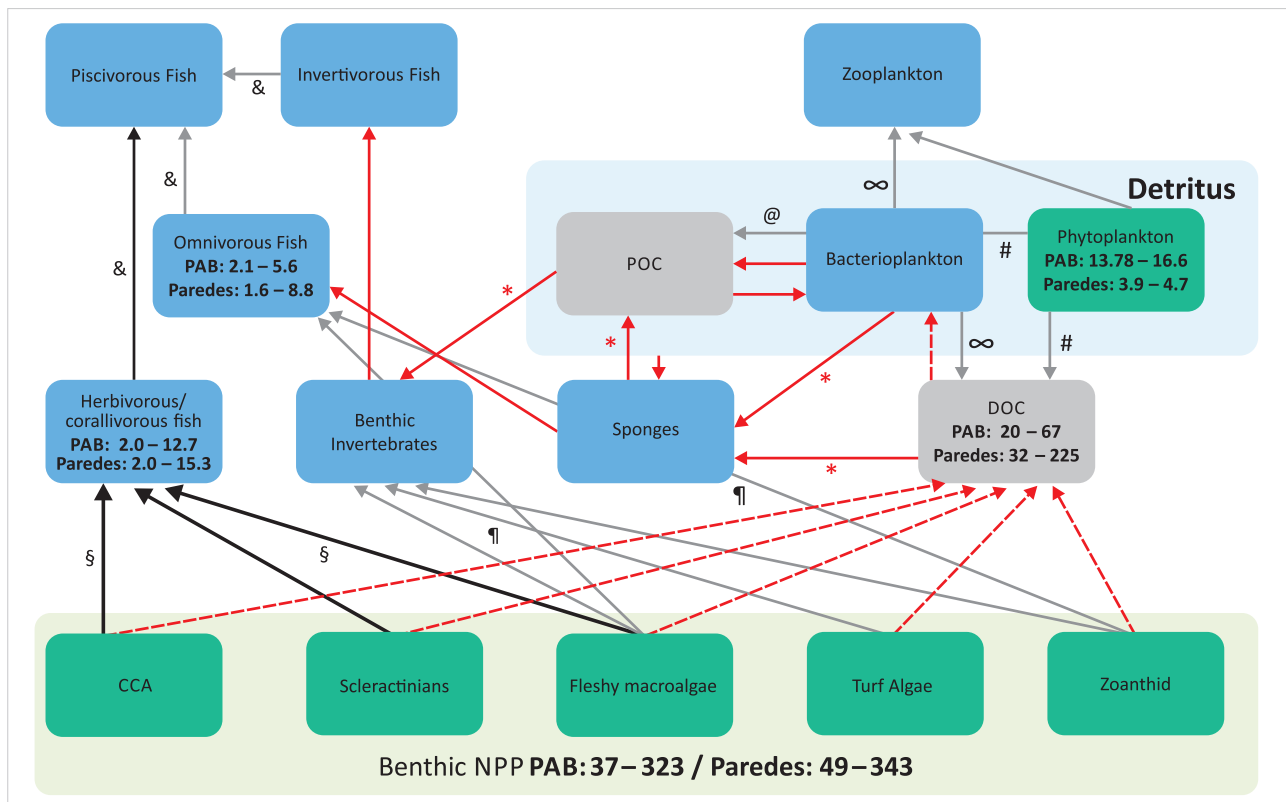


Fig. 4. Abrolhos reefs trophic web model. The diagram represents the conceptual structure of primary production and carbon recycling-based trophic model, which includes bacterial and sponge loops. Green compartments represent primary producers, blue represent consumers and gray represent DOC and POC pools. Black and grey arrows indicate transfers between the compartments shared by this model and the primary production-based model. Thick solid black arrows indicate the main carbon flux from benthos to fish in healthy reefs (i.e. Parcel dos Abrolhos). Red lines indicate benthic DOC flux through the microbial and sponge loops, exclusive of the primary production and carbon recycling-based model. Dashed red arrows indicate DOC release rates by the benthic organisms to the water column, whereas solid red arrows emphasize DOC recycling by microbial and sponge loops and subsequent channeling to fish. Gray arrows indicated the transfer fluxes with no significant differences between primary production-based and primary production and carbon recycling-based models. Values inside boxes are the net productivity of each compartment in $\text{mg C m}^{-2} \text{h}^{-1}$. Interactions and fluxes among the various compartments of the model were obtained from ¶ (Ferreira and Gonçalves, 2006; Francini-Filho *et al.*, 2009); * (de Goeij *et al.*, 2013); # (Agustí and Duarte, 2013); @ (Suttle, 2005); ∞ (Fuhrman and Noble, 1995); § (Francini-Filho *et al.*, 2009); & (Freitas *et al.*, 2011; Gathaz *et al.*, 2011).

et al., 2008; Kaczmarek and Richardson, 2011). The rapid uptake of inorganic nutrients by phytoplankton and benthic primary producers could account for the lack of differences in inorganic nutrient concentrations between sites with expected differences in runoff (Furnas *et al.*, 2005).

Exudates of benthic primary producers promote bacterioplankton growth

Although a significant correlation was found between C-phytoplankton and C-bacterioplankton in our data, the low coefficient of determination ($r^2 = 0.08$) indicates a weak coupling between these two compartments. The bacterioplankton is likely relying on DOC from an alternative source e.g. exudates of benthic primary producers, besides plankton-derived DOC. Such a weak linkage between bacteria and phytoplankton has been previously documented in the oligotrophic areas of a coral reef lagoon

in the South Pacific (Rochelle-Newall *et al.*, 2008). Likewise, Tanaka *et al.* (2011) did not find a correlation between the abundance of phytoplankton and DOC concentrations at a fringing reef in Ishigaki, Japan and concluded that the DOC pool was rather fuelled by the DOC release of the benthic primary producers. The fuelling of bacterioplankton communities by benthic-derived DOC seems to be a common feature in coral reefs. Gross primary production estimated for the Abrolhos benthic compartment was between 42 and 348 $\text{mgC m}^{-2} \text{h}^{-1}$. Daily net primary production ranged from 0 to 253 $\text{mmolC m}^{-2} \text{day}^{-1}$, as the whole reef can become net heterotrophic because of nighttime respiration rates. These values are within the production range of 0–720 $\text{mmolC m}^{-2} \text{day}^{-1}$ found for other reefs in the Atlantic, Pacific and Indic Oceans (Table 2) (Alldredge *et al.*, 2013).

Benthic DOC release rates followed the pattern observed for the Red Sea and Pacific Ocean reefs, with

fleshy macroalgae releasing significantly more DOC than corals. However, overall DOC release rates were higher in Abrolhos than in those reefs (Wild *et al.*, 2010; Haas *et al.*, 2011). Because of the relatively short acclimatization period it cannot be excluded that potential injuries or the handling prior to the incubations artificially increased the observed release rates (Mueller *et al.*, 2014b). The lower BGE of the water column microbial community observed in the highly impacted P. Leste reefs compared to the protected P. Norte reefs suggests that these communities are adapted to the distinct benthic DOC release rates in the two reefs. Higher availability of DOC at P. Leste could cause the bacterial community to have lower BGE, depleting DOC at higher rates and releasing more inorganic carbon through respiration, compared with the bacterial community at P. Norte (Haas *et al.*, 2011; 2013). This could explain the lack of differences in DOC concentrations between the two sites despite the higher algae cover and higher DOC release rates at P. Leste. Low DOC concentrations in high algae cover areas were also observed previously, while high DOC concentrations were found on pristine sites in the Line Islands (Dinsdale *et al.*, 2008). Co-metabolism of refractory and labile algae-derived DOC with low BGE is claimed to drop DOC concentrations. Higher DOC release by algae in the impacted reefs observed here may also stimulate the growth of opportunistic bacterial strains with high growth rates, maintaining low DOC concentrations and high detritus content in the form of bacterial cells (Haas *et al.*, 2011; 2013; Pedler *et al.*, 2014). Some of these opportunistic bacteria can be associated to coral diseases, fuelling the mechanism of positive feedback for coral mortality and macroalgae growth (Barott and Rohwer, 2012; Nelson *et al.*, 2013). The different BGE in both reef areas described here could be either due to different bacterial community composition or similar bacterial community composition with distinct metabolic repertoires (Nelson *et al.*, 2013; Kelly *et al.*, 2014). Because of relative size, community abundance and high per cell activity, changes in microbial biomass and metabolism may signal a large reallocation of available energy in an ecosystem: the microbialization of the coral reef (McDole *et al.*, 2012).

Microbial and sponge carbon recycling pathways are enhanced in unprotected reefs

Fish biomass predicted by the primary production-based trophic model overestimated actual observed fish biomass at Parcel das Paredes reefs (impacted reef sites) by approximately 9 gC m^{-2} . The overestimation is much greater than what could be attributed to fishery activity using catch rates of $1.67\text{--}1.86 \text{ gC year}^{-1} \text{ m}^{-2}$ from Corumbau, a reef area in close proximity with a similar reef community structure and similar fishing activity (Alves

et al., 2012). The observed discrepancy between modelled and actual fish production could be due to (i) an underestimate of catch rates for Abrolhos, (ii) the lack of an important trophic group, (iii) feeding behaviour or (iv) non-trophic interaction in the model (Kéfi *et al.*, 2012). In coral reefs, particulate organic matter formation, sinking and recycling by benthic communities through filter-feeding and particle-feeding is known to sustain high productivity (Anthony, 2000). Bacterial growth on DOC and direct DOC uptake coupled to high rates of cell shedding by sponges, the highest known for animals, has recently been shown to significantly increase the amount of particulate carbon in reef systems (de Goeij *et al.*, 2013). Carbon channeling to higher trophic levels through microbial and sponge loops was therefore implemented in a second model that included carbon recycling. These loops enhanced the biomass of invertivorous and omnivorous fish, through two different ways: (i) by the increase of food availability to spongivores of the *Pomacantidae* family, which represent a significant proportion of the omnivorous fish in Abrolhos [up to 91% (Francini-Filho and de Moura, 2008) and (ii) by cell shedding, which feeds detritivorous invertebrates, and ultimately invertivorous fish (Supporting Information Table S3). The pronounced difference between the two models in Parcel das Paredes reefs emphasizes the role of the sponge and microbial loops in the recycling of detritus that sustains the high omnivorous fish biomass in highly impacted reefs. This mechanism seems to play a role in the bottom-up control of relative fish biomass in addition to the known top-down effects of fisheries activities in selecting the large body size herbivores and apex predators over the small body size omnivorous (Newman *et al.*, 2006). It is important to note that the DOC fluxes from the benthic organisms to the water column in our model could be underestimates, because turf algae are known to be one of the benthic primary producers with the highest DOC release rates, whereas rates in the range normally observed for macroalgae were used here (Haas *et al.*, 2011; 2013). In contrary, DOC fluxes can be overestimated because of the short acclimation times (Mueller *et al.*, 2014a). The discrepancy between the primary production-based and primary production and carbon recycling-based models regarding fish productivity highlighted the importance of the sponge loop for carbon flow in trophic webs of the Abrolhos reefs. This needs to be assessed by experimental data in future studies, because its relative importance to the food web might differ from that observed in Caribbean reefs systems.

Fishery activity may have been an important driver of benthic composition and microbial metabolism shifting

It has been shown that the depletion of functionally important consumer species through exploitation can indirectly

influence coral reef ecosystem structure and function (Dulvy *et al.*, 2004; Newman *et al.*, 2006). Alteration in benthic cover patterns has been attributed to massive declines in fish biomass in the Caribbean and Pacific (Sandin *et al.*, 2008; Paddack *et al.*, 2009). At a global scale, herbivores reduce producer abundance by 68% on average, and this effect varies mainly among producer functional groups, with the filamentous and frondose macroalgae showing a higher response ratio than the crustose and calcareous algae (Poore *et al.*, 2012). Extrapolating the coral response ratio to coralivorous fish from the calcareous algae response to herbivorous fish, we could expect that lower abundance of herbivorous in non-managed Abrolhos reefs will result in faster turf and fleshy algae growth, although these fish consume all three of these three primary producer groups. Indeed, a negative correlation was observed between herbivorous/coralivorous fish biomass and macroalgae cover in Caribbean and Indo-Pacific reefs (Roff and Mumby, 2012), and also for Abrolhos, when examining turf and fleshy algae cover together (Supporting Information Fig. S6). Therefore, fishery activity may have been an important driver of the benthic composition shift in Abrolhos. Whether lower herbivory pressure at the impacted reefs is driving benthic organisms to release a higher proportion of their primary production as DOC, as observed in P. Leste, needs to be determined. Long-term adaptation of the microbial community to high DOC release rates, translated as low growth efficiency, could therefore intensify carbon loss in the food web.

A study of more than 300 surveys of shallow coral reefs from nine countries across the Indian Ocean, including Mozambique, Kenya and Tanzania, within protected and unprotected areas indicated that fish biomass of at least 85 g m⁻² appears to be necessary to maintain the reef health of Indian Ocean reefs (McClanahan *et al.*, 2011). In the Abrolhos Bank, the fish biomass ranges from approximately 50 to 150 g m⁻², with the lowest values occurring in the unprotected areas (Sebastião Gomes and Pedra de Leste) and the highest values occurring in the well-enforced protected areas (PAB). The impact of carbon recycling by microbial and sponge loops on fish biomass described here can be considered one of the frequently unexpected consequences of overfishing because of the complex nature of the species interactions and the lack of knowledge about the results of punctual disturbance (Żychaluk *et al.*, 2012; Travis *et al.*, 2014).

Caveats

One matter that could be considered a caveat in this study is the use of a strictly bottom-up model based on primary productivity, not taking in consideration the effects of top-

down controls such as fisheries. The reason for taking this approach was to test if fisheries activities could explain the differences between the biomass sustained by the system (calculated by the model) and the actual fish biomass. The model is intended to be bottom-up as a form of estimating how much fish biomass the system could sustain considering the primary production. Fish catch rate underestimates and differences in fishing activities between reef areas could also substantially influence the model interpretations. These errors are expected to be minor here as the catch rate assessments used were based on three different sampling designs covering a large reef area (Alves *et al.*, 2012). By including the microbial and sponge loop (in the carbon recycling-based model), we could improve our model and better explain the differences. A second caveat could be the relative importance of the sponge loop to the food web. The abundance of cryptic sponges, the capability of these sponges to utilize DOC, as well as their detritus production rates need to be quantified in the Abrolhos reefs in future studies in order to make appropriate comparisons to Caribbean reefs systems.

The use of the theoretical 4:1 ratio for electron flux : oxygen production for pulse amplitude modulated (PAM)-based photosynthesis estimates can also be considered a caveat, as this ratio has been shown to increase in macroalgae under high irradiances (Beer and Axelsson, 2004). This is not considered an important error in this study given the irradiances found in the Abrolhos reefs, leading to low electron leakage and cyclic photophosphorylation and allowing reliable estimates of gross carbon fixation. The gross carbon fixation is also a maximum theoretical value, which the O₂ evolution method relies on. To minimize subsequent overestimates of net production, we calculated the ranges of minimum and maximum net primary production estimates from the gross production estimates. This is the first time that PAM fluorometry is applied to vast reef areas to estimate primary production, providing remarkably large spatial coverage.

Furthermore, the benthic cover and fish biomass data used here are not contemporary with the planktonic and benthic production data, but instead were obtained previously (Francini-Filho *et al.*, 2013). This may be considered a caveat because benthic cover and fish biomass could change over time. However, it should be noted that this dataset was proven numerically and spatially robust in its original publication. It is also important to note that the web models explored in the present study were based on trophic relationships described in the literature and that realistic trophic transfer assumptions were used, such as the amount of net production at each trophic group that is transferred to higher trophic levels (10%). Nevertheless, these assumptions are widely applied to ecological

models and generate important baselines for the understanding of ecosystem functioning.

Concluding remarks

The comprehensive quantitative data presented here on reef productivity and trophic web interactions demonstrate the role of detritus production through the microbial and sponge loops in enhancing the relative biomass of omnivorous and invertivorous fishes. In the impacted, phase-shifting reefs, carbon cycling via the microbial and sponge loop appear to become increasingly important. The recycling process adds a bottom-up control of carbon fluxes in coral reefs, in addition to the top-down control exerted by fishing activity on the observed fish biomass. We also establish important baselines for ecological predictions of the Abrolhos reefs' responses to global changes and for the management of these reefs. The uncoupling between the fish biomass and the primary production observed in unprotected reefs suggests their advanced degradation stage.

Experimental procedures

Study sites

Twelve sites, within four different reef areas covering reefs under different management regimes, 25–70 km off the coast, were analysed in this study (Supporting Information Fig. S1). In Parcel das Paredes (1) unprotected reefs, four sites were sampled: Sebastião Gomes, Pedra de Leste, PA2 and Arengueira. These are unprotected coastal reefs located close to fishermen and main municipalities along the coast (Nova Viçosa, Caravelas and Alcobaça). In Timbebas (2), a poorly enforced Marine Protected Area (MPA), three sites were sampled: Tim1, Tim2 and Tim3. In Archipelago (3), rocky shore reefs located inside an enforced MPA, two sites were sampled Mato Verde and Portinho Norte. In PAB reefs (4) located inside an enforced MPA, three sites were sampled: PAB2, PAB3 and PAB4. Timbebas, Archipelago and PAB are within the National Marine Protected Area and enforcement is performed by the Brazilian Environmental Agency (ICMbio). Measurements were performed on the top of chapeirões, mushroom-like reef structures characteristic of Abrolhos reefs. These reef structures are mainly built by *M. braziliensis* (70% of the chapeirão framework), a coral species endemic to Abrolhos. Surveys were performed from 1 February to 17 February 2012 under a federal government license (SISBIO no. 27147-2).

Planktonic biomass and primary production

Water samples were taken by SCUBA diving on the top of each chapeirão, approximately 1 m above the benthic community (3–7 m deep depending on the site), three times a day: at 10:00, 14:00 and 18:00 h. For each sample, three 2 l aliquots of bulk seawater were sampled using Niskin bottles

and filtered onboard through 0.45 µm pore-size ester-cellulose filters (Millipore, Billerica, MA, USA). Filters were immediately frozen and stored in liquid nitrogen until analysis. In the laboratory, filters were then extracted overnight in 90% acetone at 4°C and analysed by fluorometry for chlorophyll *a* concentration using a Turner Designs TD-700 fluorometer (Sunnyvale, CA, USA). A carbon to chlorophyll *a* ratio of 15–167:1 (weight : weight) was used for phytoplankton biomass estimates (Sathyendranath *et al.*, 2009). Primary productivity was then calculated by a chlorophyll-based model (Platt *et al.*, 2008; Sathyendranath *et al.*, 2009) using measured chlorophyll *a* concentrations and average *in situ* irradiance for the sampled period. The DOC concentration, planktonic prokaryotic abundance and biomass measurements are described in Supplementary Methods S1.

Datasets were tested for normality and homogeneity of variance, and one-way ANOVA tests for repeated measures were used to compare Chla, DOC and bacterial abundance for different periods of the day (morning, afternoon and early night), and for different reef areas. Analyses were followed by *post hoc* testing of Tukey's honestly significant difference for multiple comparisons (significance level at $P < 0.05$). We also performed Pearson's correlation tests with the phytoplankton and the bacterial biomass, and the biomass changes with the difference of phytoplankton and bacterial biomass at the beginning and the end of the day in each station.

Benthic primary production

To assess the photosynthetic potential of the benthic primary producers in the different reef areas we used PAM fluorometry. With an underwater red-light (650 nm) model PAM fluorometer (Diving PAM, Walz, Germany) we determined the photosynthetic yield (Y) ($Y = F_m - F_0/F_m$; F_m : maximum fluorescence, F_0 : initial fluorescence) of the main benthic primary producers on reef tops (3–8 m depth). We applied saturation light pulses of 800 µmol photons $m^{-2} s^{-1}$, 0.8 s width actinic light, to dark-adapted organisms. This saturation pulse intensity is sufficient to achieve the highest maximum fluorescence, but not to cause photoinhibition to organisms living in the top of the chapeirões, as determined by at least three representative light curves for each species. We selected three representative species based on their high benthic cover: *M. braziliensis*, a scleractinian coral, *D. plagiogramma*, a fleshy macroalgae, and *P. caribaeorum*, a zoanthid, in addition to CCA and turf algae. These organisms together comprise 92.5–100.0% of benthic cover on the studied sites (Francini-Filho *et al.*, 2013). We performed a minimum of 10 saturation pulse measurements in each individual/colony. Three to five individuals/colonies were measured per species summing up to a total of 502 measurements in the five surveyed reef sites. These surveys covered three coastal sites (Tim1, Tim3, and Pedra de Leste) and two offshore reefs (Mato Verde and PAB3). The high number of measurements obtained by diving PAM reflects its advantage over standard primary production methodologies (e.g. ^{14}C incorporation and Oxygen evolution). Fleshy macroalgae were not analysed in the PAB reefs because the percentage cover was close to 0% at the time of sampling. Light intensity was measured *in situ* at the sampling depth

using the Diving PAM sensor. Measurements for all reefs were taken around noon in February 2012 and yielded a mean PAR of $189 \pm 23 \mu\text{mol photons m}^{-2} \text{ s}^{-1}$. From the photosynthetic yield and the mean PAR, we could calculate the electron transport rate ($\text{ETR} = Y \times \text{PAR} \times 0.5 \times \text{AF}$) of the benthic primary producers. The absorption factors (AF) used were: 0.81 for *Phaeophyceae* (*Stipodidium zonale* and *D. plagiogramma*), 0.725 for corals, 0.56 for CCA and 0.64 for turf algae, as previously determined (Beer and Axelsson, 2004; Ralph *et al.*, 2005). Turf algae are multi-species assemblages of *Chlorophyta*, *Phaeophyta* and *Rhodophyta* (Steneck and Dethier, 1994; Fricke *et al.*, 2011). Because there is no information available on the composition of turf algae in our sampling area, the composition of turf algae in other reefs were used for calculating the AF (Connell *et al.*, 2014). ETR is shown to have a direct correlation to O_2 evolution (4 moles electrons:1 mol O_2) and ^{14}C uptake at low irradiances ($< 500 \mu\text{mol photons m}^{-2} \text{ s}^{-1}$), when electron leakage and cyclic photophosphorylation are low, allowing reliable estimates of gross carbon fixation based on ETR (Barranguet and Kromkamp, 2000; Beer and Axelsson, 2004; Kromkamp *et al.*, 2008). The PAM technique allowed us to measure the photosynthetic yield of an extensively large number of specimens covering a broad sampling area (ca. 800 km^2) within a relatively short time period of 17 days. From the gross primary production, we estimated the net production based on ranges of photosynthesis/respiration ratios previously determined for reef organisms: 0–80% of gross production for cnidarians, 16.6–84.1% for macroalgae, 16.6–85.5% for turf algae and 0–81.5% for CCA (Hatcher, 1988; Crossland *et al.*, 1991). Net production for each reef area was estimated based on a previous assessment of the percent cover of the various types of benthic primary producers on the chapeirão tops of the Abrolhos reefs previously accessed (Francini-Filho *et al.*, 2013, publically available through the Dryad platform (<http://datadryad.org/>) and summarized in Supporting Information Table S2). Biomass of each benthic compartment was estimated based on specific productivity (gross primary production to biomass ratio) (Hatcher, 1988; Crossland *et al.*, 1991).

Benthic DOC release and bacterial yield

DOC release by benthic primary producers was determined by *in situ* incubation experiments. Incubations were performed by SCUBA diving, at the same depth where benthic organisms were collected (approx. 4 m). The primary producers used in the incubations were chosen based on their high benthic cover: *M. braziliensis*, *D. plagiogramma* and *P. caribaeorum*. Four replicate samples of each species comprising approximately 1 dm^2 covering substrate were collected, acclimated for 30 min to prevent DOC leakage and put inside translucent 2 l Niskin bottles along with a water column sample from above the reef. Four additional bottles filled with reef water only were incubated to serve as controls. The Niskin bottles were incubated hanging from a rope or placed at the bottom at natural light conditions. Incubations were performed for 24 h at Portinho Norte site in the Archipelago and at Pedra de Leste site in Parcel das Paredes. These specific sites were chosen based on operational viability for overnight experiments. At the beginning and at the end

of the incubations, we determined DOC concentration and bacterial abundance in each bottle as described in Supplementary Methods S1. Initial and final O_2 concentrations were measured using a HACH LANGE HQ40 multiparameter instrument (DO: precision 0.01 mg l^{-1} , accuracy 1%). DOC released by benthic organisms was calculated as the sum of the increments in the DOC concentration (measured as initial concentration subtracted from final concentration), bacterial biomass carbon and respired carbon, as a molar ratio of O_2 consumed. Oxygen released by photosynthesis was estimated based on PAM fluorometry and added to measured consumption rates. DOC release rates were corrected for the control bottles and the organism surface area, as determined by the image analysis of the incubated specimens using CPCe program (Kohler and Gill, 2006). We were thereby able to discriminate between the carbon release by benthic organisms and the DOC uptake by bacteria. BGE was calculated as the ratio of bacterial biomass carbon to total carbon consumed by bacteria (biomass plus respired carbon).

Trophic web model

To begin understanding the carbon flow dynamics from primary producers up to fish stocks in the Abrolhos reefs we tested the correlation between the total fish biomass (determined in 2008 within the context of the long-term reef monitoring program presented in Francini-Filho and de Moura, 2008) and the benthic primary producers biomass or phytoplankton biomass (Supporting Information Fig. S4). None of the correlations were significant. Relationships between the carbon fixed by planktonic and benthic primary producers and the fish stocks biomass were then explored in a more complex trophic web model, termed primary production-based model (Supporting Information Fig. S5). The model's conceptual trophic structure is based on the transfer of the planktonic and benthic net primary production shown in Tables 1 and 2 respectively. The model's conceptual trophic structure and transfer ratios between compartments were based on consumers diet composition as previously determined (Suttle, 2005; Ferreira and Gonçalves, 2006; Francini-Filho *et al.*, 2009; Freitas *et al.*, 2011; Gathaz *et al.*, 2011; Agustí and Duarte, 2013). From these observations, we derived the proportion of the net primary production transferred to each consumer, indicated by symbols in the arrows of Fig. 4 and Supporting Information Fig. S5 and presented in Supporting Information Table S4. A fraction of 10% of the net production of each trophic level was considered available for transfer to the next level (Lindeman, 1942; Odum *et al.*, 1971). Transfers were thus directly proportional to the compartment size following a linear function. Minimum and maximum values were calculated using photosynthesis/respiration rate ranges for net productivity production described in 'Benthic primary production'. Carbon uptake ranges by bacteria observed in 'Benthic DOC release and bacterial yield' were also used. Carbon transfer was calculated in Microsoft Excel (Microsoft, Redmond, WA, USA) using iterations between cells for resolving circular references (maximum of 100 iterations and 0.001 maximum change).

In a second model, termed primary production and carbon recycling-based model, we incorporated the effect of the

benthic DOC release on microbial growth as determined by incubation experiments in the trophic web (indicated by red arrows in Fig. 4). In this second model, we applied DOC release rates observed for corals, macroalgae and zoanths in the incubation experiments, while for turf algae we used the same rates as for macroalgae and for CCA we used values described for rhodoliths from Abrolhos (Cavalcanti *et al.*, 2014), which were similar to those observed for CCA in other reefs (Haas *et al.*, 2011; 2013; Nelson *et al.*, 2013; Mueller *et al.*, 2014a). DOC and POC release rates by phytoplankton mortality and DOC uptake by the sponges were based on previous works (Yahel *et al.*, 2003; Suttle, 2005; de Goeij *et al.*, 2008; 2013; Agustí and Duarte, 2013; Mueller *et al.*, 2014b). Production for each fish compartment was calculated for both models based on the benthic and planktonic primary production estimates. Calculations were performed in Microsoft Excel using iterations between cells for resolving circular references (maximum of 100 iterations and 0.001 maximum change).

Acknowledgements

We acknowledge the Brazilian government agencies CNPq (Conselho Nacional de Pesquisa), CAPES (Coordenação de Aperfeiçoamento de Pessoal de Nível Superior) and FAPERJ (Fundação de Amparo à Pesquisa do Estado do Rio de Janeiro) for research funding. We thank Dr Peter Mumby, Dr Linda Kelly, Dr Andreas Haas and Benjamin Mueller for their valuable insights concerning data analyses. We also acknowledge Zaira Matheus/All Angle for the *Pomacanthus paru* picture. This work is part of the PhD thesis of CBS.

Conflict of Interest

The authors declare no conflict of interest.

References

Agustí, S., and Duarte, C.M. (2013) Phytoplankton lysis predicts dissolved organic carbon release in marine plankton communities. *Biogeosciences* **10**: 1259–1264.

Alexander, B.E., Liebrand, K., Osinga, R., van der Geest, H.G., Admiraal, W., Cleutjens, J.P.M., *et al.* (2014) Cell turnover and detritus production in marine sponges from tropical and temperate benthic ecosystems. *PLoS ONE* **9**: e109486.

Allredge, A., Carlson, C., and Carpenter, R. (2013) Sources of organic carbon to coral reef flats. *Oceanography* **26**: 108–113.

Alves, D.C., Moura, R.L., and Mente-Vera, C.V. (2012) Estimativa da captura total: desenhos amostrais para pesca artesanal. *Interciencia* **37**: 899–905.

Anthony, K.R.N. (2000) Enhanced particle-feeding capacity of corals on turbid reefs (Great Barrier Reef, Australia). *Coral Reefs* **19**: 59–67.

Azam, F., and Malfatti, F. (2007) Microbial structuring of marine ecosystems. *Nat Rev Microbiol* **5**: 782–791.

Barnes, D.J., and Devereux, M.J. (1984) Productivity and calcification of coral reef: a survey using pH and oxygen electrode techniques. *J Exp Mar Bio Ecol* **79**: 213–231.

Barott, K.L., and Rohwer, F.L. (2012) Unseen players shape benthic competition on coral reefs. *Trends Microbiol* **20**: 621–628.

Barott, K.L., Rodriguez-Mueller, B., Youle, M., Marhaver, K.L., Vermeij, M.J.A., Smith, J.E., and Rohwer, F.L. (2011) Microbial to reef scale interactions between the reef-building coral *Montastraea annularis* and benthic algae. *Proc Biol Sci* doi:10.1098/rspb.2011.2155.

Barranguet, C., and Kromkamp, J. (2000) Estimating primary production rates from photosynthetic electron transport in estuarine microphytobenthos. *Mar Ecol Prog Ser* **204**: 39–52.

Beer, S., and Axelsson, L. (2004) Limitations in the use of PAM fluorometry for measuring photosynthetic rates of macroalgae at high irradiances. *Eur J Phycol* **39**: 1–7.

Bruce, T., Meirelles, P.M., Garcia, G., Paranhos, R., Rezende, C.E., de Moura, R.L., *et al.* (2012) Abrolhos bank reef health evaluated by means of water quality, microbial diversity, benthic cover, and fish biomass data. *PLoS ONE* **7**: e36687.

Cavalcanti, G.S., Gregoracci, G.B., dos Santos, E.O., Silveira, C.B., Meirelles, P.M., Longo, L., *et al.* (2014) Physiologic and metagenomic attributes of the rhodoliths forming the largest CaCO₃ bed in the South Atlantic Ocean. *ISME J* **8**: 52–62.

Connell, S., Foster, M., and Airoldi, L. (2014) What are algal turfs? Towards a better description of turfs. *Mar Ecol Prog Ser* **495**: 299–307.

Costa, O.S., Nimmo, M., and Attrill, M.J. (2008) Coastal eutrophication in Brazil: a review of the role of nutrient excess on coral reef demise. *J South Am Earth Sci* **25**: 257–270.

Crossland, C.J., Hatcher, B.G., and Smith, S.V. (1991) Role of coral reefs in global ocean production. *Coral Reefs* **10**: 55–64.

De Goeij, J.M., Van Den Berg, H., Van Oostveen, M.M., Epping, E.H.G., and Van Duyl, F.C. (2008) Major bulk dissolved organic carbon (DOC) removal by encrusting coral reef cavity sponges. *Mar Ecol Prog Ser* **357**: 139–151.

De Goeij, J.M., De Kluijver, A., Van Duyl, F.C., Vacelet, J., Wijffels, R.H., De Goeij, A.F.P.M., *et al.* (2009) Cell kinetics of the marine sponge *Halisarca caerulea* reveal rapid cell turnover and shedding. *J Exp Biol* **212**: 3892–3900.

Dinsdale, E.A., Pantos, O., Smriga, S., Edwards, R.A., Angly, F., Wegley, L., *et al.* (2008) Microbial ecology of four coral atolls in the Northern Line Islands. *PLoS ONE* **3**: e1584.

Dixson, D.L., Abrego, D., and Hay, M.E. (2014) Chemically mediated behavior of recruiting corals and fishes: a tipping point that may limit reef recovery. *Science* **345**: 892–897.

Dulvy, N.K., Freckleton, R.P., and Polunin, N.V.C. (2004) Coral reef cascades and the indirect effects of predator removal by exploitation. *Ecol Lett* **7**: 410–416.

Ferreira, C.E.L., and Gonçalves, J.E.A. (2006) Community structure and diet of roving herbivorous reef fishes in the Abrolhos Archipelago, south-western Atlantic. *J Fish Biol* **69**: 1533–1551.

Francini-Filho, R.B., and de Moura, R.L. (2008) Dynamics of fish assemblages on coral reefs subjected to different management regimes in the Abrolhos Bank, eastern Brazil. *Aquat Conserv Mar Freshw Ecosyst* **18**: 1166–1179.

- Francini-Filho, R.B., and Moura, R.L. (2008) Evidence for spillover of reef fishes from a no-take marine reserve: an evaluation using the before-after control-impact (BACI) approach. *Fish Res* **93**: 346–356.
- Francini-Filho, R.B., Ferreira, C.M., Coni, E.O.C., De Moura, R.L., and Kaufman, L. (2009) Foraging activity of roving herbivorous reef fish (Acanthuridae and Scaridae) in eastern Brazil: influence of resource availability and interference competition. *J Mar Biol Assoc U K* **90**: 481–492.
- Francini-Filho, R.B., Coni, E.O.C., Meirelles, P.M., Amado-Filho, G.M., Thompson, F.L., Pereira-Filho, G.H., et al. (2013) Dynamics of coral reef benthic assemblages of the Abrolhos Bank, eastern Brazil: inferences on natural and anthropogenic drivers. *PLoS ONE* **8**: e54260.
- Freitas, M.O., Abilhoa, V., and Costa e Silva, G.H. (2011) Feeding ecology of *Lutjanus analis* (Teleostei: Lutjanidae) from Abrolhos Bank, Eastern Brazil. *Neotrop Ichthyol* **9**: 411–418.
- Fricke, A., Teichberg, M., Beilfuss, S., and Bischof, K. (2011) Succession patterns in algal turf vegetation on a Caribbean coral reef. *Bot Mar* **54**: 111–126.
- Friedlander, A.M., and Demartini, E.E. (2002) Contrasts in density, size, and biomass of reef fishes between the north-western and the main Hawaiian islands: the effects of fishing down apex predators. *Mar Ecol Prog Ser* **230**: 253–264.
- Fuhrman, J.A., and Noble, R.T. (1995) Viruses and protists cause similar bacterial mortality in coastal seawater. *Limnol Oceanogr* **40**: 1236–1242.
- Furnas, M., Mitchell, A., Skuza, M., and Brodie, J. (2005) In the other 90%: phytoplankton responses to enhanced nutrient availability in the Great Barrier Reef Lagoon. *Mar Pollut Bull* **51**: 253–265.
- Gathaz, J.R., Goiten, R., Freitas, M.O., Bornatowski, H., and Moura, R.L. (2011) Diet of *Cephalopholis fulva* (Perciformes: Serranidae) in the Abrolhos Bank, Northeastern Brazil. *Braz J Aquat Sci Technol* **17**: 61–63.
- de Goeij, J.M., van Oevelen, D., Vermeij, M.J.A., Osinga, R., Middelburg, J.J., de Goeij, A.F.P.M., and Admiraal, W. (2013) Surviving in a marine desert: the sponge loop retains resources within coral reefs. *Science* **342**: 108–110.
- Gordon, D.C. (1971) Organic carbon budget in the Fanning island. *Pac Sci* **25**: 222–227.
- Gruner, D.S., Smith, J.E., Seabloom, E.W., Sandin, S.A., Ngai, J.T., Hillebrand, H., et al. (2008) A cross-system synthesis of consumer and nutrient resource control on producer biomass. *Ecol Lett* **11**: 740–755.
- Haas, A.F., Nelson, C.E., Wegley Kelly, L., Carlson, C.A., Rohwer, F., Leichter, J.J., et al. (2011) Effects of coral reef benthic primary producers on dissolved organic carbon and microbial activity. *PLoS ONE* **6**: e27973.
- Haas, A.F., Nelson, C.E., Rohwer, F., Wegley-Kelly, L., Quistad, S.D., Carlson, C.A., et al. (2013) Influence of coral and algal exudates on microbially mediated reef metabolism. *PeerJ* **1**: e108.
- Hatcher, B.G. (1988) Coral reef primary productivity: a beggar's banquet. *Trends Ecol Evol* **3**: 106–111.
- Hatcher, B.G. (1990) Coral reef primary productivity: a hierarchy of pattern and process. *Trends Ecol Evol* **5**: 149–155.
- Hughes, T., Rodrigues, M., Bellwood, D., Ceccarelli, D., Hoegh-Guldberg, O., McCook, L., et al. (2007) Phase shifts, herbivory, and the resilience of coral reefs to climate change. *Curr Biol* **17**: 360–365.
- Jackson, J.B., Kirby, M.X., Berger, W.H., Bjorndal, K.A., Botsford, L.W., Bourque, B.J., et al. (2001) Historical overfishing and the recent collapse of coastal ecosystems. *Science* **293**: 629–637.
- Jantzen, C., Schmidt, G.M., Wild, C., Roder, C., Khokiattiwong, S., and Richter, C. (2013) Benthic reef primary production in response to large amplitude internal waves at the Similan Islands (Andaman Sea, Thailand). *PLoS ONE* **8**: e81834.
- Kaczmarek, L., and Richardson, L.L. (2011) Do elevated nutrients and organic carbon on Philippine reefs increase the prevalence of coral disease? *Coral Reefs* **30**: 253–257.
- Kéfi, S., Berlow, E.L., Wieters, E.A., Navarrete, S.A., Petchey, O.L., Wood, S.A., et al. (2012) More than a meal... integrating non-feeding interactions into food webs. *Ecol Lett* **15**(4): 291–300.
- Kelly, L.W., Williams, G.J., Barott, K.L., Carlson, C.A., Dinsdale, E.A., Edwards, R.A., et al. (2014) Local genomic adaptation of coral reef-associated microbiomes to gradients of natural variability and anthropogenic stressors. *Proc Natl Acad Sci USA* **111**(28): 10227–10232.
- Kinsey, D., and Davies, P. (1979) Carbon turnover, calcification and growth in coral reefs. In *Biogeochemical Cycling of Mineral Forming Elements*. Trudinger, P.A., and Swaine, D.J. (eds). Amsterdam, Netherlands: Elsevier, pp. 131–162.
- Kohler, K.E., and Gill, S.M. (2006) Coral Point Count with Excel extensions (CPCe): a visual basic program for the determination of coral and substrate coverage using random point count methodology. *Comput Geosci* **32**: 1259–1269.
- Kromkamp, J.C., Dijkman, N.A., Peene, J., Simis, S.G.H., and Gons, H.J. (2008) Estimating phytoplankton primary production in Lake IJsselmeer (The Netherlands) using variable fluorescence (PAM-FRRF) and C-uptake techniques. *Eur J Phycol* **43**: 327–344.
- Leão, Z.M.A.N., Kikuchi, R.K.P., and Testa, V. (2003) Corals and coral reefs of Brazil. In *Latin American Coral Reefs*. Jorge, C. (ed.). Amsterdam, The Netherlands: Elsevier Science, pp. 9–52.
- Lesser, M.P. (2006) Benthic–pelagic coupling on coral reefs: feeding and growth of Caribbean sponges. *J Exp Mar Bio Ecol* **328**: 277–288.
- Lindeman, R.L. (1942) The trophic-dynamic aspect of ecology. *Ecology* **23**: 399–417.
- McClanahan, T.R., Graham, N.A.J., MacNeil, M.A., Muthiga, N.A., Cinner, J.E., Bruggemann, J.H., and Wilson, S.K. (2011) Critical thresholds and tangible targets for ecosystem-based management of coral reef fisheries. *Proc Natl Acad Sci USA* **108**: 17230–17233.
- McDole, T., Nulton, J., Barott, K., Felts, B., Hand, C., Hatay, M., et al. (2012) Assessing coral reefs on a Pacific-wide scale using the microbialization score. *PLoS ONE* **7**: e43233.
- Marsh, J.A. (1974) Preliminary observations on the productivity of a Guam reef flat community. In *Proceedings of the 2nd International Coral Reef Symposium*. International Society for Reef Studies (ed.). Australia: The Great Barrier Reef Province, pp. 139–145.

- Moura, R.L. (2002) Brazilian reefs as priority areas for biodiversity conservation in the Atlantic Ocean. In *Proceedings 9th International Coral Reef Symposium*. International Society for Reef Studies (ed.). Bali, Indonesia, pp. 917–920.
- Mueller, B., van der Zande, R.M., van Leent, P.J.M., Meesters, E.H., Vermeij, M.J.A., and van Duyl, F.C. (2014a) Effect of light availability on dissolved organic carbon release by Caribbean reef algae and corals. *Bull Mar Sci* **90**: 875–893.
- Mueller, B., de Goeij, J.M., Vermeij, M.J.A., Mulders, Y., van der Ent, E., Ribes, M., and van Duyl, F.C. (2014b) Natural diet of coral-excavating sponges consists mainly of dissolved organic carbon (DOC). *PLoS ONE* **9**: e90152.
- Mumby, P.J., Dahlgren, C.P., Harborne, A.R., Kappel, C., V. Micheli, F., Brumbaugh, D.R., *et al.* (2006) Fishing, trophic cascades and the process of grazing on coral reefs. *Science* **311**: 98–101.
- Nelson, C.E., Goldberg, S.J., Wegley Kelly, L., Haas, A.F., Smith, J.E., Rohwer, F., and Carlson, C.A. (2013) Coral and macroalgal exudates vary in neutral sugar composition and differentially enrich reef bacterioplankton lineages. *ISME J* **7**: 962–979.
- Newman, M.J.H., Paredes, G.A., Sala, E., and Jackson, J.B.C. (2006) Structure of Caribbean coral reef communities across a large gradient of fish biomass. *Ecol Lett* **9**: 1216–1227.
- Odum, E.P., Odum, H.T., and Andrews, J. (1971) *Fundamentals of Ecology*. Philadelphia, PA, USA: Saunders.
- Odum, H.T., and Odum, E.P. (1955) Trophic structure and productivity of a windward coral reef community on Eniwetok Atoll. *Ecol Monogr* **25**: 291–320.
- Paddack, M.J., Reynolds, J.D., Aguilar, C., Appeldoorn, R.S., Beets, J., Burkett, E.W., *et al.* (2009) Recent region-wide declines in Caribbean reef fish abundance. *Curr Biol* **19**: 590–595.
- Patterson, M.R., Sebens, K.P., and Olson, R.R. (1991) *In situ* measurements of flow effects on primary production and dark respiration in reef corals. *Limnol Oceanogr* **36**: 936–948.
- Pedler, B.E., Aluwihare, L.I., and Azam, F. (2014) Single bacterial strain capable of significant contribution to carbon cycling in the surface ocean. *Proc Natl Acad Sci USA* **111**: 7202–7207.
- Platt, T., Sathyendranath, S., Forget, M.-H., White, G.N., Caverhill, C., Bouman, H., *et al.* (2008) Operational estimation of primary production at large geographical scales. *Remote Sens Environ* **112**: 3437–3448.
- Poore, A.G.B., Campbell, A.H., Coleman, R.A., Edgar, G.J., Jormalainen, V., Reynolds, P.L., *et al.* (2012) Global patterns in the impact of marine herbivores on benthic primary producers. *Ecol Lett* **15**: 912–922.
- Ralph, P.J., Schreiber, U., Gademann, R., Kuhl, M., and Larkum, A.W.D. (2005) Coral photobiology studied with a new imaging pulse amplitude modulated fluorometer. *J Phycol* **41**: 335–342.
- Rochelle-Newall, E., Torr ton, J., Mari, X., and Pringault, O. (2008) Phytoplankton-bacterioplankton coupling in a subtropical South Pacific coral reef lagoon. *Aquat Microb Ecol* **50**: 221–229.
- Roff, G., and Mumby, P.J. (2012) Global disparity in the resilience of coral reefs. *Trends Ecol Evol* **27**: 404–413.
- Rogers, C.S., and Salesky, N.H. (1981) Productivity of *Acropora palmata* (Lamarck), macroscopic algae, and algae turf from Tague Bay reef, St. Croix, U.S. Virgin Islands. *J Exp Mar Bio Ecol* **49**: 179–187.
- Sandin, S., Smith, J., Demartini, E., Dinsdale, E., Donner, S., Friedlander, A., *et al.* (2008) Baselines and degradation of coral reefs in the Northern Line Islands. *PLoS ONE* **3**: e1548.
- Sathyendranath, S., Stuart, V., Nair, A., Oka, K., Nakane, T., Bouman, H., *et al.* (2009) Carbon-to-chlorophyll ratio and growth rate of phytoplankton in the sea. *Mar Ecol Prog Ser* **383**: 73–84.
- Smith, J.E., Shaw, M., Edwards, R.A., Obura, D., Pantos, O., Sala, E., *et al.* (2006) Indirect effects of algae on coral: algae-mediated, microbe-induced coral mortality. *Ecol Lett* **9**: 835–845.
- Smith, S.V., and Marsh, J.A. (1973) Organic carbon production on the windward reef plat of Eniwetok Atoll. *Limnol Oceanogr* **18**: 953–961.
- Steneck, R.S., and Dethier, M.N. (1994) A functional group approach to the structure of algal-dominated communities. *Oikos* **68**: 476–498.
- Suttle, C. (2005) Viruses in the sea. *Nature* **437**: 356–361.
- Tanaka, Y., Miyajima, T., Watanabe, A., Nadaoka, K., Yamamoto, T., and Ogawa, H. (2011) Distribution of dissolved organic carbon and nitrogen in a coral reef. *Coral Reefs* **30**(2): 533–541.
- Travis, J., Coleman, F.C., Auster, P.J., Cury, P.M., Estes, J.A., Orensanz, J., *et al.* (2014) Integrating the invisible fabric of nature into fisheries management. *Proc Natl Acad Sci USA* **111**: 581–584.
- Tun, K.P.P., Cheshire, A.C., and Chou, L.M. (1997) Twenty-four hour *in situ* monitoring of oxygen production and respiration of the colonial zoanthid *Palythoa*. *Environ Monit Assess* **44**: 33–43.
- Wanders, J.B.W. (1976) The role of benthic algae in the shallow reef of Cura ao (Netherlands Antilles). i: primary productivity in the coral reef. *Aquat Bot* **2**: 235–270.
- Wild, C., Huettel, M., Klueter, A., Kremb, S.G., Rasheed, M.Y.M., and Jørgensen, B.B. (2004) Coral mucus functions as an energy carrier and particle trap in the reef ecosystem. *Nature* **428**: 63–66.
- Wild, C., Niggli, W., Naumann, M., and Haas, A. (2010) Organic matter release by Red Sea coral reef organisms – potential effects on microbial activity and *in situ* O₂ availability. *Mar Ecol Prog Ser* **411**: 61–71.
- Yahel, G., Sharp, J.H., and Marie, D. (2003) *In situ* feeding and element removal in the symbiont-bearing sponge *Theonella swinhoei*: Bulk DOC is the major source for carbon. *Limnol Oceanogr* **48**: 141–149.
- Zychaluk, K., Bruno, J.F., Clancy, D., McClanahan, T.R., and Spencer, M. (2012) Data-driven models for regional coral-reef dynamics. *Ecol Lett* **15**: 151–158.

Supporting information

Additional Supporting Information may be found in the online version of this article at the publisher's web-site:

Fig. S1. Map of Abrolhos sampling sites. Red lines indicate Marine National Park limits. Dark red symbols indicate Parcel dos Abrolhos reefs and light red indicate Archipelago rocky

shore reefs. Light blue symbols indicate sites under no management regime at Parcel das Paredes, and dark blue symbols indicate the poorly enforced National Park sites of Timbebas.

Fig. S2. Variation of the nutrient concentrations over time at three sites. Asterisks indicate significant difference over time ($P < 0.05$), error bars show standard deviation. Values of 2009 and 2010 originate from (Bruce *et al.*, 2012).

Fig. S3. Bacterial abundance. (a) Total prokaryotic cell abundance discriminated as autotrophs and heterotrophs, and (b) High Nucleic Acid Content (HNA) and Low Nucleic Acid Content (LNA); $n = 9$ for each reef, error bars indicate SE.

Fig. S4. Correlation test between fish biomass and phytoplankton biomass (A) or benthic primary producer biomass (B). No significant correlation was observed.

Fig. S5. Abrolhos reefs trophic web in primary production-based model. In this model no carbon recycling by microbial or sponge loops is included. Green compartments represent primary producers, blue represent consumers and gray represent DOC and POC pools. Thick solid black arrows indicate the main carbon flux from benthos to fish in healthy reefs (i.e. Parcel dos Abrolhos). Values inside boxes are net productivity of each compartment in $\text{mg C m}^{-2} \text{ h}^{-1}$. Interactions and fluxes among the various compartments of the model were obtained from ¶ (Ferreira and Gonçalves, 2006; Francini-Filho *et al.*, 2009); * (De Goeij *et al.*, 2013); # (Agusti and Duarte, 2013); @ (Suttle, 2005); ∞ (Fuhrman and Noble,

1995); § (Francini-Filho *et al.*, 2009); & (Freitas *et al.*, 2011; Gathaz *et al.*, 2011).

Fig. S6. Correlation between herbivore fish biomass and algae benthic cover, including turfs and fleshy macroalgae.

Table S1. Physical and chemical parameters for each reef in February, 2012 ($n = 3$, values after \pm are standard error values; nd = not determined).

Table S2. Benthic percent cover on reef tops of the studied sites (Francini-Filho *et al.*, 2013). Benthic species were grouped in functional groups (coral, CCA, fleshy macroalgae and turf algae).

Table S3. Actual fish biomass and net production predicted by Model 1 (primary production-based) and Model 2 (primary production and carbon recycling-based) for each functional group at each site. Biomass is in mg C m^{-2} and production in $\text{mg C m}^{-2} \text{ h}^{-1}$. Values inside brackets are relative to total fish production and biomass.

Table S4. Proportion of net production in each trophic group transferred to the next trophic level. Producers are in the rows and consumers in the columns. As DOC and POC are abiotic compartments their production are not included in the 10% of net production transferred to the next trophic level. Cells colored in orange indicate the microbial and sponge loops only included in the model 2. Detritus compartment is the sum of POC, phytoplankton and bacterioplankton.

Methods S1. Water physical and chemical parameters.

Results S1. Water physical and chemical parameters.

An extensive reef system at the Amazon River mouth

Rodrigo L. Moura,^{1,2} Gilberto M. Amado-Filho,³ Fernando C. Moraes,^{3,9} Poliana S. Brasileiro,³ Paulo S. Salomon,^{1,2} Michel M. Mahiques,⁴ Alex C. Bastos,⁵ Marcelo G. Almeida,⁶ Jomar M. Silva Jr.,⁶ Beatriz F. Araujo,⁶ Frederico P. Brito,⁶ Thiago P. Rangel,⁶ Braulio C. V. Oliveira,⁶ Ricardo G. Bahia,³ Rodolfo P. Paranhos,¹ Rodolfo J. S. Dias,⁴ Eduardo Siegle,⁴ Alberto G. Figueiredo Jr.,⁷ Renato C. Pereira,⁸ Camille V. Leal,^{1,9} Eduardo Hajdu,⁹ Nils E. Asp,¹⁰ Gustavo B. Gregoracci,¹¹ Sigrid Neumann-Leitão,¹² Patricia L. Yager,¹³ Ronaldo B. Francini-Filho,¹⁴ Adriana Fróes,¹ Mariana Campeão,¹ Bruno S. Silva,¹ Ana P. B. Moreira,¹ Louisi Oliveira,¹ Ana C. Soares,¹ Lais Araujo,¹ Nara L. Oliveira,¹⁵ João B. Teixeira,¹⁵ Rogério A. B. Valle,² Cristiane C. Thompson,¹ Carlos E. Rezende,^{6*} Fabiano L. Thompson^{1,2*}

2016 © The Authors, some rights reserved; exclusive licensee American Association for the Advancement of Science. Distributed under a Creative Commons Attribution NonCommercial License 4.0 (CC BY-NC). 10.1126/sciadv.1501252

Large rivers create major gaps in reef distribution along tropical shelves. The Amazon River represents 20% of the global riverine discharge to the ocean, generating up to a 1.3×10^6 -km² plume, and extensive muddy bottoms in the equatorial margin of South America. As a result, a wide area of the tropical North Atlantic is heavily affected in terms of salinity, pH, light penetration, and sedimentation. Such unfavorable conditions were thought to imprint a major gap in Western Atlantic reefs. We present an extensive carbonate system off the Amazon mouth, underneath the river plume. Significant carbonate sedimentation occurred during lowstand sea level, and still occurs in the outer shelf, resulting in complex hard-bottom topography. A permanent near-bottom wedge of ocean water, together with the seasonal nature of the plume's eastward retroflexion, conditions the existence of this extensive (~9500 km²) hard-bottom mosaic. The Amazon reefs transition from accretive to erosional structures and encompass extensive rhodolith beds. Carbonate structures function as a connectivity corridor for wide depth-ranging reef-associated species, being heavily colonized by large sponges and other structure-forming filter feeders that dwell under low light and high levels of particulates. The oxycline between the plume and subplume is associated with chemoautotrophic and anaerobic microbial metabolisms. The system described here provides several insights about the responses of tropical reefs to suboptimal and marginal reef-building conditions, which are accelerating worldwide due to global changes.

INTRODUCTION

Biogenic reefs are topographically significant structures built by benthic animals, plants, and microbes that mineralize carbonate or siliceous skeletons and/or induce carbonate precipitation (1). The most conspicuous biogenic reefs are the highly biodiverse coral reefs that occur in shallow, warm, and oligotrophic waters with a higher saturation state of calcium carbonate (Ω CaCO₃). Under such optimal mineralization conditions, carbonate accumulation reaches up to 10 kg m⁻² year⁻¹, and structures may extend for thousands of kilometers (2). However,

biogenic reefs develop under a much wider array of conditions that constrain mineralization and other core ecosystem processes typical of tropical coral reefs (for example, grazing by metazoans) (3, 4). The main controls over reef ecosystems interact and vary in a wide range of spatial and temporal scales. As a result, many types of reefs have been subjected to fruitless nomenclatural controversies since the 19th century (3).

Because of their impact on salinity, pH, light penetration, sedimentation, and nutrients, large tropical rivers typically exclude carbonate reef builders from continental shelves. The Amazon-Orinoco and the Ganges-Brahmaputra mouths are textbook examples of such major reef gaps (2). The wide (~300 km) Amazon continental shelf evolved from a carbonate to a siliciclastic system during the early Late Miocene (9.5 to 8.3 million years ago) (5, 6). By this time, under lowstand sea level, an incised canyon system directed sediment influx toward the slope and basin floor (7). Shelf edge reef buildups occurred peripherally to this deep Amazon Fan and were gradually overlain by siliciclasts during Neogene and Quaternary highstands (7, 8). At present, the high sediment load from the river settles relatively quickly in the inner and mid shelves, conditioning an unstable muddy benthic habitat with high bacterial biomass and low diversity and abundance of epifauna and meiofauna (9, 10). The region is also subjected to a highly energetic physical regime because of the fast-flowing North Brazil Current (NBC), strong wind stress, and high semidiurnal tidal ranges. Such conditions create a stressful habitat for benthic megafauna, especially in the areas with

¹Instituto de Biologia, Universidade Federal do Rio de Janeiro (UFRJ), Rio de Janeiro RJ CEP 21941-599, Brazil. ²Laboratório de Sistemas Avançados de Gestão da Produção, Instituto Alberto Luiz Coimbra de Pós-Graduação e Pesquisa de Engenharia, COPPE, UFRJ, Rio de Janeiro RJ CEP 21941-972, Brazil. ³Instituto de Pesquisas Jardim Botânico do Rio de Janeiro, Rio de Janeiro RJ CEP 22460-030, Brazil. ⁴Instituto Oceanográfico, Universidade de São Paulo, São Paulo SP CEP 05508-120, Brazil. ⁵Departamento de Oceanografia, Universidade Federal do Espírito Santo, Vitória ES CEP 29199-970, Brazil. ⁶Laboratório de Ciências Ambientais, Centro de Biociências e Biotecnologia, Universidade Estadual do Norte Fluminense, Campos dos Goytacazes RJ CEP 28013-602, Brazil. ⁷Instituto de Geociências, Universidade Federal Fluminense, Niterói RJ CEP 24210-346, Brazil. ⁸Instituto de Biologia, Universidade Federal Fluminense, Niterói RJ CEP 24210-130, Brazil. ⁹Museu Nacional, Universidade Federal do Rio de Janeiro, Rio de Janeiro RJ 20940-040, Brazil. ¹⁰Instituto de Estudos Costeiros, Universidade Federal do Pará, Bragança PA CEP 68600-000, Brazil. ¹¹Departamento de Ciências do Mar, Universidade Federal de São Paulo, Santos SP CEP 11070-100, Brazil. ¹²Departamento de Oceanografia, Universidade Federal de Pernambuco, Recife PE CEP 50670-901, Brazil. ¹³Department of Marine Sciences, University of Georgia, Athens, GA 30602-2626, USA. ¹⁴Universidade Federal da Paraíba, Rio Tinto PB CEP 58297000, Brazil. ¹⁵Departamento de Ciências Biológicas, Universidade Estadual de Santa Cruz, Ilhéus, BA CEP 45650-000, Brazil. *Corresponding author: E-mail: fabianothompson1@gmail.com (F.L.T.); crezendeuenf@yahoo.com.br (C.E.R.)

soft, fluid sediments. The massive sedimentation and sediment reworking in the inner and mid shelves have been comprehensively surveyed in the last decades, including the core river-ocean biogeochemical processes (9). On the other hand, the “relict magnesian calcite ooids” (11) and other carbonate sediments recorded along the outer shelf (5, 8) have received much less attention. For instance, it is unknown whether this surficial carbonate layer comprises living biomineralizers and other reef-associated organisms and how this benthic system may be coupled to the pelagic compartments. The only noteworthy exceptions to such knowledge gap about the outer shelf is a brief description of reef fishes associated with sponge bottoms (12) and a checklist of corals produced from specimens deposited in museums (13), both of which fail to report the presence of carbonate structures and rhodolith beds.

The Amazon River represents ~20% of the global riverine discharge to the ocean [$\sim 120 \times 10^3 \text{ m}^3 \text{ s}^{-1}$ in December to $\sim 300 \times 10^3 \text{ m}^3 \text{ s}^{-1}$ in May; (14)], generating an up to $1.3 \times 10^6 \text{ km}^2$ offshore plume enriched with chromophoric dissolved organic matter (15, 16). This relatively shallow (5 to 25 m deep) and hyposaline layer is driven by seasonal winds and currents, flowing northward into the Caribbean and retroflecting eastward during September and October. Phytoplankton productivity is limited by low light penetration in the inner shelf, increasing only once sediments have cleared (16, 17). The resulting downward particle flow occurs away from the continental shelf (18). On the shelf break, sedimentation under the plume is limited by a permanent frontal process that draws near-bottom seawater landwards, coupled with Ekman veering (9). Oxygen levels are lowered in the subplume and near the bottom because of the high rates of organic matter mineralization in the inner and mid-shelf (10, 19). Although the plume has been the focus of recent studies (16, 17, 20), the subplume and the coupling between the plume, subplume, and outer-shelf benthic systems have been largely ignored.

The Amazon River mouth represents the distribution boundary for several sponges, scleractinian corals, and shallow water fishes, among other groups of coastal and reef-associated organisms, as a consequence of the massive oceanographic discontinuities that it imprints in the West Atlantic continental margin (21). On the other hand, many reef-associated species occur at both sides of the river mouth, with possible connectivity mechanisms related to long-range larval dispersal, rafting, or demersal migration through stepping stones (22). The operation of the Amazon mouth biogeographic filter is not completely known because information about the nature and extension of reef habitats off the Amazon mouth is still limited (11–13, 23, 24).

Here, we present the results of a multidisciplinary assessment of the outer Amazon shelf, where we found a unique carbonate reef system of $\sim 9500 \text{ km}^2$, between the French Guiana–Brazil border and the Maranhão State in Brazil ($\sim 1000 \text{ km}$). Our survey was carried out near the shelf edge and in the upper slope (25 to 120 m), and included geophysical and physical-chemical surveys, radiocarbon dating and petrographic characterization of reef samples, biogeochemical tracers, and microbial metagenomics. We provide a description of macrobenthic and demersal assemblages, including extensive rhodolith beds built by coralline algae and sponge-dominated hard bottom, and also adding primary and gray literature data about the large reef fisheries that operate off the Amazon mouth [for example, CREOCEAN (25) and IBAMA (26)]. The novel system presented here adds to the repertoire of “marginal” reef types shaped by conditions deviating from those of the archetypal tropical coral reefs. The ubiquity of large sponges and other filter feeders, as well as the increase of chemoautotrophic and

anaerobic microbial metabolisms recorded in the subplume, provides insights about ecosystem-level responses to the globally accelerating conditions that select against photosymbiotic biocalifiers (for example, scleractinian corals).

RESULTS

Structure, composition, and age of reef structures

An extensive carbonate reef system of $\sim 9500 \text{ km}^2$, spanning from 5°N to 1°S and 44° to 51°W , was recorded between the Brazil–French Guiana border and Maranhão State, Brazil (Fig. 1). Rhodolith beds and higher-relief structures were recorded across a relatively long ($\sim 1000 \text{ km}$) and narrow ($\sim 50 \text{ km}$) stretch in the outer shelf and upper slope, in depths ranging from 30 m to the shelf break at 90 to 120 m. This extensive submerged carbonate system extends from French Guiana southward to the Manuel Luis reef, the northernmost emerging reef within the Brazilian Biogeographic Province.

In the Northern Sector of the study region, structures were recorded near the shelf edge, comprising widely spaced (hundreds to thousands of meters) patches with lengths of up to 300 m and heights of up to 30 m. These irregularly shaped reefs tended to be elongated with a parallel shelf edge orientation, resembling erosive structures (Fig. 1B). Dredged materials consist of carbonate fragments with incipient living cover of crustose coralline algae (<5%) and low-vitality rhodoliths recovered in the vicinity of the larger reef patches, and also include lateritic crusts. The dated sample (surficial carbonate fragment) presented a 2σ radiocarbon calibrated age of 13,382 to 13,749 years before present (BP), with microfacies typical of grainstone composed of skeleton fragments of tube worms, foraminifera, barnacles, bryozoans, and molluscs (Fig. 2, A and B). Dredge casts that did not hit structures recovered large sponges among soft sediments (fig. S1). In the Central Sector, the bottom was dominated by rhodoliths with high vitality (>50% of live coralline algae cover), as well as by complex sandwaves and gravel ripples between 20- and 100-m depths (Fig. 1C). Patches of carbonate blocks were small (< 10 m^2) and sparsely distributed. The core and surface of a $\sim 70 \times 40\text{-cm}$ block collected in this sector presented 2σ radiocarbon calibrated ages of 4487 to 4846 and 4157 to 4562 years BP, respectively. Microfacies is typical of boundstone and is mainly composed of crustose coralline algae and bryozoans (Fig. 2, C and D). The surface of this block presented small and sparse patches of living coralline algae. In the Southern Sector, structures were widespread and occurred between 30- and 90-m depths. Reef morphology consists of ridge-like features <5 m in height and irregular and low-relief patch reefs (<5 m in height) (Fig. 1D). Structures are surrounded by a high backscatter and flat hardground (fig. S2) dominated by high-vitality rhodoliths and carbonate sand. The dated sample (surficial carbonate fragment) presented a modern radiocarbon age (<150 years), with microfacies typical of boundstone composed of hydrocorals, crustose coralline algae, and corals (Fig. 2, E and F). The southern part of this sector encompasses one relatively shallow (<10-m depth) submerged reef (Banco do Álvaro reef) and the emerging Manoel Luis reef ($\sim 450 \text{ km}^2$), both consisting of isolated and coalesced coralline pinnacles. None of the benthic casts in the Central and Southern Sectors recovered mud.

Macrobenthos, demersal fish, and reef fisheries

Red algae (Rhodophyta, 25 species) were the predominant benthic plant group, followed by green (Chlorophyta, 6 species) and brown algae

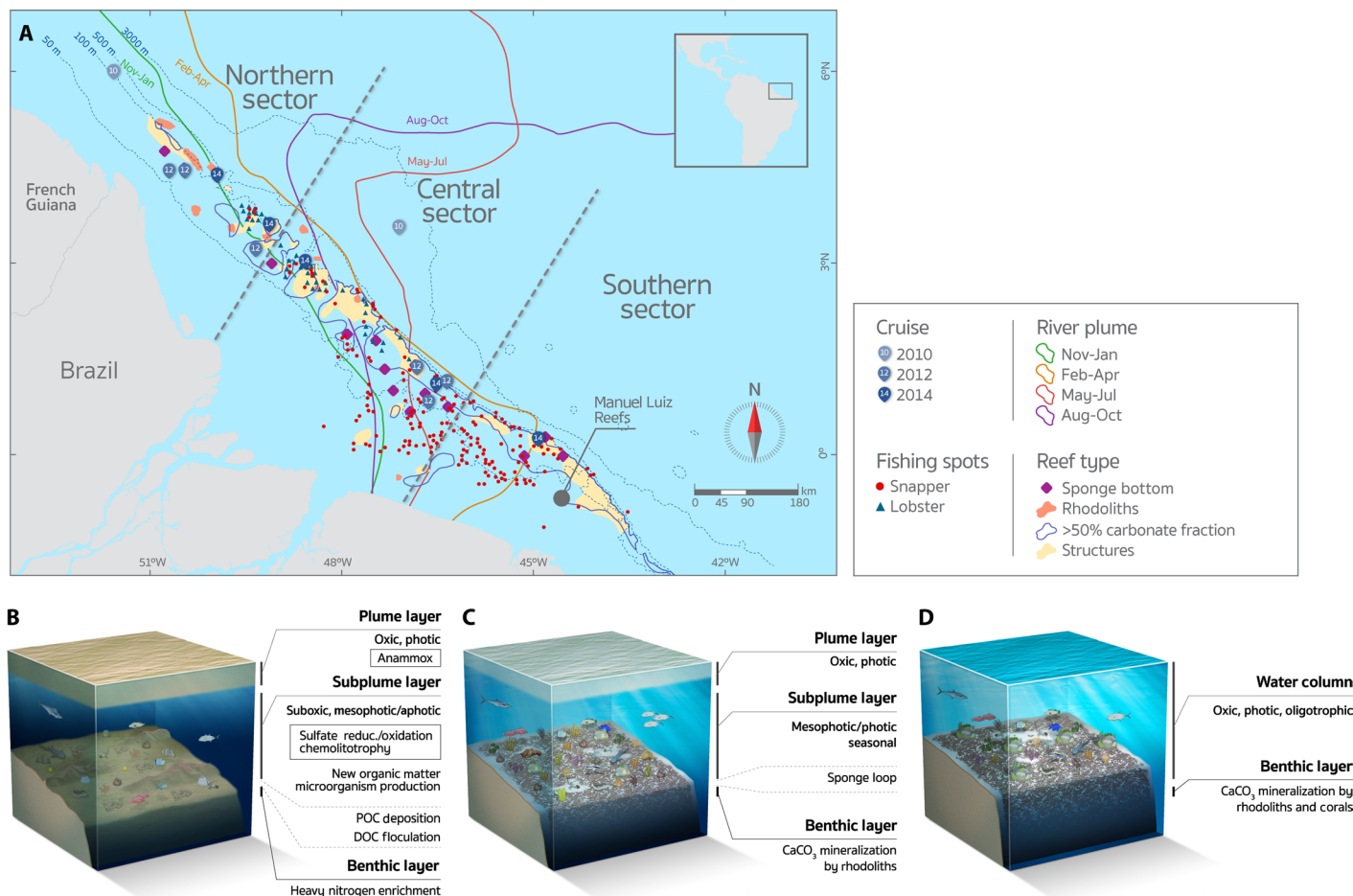


Fig. 1. Map of the Amazon shelf showing the benthic megahabitats and seasonal influence of the river plume. (A) Distribution of reef fisheries and oceanographic stations. Manuel Luis reefs are the northernmost emerging reefs in Brazil. (B to D) Main structural and functional traits of the reefs in the Northern (120 m), Central (55 m), and Southern Sectors (25 m), respectively. Plume POC $\delta^{13}\text{C} = -22.9 \pm 0.7$, $\delta^{15}\text{N} = 4.0 \pm 1.2$; Plume DOC $\delta^{13}\text{C} = -27.7 \pm 1.0$, $\delta^{15}\text{N} = 1.3 \pm 0.3$. Subplume POC $\delta^{13}\text{C} = -24.2 \pm 1.3$, $\delta^{15}\text{N} = 5.1 \pm 1.7$; Subplume DOC $\delta^{13}\text{C} = -26.6 \pm 1.7$, $\delta^{15}\text{N} = 0.1 \pm 1.8$. Benthic (sediment) $\delta^{13}\text{C} = -26.2 \pm 0.6$, $\delta^{15}\text{N} = 2.2 \pm 0.5$. Some graphic elements are courtesy of the Integration and Application Network, University of Maryland Center for Environmental Science (<http://ian.umces.edu/symbols/>). The plume lines represent the outer edge of the plume during that season, according to satellite climatology (80).

(Ochrophyta, 4 species) (table S1). Calcareous algae were ubiquitous (fig. S3), with a clear impoverishment gradient northward. Five encrusting calcareous algae taxa were identified in the surface of rhodoliths and carbonate blocks, with living *Lithothamnion crispatum* and *Sporolithon ptychoides* distributed across the entire outer shelf, including the sub-plume environment of the Northern Sector. A low-diversity assemblage (34 species) of typically tropical-subtropical and wide depth-ranging seaweeds was recorded in association with the rhodoliths in the Central and Southern Sector. These assemblages included greater functional diversity than those of the Northern Sector (table S1). Seaweeds recovered from the Northern Sector (for example, *Gelidium* and *Anadyomene*) consisted of detached and low-vitality fragments. With the exception of *Anadyomene*, green and brown algae were restricted to the South Sector.

The sponge assemblage comprised 61 species and was dominated by massive forms that were wide depth-ranging within the photic and mesophotic zones, but also included a few deep-water species (table S2

and fig. S4). Three Northern Sector stations were remarkable as they recovered sponges among soft sediments, including large-sized *Xestospongia muta* with unusual pale coloration and narrow atria and *Tribrachium schmidtii* with a buried bulbous base and an upward long papilla (fig. S4). The highest sponge diversity and biomass was recorded on the flatter rhodolith beds of the Central Sector. For instance, a single 20 minutes trawl (station 2014-6; 55-m depth) recovered about 30 species (150 specimens, ~900 kg), most of which exhibited large, erect, cup-like, and massive forms, growing attached to rhodoliths (table S2, fig. S4, and movie S1). The most common sponge species in the Central Sector were *Agelas* spp., *Aplysina* spp., *Callyspongia vaginalis*, *Clathria nicoleae*, *Geodia* spp., *Monanchora arbuscula*, and *Oceanapia bartschi*. Encrusting species (for example, *Clathria* cf. *calla*) were overall rare and restricted to grow on other sponges. *Lissodendoryx* sp. and *O. bartschi* were heavily colonized by epibionts (ascidians, hydroids, and other sponges). Two excavating species of genus *Cliona* were found associated

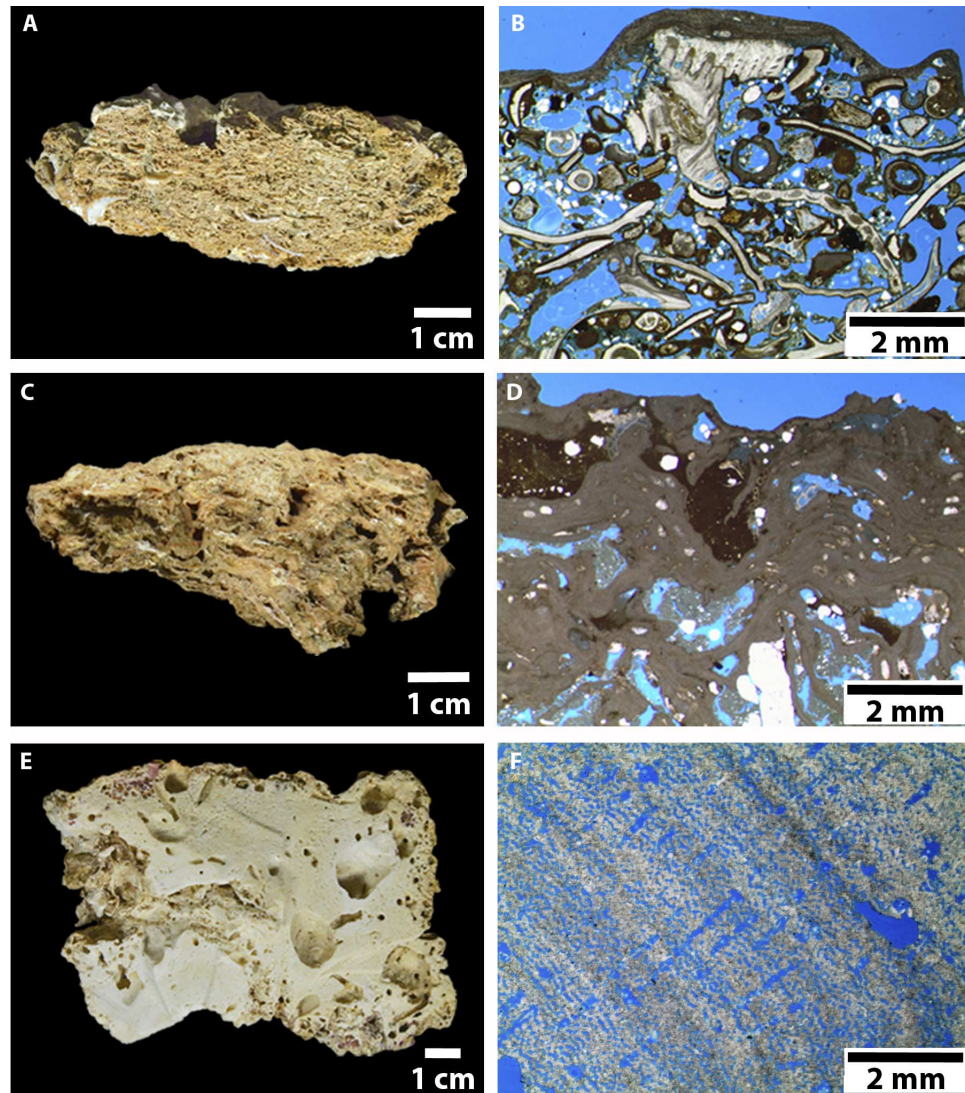


Fig. 2. Surficial reef fragments (left) and corresponding petrographic images (right) from the Northern (A and B, 120-m depth), Central (C and D, 60 m), and Southern Sectors (E and F, 23 m). Microfacies transition from an older grainstone ($12,100 \pm 30$ thousand years BP) composed of filter feeders (polychaetes, foraminifera, barnacles, bryozoans, and molluscs) under a thin veneer of coralline algae in the Northern Sector (A and B) to a more recently turned-off (5220 ± 110 thousand years BP) boundstone composed of photosynthesizers (crustose coralline algae) and filter feeders (bryozoans) in the Central Sector (C and D) and, finally, to a recent boundstone typical of turbid zone reefs (hydrocorals, crustose coralline algae, and corals) in the Southern Sector (E and F).

with scleractinian corals in the Southern Sector (table S2 and figs. S4 and S5), whereas no boring sponges were recorded in the Northern Sector.

Cnidarians were present at all stations, with hydroids (benthic colonial life stage of hydrozoans) being particularly abundant across the region. Two black coral species (*Antipatharia*), *Antipathes furcata* and *Tanacetipathes tanacetum*, typical of mesophotic zone reefs, were recorded at the Northern Sector (table S3). Octocorallia was the most speciose group (26 species), but most records are from sparse museum specimens without precise locality records (13). Scleractinians with symbiotic dinoflagellates (*Symbiodinium* spp.) were largely restricted to the Central and Southern Sectors. Where present (Central and Southern Sectors), scleractinians comprised impoverished (12 species,

table S3) and low-density/cover assemblages (fig. S5) encompassing encrusting colonies of small-sized species (*Meandrina braziliensis*, *Agaricia* spp., *Scolymia wellsii*, and *Favia gravida*), small colonies of massive species (*Montastraea cavernosa* and *Madracis decactis*), and branching colonies of *Millepora* cf. *alcicornis*. With the exception of *F. gravida* and *Millepora* cf. *alcicornis*, all corals recorded off the Amazon mouth were wide depth-ranging species, occurring in photic and mesophotic habitats. An alien brittle star from the Pacific Ocean, *Ophiothela mirabilis*, was recorded in association with *Leptogorgia miniata*.

We recorded 73 reef fish species in the study region, most of them with wide depth and geographic ranges (table S4 and fig. S6). Most fish species were carnivores (86%), including piscivores and invertivores,

whereas a few were planktivores or herbivore/detritivores (two species, 3% each). Four species (5.5%) of sponge-eating fishes of family Pomacanthidae (angelfishes) were recorded across the region. Significant fisheries for the Southern red snapper, *Lutjanus purpureus* (2900 metric tons year⁻¹), and spiny lobsters, *Palinurus* spp. (1360 metric tons year⁻¹), were recorded across the region, the latter being concentrated in the Northern and Central Sectors (Fig. 1). Reef fisheries are carried out by small- to medium-sized boats (8 to 20 m lengths) operating with traps (for lobsters) and hand lines or long lines (for reef fishes) in the outer shelf. Smaller dinghies with one to two crew (fig. S7) operating hand lines are also regularly spotted, and are used to increase fishing area and the chance of finding reef structures where fishes aggregate. At least 131 boats are currently registered to fish lobsters with traps (~3 boats per 10 km of the linear extension of the reef system), but a larger number of unregistered boats target reef fishes. Targeted species include a diverse assemblage of groupers (Serranidae, 321 metric tons year⁻¹) and snappers (Lutjanidae, 4220 metric tons year⁻¹), which are landed mainly in Pará and Amapá (26). Such intense reef fisheries (fig. S8) represent additional evidence for the wide distribution and importance of the reefs close to the Amazon mouth. In the inner shelf, fisheries are carried out over soft sediments, mostly with gillnets, trawls, and long lines.

Biogeographic patterns. All macroalgae recorded off the Amazon mouth are wide-ranging species that are distributed across large expanses of the Atlantic and Pacific basins. The sponge fauna was a typical tropical West Atlantic reef assemblage, with only three Brazilian endemics and two species that also occur in West Africa. Three new records were added to the Brazilian sponge fauna: *Theonella atlantica*, a typical deep-water species previously recorded in the Southern Caribbean; *Clathria echinata*, previously known from the Caribbean; and *Didiscus verdensis*, previously known from shallow waters in the Cape Verde Archipelago (27). The octocoral fauna (26 species) included typically mesophotic species, with 18 species that are wide-ranging in the West Atlantic, 7 Brazilian endemics, and 1 circum-globally distributed gorgonian. Anthipatarians included only three species that are widely distributed in the West Atlantic, including the black coral *Anthipathes furcate*, which is a new record to Brazilian tropical waters (previously known from the Caribbean and Southeastern Brazil). Of the 6 recorded scleractinians, 2 are Brazilian endemics and the remaining 4 are wide-ranging in the Atlantic Ocean. Brazilian-endemic scleractinians were restricted to the Central and Southern Sectors. The reef fish assemblage was also dominated by wide-ranging species (63% are widely distributed in the West Atlantic, 22% occur in the West and East Atlantic, and 11% occur in the Atlantic and Pacific), with the exception of *Stegastes pictus*, *Halichoeres dimidiatus*, and *Sparisoma frondosum*, which are Brazilian endemics with occasional records northward into the Caribbean and West Africa (*S. frondosum*). Pelagic spawners with high dispersal capabilities (80%) dominated the reef fish assemblage. Most recorded species (algae, sponges, cnidarians, and fishes) are wide depth-ranging, with a few exceptions restricted to the Southern Sector (tables S1 to S4).

Plume and nonplume water column. Water column profiles under nonplume conditions encompassed outer shelf, slope, and open-ocean/deep-sea stations (Fig. 3 and fig. S9). These profiles were well mixed to about 100 m, with near constant salinity at ~35.5 to 36. Temperatures near the surface were consistently ~28°C, cooling rapidly below 50 m, with 1% light level [photosynthetically active radiation (PAR)] reaching ~100 m. Dissolved inorganic nitrogen (DIN), a lim-

iting nutrient, was near the detection limit in the upper 70 m, and particulate organic carbon (POC) and dissolved organic carbon (DOC) concentrations were generally low throughout the upper water column (Fig. 3). Oxygen was uniform at around 4 ml liter⁻¹ throughout the upper 100 m (Fig. 3). Conversely, in profiles associated with the plume (Fig. 3 and fig. S9), the water column was strongly stratified with an evident lower salinity and higher temperature signal in the upper 10 to 15 m. Light attenuation was much stronger in plume profiles, with 1% levels no deeper than 50 m (Fig. 3), and nutrient concentrations (such as DIN) were consistently >0, with values depending on proximity to river mouth. Concentrations of POC and DOC were higher in the plume (Fig. 3), reflecting both riverine and marine organic inputs. Oxyclines were detectable at depths of ~5 to 10 m across the plume interface and 35 to 50 m within the subplume. Dissolved oxygen (DO) levels dropped to ≤ 3.5 ml liter⁻¹ near the bottom at some stations on the outer shelf (fig. S9).

Isotopic analysis. The isotopic composition of POC was heavier in the plume (-22.9 ± 0.7‰) than in the subplume (-24.2 ± 1.3‰) and benthic (sediment) layers (-26.2 ± 0.6‰), whereas DOC showed a slight but not significant difference between the plume (-27.7 ± 1.0‰) and subplume (-26.6 ± 1.7‰) layers. The same trend was observed for nitrogen isotopic composition of particulate organic nitrogen (PON) in the plume (4.0 ± 1.2‰) and subplume (5.1 ± 0.7‰) layers, respectively, but significantly lower values were found in the benthic layer (2.2 ± 0.5‰) (Fig. 1). Dissolved organic nitrogen showed an opposite trend when compared with PON, with higher values in the plume (1.3 ± 0.3‰) than in the subplume (-0.1 ± 1.8‰) layer.

Transcriptome analysis. Compared to nonplume (oceanic) meta-transcriptomes, more gene transcripts related to anaerobic metabolism were detected in the plume and subplume layers (fig. S10), corroborating the water column physical-chemical features. An opposite trend was observed for photosynthesis gene transcripts, except for the particle-associated fraction of the plume, reinforcing the increased contribution of chemosynthesis in the subplume. The adenylyl sulfate reductase subunits α and β (*aprAB*; responsible for dissimilatory sulfate reduction) and sulfur (thiosulfate and sulfide) oxidation (*soxB*) transcripts from free-living microbes were more abundant in the subplume layer. Anammox gene transcripts and respiratory nitrate/nitrite reductase (*narB* and *nirB*; responsible for nitrate respiration) transcripts were more abundant in the plume layer, from both free-living and particle-attached microbes in the plume.

DISCUSSION

Despite the iconic depiction of reefs as megadiverse systems thriving in warm, shallow, and oligotrophic waters, biogenic reefs develop under a much wider range of conditions. The benthic production by efficient mixotrophic holobionts that build carbonate structures (for example, scleractinian corals), together with the grazing by fish and macroinvertebrates, have been important drivers in the evolution of coral reef ecosystems (28, 29). However, these processes are constrained in the so-called marginal reef systems (4), which may share parts of their taxonomic structure and some functional properties with tropical coral reefs (29). Marginal reefs are subjected to environmental forcing that depart from the optimal mineralization conditions for corals, such as the rhodolith beds that occur at great depths and latitudes (30, 31), aphotic zone coralline and sponge reefs (32), and stromatolites that

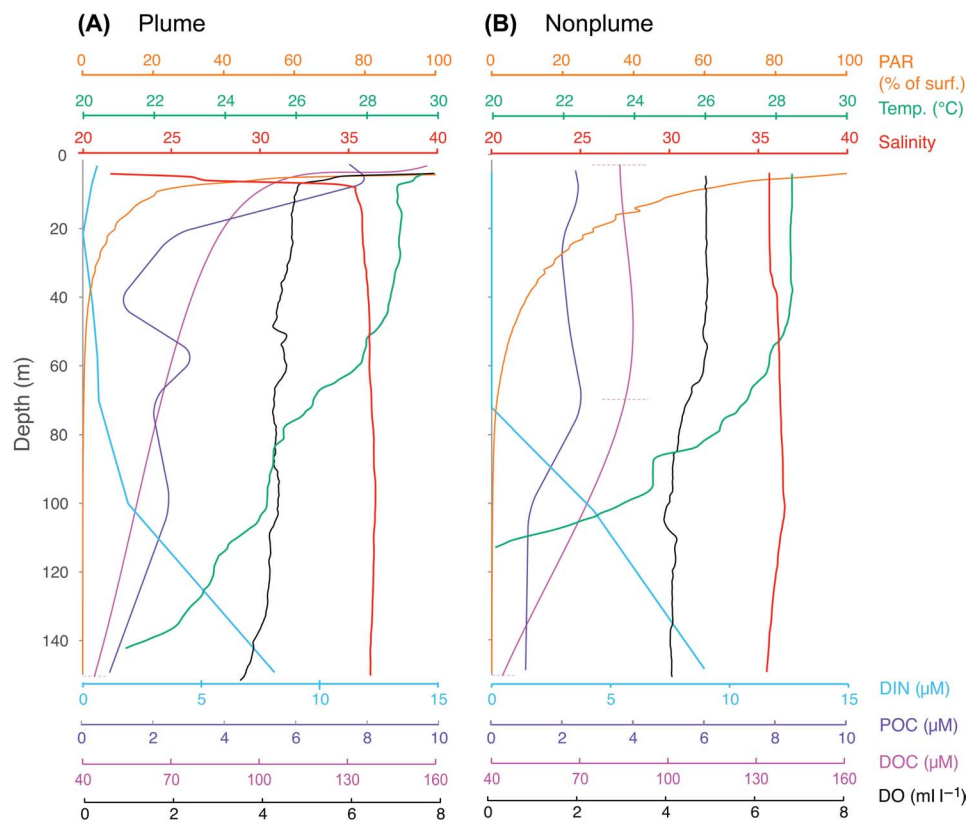


Fig. 3. Water column profiles under plume (A) and nonplume (B) conditions. (A) Station 2010-04 (5.495°N, 51.488°W), under intense plume influence, Northern Sector. (B) Station 2010-08 (4.349°N, 46.852°W) under nonplume condition, Central Sector.

develop under extreme physicochemical conditions (3). These marginal reef systems share some common trends such as a lowered importance of photosymbioses, reduced diversity of macroorganisms (macroalgae and metazoans), reduced grazing, and increased microbial diversity. With a greater areal extent, depth range, and latitudinal extent than that of coral reefs, marginal reefs have been relatively neglected by science, especially because of the logistical constraints for direct observation and mapping with remote sensing in turbid waters (33). Here, we presented a major carbonate system that occurs off the Amazon River mouth, adding to the wide repertoire of marginal reefs that includes large megahabitats (thousands of square kilometers) that were only recently mapped (31, 34), despite occurring in continental shelves.

The extensive reef system off the Amazon River mouth presents erosive structures that ceased to grow during the late stages of the last post-glacial maximum transgression, as revealed by the carbonate rocks dated in the Northern (13,382 to 12,749 calibrated years BP) and Central Sectors (4487 to 4846 and 4157 to 4562 calibrated years BP). Dead rhodolith beds and relict magnesium calcite ooids (11) are recorded in the Northern Sector, extending into southern French Guiana (25), and their ages are compatible to the surface of the dated structure from this sector. The age of this structure also corresponds to the transitional period of the last turn off of the Amazon Fan because of widespread shelf flooding (sea level reaching 40 to 50 m below present-day sea level) (7). Besides the last post-glacial transgression and shifts in the sediment budget because of fluvial, oceanographic, and meteorological processes (35), the reef building turnoff (36) in the Northern Sector also seems related to shelf subsidence, which reached more than 100 m between 16 and 21 thousand years BP

(35). Despite encompassing assemblages adapted to low light penetration, turbid zone reefs develop under narrow depth ranges and can be especially vulnerable to relative sea level changes (4).

Turbidity is elevated across the entire Equatorial Margin, but deposition is low in the outer shelf, especially in the Northern Sector, where the NBC reaches maximum speed (9) and prevents the burial of reefs by terrigenous sediments. Such high turbidity–low net sediment accumulation is also associated with the permanent frontal processes and Ekman pumping into the platform (9). From the Central Sector southward, turbidity decreases and the plume influence becomes more seasonal. The carbonate balance becomes positive from the Central Sector southward, mainly due to the high density of living rhodoliths covered by red algae (Corallinales), which are able to mineralize under very low light levels.

Although reef framework building has been “turned off” (35) in a significant portion of the Amazon reef range, in all sectors, there is a living assemblage of reef-associated organisms typical of West Atlantic mesophotic and deep reefs (37–39). The benthic assemblage of the Northern Sector is dominated by filter feeders adapted to strong currents, high suspended sediment, and lowered light and oxygen, such as octocorals and black corals, and especially by massive sponges with long papilla (*O. bartschi*), ball-shaped sponges (*Cinachyrella kuekenethali*), barrels with narrow atrium and high pumping rates (*X. muta*), and bulbs (*T. schmidtii*) (40). Besides bearing narrower atria typical of high current settings, the large barrel sponges, *X. muta*, were remarkable for being pale, possibly due to the lack of photosymbionts (fig. S1). An even more diverse assemblage of large sponges develops in association

to the high-vitality rhodolith beds of the Central Sector, including growth forms adapted to steady currents, to light capture by photosynthetic symbionts, and to sediment resistance (for example, tubes—*A. lacunosa*; curled fan—*C. vaginalis*; branched—*C. nicoleae*; massive with long inhaling papillae and narrow elevated central oscule—*O. bartschi*) (table S2). There are few larger coalesced structures in the Central Sector, and the topography of the rhodolith beds is limited by the size of the nodules (centimeters to tens of centimeters). However, the great sponge abundance significantly increases habitat complexity and enhances nutrient supply to other organisms, reducing DOC concentration and providing significant benthic production (41). The high abundance of sponges in the outer shelf was recorded in an early survey targeting the discovery of shrimp-trawling beds (12), but it is now clear that sponge diversity and abundance peaks in the intermediary portion of the plume influence gradient. Turbidity and extreme limitations in light penetration may control the diversity and abundance of sponges in the Northern Sector, whereas competition with other benthic organisms (coralline algae, macroalgae, and corals) and predation by reef fishes may be the most important controls southward.

Large sponge reefs are well documented in aphotic areas in different oceans, but they are generally dominated by Hexactinellida (glass sponges), with a few exceptions in which Demospongiae dominate. Reefs dominated by few species of hexactinellids are well documented in the Northeast Canadian shelf, between 30- and 240-m depths (32). Deep-water aggregates of large Demospongiae are known as “sponge grounds” or “sponge gardens” and are widely distributed in the North Atlantic (42). These habitats may encompass up to 50 sponge species, including a strong contribution of *Geodia* spp. (42, 43), which is a ubiquitous genus in the Amazon reefs (table S2). A sponge garden hotspot in West Australia (tropical Carnarvon Shelf) also has high richness and biomass concentrated between 40- and 100-m depths (40). The Central Sector of the Amazon reefs system is similar to such sponge gardens, presenting (i) high sponge diversity and biomass in the mesophotic zone; (ii) large, erect, cup-like, and massive forms adapted to sedimentation; and (iii) species with low inorganic content (with few or no spicules) concentrated where the shelf is wider and currents are weaker.

The shallower Southern Sector is an area with higher wave energy and episodic plume influence (23, 44), resembling the typical turbid zone reefs [for example, Perry and Larcombe (4)] with few species and sparse corals and hydrocorals (Fig. 1C). When compared to other reefs within the Brazilian Province and the Caribbean [for example, Wilkinson (45)], coral and coralline algal diversity is still relatively low, but carbonate accumulation is positive, as indicated by the dating of the structures. Indeed, high coral diversity and framework accumulation are often uncoupled, and the former may not be a universal surrogate of reef health (4).

The Amazon reefs are also noteworthy for supporting considerable fisheries yields that span all sectors, especially lobsters (Crustacea: Palinuroidea) and snappers (Perciformes: Lutjanidae). Although extensive shrimp trawling and other fisheries (for example, gill nets and long lines) are well documented in the soft sediments of the inner and mid-shelf [for example, Pinheiro and Frédo (46)], hundreds of artisanal and commercial boats operate in the outer shelf with hand lines and traps. For instance, lobster yields in the Amazon reefs (mostly *Panulirus argus*, but also including five other species) (47) are equivalent to 5% of the total lobster capture in the 23 Caribbean countries that explore this resource (48, 49). Because of Brazil incipient fisheries management, the exact number of boats that operate in the Amazon reefs remains undisclosed, but tracking data show that fishing effort with hand lines

and traps is concentrated in the outer shelf (fig. S8). Although some typical reef fisheries resources are lacking from the Amazon reefs (for example, parrot fishes), lobsters and other species (for example, red snapper and large groupers) may benefit from plume-related resources and conditions, showing that low-diversity reefs with incipient coral cover may still provide relevant and valuable ecosystem services.

The Amazon River mouth is the distribution boundary for several reef-associated organisms. Southward, the reef biota of the Brazilian Biogeographic Province is less diverse than that of the Caribbean and presents high endemism levels (24, 50). Although such lowered species richness seems to result from the relatively smaller area and sub-optimal conditions for reef development (for example, high turbidity and river runoff), endemism seems to be largely driven by the partial isolation of the Southwestern Atlantic. The selective and intermittent nature of the Amazon mouth biogeographic filter may drive parapatric divergence (instead of allopatric speciation) because this model allows for restricted gene flow between diverging populations (51). Indeed, the novel information about the characteristics and extension of the Amazon mouth reef system provides additional support to the phylogeographic evidence for the operation of parapatric speciation, whereas our updated checklist of reef-associated organisms (tables S1 to S4) clarifies the selective nature of the biogeographic corridor.

The relatively low-diversity assemblage of algae, sponges, corals, and reef fishes is dominated by wide depth-ranging species that are broadly distributed in the Atlantic (or in the West Atlantic) (tables S1 to S4). Shallow-water dwellers, or species that depend on specific coralline microhabitats or resources, are not able to use the Amazon reef system as a stepping stone because reef structures and rhodolith beds are largely located in relatively deep areas (>40 m) with limited availability of habitat and food resources. At ecological time frames, such shallow-water dwellers must rely on larval dispersal or rafting (22) across the hyposaline plume within the unidirectional NBC, a fact that helps explain the higher Brazilian-endemism level within fish groups such as blennies (shallow-water dwellers) and parrot fishes (specialized herbivores) (52–54). Brazilian-endemic corals such as *Mussimilia* spp., which have expressive cover southward (55), are also shallow-water dwellers. These species only occur in deeper habitats in oceanic islands and offshore banks, where light penetration reaches greater depths. At larger time scales (thousands to tens of thousands years), lowered relative sea level (7) and other environmental fluctuations may “turn on” the Amazon Fan and widespread reef development in the Amazon reef system, providing a more permeable connectivity matrix between the Caribbean and the South Atlantic.

At least 29 sponge taxa are still identified only at supraspecific levels, indicating a source for new species. An alien brittle star from the Pacific Ocean, *O. mirabilis*, which was known from Brazil and French Guiana (56), was recorded in the Amazon reefs, showing that invasive species introduced in the Caribbean (for example, lionfishes) may reach the South Atlantic through this countercurrent dispersal route (57). Modeling of potential bioinvasions through this route may take depth range into account because of depth selectivity of the Amazon mouth biogeographic filter.

The inner Amazon shelf is known for high rates of benthic respiration, which is associated with the river-sourced terrestrial material (19). In the Amazon reefs, microbial metabolisms deviate from those commonly found in coralline reefs (39, 58) because they include chemosynthesis and heterotrophy, particularly in the Northern and Central Sectors. This particular functional structure is better understood from

the layered structure comprising the plume, the subplume, and the benthic mosaic (Fig. 1 and fig. S2). Light reduction may condition heterotrophic and chemosynthetic microbial metabolisms (Fig. 3 and figs. S9 and S10). Whereas photosynthesis is the major carbon fixation process in nonplume waters, the subplume presents significant amounts of gene transcripts related to anaerobic respiration, resembling an oxygen minimum zone (OMZ), and corroborates the observed oxycline. Oxygen depletion in the subplume is not as drastic as in other OMZs (54), but oxygen levels near the bottom can be as low as 3 ml liter⁻¹ and can potentially limit some benthic organisms.

At the Northern and Central Sectors, calcareous algae may photosynthesize at low light levels, and sponges may tolerate anoxic and suboxic conditions for several days (59). The sponge assemblage includes both high microbial abundance (HMA) and low microbial abundance (LMA) species (60); the former rely heavily on microbial symbionts, whereas the latter use water column microbes for nourishment. Symbiotic microbes associated with HMA sponges include chemosynthetic and fermenting taxa (for example, *Proteobacteria*, *Firmicutes*, *Actinobacteria*, *Planctomycetes*, and *Thaumarchaeota*) and *Cyanobacteria* (60) that help sponge metabolism. On the other hand, the high POC and DOC concentration in the Amazon mouth reefs may promote an intense development of LMA sponge loop (61, 62).

Although the low-salinity plume stays well above the seafloor, the plume may interact dynamically with benthic organisms through particle flux, shear, and enhanced eddy stirring and mixing (15). The clear marked difference in isotopic composition can be related to increased anoxia, with heavier N increased in the subplume (higher subplume N₂ concentration). A significant fractionation in isotopic composition of N between suspended particles (plume and subplume layers) and surface sediment corroborates the presence of processes such as nitrogen fixation and denitrification/anammox (63). In addition, the isotopic analysis of plume and subplume DOC and POC indicates a strong contribution from terrestrial and mangrove-derived material, suggesting that the reefs in the Northern and Southern Sector are subjected to very specific biogeochemical conditions. Previous studies have suggested a rapid turnover of organic matter from terrestrial and mangrove origins, with a longer persistence of mangrove-derived DOC, with contribution to oceanic areas accounting for >10% of DOC (64, 65). Our results are in agreement with these patterns, and the isotopic signatures for Amazon rivers [−26.8 to −30.4‰ (DOC) and −27.4 ± 0.8‰ (POC)], mangrove waters [−31.4‰ (DOC) and −28.1 ± 1.5‰ (POC)], surface Atlantic waters [−20.8 ± 1.1‰ (DOC)], and deep Atlantic waters [−23.7‰ (DOC)] reinforce the contribution from terrestrial and mangrove-derived material to the reefs' DOC and POC pools.

The rapid decline of coral reefs is drawing considerable attention because of the alarming forecasts of biodiversity losses from local (for example, pollution and overfishing) and global stressors (temperature anomalies and ocean acidification) (66, 67). Understanding the distribution of the several reef subtypes and how their biodiversity and functional properties are associated with different environmental forcing is a major and basic step toward forecasting generalized trajectories for reef systems (41, 68). In this regard, studies of marginal reef ecosystems have a major role to play in reef ecology because scleractinian-dominated communities may not be a universal baseline. The Amazon reef system comprises a gradient from marginal mineralization conditions (South Sector) to structures that are beyond CaCO₃ mineralization thresholds for thousands of years (North Sector) but still supports significant reef-associated biodiversity and relevant ecosystem

services. For low trophic level fisheries resources, such as lobsters, the system seems to support higher yields than coral-dominated reefs (49). The CaCO₃ production by rhodolith beds (1.3 to 2.7 kg m⁻² year⁻¹), the dominant megahabitat in vast expanses of tropical and temperate shelves (30), as well as in the Amazon mouth, is close to the mean global coral reef rate (1.5 kg m⁻² year⁻¹) (31). Although the impoverished coral reefs in the Brazilian Province represent only 5% of the Atlantic reef area (33), the region's extensive rhodolith beds produce >0.025 gigatons year⁻¹, rivaling with the total CaCO₃ production by coral reefs in the Caribbean (0.04 to 0.08 gigatons year⁻¹). Although corals appear biologically fragile, they are geologically robust (“the most ingenious paradox”) (69), and there is mounting evidence that peripheral areas with reef-associated organisms may be a key to the evolution and survival of coral reef biota through geological time (70, 71).

The sponge dominance in the Central Sector provides support to the idea that coral domination may phase-shift to sponge domination as climate changes and some local stressors escalate (for example, nutrients) (40, 70). Sponges, corals, and coralline algae respond differently to ocean chemistry and environmental conditions, with sponges benefitting from increased DOC and POC while having broader tolerance to acidification and temperature anomalies. Indeed, sponges are the oldest reef-associated organisms; they dominated reef building during various stages of the Paleozoic and Mesozoic when conditions to biomineralizers deteriorated (28).

In conclusion, the novel reef system off the Amazon River is extensive, is impoverished in terms of biodiversity, and presents unique functional attributes due to the plume influence. The system provides relevant ecosystem services and functions as a selective biogeographic corridor between the Caribbean and the South Atlantic Ocean, and may give important insights in terms of future scenarios for forecasting coralline reefs trajectories under acute climate changes. Remarkably, 125 exploratory blocks for oil drilling in the Amazon shelf were offered in an international auction in 2013, 35 of which were acquired by domestic and transnational companies. In the past decade, a total of 80 exploratory blocks have been acquired for oil drilling in the study region, 20 of which are already producing. These blocks will soon be producing oil in close proximity to the reefs, but the environmental baseline compiled by the companies and the Brazilian government is still incipient and largely based on sparse museum specimens (13). Such large-scale industrial activities present a major environmental challenge, and companies should catalyze a more complete social-ecological assessment of the system before impacts become extensive and conflicts among the stakeholders escalate. The feasibility of oil and gas operations may be assessed by considering environmental and social sensibilities, but even the extent of the overlap of exploratory blocks with sensitive areas remains unclear. The context of great proximity to international waters and to the French border adds complexity. It is relevant to consider further studies on regional marine spatial planning, the functioning of the new reef biome in face of global changes, and sensitivities related to the hydrologic cycle of the Amazon—where extreme droughts and floods are on the increase and will influence the functioning of this novel carbonate reef system.

MATERIALS AND METHODS

Experimental design

Sampling was carried out onboard R/V Knorr (May 2010), R/V Atlantis (July 2012), and NHO Cruzeiro do Sul (September 2014). A

complete station list of the three cruises is provided in table S5. To assess the effects of the dynamic river-ocean interface, sampling was stratified in (i) Northern Sector, representing the area under the strongest and permanent plume influence; (ii) Central Sector, under seasonal plume influence; and (iii) Southern Sector, under intermittent riverine influence (Fig. 1). Water column profiles were acquired with a conductivity-temperature-depth with a recorder (CTD), which was also equipped with sensors of PAR and DO at eight stations in 2010 and at nine stations in 2014 (table S5). Water was collected from near the surface, bottom, and in the chlorophyll maximum using Niskin bottles or surface pumps, and was analyzed for inorganic nutrients (16), DOC and POC (16, 72), and microorganisms (20, 73).

Bottom topography. We obtained 800 km of acoustic data with a Kongsberg EM122 Multibeam Echosounder in 2012. In 2014, we surveyed 500 km with two EdgeTech side scan sonars (model 4200, 100 to 400 kHz at stations 1 to 56; model 4100, 100 to 500 kHz at stations 67 to 100). Both surveys were carried out with ~300-m swath widths. Sonograms were processed with Sonar WizMap 5.03, converted into 1-m pixel images, and further vectored and submitted to supervised qualitative classification in a GIS environment. Classification was based on backscatter intensity and indirect topography (74).

Macrobenthic and demersal assemblages. We sampled 14 stations (5 in 2012 and 9 in 2014; Fig. 1) with heavy (150 kg) metal dredges with mouths of 100 to 150 by 40 to 80 cm and mesh nets of 1 cm² that were trawled at 1 to 1.5 knots for 5 to 20 min. Two box corer launches were done in six stations of the 2014 cruise, and a flat shrimp net (15-m mouth, 1.5-cm mesh in the cod end, and two 150-kg trawl doors) was trawled in three stations. Dredging, trawling, or box-coring covered stations in all three sectors. Specimens were washed in seawater, sorted, and photographed on board, and were further preserved in 80% ethanol or 5% formalin. Frozen or dried subsamples were kept for microbiological, genetic, and chemical analyses. Vouchers were deposited at the Museu Nacional, Universidade Federal do Rio de Janeiro, and at the Jardim Botânico do Rio de Janeiro. Crustose coralline algae, sponges, and fishes were identified with standard methods (75, 76). Fisheries yields were obtained from unpublished governmental reports that refer to the last year during which Brazil monitored fisheries (2007). Only landings in Pará and Amapá were accounted for (Maranhão was excluded because its fleet extends southward to the Amazon River mouth).

Petrographic and isotopic analyses. Petrographic thin sections (30 µm) of carbonate rocks recovered in each sector were used to assess reef builders' identities and relative importance. Radiocarbon (¹⁴C) ages were determined from the same samples, which included the surface and core of a larger carbonate block (~45 cm) from the Central Sector (80-m depth), and two superficial smaller (~20 cm) framework fragments from the North and Central Sector, obtained at depths of 120 and 23 m, respectively. Radiocarbon ages were derived from carbon reduction to graphite (100% C) after acid etch pretreatment, with subsequent detection in Accelerator Mass Spectrometry (Center for Applied Isotope Studies, University of Georgia). Dates were reported as 2σ calibrated (95% confidence) radiocarbon ages BP. Calibration was carried out using Calib 7.1 (available at <http://calib.qub.ac.uk/calib/>), Marine13 calibration curve, and assuming a global marine reservoir effect of 400 years (radiocarbon years before present, "present" = AD 1950). Organic matter samples were analyzed for C and N isotopes using an isotope ratio mass spectrom-

eter (model DELTA V Advantage, Thermo Fisher Scientific) as described previously (77).

Secondary data sets. Literature data indicative of reefs and reef-associated biota were compiled and incorporated in the GIS (Fig. 2), including observations of high CaCO₃ sediments, magnesium calcite ooids [for example, Barreto *et al.* (8)], sponges and reef fish (12), and reef fisheries (26).

Metatranscriptomes from the plume and subplume. Microbial genes and transcripts were obtained from water samples obtained at six stations of the 2010 cruise (73) and two stations of the 2012 cruise, inside and outside the plume, and in the subplume. Data sets were generated by Illumina sequencing (150 × 150 base pairs overlapping paired-end reads) and were deposited in GenBank under accession number SRP037995 (73). Ribosomal sequences in RNA-seq data (complementary DNA sequencing) were identified and removed from metatranscriptome data sets using riboPicker tool (73). Identification of chemosynthesis-related genes (that is, sulfur oxidation, sulfate reduction, and anammox transcripts in the plume and subplume interface) was performed based on profile hidden Markov model (pHMM) approach. Full-length sulfur oxidation (SoxA, SoxB, SoxX, SoxY, and SoxZ), sulfate reduction (DsrA, DsrB, DsrJ, DsrK, DsrL, DsrM, DrsO, DrsP, AprA, and AprB), and anammox (NarB, NarG, NarH, NarI, NirA, NirB, NirK, and NirS) amino acid sequences obtained from the UniProtKB database (www.uniprot.org) were used as seed alignments. pHMM profiles of protein subunits families related to photosynthesis were also used for contrasting water layers, using both photosystem complexes: I (PsaF, PsaM, PsaN, and PsaAB) and II (PsbN, PsbI, PsbH, and PSII). Profiles were obtained directly from the Pfam database (PsaN-PF05479, PsaM-PF07465, PsaAB-PF00223, PsaF-PF02507, PsbN-PF02468, PsbI-PF02532, PSII-PF00421, and PsbH-PF00737). Multiple alignments were conducted using MAFFT (version 6.717b) (78, 79) with the auto mode option, and pHMMs were built using hmmbuild functionality from HMMER package (version 3.0). Contigs assembled from metatranscriptomes were translated into six frames using the Transeq program from the EMBOSS package (v6.1.0) and used as the database for searching genes related to sulfur oxidation, sulfate reduction, and anammox metabolisms. Search was conducted using hmmersearch functionality from HMMER package of the pHMMs built against the plume database. Results were parsed and counted using Python, and shell scripts and relative abundance were calculated.

SUPPLEMENTARY MATERIALS

Supplementary material for this article is available at <http://advances.sciencemag.org/cgi/content/full/2/4/e1501252/DC1>

- fig. S1. Trawl and dredge casts on ships' deck.
- fig. S2. Sonographic images of the main reef megahabitats off the Amazon River mouth.
- fig. S3. Carbonate fragments (A and B) and rhodoliths (C and D) sampled off the Amazon River mouth.
- fig. S4. Representative species of sponges collected off the Amazon River mouth.
- fig. S5. Representative species of corals and hydrocoral collected off the Amazon River mouth.
- fig. S6. Representative reef fish species collected off the Amazon River mouth.
- fig. S7. Fishing boat operating dinghies with hand lines and long lines near the shelf edge in the Northern Sector during the 2014 cruise.
- fig. S8. Density of fishing operations targeting red snapper (*L. purpurus*) in 2010 off the Amazon mouth.
- fig. S9. Depth profiles of salinity and DO measured during the R/V Cruzeiro do Sul cruise (September 2014).
- fig. S10. Relative contribution of functions related to chemosynthesis and photosynthesis recorded outside, within, and underneath the Amazon River plume.

table S1. Algae recorded off the Amazon River mouth.
 table S2. Sponges recorded off the Amazon River mouth.
 table S3. Corals, hydrocorals, and gorgonians recorded off the Amazon River mouth.
 table S4. Reef fish species recorded off the Amazon mouth [does not include species recorded at the Manuel Luis reefs; see de Moura *et al.* (23) and Rocha and Rosa (44)].
 table S5. Oceanographic stations (primary data sources).
 movie S1. Sampling the plume, subplume, and reefs off the Amazon river mouth during the NHo Cruzeiro do Sul cruise (2014).
 Supplementary file. Shape files.
 References (81–85)

REFERENCES AND NOTES

1. C. Birkeland, Ed. *Life and Death of Coral Reefs* (Chapman & Hall, New York, 1997).
2. W. N. Goldberg, *The Biology of Reefs and Reef Organisms* (The University of Chicago Press, Chicago, IL, 2013).
3. R. Riding, Structure and composition of organic reefs and carbonate mud mounds: Concepts and categories. *Earth Sci. Rev.* **58**, 163–231 (2002).
4. C. T. Perry, P. Larcombe, Marginal and non-reef-building coral environments. *Coral Reefs* **22**, 427–432 (2003).
5. J. D. Milliman, C. P. Summerhayes, H. T. Barreto, Quaternary sedimentation on the Amazon continental margin: A model. *Geol. Soc. Amer. Bull.* **86**, 610–614 (1975).
6. C. Gorini, B. U. Haq, A. T. dos Reis, C. G. Silva, A. Cruz, E. Soares, D. Grangeon, Late Neogene sequence stratigraphic evolution of the Foz do Amazonas Basin, Brazil. *Terra Nova* **26**, 179–185 (2014).
7. M. A. Maslin, E. Durham, S. J. Burns, E. Platzman, P. Grootes, S. E. J. Greig, M.-J. Nadeau, M. Schleicher, U. Pflaumann, B. Lomax, N. Rimington, Paleoreconstruction of the Amazon River freshwater and sediment discharge using sediments recovered at site 942 on the Amazon Fan. *J. Quaternary Sci.* **15**, 419–434 (2000).
8. L. A. Barreto, J. D. Milliman, C. A. B. Amaral, O. Francisconi, Upper continental margin sedimentation off Brazil, northern Brazil. *Contr. Sedimentol.* **4**, 11–43 (1975).
9. C. A. Nittrouer, D. J. DeMaster, The Amazon shelf setting: Tropical, energetic, and influenced by a large river. *Cont. Shelf Res.* **16**, 553–573 (1996).
10. J. Y. Aller, I. Stupakoff, The distribution and seasonal characteristics of benthic communities on the Amazon shelf as indicators of physical processes. *Cont. Shelf Res.* **16**, 717–751 (1996).
11. J. D. Milliman, H. T. Barreto, Relict magnesian calcite oolite on the Amazon shelf. *Sedimentology* **22**, 137–145 (1975).
12. B. B. Collette, K. Rützel, Reef fishes over sponge bottoms off the mouth of the Amazon river. *Proceedings of the 3rd International Coral Reef Symposium*, Miami, FL, 1977 May.
13. R. T. S. Cordeiro, B. M. Neves, J. S. Rosa-Filho, C. D. Pérez, Mesophotic coral ecosystems occur offshore and north of the Amazon River. *Bull. Mar. Sci.* **91**, 491–510 (2015).
14. N. D. Ward, A. V. Krusche, H. O. Sawakuchi, D. C. Brito, A. C. Cunha, J. M. S. Moura, R. da Silva, P. L. Yager, R. G. Keil, J. E. Richey, The compositional evolution of dissolved and particulate organic matter along the lower Amazon River—Óbidos to the ocean. *Mar. Chem.* **177**, 244–256 (2015).
15. V. J. Coles, M. T. Brooks, J. Hopkins, M. R. Stukel, P. L. Yager, R. R. Hood, The pathways and properties of the Amazon River plume in the tropical North Atlantic Ocean. *J. Geophys. Res.* **118**, 6894–6913 (2013).
16. J. I. Goes, H. do Rosario Gomes, A. M. Chekalyuk, E. J. Carpenter, J. P. Montoya, V. J. Coles, P. L. Yager, W. M. Berelson, D. G. Capone, R. A. Foster, D. K. Steinberg, A. Subramaniam, M. A. Hafez, Influence of the Amazon River discharge on the biogeography of phytoplankton communities in the western tropical north Atlantic. *Prog. Oceanogr.* **120**, 29–40 (2014).
17. A. Subramaniam, P. L. Yager, E. J. Carpenter, C. Mahaffey, K. Björkman, S. Cooley, A. B. Kustka, J. P. Montoya, S. A. Sañudo-Wilhelmy, R. Shipe, D. G. Capone, Amazon River enhances diazotrophy and carbon sequestration in the tropical North Atlantic Ocean. *Proc. Natl. Acad. Sci. U.S.A.* **105**, 10460–10465 (2008).
18. L. S. Chong, W. M. Berelson, J. McManus, D. E. Hammond, N. E. Rollins, P. L. Yager, Carbon and biogenic silica export influenced by the Amazon River Plume: Patterns of remineralization in deep-sea sediments. *Deep Sea Res. Pt. I* **85**, 124–137 (2014).
19. N. E. Blair, R. C. Aller, Anaerobic methane oxidation on the Amazon shelf. *Geochim. Cosmochim. Acta* **59**, 3707–3715 (1995).
20. B. M. Satinsky, B. C. Crump, C. B. Smith, S. Sharma, B. L. Zielinski, M. Doherty, J. Meng, S. Sun, P. M. Medeiros, J. H. Paul, V. J. Coles, P. L. Yager, M. A. Moran, Microspatial gene expression patterns in the Amazon River Plume. *Proc. Natl. Acad. Sci. U.S.A.* **111**, 11085–11090 (2014).
21. P. Milosavljević, E. Klein, J. M. Díaz, C. E. Hernández, G. Bigatti, L. Campos, F. Artigas, J. Castillo, P. E. Penchaszadeh, P. E. Neill, A. Carranza, M. V. Retana, J. M. Díaz de Astarloa, M. Lewis, P. Yorío, M. L. Piriz, D. Rodríguez, Y. Yoneshigue-Valentin, L. Gamboa, A. Martín, Marine biodiversity in the Atlantic and Pacific coasts of South America: Knowledge and gaps. *PLOS One* **6**, e14631 (2011).
22. O. J. Luiz, J. S. Madin, D. R. Robertson, L. A. Rocha, P. Wirtz, S. R. Floeter, Ecological traits influencing range expansion across large oceanic dispersal barriers: Insights from tropical Atlantic reef fishes. *Proc. R. Soc. B* **279**, 1033–1040 (2011).
23. R. L. de Moura, M. C. Martins Rodrigues, R. B. Francini-Filho, I. Szazima, Unexpected richness of reef corals near the southern Amazon River mouth. *Coral Reefs* **18**, 170 (1999).
24. L. A. Rocha, Patterns of distribution and processes of speciation in Brazilian reef fishes. *J. Biogeogr.* **30**, 1161–1171 (2003).
25. CREOCEAN, Évaluation de l'évolution des peuplements halieutiques des zones adjacentes éloignées au site. Première campagne—avant acquisition sismique (Shell E&P France, Le Lamentin, Martinique, 2012).
26. IBAMA, *Instituto Brasileiro do Meio Ambiente e dos Recursos Naturais Renováveis. Estatística da Pesca no Brasil. Grandes regiões e unidades da federação* (Ministério do Meio Ambiente, Brasília, Brasil, 2007); <http://www.ibama.gov.br/documentos-recursos-pesqueiros/estatistica-pesqueira>.
27. F. Hiemstra, R. W. M. van Soest, *Didiscus verdensis* spec. nov. (Porifera: Halichondrida) from the Cape Verde Islands, with a revision and phylogenetic classification of the genus *Didiscus*. *Zoologische Mededelingen* **65**, 39–52 (1991).
28. W. Kiessling, Geologic and biologic controls on the evolution of reefs. *Annu. Rev. Ecol. Evol. Syst.* **40**, 173–192 (2009).
29. D. R. Bellwood, C. H. R. Goatley, S. J. Brandl, O. Bellwood, Fifty million years of herbivory on coral reefs: Fossils, fish and functional innovations. *Proc. R. Soc. B.* **281**, 20133046 (2014).
30. M. S. Foster, Rhodoliths: Between rocks and soft places. *J. Geophys. Res.* **37**, 659–667 (2001).
31. G. M. Amado-Filho, R. L. Moura, A. C. Bastos, L. T. Salgado, P. Y. Sumida, A. Z. Guth, R. B. Francini-Filho, G. H. Pereira-Filho, D. P. Abrantes, P. S. Brasileiro, R. G. Bahia, R. N. Leal, L. Kaufman, J. A. Kleypas, M. Farina, F. L. Thompson, Rhodolithbeds are major CaCO₃ bio-factories in the Tropical South West Atlantic. *PLOS One* **7**, e35171 (2012).
32. L. S. Eluik, Siliceous sponge communities, biological zonation, and recent sea-level change on the Arctic margin: Ice island results: Discussion. *Can. J. Earth Sci.* **28**, 459–462 (1991).
33. M. D. Spalding, C. Ravillious, E. P. Green, *World Atlas of Coral Reefs* (University of California Press, Berkeley, CA, 2001).
34. R. L. Moura, N. A. Secchin, G. M. Amado-Filho, R. B. Francini-Filho, M. O. Freitas, C. V. Mente-Vera, J. B. Teixeira, F. L. Thompson, G. F. Dutra, P. Y. G. Sumida, A. Z. Guth, R. M. Lopes, A. C. Bastos, Spatial patterns of benthic megahabitats and conservation planning in the Arolhos Bank. *Cont. Shelf Res.* **70**, 109–117 (2013).
35. C. K. Sommerfield, C. A. Nittrouer, A. G. Figueiredo, Stratigraphic evidence of changes in Amazon shelf sedimentation during the late Holocene. *Mar. Geol.* **125**, 351–371 (1995).
36. C. T. Perry, S. G. Smithers, Evidence for the episodic “turn-on” and “turn-off” of turbid-zone coral reefs during the late Holocene sea-level highstand. *Geology* **38**, 119–122 (2010).
37. G. Olavo, P. C. S. Costa, A. S. Martins, B. P. Ferreira, Shelf-edge reefs as priority areas for conservation of reef fish diversity in the tropical Atlantic. *Aquat. Conserv.* **21**, 199–209 (2011).
38. H. T. Pinheiro, E. Mazzei, R. L. Moura, G. M. Amado-Filho, A. Carvalho-Filho, A. C. Braga; P. A. S. Costa, B. P. Ferreira, C. E. L. Ferreira, S. R. Floeter, R. B. Francini-Filho, J. L. Gasparini, R. M. Macieira, A. S. Martins, G. Olavo, C. R. Pimentel, L. A. Rocha, I. Szazima, T. Simon, J. B. Teixeira, L. B. Xavier, J.-C. Joyeux, Fish biodiversity of the Vitória-trindade seamount chain, Southwestern Atlantic: An updated database. *PLOS One* **10**, e0118180 (2015).
39. P. M. Meirelles, G. M. Amado-Filho, G. H. Pereira-Filho, H. T. Pinheiro, R. L. de Moura, J.-C. Joyeux, E. F. Mazzei, A. C. Bastos, R. A. Edwards, E. Dinsdale, R. Paranhos, E. O. Santos, T. Iida, K. Gotoh, S. Nakamura, T. Sawabe, C. E. Rezende, L. M. R. Gadelha Jr., R. B. Francini-Filho, C. Thompson, F. L. Thompson, Baseline assessment of mesophotic reefs of the Vitória-Trindade seamount chain based on water quality, microbial diversity, benthic cover and fish biomass data. *PLOS One* **10**, e0130084 (2015).
40. C. H. L. Schönberg, J. Fromont, Sponge gardens of Ningaloo Reef (Camarvon Shelf, Western Australia) are biodiversity hotspots. *Hydrobiologia* **687**, 143–161 (2011).
41. J. J. Bell, S. K. Davy, T. Jones, M. W. Taylor, N. S. Webster, Could some coral reefs become sponge reefs as our climate changes? *Glob. Change Biol.* **19**, 2613–2624 (2013).
42. A. B. Klitgaard, O. S. Tendal, Distribution and species composition of mass occurrences of large-sized sponges in the northeast Atlantic. *Prog. Oceanogr.* **61**, 57–98 (2004).
43. L. I. Beazley, E. L. Kenchington, F. J. Murillo, M. del Mar Sacau, Deep-sea sponge grounds enhance diversity and abundance of epibenthic megafauna in the Northwest Atlantic. *ICES J. Mar. Sci.* **70**, 1471–1490 (2013).
44. L. A. Rocha, I. L. Rosa, Baseline assessment of reef fish assemblages of Parcel Manuel Luiz Marine State Park, Maranhão, north-east Brazil. *J. Fish Biol.* **58**, 985–998 (2001).
45. C. R. Wilkinson, Ed., *Status of Coral Reefs of the World: 2008* (Global Coral Reef Monitoring Network and Reef and Rainforest Research Centre, Townsville, Australia, 2008).
46. L. A. Pinheiro, F. L. Frédou, Caracterização geral de pesca industrial desembarcada no estado do Pará. *Rev. Cient. Universidade Federal do Pará* **4**, 1–16 (2004).
47. K. C. Araujo-Silva, I. H. A. Cintra, M. Ramos-Porto, G. F. S. Viana, Lagostas capturadas na plataforma continental do estado do Amapá (Crustacea, Nephropoidea, Palinuroidea). *Bol. Téc. Cient. CEPNOR* **7**, 173–184 (2007).
48. A. A. Fonteles-Filho, Síntese sobre distribuição, abundância, potencial pesqueiro e biologia lagosta-vermelha *Panulirus argus* (Latreille) e a lagosta-verde *Panulirus laeviscauda* (Latreille) do nordeste do Brasil (Ministério do Meio Ambiente/Recursos Vivos na Zona Econômica Exclusiva, Brasília, Brasil, 2008).
49. E. A. Chávez, Potential production of the Caribbean spiny lobster (Decapoda, Palinura) fisheries. *Crustaceana* **82**, 1393–1412 (2009).

50. G. Muricy, D. A. Lopes, E. Hajdu, M. S. Carvalho, F. C. Moraes, M. Klautau, C. Menegola, U. Pinheiro, *Catalogue of Brazilian Porifera* (Museu Nacional, Rio de Janeiro, 2011).
51. L. A. Rocha, B. W. Bowen, Speciation in coral reef fishes. *J. Fish Biol.* **72**, 1101–1121 (2008).
52. R. L. Moura, I. Szazima, Species richness and endemism levels of the Southwestern Atlantic reef fish fauna, *Ninth International Coral Reef Symposium*, Bali, Indonesia, 23–27 October 2000.
53. S. R. Floeter, L. A. Rocha, D. R. Robertson, J. C. Joyeux, W. F. Smith-Vaniz, P. Wirtz, A. J. Edwards, J. P. Barreiros, C. E. L. Ferreira, J. L. Gasparini, A. Brito, J. M. Falcón, B. W. Bowen, G. Bernardi, Atlantic reef fish biogeography and evolution. *J. Biogeogr.* **35**, 22–47 (2008).
54. D. E. Canfield, F. J. Stewart, B. Thamdrup, L. De Brabandere, T. Dalsgaard, E. F. Delong, N. P. Revsbech, O. Ulloa, A cryptic sulfur cycle in oxygen-minimum-zone waters off the Chilean coast. *Science* **330**, 1375–1378 (2010).
55. R. B. Francini-Filho, E. O. C. Coni, P. M. Meirelles, G. M. Amado-Filho, F. L. Thompson, G. H. Pereira-Filho, A. C. Bastos, D. P. Abrantes, C. M. Ferreira, F. Z. Gibran, A. Z. Güth, P. Y. G. Sumida, N. L. Oliveira, L. Kaufman, C. V. Minte-Vera, R. L. Moura, Dynamics of coral reef benthic assemblages of the Abrolhos Bank, Eastern Brazil: Inferences on natural and anthropogenic drivers. *PLOS One* **8**, 54260 (2013).
56. G. Hendler, S. J. Brugneaux, New records of brittle stars from French Guiana: *Ophiactissavignyi* and the alien species *Ophiothela mirabilis* (Echinodermata: phiueroidea). *Mar. Biodiv. Res.* **6**, 113 (2013).
57. O. J. Luiz, S. R. Floeter, L. A. Rocha, C. E. L. Ferreira, Perspectives for the lionfish invasion in the South Atlantic: Are Brazilian reefs protected by the currents? *Mar. Ecol. Prog. Ser.* **485**, 1–7 (2013).
58. T. Bruce, P. M. Meirelles, G. Garcia, R. Paranhos, C. E. Resende, R. L. de Moura, R.-F. Filho, E.O. C. Coni, A. T. Vasconcelos, G. A. Filho, M. Hatay, R. Schmieder, R. Edwards, E. Dinsdale, F. L. Thompson, Abrolhos bank reef health evaluated by means of water quality, microbial diversity, benthic cover, and fish biomass data. *PLOS One* **7**, e36687 (2012).
59. D. B. Mills, L. M. Warda, C. Jones, B. Sweetenham, M. Forth, A.H. Treusch, D. E. Canfield, Oxygen requirements of the earliest animals. *Proc. Natl. Acad. Sci. U.S.A.* **111**, 4168–4172 (2014).
60. V. Gloeckner, M. Wehr, L. Moitinho-Silva, C. Gernert, P. Schupp, J. R. Pawlik, N. L. Lindquist, D. Erpenbeck, G. Wörheide, U. Hentschel, The HMA-LMA dichotomy revisited: An electron microscopical survey of 56 sponge species. *Biol. Bull.* **227**, 78–88 (2014).
61. J. M. de Goeij, D. van Ovelen, M. J. A. Vermeij, R. Osinga, J. J. Middelburg, A. F. P. M. Goeij, W. Admiraal, Surviving in a marine desert: The sponge loop retains resources within coral reefs. *Science* **342**, 108–110 (2013).
62. C. B. Silveira, A. W. Silva-Lima, R. B. Francini-Filho, J. S.M. Marques, M. G. Almeida, C. C. Thompson, C. E. Rezende, R. Paranhos, R. L. Moura, P. S. Salomon, F. L. Thompson, Microbial and sponge loops modify fish production in phase-shifting coral reefs. *Environ. Microbiol.* **17**, 3832–3846 (2015).
63. R. S. Robinson, M. Kienast, A. L. Albuquerque, M. Altabet, S. Contreras, R. De Pol Holz, N. Dubois, R. Francois, E. Galbraith, T.-C. Hsu, T. Ivanochko, S. Jaccard, S.-J. Kao, T. Kiefer, S. Kienast, M. Lehmann, P. Martinez, M. M. Carthy, J. Möbius, T. Pedersen, T. M. Quan, E. Ryabenko, A. Schmittner, R. Schneider, A. Schneider-Mor, M. Shigemitsu, D. Sinclair, C. Somes, A. Studer, R. Thunell, J.-Y. Yang, A review of nitrogen isotopic alteration in marine sediments. *Paleoceanography* **27**, PA4203 (2012).
64. T. Dittmar, R. J. Lara, G. Kattner, River or mangrove? Tracing major organic matter sources in tropical Brazilian coastal waters. *Mar. Chem.* **73**, 253–271 (2001).
65. T. Dittmar, N. Hertkorn, G. Kattner, R. J. Lara, Mangroves, a major source of dissolved organic carbon to the oceans. *Global Biogeochem. Cycles* **20**, GB1012 (2006).
66. O. Hoegh-Guldberg, P. J. Mumby, A. J. Hooten, R. S. Steeneck, P. Greenfield, E. Gomez, C. D. Harvell, P. F. Sale, A. J. Edwards, K. Caldeira, N. Knowlton, C. M. Eakin, R. Iglesias-Prieto, N. Muthiga, R. H. Bradbury, A. Dubi, M. E. Hatzitolos, Coral reefs under rapid climate change and ocean acidification. *Science* **318**, 1737–1742 (2007).
67. P. Descombes, M. S. Wisz, F. Leprieur, V. Parravicini, C. Heine, S. M. Olsen, D. Swingedouw, M. Kulbicki, D. Mouillot, L. Pellissier, Forecasted coral reef decline in marine biodiversity hotspots under climate change. *Glob. Change Biol.* **21**, 2479–2487 (2015).
68. J. M. Pandolfi, S. R. Connolly, D. J. Marshall, A. L. Cohen, Projecting coral reef futures under global warming and ocean acidification. *Science* **333**, 418–422 (2011).
69. A. J. Andersson, F. T. Mackenzie, A. Lerman, Coastal ocean and carbonate systems in the high CO₂ world of the anthropocene. *Am. J. Sci.* **305**, 875–918(2005).
70. B. W. Bowen, L. A. Rocha, R. J. Toonen, S. A. Karl; ToBo Laboratory, The origins of tropical marine biodiversity. *Trends Ecol. Evol.* **28**, 359–366(2013).
71. A. V. Norström, M. Nyström, J. Lokrantz, C. Folke, Alternative states on coral reefs: Beyond coral–macroalgal phase shifts. *Mar. Ecol. Prog. Ser.* **376**, 295–306 (2009).
72. P. M. Medeiros, M. Seidel, N. D. Ward, E. J. Carpenter, H. R. Gomes, J. Niggemann, A. V. Krusche, J. E. Richey, P. L. Yager, T. Dittmar, Fate of the Amazon River dissolved organic matter in the tropical Atlantic Ocean. *Global Biogeochem. Cy.* **29**, 677–690 (2015).
73. B. M. Satinsky, B. L. Zielinski, M. Doherty, C. B. Smith, S. Sharma, J. H. Paul, B.C. Crump, M. A. Moran, The Amazon continuum dataset: Quantitative metagenomic and metatranscriptomic inventories of the Amazon River plume, June 2010. *Microbiome* **2**, 17 (2014).
74. G. S. Cavalcanti, G. B. Gregoracci, E. O. dos Santos, C. B. Silveira, P. M. Meirelles, L. Longo, K. Gotoh, S. Nakamura, T. Iida, T. Sawabe, C. E. Rezende, R. B. Francini-Filho, R. L. Moura, G. M. Amado-Filho, F. L. Thompson, Physiologic and metagenomic attributes of the rhodoliths forming the largest CaCO₃ bed in the South Atlantic Ocean. *ISME J.* **8**, 52–62 (2014).
75. H. G. Greene, J. J. Bizzarro, V. M. O’Connell, C. K. Brylinsky, Mapp. *Seafloor Habitat Charact.* 141–155 (2007).
76. J. N. A. Hooper, R. W. M. van Soest, Eds., *Systema Porifera: A Guide to the Classification of Sponges* (Kluwer Academic/Plenum Press, New York, 2002).
77. G. D. Farquhar, J. R. Ehleringer, K. T. Hubick, Carbon isotope discrimination and photosynthesis. *Annu. Rev. Plant Phys.* **40**, 503–537 (1989).
78. R. Schmieder, Y. W. Lim, R. Edwards, Identification and removal of ribosomal RNA sequences from metatranscriptomes. *Bioinformatics* **28**, 433–435 (2012).
79. K. Katoh, K. Misawa, K.-i. Kuma, T. Miyata, MAFFT: A novel method for rapid multiple sequence alignment based on fast Fourier transform. *Nucleic Acids Res.* **30**, 3059–3066 (2002).
80. J. Salisbury, D. Vandemark, J. Campbell, C. Hunt, D. Wisser, N. Reul, B. Chapron, Spatial and temporal coherence between Amazon River discharge, salinity, and light absorption by colored organic carbon in western tropical Atlantic surface waters. *J. Geophys. Res.* **116**, C00H02 (2011).
81. R. W. Buddemeier, S. V. Smith, Coral adaptation and acclimatization: A most ingenious paradox. *AmerZool* **39**, 1–9 (1999).
82. P. S. Brasileiro, thesis, Escola Nacional de Botânica Tropical, Rio de Janeiro (2013).
83. R. G. Bahia, thesis, Escola Nacional de Botânica Tropical, Rio de Janeiro (2014).
84. R. K. Pang, The systematics of some Jamaican excavating sponges (Porifera). *Postilla* **161**, 1–75 (1973).
85. L. V. Barros, G. G. Santos, U. Pinheiro, *Clathria* (*Clathria*) Schmidt, 1862 from Brazil with description of a new species and a review of records (Poecilosclerida: Demospongiae: Porifera). *Zootaxa* **3640**, 284–295 (2013).

Acknowledgments: We thank J. C. Braga for the help with petrographic interpretations and J. Montoya, P. Medeiros, and V. Coles for providing oceanographic data. **Funding:** Conselho Nacional de Desenvolvimento Científico e Tecnológico (CNPq), Coordenadoria de Aperfeiçoamento de Pessoal de Nível Superior (CAPES), Fundação Carlos Chagas Filho de Amparo à Pesquisa do Estado do Rio de Janeiro (FAPERJ), Fundação de Amparo à Pesquisa do Estado de São Paulo (FAPESP), and Brasão provided essential funding. MCTI and the Brazilian Navy provided support with the NHO Cruzeiro do Sul in 2014. Expeditions in 2010 (R/V Knorr) and 2012 (R/V Atlantis) were funded by U.S. NSF (OCE-0934095 to P.L.Y.). Additional support was provided by the Gordon and Betty Moore Foundation (GBMF #2293 and #2928 to P.L.Y.). **Author contributions:** C.E.R. and F.L.T. coordinated the project. R.L.M., P.L.Y., C.E.R., and F.L.T. designed and coordinated the fieldwork. R.L.M., C.E.R., G.M.A.-F., A.C.B., F.C.M., P.L.Y., and F.L.T. wrote the paper. P.S.B., P.S.S., M.M.M., M.G.A., J.M.S., B.F.A., F.P.B., T.P.R., B.C.V.O., R.G.B., R.P.P., R.J.S.D., E.S., A.G.F., C.V.L., E.H., N.E.A., G.B.G., S.N.-L., P.L.Y., R.B.F.-F., A.F., M.C., B.S.S., A.P.B.M., L.O., A.C.S., R.C.P., L.A., N.L.O., J.B.T., C.C.T., and R.A.B.V. contributed with data and data analyses. **Competing interests:** The authors declare that they have no competing interests. **Data and materials availability:** All data used to obtain the conclusions in this paper are available online in the Brazilian Marine Biodiversity database (<http://marinebiodiversity.lncc.br/files/index.php/s/TaLwiK6CqCQI0vN>) and in the Biological and Chemical Oceanography Data Management Office (www.bco-dmo.org/project/2097).

Submitted 10 September 2015

Accepted 25 March 2016

Published 22 April 2016

10.1126/sciadv.1501252

Citation: R. L. Moura, G. M. Amado-Filho, F. C. Moraes, P. S. Brasileiro, P. S. Salomon, M. M. Mahiques, A. C. Bastos, M. G. Almeida, J. M. Silva Jr., B. F. Araujo, F. P. Brito, T. P. Rangel, B. C. V. Oliveira, R. G. Bahia, R. P. Paranhos, R. J. S. Dias, E. Siegle, A. G. Figueiredo Jr., R. C. Pereira, C. V. Leal, E. Hajdu, N. E. Asp, G. B. Gregoracci, S. Neumann-Leitão, P. L. Yager, R. B. Francini-Filho, A. Fróes, R. M. Campeão, B. S. Silva, A. P. B. Moreira, L. Oliveira, A. C. Soares, L. Araujo, N. L. Oliveira, J. B. Teixeira, R. A. B. Valle, C. C. Thompson, C. E. Rezende, F. L. Thompson, An extensive reef system at the Amazon River mouth. *Sci. Adv.* **2**, e1501252 (2016).

An extensive reef system at the Amazon River mouth

Rodrigo L. Moura, Gilberto M. Amado-Filho, Fernando C. Moraes, Poliana S. Brasileiro, Paulo S. Salomon, Michel M. Mahiques, Alex C. Bastos, Marcelo G. Almeida, Jomar M. Silva, Jr, Beatriz F. Araujo, Frederico P. Brito, Thiago P. Rangel, Bráulio C. V. Oliveira, Ricardo G. Bahia, Rodolfo P. Paranhos, Rodolfo J. S. Dias, Eduardo Siegle, Alberto G. Figueiredo, Jr, Renato C. Pereira, Camille V. Leal, Eduardo Hajdu, Nils E. Asp, Gustavo B. Gregoracci, Sigrid Neumann-Leitão, Patricia L. Yager, Ronaldo B. Francini-Filho, Adriana Fróes, Mariana Campeão, Bruno S. Silva, Ana P. B. Moreira, Louisi Oliveira, Ana C. Soares, Lais Araujo, Nara L. Oliveira, João B. Teixeira, Rogerio A. B. Valle, Cristiane C. Thompson, Carlos E. Rezende and Fabiano L. Thompson (April 22, 2016)
Sci Adv 2016, 2:
doi: 10.1126/sciadv.1501252

This article is published under a Creative Commons license. The specific license under which this article is published is noted on the first page.

For articles published under [CC BY](#) licenses, you may freely distribute, adapt, or reuse the article, including for commercial purposes, provided you give proper attribution.

For articles published under [CC BY-NC](#) licenses, you may distribute, adapt, or reuse the article for non-commercial purposes. Commercial use requires prior permission from the American Association for the Advancement of Science (AAAS). You may request permission by clicking [here](#).

The following resources related to this article are available online at <http://advances.sciencemag.org>. (This information is current as of March 19, 2017):

Updated information and services, including high-resolution figures, can be found in the online version of this article at:
<http://advances.sciencemag.org/content/2/4/e1501252.full>

Supporting Online Material can be found at:
<http://advances.sciencemag.org/content/suppl/2016/04/19/2.4.e1501252.DC1>

This article **cites 71 articles**, 14 of which you can access for free at:
<http://advances.sciencemag.org/content/2/4/e1501252#BIBL>

Science Advances (ISSN 2375-2548) publishes new articles weekly. The journal is published by the American Association for the Advancement of Science (AAAS), 1200 New York Avenue NW, Washington, DC 20005. Copyright is held by the Authors unless stated otherwise. AAAS is the exclusive licensee. The title *Science Advances* is a registered trademark of AAAS



Dissolved Black Carbon in the Headwaters-to-Ocean Continuum of Paraíba Do Sul River, Brazil

Jomar S. J. Marques^{1,2*}, Thorsten Dittmar², Jutta Niggemann², Marcelo G. Almeida¹, Gonzalo V. Gomez-Saez² and Carlos E. Rezende¹

¹ Research Group for Biogeochemistry of Aquatic Ecosystems, Laboratório de Ciências Ambientais, Centro de Biociências e Biotecnologia Universidade Estadual do Norte Fluminense, Campos dos Goytacazes, Brazil, ² Research Group for Marine Geochemistry (ICBM—MPI Bridging Group), Institute for Chemistry and Biology of the Marine Environment, Carl von Ossietzky University, Oldenburg, Germany

OPEN ACCESS

Edited by:

Samuel Abiven,
University of Zurich, Switzerland

Reviewed by:

Philippa Louise Ascough,
Scottish Universities Environmental
Research Centre, UK
Alysha Coppola,
University of Zurich, Switzerland

*Correspondence:

Jomar S. J. Marques
jomar.uenf@gmail.com

Specialty section:

This article was submitted to
Biogeoscience,
a section of the journal
Frontiers in Earth Science

Received: 12 November 2016

Accepted: 31 January 2017

Published: 27 February 2017

Citation:

Marques JSJ, Dittmar T,
Niggemann J, Almeida MG,
Gomez-Saez GV and Rezende CE
(2017) Dissolved Black Carbon in the
Headwaters-to-Ocean Continuum of
Paraíba Do Sul River, Brazil.
Front. Earth Sci. 5:11.
doi: 10.3389/feart.2017.00011

Rivers annually carry 25–28 Tg carbon in the form of pyrogenic dissolved organic matter (dissolved black carbon, DBC) into the ocean, which is equivalent to about 10% of the entire riverine land-ocean flux of dissolved organic carbon (DOC). The objective of this study was to identify the main processes behind the release and turnover of DBC on a riverine catchment scale. As a model system, we chose the headwater-to-ocean continuum of Paraíba do Sul River (Brazil), the only river system with long-term DBC flux data available. The catchment was originally covered by Atlantic rain forest (mainly C3 plants) which was almost completely destroyed over the past centuries by slash-and-burn. As a result, large amounts of wood-derived charcoal reside in the soils. Today, fire-managed pasture and sugar cane (both dominated by C4 plants) cover most of the catchment area. Water samples were collected along the river, at the main tributaries, and also along the salinity gradient in the estuary and up to 35 km offshore during three different seasons. DBC was determined on a molecular level as benzenepolycarboxylic acids (BPCAs). Stable carbon isotopes ($\delta^{13}\text{C}$) were determined in solid phase extractable DOC (SPE-DOC) to distinguish C4 and C3 sources. Our results clearly show a relationship between hydrology and DBC concentrations in the river, with highest DBC concentrations and fluxes in the wet season (flux of 770 moles s^{-1} in 2013 and 59 moles s^{-1} in 2014) and lowest in the dry season (flux of 27 moles s^{-1}). This relationship indicates that DBC is mainly mobilized from the upper soil horizons during heavy rainfalls. The relationship between DBC concentrations and $\delta^{13}\text{C}$ -SPE-DOC indicated that most of DBC in the river system originated from C3 plants, i.e., from the historic burning event of the Atlantic rain forest. A conservative mixing model could largely reproduce the observed DBC fluxes within the catchment and the land to ocean continuum. Comparably slight deviations from conservative mixing were accompanied by changes in the molecular composition of DBC (i.e., the ratio of benzenepenta- to benzenhexacarboxylic acid) that are indicative for photodegradation of DBC.

Keywords: headwaters-to-ocean, black carbon, dissolved black carbon, dissolved organic carbon, Paraíba do Sul River

INTRODUCTION

Forest fires produce airborne combustion products and charred residues on and in the ground (Preston and Schmidt, 2006). Charred materials include a wide range of compounds, from dehydrated sugars formed at low charring temperature to highly-condensed graphite-like material produced at high temperatures, and secondary condensation products like soot (Santín et al., 2016). Also fuel characteristics are important, charcoal from woody and soft plant tissues often have different levels of condensation and oxygen content (Forbes et al., 2006; Schneider et al., 2010; Ding et al., 2014). The entire continuum of charred material is considered pyrogenic organic matter, of which the most condensed fraction is commonly referred to as black carbon (BC; Forbes et al., 2006).

Black carbon, which is largely derived from high-temperature woody chars, has received large attention in the literature, because it is more resistant to further biological and chemical degradation than the biomolecular precursors (Forbes et al., 2006). As a consequence, BC is ubiquitous in soils, sediments, and aquatic environments (Forbes et al., 2006; Jaffé et al., 2013). Important removal mechanisms of BC from soils are solubilization and subsequent transport in the dissolved phase (Dittmar et al., 2012a) and lateral transport of BC particles in the landscape (Major et al., 2010). During degradation in soils, oxygen atoms can be introduced into condensed aromatic structures of charcoal (Abiven et al., 2011). The resulting carboxylated molecular subunits partially dissolve in water and migrate through the soil as dissolved BC (DBC; Cheng and Lehmann, 2009). There is a significant time lag between wildfire induced BC production, incorporation into soils, and the actual release of DBC to aquatic systems (Dittmar et al., 2012a; Ding et al., 2014). Microbial reworking of charcoal may be required to enhance the translocation of soil BC to DBC (Ding et al., 2014). This translocation process can explain the presence of DBC in dissolved organic matter (DOM) in rivers, estuaries, and the ocean (Kim et al., 2004; Mannino and Harvey, 2004; Ziolkowski and Druffel, 2010). Global export of DBC from land to ocean amounts to ~ 27 Tg carbon year⁻¹, which is equivalent to 10% of the entire riverine dissolved organic carbon (DOC) flux (Jaffé et al., 2013). DBC is distributed throughout the ocean and may impact biogeochemical processes on a global scale (Ziolkowski and Druffel, 2010). Even in the most remote basins of the deep ocean, $\sim 2\%$ of DOM contains a heat-induced molecular signature (Dittmar and Koch, 2006; Dittmar and Paeng, 2009).

Very little is known on how DBC behaves in aquatic environments. While there is evidence that DBC is very stable in the deep ocean having conservative, salt-like properties (Dittmar and Paeng, 2009; Ziolkowski and Druffel, 2010), it is very susceptible to UV radiation in sunlit waters (Stubbins et al., 2012). Once exposed to sunlight, most of DBC is lost from seawater (Stubbins et al., 2012) and river water (Riedel et al., 2016). It is unclear what proportion of DBC that is introduced from soils and groundwater into the rivers eventually survives riverine transport from the headwaters to the estuaries and from there into the open ocean. The objective of this study was to fill this gap of knowledge for one of the best studied

rivers in this context. Paraíba do Sul River (PSR) in Brazil is the only river system for which long-term DBC flux data are available (Dittmar et al., 2012a). In this river, DBC annual export exceeds by far present BC production rates, and charcoal still residing in the soils after historic forest fires is the most likely source of DBC in the river today. PSR drains an area formerly covered entirely by Brazilian Atlantic Forest. Its original area comprised 1.3 million km², but nowadays, only 12–15% of its original extension remains as secondary forest distributed as isolated, disconnected patches (Ribeiro et al., 2009; Fundação SOS Mata Atlântica Instituto Nacional de Pesquisas Espaciais, 2011; Lira et al., 2012). Deforestation occurred mainly between 1850 and 1970 via slash-and-burn (Warren, 1995). Today, 74% of the watershed is covered by fire-managed grassland and, in the area close to the coastal region, fire-managed sugar cane plantations. DBC concentration in PSR fluctuates with seasons, with highest concentrations during wet seasons and lowest ones during dry seasons, excluding direct deposition as a significant source (Dittmar et al., 2012a).

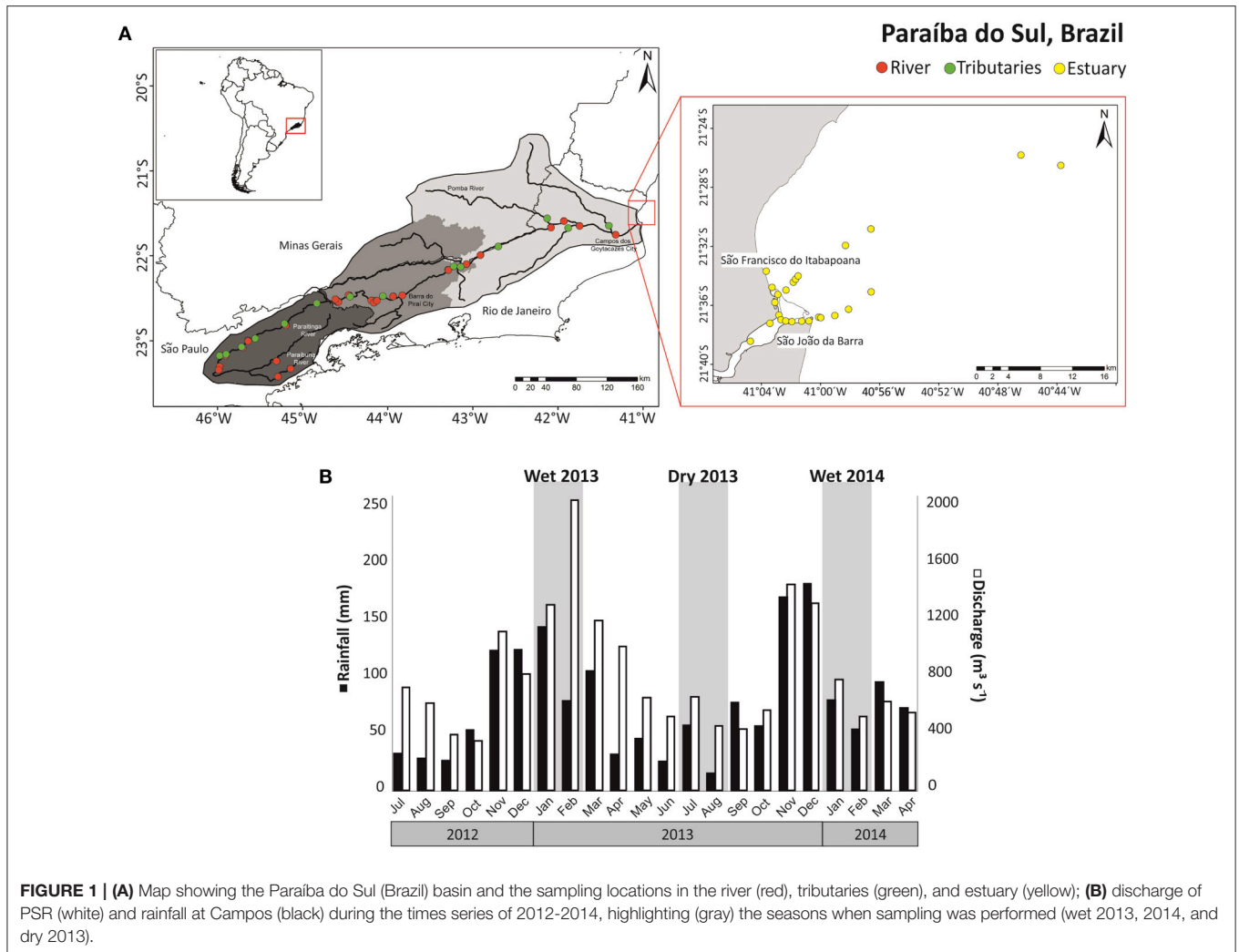
In this study we tested the hypothesis that due to limited light penetration and bio-recalcitrant properties, DBC is funneled unmodified within the PSR from the headwaters to the estuary and into the open ocean. We focused on the polycyclic aromatic fraction of DBC that can be quantified in natural waters with help of molecular proxies, i.e., benzenepolycarboxylic acids that are released from DBC during nitric acid oxidation (Hammes et al., 2007; Dittmar, 2008). We tested for conservative behavior of DBC in the headwaters-to-ocean continuum in three sampling campaigns, two in the rainy and one in the dry season.

Furthermore, we searched for chemical evidence that DBC in PSR is indeed mainly released from charcoal produced in historic forest fires and not primarily derived from today's fire management practice, as deduced previously from budget calculations (Dittmar et al., 2012a). We took advantage of the fact that the historic Atlantic forest vegetation was composed mainly of C3 plants, while today's pastures and sugar cane plantations are dominated by plants with the C4 photosynthetic pathway. Both types of plants carry a distinct carbon isotopic signature ($\delta^{13}\text{C}$) in their organic tissue. We determined $\delta^{13}\text{C}$ on bulk SPE-DOM along the headwater-to-ocean continuum, which provided us with information about the main sources of DOM, of which DBC is a significant fraction.

MATERIALS AND METHODS

Study Area

The PSR watershed occupies an area of 57,300 km² in the states of São Paulo, Minas Gerais and Rio de Janeiro, located between 20°26' and 23°28'S latitude and 41°00' and 46°30'W longitude (Ovalle et al., 2013). The headwaters of the PSR are formed by the confluence of the Paraitinga and Paraíba Rivers. The total length of the river channel is ~ 1150 km. The PSR basin can be divided into three macro-sectors (**Figure 1A**): (1) An upper basin sector with an area of 7,300 km², where the river descends from an altitude of around 1800 to 600 m through narrow and embedded valleys carved out of crystalline rocks; (2) A middle



basin sector with an area of 27,500 km² and average elevation of 510 m, this sector is most influenced by industry, mainly for steel, chemicals, food, and paper; (3) A lower basin sector with an area of 22,500 km² that is mainly occupied by coastal plain with numerous riverine meanders and islands.

The area within the PSR watershed is highly urbanized and industrialized, with about 5 million inhabitants. The PSR is used for supplying drinking water to over 14 million people. Close to Barra do Pirai city, ~160 m³ s⁻¹ of water is diverted from PSR for water supply to Rio de Janeiro city. There is a strong seasonality in water discharge in PSR. The high and low water periods range from December to February and from June to August, respectively. Major industrial areas are concentrated in the middle and upper sector basin and in the sub-basins of the Pomba and Paraíba Rivers (Ovalle et al., 2013). In the lower basin sector, extensive farming prevails, especially sugar cane production. In addition, 47 different reservoirs and hydroelectric dams with varying sizes influence the hydrology of the river system throughout the basin (Ovalle et al., 2013). The Paraíba do Sul estuary is located at the coastal plain formed by the PSR delta

in the North of Rio de Janeiro state, near São João da Barra city (Souza et al., 2010).

Sampling

Samples from rivers, estuary, and adjacent ocean (Figure 1A) were collected during the wet seasons in January 2013 and February 2014. Average fluvial discharge in the lower reaches of PSR (Campos dos Goytacazes) was 1875 m³ s⁻¹ in January 2013 and 719 m³ s⁻¹ in February 2014. Sampling in the dry season was done in July and August of 2013, with an average discharge of 478 m³ s⁻¹. The discharge value was estimated using river velocity and cross-sectional area measurements (General Oceanic model 2030 current meter). Surface water samples (3 L) were collected in acid rinsed bottles at 24 sites along the main channel of the PSR (Figure 1A, red symbols) and 14 sites at the PSR tributaries (Figure 1A, green symbols). In the estuary and adjacent ocean up to 35 km offshore, 24 samples were collected along the salinity gradient in the wet season of 2013, and 21 sites during the other campaigns (Figure 1A, yellow symbols). The PSR and tributaries were sampled from bridges while the estuary and ocean were

sampled from a trawler. All samples were retrieved from the water surface with acid-rinsed buckets. We collected superficial soil samples in the forest and pasture sites (three samples at each site) to constrain the end-members used in the two-source isotopic model as C3 plants (forest site) and C4 plants (pasture site).

Sample Processing

Immediately after sampling, samples were filtered through pre-combusted GF/F filters (Whatman, nominal pore size 0.7 μm). After filtration, samples were acidified with HCl (32%, analytical grade) to pH 2 and DOM was isolated from the water samples via solid-phase extraction (SPE; Dittmar et al., 2008). In brief, filtered and acidified samples were passed by gravity through solid-phase cartridges (1 g PPL, Agilent). The cartridges were desalted with 0.01 mol L⁻¹ HCl, dried with a stream of N₂, and DOM was eluted with 8 mL of methanol (HPLC grade). The DOC extraction efficiency was determined for each sample by evaporating an aliquot of the methanol extract to dryness, re-dissolving it in ultrapure water at pH 2, and relating the DOC concentration of this solution to that of the original sample. On average among all samples ($n = 177$), 45% (SE $\pm 13\%$) of DOC was recovered by the SPE. Extraction efficiency did not systematically vary along the river and along the salinity gradient. Soil samples were freeze-dried and the fraction $>2.0\text{ mm}$ removed by sieving.

Dissolved Organic Carbon and Stable Carbon Isotope Determination

The concentration of DOC in filtered samples was determined by the high-temperature catalytic oxidation method on an automated TOC analyzer (Shimadzu TOC 5000), using five calibration solutions spanning the concentration range of the samples. All DOC data reported are the mean of three replicate injections, for which the coefficient of variance was $<5\%$. Procedural blanks, including the filtration step, were obtained using ultrapure water. These blank samples did not contain any detectable amounts of DOC. The detection limit for DOC was 5 μM , and the analytical accuracy (relative to the reference material) and precision (replicate injections) were within $\pm 1\ \mu\text{M}$. The deep sea reference material provided by D. Hansell (University of Miami, USA) was repeatedly analyzed in each run to control accuracy.

The stable carbon isotope composition of SPE-DOM was determined following an established protocol (Seidel et al., 2015). In brief, an aliquot of 800–1600 μL of SPE-DOM extract, corresponding to $\sim 20\ \mu\text{g}$ of SPE-DOC, was dried under N₂ flux. Then, it was re-dissolved in 50 μL of methanol, transferred into Sn combustion capsules (Elemental) and dried in an oven at 60°C for 24 h. Soil samples were weighed (10 mg) in Sn combustion capsules (Elemental). The isotopic composition was analyzed on an elemental analyzer (Flash 2000) coupled to an isotope-ratio mass spectrometer Delta V Advantage (Thermo Scientific, Germany). Stable carbon isotope ratio is expressed as $\delta^{13}\text{C}$ (%) relative to the Pee Dee Belemnite (PDB) standard reference.

Dissolved Black Carbon

The benzenepolycarboxylic acids (BPCAs) method (Dittmar, 2008) was used to quantify the condensed polyaromatic fraction of DBC. This method is the most sensitive and unequivocal method for the determination of BC in fluvial and marine DOM (Dittmar et al., 2012b). Moreover, the proportions of the different detectable BPCAs are indicative of the extent of condensation and size of the polycyclic aromatics. For example, char produced at 1000°C is typically highly condensed and BPCAs released by nitric acid oxidation are basically composed of benzenhexacarboxylic acid. Charcoal produced at 200°C is characterized by a low number of condensed aromatic rings, and BPCAs are less carboxylated compared to high-temperature chars (Schneider et al., 2010). For BPCA analysis, 300–500 μL of the methanol extracts, corresponding to 1–10 μmol of SPE-DOC, were transferred into 2 mL glass ampoules, evaporated to dryness in an oven at 60°C and dissolved in 0.5 mL of concentrated HNO₃ (65%). The ampoules were flame sealed, placed in a stainless-steel pressure bomb and kept for 9 h at 170°C in a furnace. After the ampoules had cooled, the HNO₃ was evaporated to dryness in a speed vacuum centrifuge (60°C, Christ RV2-18). Samples were dissolved in 100 μL of phosphate buffer at pH 7.2 (Na₂HPO₄ and NaH₂PO₄, each 0.5 mM) and analyzed on an ultrahigh performance liquid chromatography system (Waters Acquity UPLC), equipped with a photodiode array light-absorbance detector. BPCAs were identified in accordance to retention time and absorbance spectra (220–380 nm). Quantification was performed using the absorbance signal at 240 nm and an external calibration. The injection volume was 1 μL . BPCA concentrations were converted into DBC concentrations after the equation of Dittmar (2008), with the slight modification outlined in Stubbins et al. (2015), where the most robustly quantified B6CA and B5CA are used for estimating DBC. For the equations we refer to Stubbins et al. (2015).

Two Source Isotopic Model

To estimate the contribution of C₄ plant derived organic matter to PSR and tributaries DOM, we used a linear two-source mixing model (Martinelli et al., 2002):

$$C4(\%) = \frac{\delta^{13}\text{C}_{\text{sample}} - \delta^{13}\text{C}_{\text{C3 soil}}}{\delta^{13}\text{C}_{\text{C4 soil}} - \delta^{13}\text{C}_{\text{C3 soil}}} \times 100 \quad (1)$$

where $\delta^{13}\text{C}_{\text{sample}}$ is the isotopic composition of SPE-DOM in a given sample, $\delta^{13}\text{C}_{\text{C3 soil}}$ ($-29.4 \pm 0.4\%$) is the isotopic composition of the forest soil and $\delta^{13}\text{C}_{\text{C4 soil}}$ ($-14.9 \pm 0.3\%$) is the isotopic composition of the pasture soil. An underlying assumption of our calculations is that there are only two main sources of SPE-DOM. Other sources, like sewage or autochthonous production by algae reduce the accuracy of our calculations. Also isotope fractionation during DOM decomposition is not considered in our model.

Hydrological and Conservative Mixing Models

Daily water discharge data are available for the lower reach of PSR, at the city of Campos dos Goytacazes. We used

electric conductivity as a tracer to backwards calculate the water discharge of the tributaries and at each sampling point of PSR. Electrical conductivity was determined *in situ* with a WTW portable probe calibrated directly before each measurement. Under the reasonable assumption that electrical conductivity behaves conservatively during mixing, the relative proportion of water discharge of a tributary and the mainstream before and after the effluent was calculated, based on the principles of mass conservation:

$$Q_{\text{after}} = Q_{\text{before}} + Q_{\text{tributary}} \quad (2)$$

$$\sigma_{\text{after}} \cdot Q_{\text{after}} = \sigma_{\text{before}} \cdot Q_{\text{before}} + \sigma_{\text{tributary}} \cdot Q_{\text{tributary}} \quad (3)$$

Q is the water discharge after the tributary (Q_{after}), before the tributary (Q_{before}), and of the tributary ($Q_{\text{tributary}}$); and σ is the electrical conductivity at the respective position. For example, the water discharge in Campos dos Goytacazes (Q_{after}) was $1875 \text{ m}^3 \text{ s}^{-1}$ in January 2013 and σ_{after} at that site was $65 \text{ } \mu\text{S cm}^{-1}$. From the electrical conductivity of the next upstream tributary ($\sigma_{\text{tributary}}$; $73 \text{ } \mu\text{S cm}^{-1}$) and the river sample before the tributary (σ_{before} ; $59 \text{ } \mu\text{S cm}^{-1}$), we calculated a water discharge of $803 \text{ m}^3 \text{ s}^{-1}$ from the tributary and $1071 \text{ m}^3 \text{ s}^{-1}$ from the PSR upstream the tributary. Loss of water (e.g., through evaporation) and unknown sources of water (e.g., groundwater inputs) are sources of errors in this model.

As a second step we calculated the respective fluxes of DBC (F_{DBC}) as water discharge multiplied by DBC concentration (c_{DBC}) at each site.

$$F_{\text{DBC}} = Q \cdot c_{\text{DBC}} \quad (4)$$

DBC fluxes were then compared to the theoretical DBC fluxes for ideal conservative behavior at each site. Deviations of the measured fluxes from these conservative fluxes indicate additional source and sink terms along the river. Conservative fluxes were calculated on the assumption that DBC behaves like electrical conductivity in the conservative case. Consequently, the theoretical, conservative DBC flux at a given station is the DBC flux of the uppermost station in PSR, plus the additive flux of each tributary upstream of a given station:

$$F_{\text{DBC, conservative}} = F_{\text{DBC, uppermost station}} + \Sigma F_{\text{DBC, all tributaries upstream}} \quad (5)$$

The theoretical, conservative DBC concentration ($c_{\text{DBC, conservative}}$) at each station is:

$$c_{\text{DBC, conservative}} = F_{\text{DBC, conservative}}/Q \quad (6)$$

Similar calculations were done for the estuary. The proportion of freshwater ($\%_{\text{fresh}}$) and seawater ($\%_{\text{sea}}$) in each estuarine sample was calculated from electrical conductivity. We considered the samples taken in PSR in Campos dos Goytacazes (freshwater) and the outermost marine station (seawater) as endmembers for these calculations. Based on the principles of mass conservation:

$$c_{\text{DBC, conservative}} = \text{fresh}(\%) \cdot c_{\text{DBC, fresh}} + \text{sea}(\%) \cdot c_{\text{DBC, sea}} \quad (7)$$

$c_{\text{DBC, fresh}}$ and $c_{\text{DBC, sea}}$ are the DBC concentrations of the endmembers.

In the conservative case, the freshwater flux of DBC throughout the entire estuary is equal to the DBC flux in the lowermost riverine station:

$$F_{\text{DBC, conservative}} = F_{\text{fresh}} \quad (8)$$

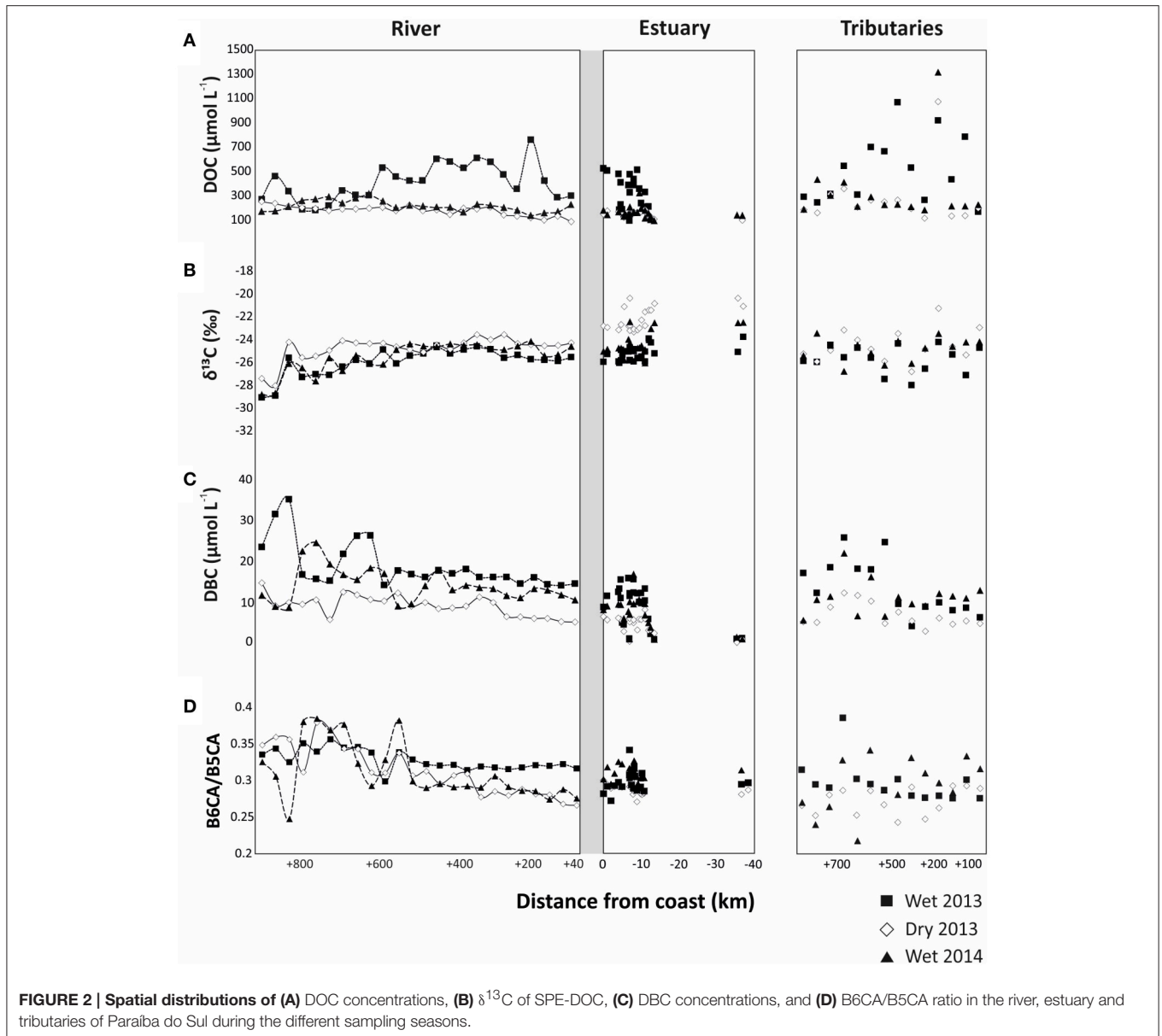
The real flux of freshwater-derived DBC in the estuary is approximated from the deviations of DBC concentration from conservative mixing:

$$F_{\text{DBC}} = c_{\text{DBC}}/c_{\text{DBC, conservative}} \cdot F_{\text{fresh}} \quad (9)$$

RESULTS

DOC and DBC concentrations were highly variable between sites and seasons in the main stem of the river, the tributaries, and the estuary. The DOC concentration in the PSR system ranged between 168 and $894 \text{ } \mu\text{mol L}^{-1}$ in riverine samples, 72 – $529 \text{ } \mu\text{mol L}^{-1}$ in estuarine samples and 143 – $1381 \text{ } \mu\text{mol L}^{-1}$ in tributaries (Figure 2A, Tables S1–S3). Riverine and estuarine DOC concentrations were distinctly higher during the wet season of 2013, while during the dry season of 2013 and the wet season of 2014 DOC concentrations were lower (Student's *t*-test, $p < 0.01$, Figure 2A, Tables S1–S3). In contrast, DOC concentrations in the tributaries were not significantly different between both wet seasons, but differed between wet and dry seasons (Student's *t*-test, $p < 0.05$, Figure 2A, Tables S1–S3). DOC concentrations in the estuary decreased with distance offshore. In all the sampling periods, DOC concentrations slightly deviated from conservative mixing in the river and estuary (Figure 2A), but the resulting DBC fluxes were not significantly different from those calculated from the conservative mixing model. The stable carbon isotopic composition ($\delta^{13}\text{C}$) of SPE-DOM ranged between -29.0 and -23.5% in the main stem of PSR, and from -28.0 to -21.3% in the tributaries. In the estuary, $\delta^{13}\text{C}$ increased from a minimum of -25.7% inshore to -20.0% in the marine endmember offshore (Figure 2B, Tables S1–S3). Riverine and estuarine $\delta^{13}\text{C}$ were more depleted (more negative $\delta^{13}\text{C}$ values) in the wet season of 2013 (Student's *t*-test, $p < 0.05$, Figure 2B), followed by the wet season of 2014 and finally of dry season of 2013 (Student's *t*-test, $p < 0.05$, Figure 2B). The $\delta^{13}\text{C}$ of forest soil sample was $-29.4 \pm 0.4\%$ whilst it was $-14.9 \pm 0.3\%$ for the pasture soil sample.

DBC concentrations in PSR ranged between 5 and $35 \text{ } \mu\text{mol L}^{-1}$, with significantly higher values during the wet season of 2013 compared to the other sampling campaigns (Student's *t*-test, $p < 0.01$, Figure 2C, Table S1). DBC concentrations in the tributaries ranged from 3 to $26 \text{ } \mu\text{mol L}^{-1}$, and were similar in both wet seasons, but distinctly different between wet and dry seasons (Student's *t*-test, $p < 0.01$, Figure 2C, Table S2). Estuarine DBC concentrations ranged from 0.3 to $17 \text{ } \mu\text{mol L}^{-1}$, strongly decreasing from in- to offshore; they were similar in both wet seasons, and distinctly different between wet and dry seasons (Student's *t*-test, $p < 0.01$, Figure 2C, Table S3). The concentration ratio of benzenehexa- to benzenepentacarboxylic acids (B6CA/B5CA) in PSR ranged between 0.27 and 0.36 , in the



tributaries between 0.22 and 0.34 and in the estuary between 0.27 and 0.34 (Figure 2D, Tables S1–S3), with a decreasing trend from in- to offshore.

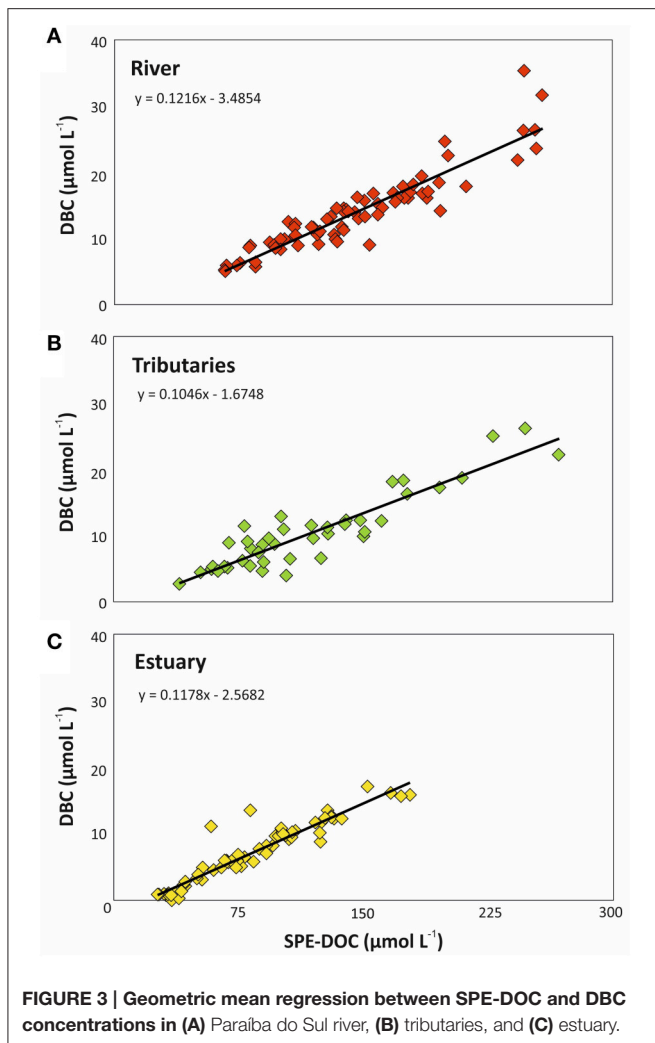
DISCUSSION

The Source of DBC

The PSR catchment area was once covered by Atlantic forest. Due to almost complete destruction via the slash-and-burn practice until the mid-1970's large amounts of charcoal had been deposited in the soils of the catchment. DBC is slowly released when charcoal ages in soils (Ding et al., 2013). Simultaneous microbial oxidation of soil organic matter and charcoal likely results in a strong relationship between DOC and DBC concentrations in the rivers draining the area (Ding et al., 2013).

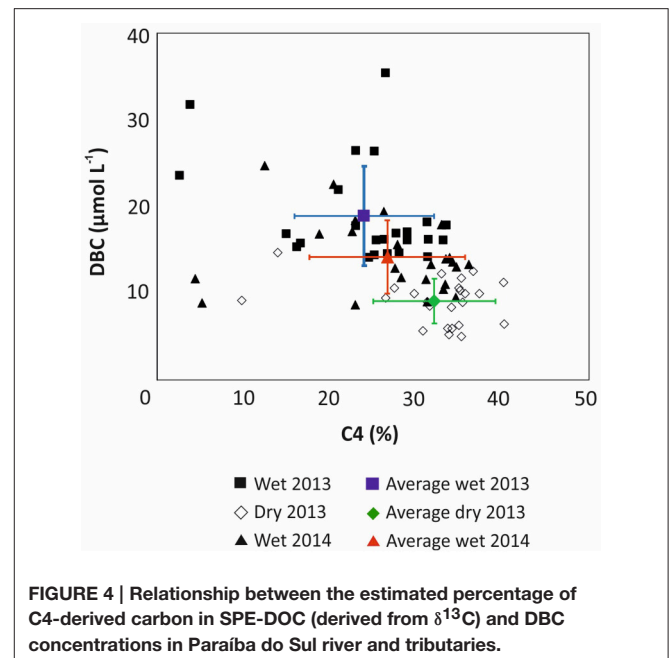
Consistent with this concept, statistically significant correlations between DBC and DOC concentrations were observed for PSR, tributaries, and estuary (Figure 3). Similar relationships were previously found in intertidal systems (Dittmar et al., 2012b), intermittent grassland streams (Ding et al., 2013), and fluvial systems (Dittmar et al., 2012a; Jaffé et al., 2013; Stubbins et al., 2015). In our study, the slope of the resulting regressions indicated that the DOC pool in the river contained 12.2% of DBC, followed by the estuary with 11.8% and the tributaries with 10.5%, which is close to the previously reported global riverine average (Jaffé et al., 2013).

It was proposed that DBC in PSR is largely derived from historic charcoal deposits in the soils, and only to a minor degree from today's fire-management practice (Dittmar et al., 2012a). The historic forest vegetation was composed mainly of C3 plants,



while today's pastures and sugar cane plantations are dominated by C4 plants. DBC concentrations in the river system inversely correlated with the percentage of DOC that was derived from C4 plants (Figure 4; Figure S1). The higher the contribution of C3 plants the higher was the concentration of DBC in the river. The relationship between all samples presented a strong negative correlation ($r_s = -0.605$, $p < 0.001$, $n = 114$) indicating that historical fire events from Atlantic Forest represented a more important source of DBC to the river water today than recent burning activities.

The source of DOC shifted between the seasons and was consistent with DBC concentrations. During the rainy season, DBC concentrations were high, and the DOC was largely derived from historic carbon sources (C3) with more depleted $\delta^{13}\text{C}$ values. In the dry season, DBC concentration was lower and the contribution of today's vegetation (C4) was higher, with $\delta^{13}\text{C}$ values more enriched. The identification of C3 or C4 plants with carbon isotopic composition was possible due the marked differences in $\delta^{13}\text{C}$ values between each kind of plants. C3 plants have $\delta^{13}\text{C}$ values depleted close to -31% , while C4 plants have $\delta^{13}\text{C}$ values less depleted close to -14% (Kruche et al., 2002). This

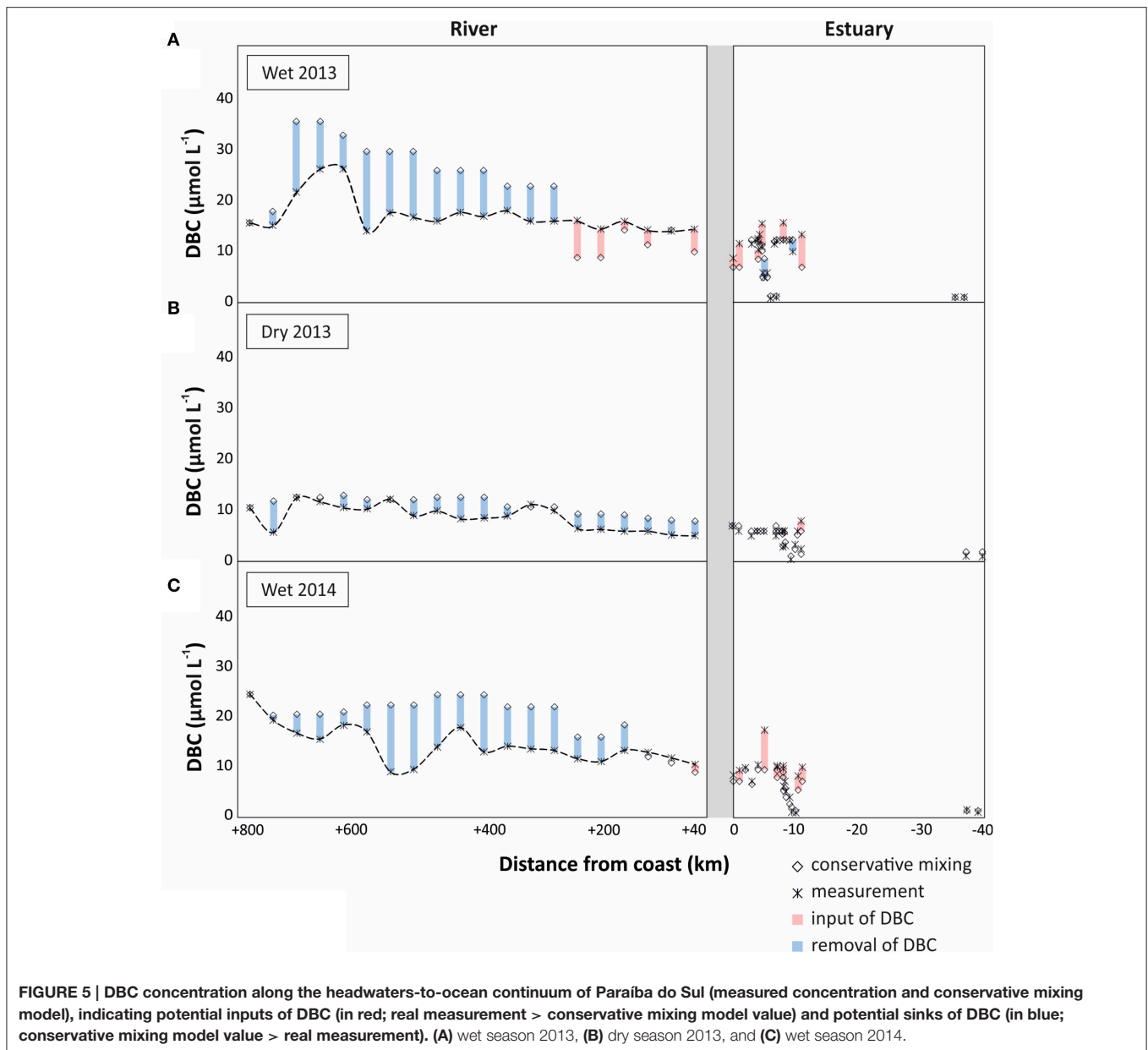


observation is probably a reflection of water flow paths. During the rainy season, upper soil horizons, where most (historic) charcoal deposits are flushed. Deeper groundwater that fuels the river during base flow seems to be less influenced by soil-derived DOM. In accordance, in the Amazon Forest, the upper soil horizons (upper 60 cm) contain higher amounts of BC and char than deeper horizons (Glaser et al., 2001). The char in soil in the Amazon had an apparent radiocarbon age of 1775 ± 325 years (Glaser et al., 2001), indicating a long residence time of char in tropical soils. In addition, enhanced *in-situ* production by algae during the dry season caused by deeper light penetration should be taken into account. Algae are potentially another source of isotopically heavy and DBC-poor DOC to the river. Nevertheless, the historic C3 vegetation is apparently the predominant source of bulk DOC and associated DBC to the river system.

Processing of DBC in the River-to-Ocean Continuum

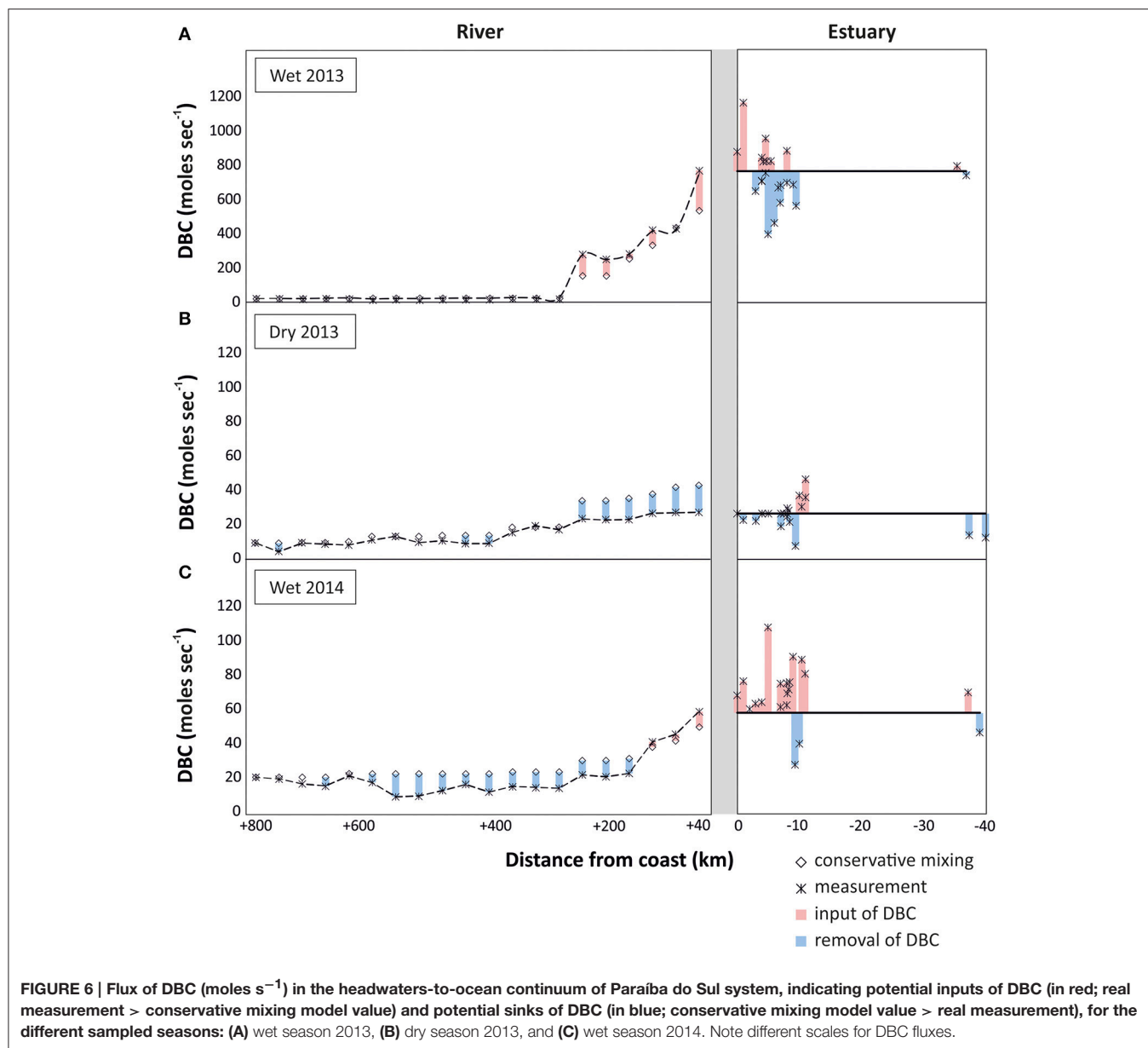
In the headwaters-to-ocean continuum of PSR, the DBC concentrations varied over one order of magnitude. Within the main river, the DBC concentrations matched those reported earlier for PSR in Campos dos Goytacazes (Dittmar et al., 2012a), and are within the range of global rivers (Jaffé et al., 2013) and coastal wetlands (Dittmar et al., 2012b; Ding et al., 2014). The much lower concentrations offshore are consistent with the low DBC concentrations reported for the sea surface in the Gulf of Mexico (Dittmar, 2008) and the Southern Indian Ocean (Dittmar and Paeng, 2009).

To identify potential sources and sinks along the PSR and estuary we compare the observed trends with those expected from conservative mixing, i.e., a scenario in which DBC has salt-like characteristics in the headwater-to-ocean continuum. In all sampling campaigns a cumulative net-removal of DBC was



observed from the headwaters down to the lower reaches of the riverine system (300 km inland, **Figure 5**). This apparent non-conservative behavior of DBC was restricted to few sites and the introduced deviation propagated downstream. An apparent net-removal of DBC persisted all the way to the estuary in the dry season of 2013, but was counteracted or even outbalanced by inputs of DBC in the lower reaches of the river during the wet seasons. In the estuary, a net-input was observed in both rainy seasons; in the dry season, DBC mixed conservatively in the estuary and inner shelf. Overall, the slight deviations of DBC concentration from the conservative mixing model had comparatively little effect on DBC fluxes in the rivers system that were dominated by the large discharge of few tributaries in the lower reaches of PSR (**Figure 6**).

In principle, two explanations can be put forward for a non-conservative behavior of DBC in the river-to-ocean continuum. First, unknown sources of water with different DBC to conductivity ratios than the sampled tributaries introduce errors in our mass balance calculations. Deep groundwater is generally poor in DBC (Dittmar et al., 2012a; Stubbins et al., 2015). With increased rainfall, the hydrological pathway also incorporates active soil layers that are rich in organic compounds and charcoal (Guggenberger et al., 2008; Stubbins et al., 2015). At base flow during the dry season, deep groundwater is the main source of water to PSR and the DBC concentrations are consequently lower than during the rainy season when upper soil horizons are flushed (Dittmar et al., 2012a). Lateral input of groundwater into the tributaries is indirectly considered in our



mass balance model, but direct inputs of groundwater into the main stem not. Depending on the source of groundwater, these undetected inputs may cause net-inputs from upper soil horizons (rainy seasons) or an apparent net-removal due to dilution with deep groundwater (dry season). Because we observed an overall consistent pattern of net-removal of DBC during wet and dry seasons we consider methodological artifacts as an unlikely reason for the observed net-removal. About 23–40% of DBC was lost along the transect from river to estuary during the various seasons.

DBC consists of condensed organic compounds, and is thus sensible to photooxidation (Stubbins et al., 2008; Spencer et al., 2009). This could be an important sink for DBC in the riverine system, and explain the observed net-removal. One way to

assess whether photooxidation indeed occurred is provided by changes of the B6CA/B5CA ratio. Benzenhexacarboxylic acid (B6CA) is indicative of highly condensed aromatics, whereas benzenepolycarboxylic acids with a lower number of carboxylic substitutes are indicative of molecules with a lower number of condensed rings in their core structure (Schneider et al., 2010). Thus, the B6CA/B5CA ratio was proposed as a measure for the degree of condensation of DBC (Stubbins et al., 2012). Highly condensed structures are preferentially degraded by irradiation, and 28 days of exposure to sunlight of North Atlantic Deep Water caused a decrease of B6CA/B5CA from 0.32 to 0.23 (Stubbins et al., 2012). Similarly in our study, apparent loss of DBC was associated with a decrease of B6CA/B5CA (Figure 2D). In the dry season of 2013 and the wet season of 2014, the B6CA/B5CA

ratio decreased from 0.38 to 0.27 along the river, which is a clear indication for photodegradation. In the wet season of 2013, the change in B6CA/B5CA was not as pronounced, as there was a net-input of DBC in the lower reaches of the river. In the lower reaches of PSR and next to the estuary, there are extensive fire-managed sugar cane plantations located in direct vicinity of the estuary. These areas of sugar cane plantations have been managed since 1538 (Oscar, 1985). It is plausible that lateral inputs from these areas especially during the rainy season caused the observed net-inputs in the corresponding areas. DBC from upper soil horizons has not been exposed to sunlight yet, which is consistent with the relatively high B6CA/B5CA in the respective area and season. Furthermore, during the wet season of 2013, the load of suspended particles in the river was almost one order of magnitude higher than during the other campaigns at station Campos dos Goytacazes (120 mg L^{-1} , compared to 15 mg L^{-1} , unpublished data). Particles shade the water and reduce photodegradation. In addition, DBC may desorb from the particles thereby contributing to the apparent net-input of DBC in the lower reaches of the river during the rainy season of 2013.

In the rainy seasons, DBC concentrations were higher than during the dry season. In conjunction with the higher water discharge, DBC fluxes were even more enhanced during the rainy seasons (Figure 6). This cumulative effect of higher DBC concentration and higher water discharge was most pronounced during the wet season of 2013. During this campaign water discharge was more than one order of magnitude higher at the lowest reaches of PSR compared to the other sampling campaigns, resulting in correspondingly high fluxes of DBC from the river to the ocean. The flux of DBC fluctuated in the estuary, but there was no indication for net-removal of DBC. Fluctuations are likely due to spatial heterogeneity of DBC concentration and local inputs from resuspended sediments, tidal creeks and groundwater discharge. Overall, it appears that a large fraction of the DBC survived transport through the estuary and onto the inner shelf, and possibly over larger scales in the ocean.

CONCLUSIONS

This study presents the first data about the DBC spatial and seasonal behavior in a tropical basin. As model system, we chose the Paraíba do Sul system (Brazil), the only river system for which long-term DBC flux data exist. Our study indicates that hydrology plays an important role in DBC dissolution and migration, with highest DBC concentrations in the wet season and lowest in the dry season. This relationship suggests that DBC is mainly mobilized from the upper soil horizons during heavy rainfalls. Therefore, lateral transport to the ocean seems to be an important removal mechanism for BC in soils. A direct relationship between DOC and DBC concentrations was observed, indicating fire-altered carbon as an intrinsic component of the DOC pool. The similarities in the mechanisms of DOC and DBC stabilization and loss, suggested that DOC may contribute to the mobilization of soil BC to the aquatic systems. In addition, a statistically significant relationship between DBC and $\delta^{13}\text{C}$ -SPE-DOC is consistent with previous

literature suggestion (Dittmar et al., 2012a), that DBC in the PSR system is derived from aged charcoal, produced during the Atlantic forest destruction and historically accumulated in soils. Future studies should be directed toward compound-specific carbon isotope analysis on BPCAs to unambiguously confirm the source and age of DBC.

A simple mixing model could largely reproduce the observed DBC fluxes within the catchment and the headwaters-to-ocean continuum. Photooxidation likely removed some DBC along the course of the river-to-ocean-continuum. High water discharge and increased DBC concentrations had a cumulative effect on DBC flux during the rainy seasons. We found no evidence for net DBC removal in the estuary or inner shelf, thus large-scale transport in the ocean is likely. Anticipated temperature increase and changes in the water cycle may result in an increase of fire frequency. As global climate change effects promote extreme dry and wet seasons, the DBC export may increase proportionally and alter the size of the refractory DOM pool in the deep ocean.

AUTHOR CONTRIBUTIONS

All authors contributed to the design of the study. JM and MA analyzed samples for stable carbon isotopic composition. JM and JN analyzed samples for dissolved black carbon. TD, CR, and JM conducted modeling studies. All authors contributed to data interpretation and writing of the manuscript. JM and GG built the figures.

FUNDING

INCT-TMCOcean on the Continent-Ocean Materials Transfer (CNPq; 573.601/08-9). CR received financial support from CNPq (506.750/2013-2) and FAPERJ (E-26/111.616/2011 and E-26/201.188/2014). The Science without Border (CNPq CSF 400.963/2012-4) provided financial support for JM 1 year in a sandwich program at the University of Oldenburg; MA 1 year of Post Doctor position in Environmental Sciences Laboratory (UENF) and TD 3 months as a Visiting Professor at Universidade Estadual do Norte Fluminense.

ACKNOWLEDGMENTS

The authors are grateful to the *Laboratório de Ciências Ambientais* of the *Centro de Biociências e Biotecnologia* at the *Universidade Estadual do Norte Fluminense* and the University of Oldenburg Research Group for Marine Geochemistry (ICBM—MPI Bridging Group), Institute for Chemistry and Biology of the Marine Environment (ICBM) for the use of its facilities. We thank Thiago Rangel, Diogo Quitete for sampling assistance and Ina Ulber and Matthias Friebe for assistance in the lab.

SUPPLEMENTARY MATERIAL

The Supplementary Material for this article can be found online at: <http://journal.frontiersin.org/article/10.3389/feart.2017.00011/full#supplementary-material>

REFERENCES

- Abiven, S., Hengartner, P., Schneider, M. P. W., Singh, N., and Schmidt, M. W. I. (2011). Pyrogenic carbon soluble fraction is larger and more aromatic in aged charcoal than in fresh charcoal. *Soil Biol. Biochem.* 43, 1615–1617. doi: 10.1016/j.soilbio.2011.03.027
- Cheng, C. H., and Lehmann, J. (2009). Ageing of black carbon along a temperature gradient. *Chemosphere* 75, 1021–1027. doi: 10.1016/j.chemosphere.2009.01.045
- Ding, Y., Cawley, K. M., Cunha, C. N., and Jaffé, R. (2014). Environmental dynamics of dissolved black carbon in wetlands. *Biogeochemistry* 119, 259–273. doi: 10.1007/s10533-014-9964-3
- Ding, Y., Yamashita, Y., Dodds, W. K., and Jaffé, R. (2013). Dissolved black carbon in grassland streams: is there an effect of recent fire history? *Chemosphere* 90, 2557–2562. doi: 10.1016/j.chemosphere.2012.10.098
- Dittmar, T. (2008). The molecular level determination of black carbon in marine dissolved organic matter. *Organ. Geochem.* 39, 396–407. doi: 10.1016/j.orggeochem.2008.01.015
- Dittmar, T., and Koch, B. P. (2006). Thermogenic organic matter dissolved in the abyssal ocean. *Mar. Chem.* 102, 208–217. doi: 10.1016/j.marchem.2006.04.003
- Dittmar, T., Koch, B., Hertkorn, N., and Kattner, G. (2008). A simple and efficient method for the solid-phase extraction of dissolved organic matter (SPE-DOM) from seawater. *Limnol. Oceanogr. Methods* 6, 230–235. doi: 10.4319/lom.2008.6.230
- Dittmar, T., and Paeng, J. (2009). A heat-induced molecular signature in marine dissolved organic matter. *Nat. Geosci.* 2, 175–179. doi: 10.1038/ngeo440
- Dittmar, T., Paeng, J., Gihring, T. M., Suryaputra, I. G. N. A., and Huettel, M. (2012b). Discharge of dissolved black carbon from a fire-affected intertidal system. *Limnol. Oceanogr.* 57, 1171–1181. doi: 10.4319/lo.2012.57.4.1171
- Dittmar, T., Rezende, C. E., Manecki, M., Niggemann, J., Ovalle, A. R. C., Stubbins, A., et al. (2012a). Continuous flux of dissolved black carbon from a vanished tropical forest biome. *Nat. Geosci.* 5, 618–622. doi: 10.1038/ngeo1541
- Forbes, M. S., Raison, R. J., and Skjemstad, J. O. (2006). Formation, transformation and transport of black carbon (charcoal) in terrestrial and aquatic ecosystems. *Sci. Total Environ.* 370, 190–206. doi: 10.1016/j.scitotenv.2006.06.007
- Fundação SOS Mata Atlântica and Instituto Nacional de Pesquisas Espaciais (2011). *Atlas dos Remanescentes Florestais da Mata Atlântica, Período 2008–2010*.
- Glaser, B., Haumaier, L., and Guggenberger, G., Zech, W. (2001). The ‘Terra Preta’ phenomenon: a model for sustainable agriculture in the humid tropics. *Naturwissenschaften* 88, 37–41. doi: 10.1007/s00114000193
- Guggenberger, G., Rodionov, A., Shibistova, O., Grabe, M., Kasansky, O., Fuchs, H., et al. (2008). Storage and mobility of black carbon in permafrost soils of the forest tundra ecotone in Northern Siberia. *Glob. Change Biol.* 14, 1397–1381. doi: 10.1111/j.1365-2486.2008.01568.x
- Hammes, K., Schmidt, M. W. I., Smernik, R. J., Currie, L. A., Ball, W. P., Nguyen, T. H., et al. (2007). Comparison of quantification methods to measure fire-derived (black/elemental) carbon in soils and sediments using reference materials from soil, water, sediment and the atmosphere. *Glob. Biogeochem. Cycles* 21:GB3016. doi: 10.1029/2006GB002914
- Jaffé, R., Ding, Y., Niggemann, J., Vähätalo, A. V., Stubbins, A., Spencer, R. G. M., et al. (2013). Global charcoal mobilization from soils via dissolution and riverine transport to the oceans. *Science* 340, 345–347. doi: 10.1126/science.1231476
- Kim, S., Kaplan, L. A., Benner, R., and Hatcher, P. G. (2004). Hydrogen-deficient molecules in natural riverine water sample – evidence for existence of black carbon in DOM. *Mar. Chem.* 92, 225–234. doi: 10.1016/j.marchem.2004.06.042
- Kruche, A. V., Martinelli, L. A., Victoria, R. L., Bernades, M. C., Camargo, P. B., Ballester, M. V., et al. (2002). Compositional of particulate and dissolved organic matter in a disturbed watershed of southeast Brazil (Piracicaba River basin). *Water Res.* 36, 2743–2752. doi: 10.1016/S0043-1354(01)00495-X
- Lira, P. K., Tambosi, L. R., Ewers, R. M., and Metzger, J. P. (2012). Land-use and land-cover change in Atlantic Forest landscapes. *Forest Ecol. Manage.* 15, 80–89. doi: 10.1016/j.foreco.2012.05.008
- Major, J., Lehmann, J., Rondon, M., and Goodale, C. (2010). Fate of soil-applied black carbon: downward migration, leaching and soil respiration. *Glob. Change Biol.* 16, 1366–1379. doi: 10.1111/j.1365-2486.2009.02044.x
- Mannino, A., and Harvey, H. R. (2004). Black carbon in estuarine and coastal ocean dissolved organic matter. *Limnol. Oceanogr.* 49, 735–740. doi: 10.4319/lo.2004.49.3.0735
- Martinelli, L. A., Camargo, P. B., Lara, L. B. L. S., Victoria, R. L., and Artaxo, P. (2002). Stable carbon and nitrogen isotopic composition of bulk aerosol particles in a C4 landscape of southeast Brazil. *Atmos. Environ.* 36, 2427–2432. doi: 10.1016/S1352-2310(01)00454-X
- Oscar, J. (1985). *Escravidão and Engenhos: Campos, São João da Barra, Macaé, e São Fidélis*. Rio de Janeiro: Rio de Janeiro Achiamé.
- Ovalle, A. R. C., Silva, C. F., Rezende, C. E., Gatts, C. E. N., Suzuki, M. S., and Figueiredo, R. O. (2013). Long-term trends in hydrochemistry in the Paraíba do Sul River, southeastern Brazil. *J. Hydrol.* 481, 191–203. doi: 10.1016/j.jhydrol.2012.12.036
- Preston, C. M., and Schmidt, M. W. I. (2006). Black (pyrogenic) carbon in boreal forests: a synthesis of current knowledge and uncertainties. *Biogeosciences* 3, 211–271. doi: 10.5194/bg-3-397-2006
- Ribeiro, M. C., Metzger, J. P., Martensen, A. C., Ponzoni, F. J., and Hirota, M. M. (2009). The Brazilian Atlantic Forest: how much is left, and how the remaining forest distributed? *Implications for conservation. Biol. Conserv.* 142, 1141–1153. doi: 10.1016/j.biocon.2009.02.021
- Riedel, T., Zark, M., Vähätalo, A. V., Niggemann, J., Spencer, R. G. M., Hernes, P. J., et al. (2016). Molecular signatures of biogeochemical transformations in dissolved organic matter from ten World Rivers. *Front. Earth Sci.* 4:85. doi: 10.3389/feart.2016.00085
- Santín, C., Doerr, S. H., Kane, E. S., Masiello, C. A., Ohlson, M., Rosa, J. M., et al. (2016). Towards a global assessment of pyrogenic carbon from vegetation fires. *Glob. Change Biol.* 22, 76–91. doi: 10.1111/gcb.12985
- Schneider, M. P. W., Hilf, M., Vogt, U. F., and Schmidt, M. W. I. (2010). The benzene polycarboxylic acid (BPCA) pattern of wood pyrolyzed between 200 °C and 1000 °C. *Organ. Geochem.* 41, 1082–1088. doi: 10.1016/j.orggeochem.2010.07.001
- Seidel, M., Yager, P. L., Ward, N. D., Carpenter, E. J., Gomes, H. R., Kruske, A. L., et al. (2015). Molecular-level changes of dissolved organic matter along the Amazon River-to-ocean continuum. *Mar. Chem.* 177, 218–231. doi: 10.1016/j.marchem.2015.06.019
- Souza, T. A., Godoy, J. M., Godoy, M. L., Moreira, I., Carvalho, Z. L., Salomão, M. S., et al. (2010). Use of multitracers of the study of water mixing in the Paraíba do Sul River estuary. *J. Environ. Radioact.* 101, 564–570. doi: 10.1016/j.jenvrad.2009.11.001
- Spencer, R. G. M., Stubbins, A., Hernes, P. J., Baker, A., Mopper, K., Aufdenkampe, A. K., et al. (2009). Photochemical degradation of dissolved organic matter and dissolved lignin phenols from the Congo River. *J. Geophys. Res.* 114:G03010. doi: 10.1029/2009jg000968
- Stubbins, A., Hubbard, V., Uher, G., Law, C. S., Upstill-Goddard, R. C., et al. (2008). Relating carbon monoxide photoproduction to dissolved organic matter functionality. *Environ. Sci. Technol.* 42, 3271–3276. doi: 10.1021/es703014q
- Stubbins, A., Niggemann, J., and Dittmar, T. (2012). Photo-lability of deep ocean dissolved black carbon. *Biogeosciences* 9, 1661–1670. doi: 10.5194/bg-9-1661-2012
- Stubbins, A., Spencer, R. G. M., Mann, P. J., Holmes, R. M., McClelland, J. W., Niggemann, J., et al. (2015). Utilizing colored dissolved organic matter to derive dissolved black carbon export

by Arctic Rivers. *Front. Earth Sci.* 3:63. doi: 10.3389/feart.2015.00063

Warren, D. (1995). *With Broadax and Firebrand. The Destruction of the Brazilian Atlantic forest*. California: University of California Press.

Ziolkowski, L. A., and Druffel, E. R. M. (2010). Aged black carbon identified in marine dissolved organic carbon. *Geophys. Res. Lett.* 37:L16601. doi: 10.1029/2010GL043963

Conflict of Interest Statement: The authors declare that the research was conducted in the absence of any commercial or financial relationships that could be construed as a potential conflict of interest.

The reviewer AC and handling Editor declared their shared affiliation, and the handling Editor states that the process nevertheless met the standards of a fair and objective review.

Copyright © 2017 Marques, Dittmar, Niggemann, Almeida, Gomez-Saez and Rezende. This is an open-access article distributed under the terms of the Creative Commons Attribution License (CC BY). The use, distribution or reproduction in other forums is permitted, provided the original author(s) or licensor are credited and that the original publication in this journal is cited, in accordance with accepted academic practice. No use, distribution or reproduction is permitted which does not comply with these terms.

Regional aerosol emissions contribute to the riverine export of dissolved black carbon

M. W. Jones¹, T. A. Quine¹, L. E. O. C. de Aragão^{1,2}, C. E. de Rezende³, T. Dittmar⁴, M. Manecki⁴, B. Johnson⁵, J. S.J. Marques³

¹University of Exeter, UK.

²Instituto Nacional de Pesquisas Espaciais (INPE), Brazil.

³Universidade Estadual do Norte Fluminense, Brazil.

⁴Institute for Chemistry and Biology of the Marine Environment (ICBM), University of Oldenburg, Germany.

⁵Met Office, UK.

Corresponding author: Matthew Jones (m.jones@exeter.ac.uk)

Key Points:

- Both charcoal and aerosol sources contribute towards fluvial dissolved black carbon loads
- Dissolved black carbon exported by rivers reaches extremely recalcitrant oceanic stores
- Regional aerosol emission sources include intensive agricultural systems and population centres

Abstract

The fate of fire-altered black carbon (BC) remains an area of uncertainty in the global carbon cycle. Its role as a long-term storage mechanism in the carbon cycle is augmented by its transfer to particularly long-term oceanic stores by rivers. Significant fluvial fluxes of dissolved BC to oceans result from the slow release of BC from degrading charcoal stocks but may also include undetermined contributions from aerosols produced by biomass and fuel combustion. By investigation of the Paraíba do Sul River catchment in Southeast Brazil we show that aerosol deposits can be substantial contributors to fluvial fluxes of BC. We estimated stocks of BC associated with soil charcoal and aerosol deposited within the catchment from biomass and fossil fuel combustion sources during the 2009 dry season. We then modelled the fluvial concentrations of dissolved BC that would result from scenarios of loss from these stocks and analysed the ability of each scenario to reproduce the variability in concentrations measured in a dataset of river water samples. The goodness-of-fit between modelled and measured concentrations was greatly improved by inclusion of the aerosol sources. Scenarios in which charcoal contributed ~80% of the DBC and aerosols contributed ~20% were the best predictors of the observed concentrations. We therefore suggest that BC aerosol deposits can contribute towards fluvial fluxes of BC to long-term ocean stores in a manner that is disproportionate to the magnitude of their stocks in river catchments.

1 Introduction

The term black carbon (BC) describes a continuum of organic materials formed by the thermal alteration of organic carbon (OC) during biomass, fossil fuel and biofuel combustion and characterised by a stable structure and a depletion in hydrogen and oxygen [Bird and Ascough, 2012]. BC accumulates as charcoal at the surface of burning biomass as oxygen reacts exothermically with carbon [Schmidt and Noack, 2000] and also as aerosol particles (soot) formed when tars condense in flames [Preston and Schmidt, 2006]. The crucial property of BC relevant to its global cycling is its condensed aromatic structure, which results in its low reactivity and resistance to thermal and chemical oxidation [Schmidt and Noack, 2000]. This recalcitrance leads to the accumulation of BC in terrestrial and aquatic stores that are frequently dated to 10^3 to 10^4 years [Schmidt and Noack, 2000], which evidence a fraction of the BC continuum that is exceptionally slow to degrade.

During a fire, the majority of the OC stored in biomass is converted to CO_2 and a portion (5-15% of biomass [Santín *et al.*, 2015b]) is converted to BC. Upon complete recovery of the affected biomass stocks through re-sequestration of atmospheric CO_2 , BC represents an additional terrestrial store of carbon [Santín *et al.*, 2015a]. Consequently, many have proposed that the production of BC by open biomass burning functions as a sink for atmospheric CO_2 by sequestering carbon to stocks that exhibit slow rates of mineralisation relative to the parent biomass from which it derives; it reduces the turnover rate of the terrestrial stock of organic carbon [Kuhlbusch, 1998; Santín *et al.*, 2015a]. Estimates for the modern rate of global charcoal BC production by open biomass burning range from 40 to 379 Tg BC year⁻¹ [Kuhlbusch and Crutzen, 1995; Santín *et al.*, 2015b]. Aerosol emission inventories suggest that biomass burning and energy-related (fossil fuels and biofuel) combustion emit an additional 2 – 11 Tg BC year⁻¹ and 4.5 – 12.6 Tg BC year⁻¹, respectively [Bond *et al.*, 2013]. Total BC production thus equates to up to 0.8% of terrestrial net primary production (50 – 60 PgC year⁻¹) [Ciais *et al.*, 2013].

For several decades there was consensus that BC resides in soils and sediments for millennia [Crutzen, P. J., Andreae, 1990; Kuhlbusch and Crutzen, 1995; Kuhlbusch, 1998]. However, recent field evidence has shown that the residence time of BC in soils is far shorter than previously thought, probably lying within centennial timescales [Czimczik *et al.*, 2003; Ohlson *et al.*, 2009; Singh *et al.*, 2012]. BC is lost from soil and sediments both by mineralisation and by fluvial transport triggered by erosion, dislocation and dissolution, but the balance of these loss mechanisms is yet to be resolved. Rivers play a crucial role in the loss for terrestrial BC stores by transporting it in suspension as particulate BC (PBC) with eroded sediments [Mitra *et al.*, 2002; Elmquist *et al.*, 2008] or as dissolved BC (DBC) [Hockaday *et al.*, 2007; Dittmar *et al.*, 2012; Jaffé *et al.*, 2013]. BC transported by rivers has the potential to reach oceanic stores where the rate of oxidation is limited by anoxic conditions. Millennial storage times are typically observed in suspended particulates and sediments from coastal and deep ocean sites, while BC persists in the oceanic dissolved pool for thousands of years in advance of its sorption to sinking particulate matter [Masiello and Druffel, 1998; Middelburg *et al.*, 1999; Dittmar and Paeng, 2009; Flores-Cervantes *et al.*, 2009; Ziolkowski and Druffel, 2010; Coppola *et al.*, 2014].

It has been estimated that, globally, 27 Tg BC year⁻¹ is discharged by rivers to the oceans as DBC [Jaffé *et al.*, 2013] and 8 Tg BC year⁻¹ is exported as PBC [Mitra *et al.*, 2013]. These fluxes are 10-15% and 4-5% of the total dissolved organic carbon (DOC; 170-250 Tg year⁻¹) and particulate organic carbon (POC; 150-200 Tg year⁻¹) transported by rivers, respectively [Ludwig *et al.*, 1996; Hedges *et al.*, 1997; Seitzinger *et al.*, 2005]. Fluvial fluxes of DBC have been linked with noteworthy stocks of degrading charcoal BC in drainage catchments [Hockaday *et al.*, 2007; Ding *et al.*, 2012; Dittmar *et al.*, 2012]. However, the contribution of BC aerosol to fluvial transport fluxes of DBC has not yet been evaluated, probably because its production is the smaller term of the global production budget. Direct chemical fingerprinting for the source apportionment of fluvial DBC is hampered by overlap in the chemical signatures of BC from the multiple sources and isotopic fractionation during combustion and diagenesis [Mannino and Harvey, 2004; Mitra *et al.*, 2013].

BC aerosol is mobile in the atmosphere, residing there on average for around one week before being deposited over the land and ocean [Textor *et al.*, 2006]. While fresh BC aerosol is initially

extremely hydrophobic and thus insoluble, oxidation at the surface of particles leads to the substitution of highly aromatic compounds with functional groups containing oxygen, hydrogen and nitrogen [Fierce *et al.*, 2014]. This degradation, combined with the coagulation of BC with other aerosol species during its time in the atmosphere, creates a hydrophilic coating that promotes cloud droplet condensation [McMeeking *et al.*, 2011; Fierce *et al.*, 2014]. It is estimated that approximately 80% of BC aerosol deposition occurs by deposition with rain droplets [Textor *et al.*, 2006]. Similarities in the ratios of concomitant polycyclic aromatic hydrocarbon (PAH) have been observed in smoke plumes and river and coastal sediments, implying that aerosol deposits may contribute meaningfully towards fluvial BC fluxes [Mitra *et al.*, 2002; Yunker *et al.*, 2002; Elmquist *et al.*, 2008]. However, further evidence is needed to understand and quantify the significance of this contribution to BC dynamics in fluvial systems.

We implemented an inverse-modelling approach using measured concentrations of DBC in the Paraíba do Sul River in Southeast Brazil to identify the contributions of various BC source stocks to fluvial load. We utilised satellite-derived datasets of land cover and open biomass burning and spatially resolved estimates for aerosol emissions from fossil fuel and biofuel in conjunction with the HYSPLIT atmospheric trajectory model to produce estimates of BC stocks in the catchment. By modelling the DBC concentrations in the river for various scenarios of transfer from these stocks to and comparing modelled concentrations to a reference dataset of observed concentrations in the river, we demonstrate that BC aerosol deposits contribute significantly towards fluvial DBC loads.

2 Study region

The Paraíba do Sul River drains a catchment of 58,000 km² in a region of high agricultural intensity and population density and a history of extensive slash-and-burn deforestation of tropical forests. DBC in this river network has three potential sources: charcoal-rich soils in deforested sub-catchments (BC_{CHAR}); deposited BC aerosol from regional biomass burning (BC_{BBA}), and; deposited aerosol from regional fossil fuel and biofuel combustion (BC_{FFA}). BC_{CHAR} is derived from slash-and-burn deforestation of the tropical Atlantic Forest of the region, which occurred predominantly between 1850 and 1980 (figure 1) [Dittmar *et al.*, 2012]. BC_{BBA} is a product of natural fire regimes in the Cerrado biome of south-central and southeast Brazil that have been amplified by the expansion and edge effects of cropland and pasture (figure 1) [Klink and Machado, 2005; Lapola *et al.*, 2014]. The use of fire for land clearing, maintenance and crop waste removal in the region is well documented [Oliveira and Marquis, 2002; Lapola *et al.*, 2014]. The clearest example of this is the widespread practice of sugarcane crop waste burning, which impacts the air and rainwater chemical composition in downwind regions [Lara *et al.*, 2001, 2005]. Around two-thirds of Brazil's sugarcane production occurs in the Southeast of the country [Martinelli and Filoso, 2014], amounting to 20% of global production [Martines-filho *et al.*, 2006], and 50% of this area is burned in preparation for harvest [Rudorff *et al.*, 2010]. Meanwhile, in global aerosol emissions datasets BC_{FFA} emissions peak in the densely populated centres of Southeast Brazil, most notably the cities of São Paulo and Rio de Janeiro (figure 1).

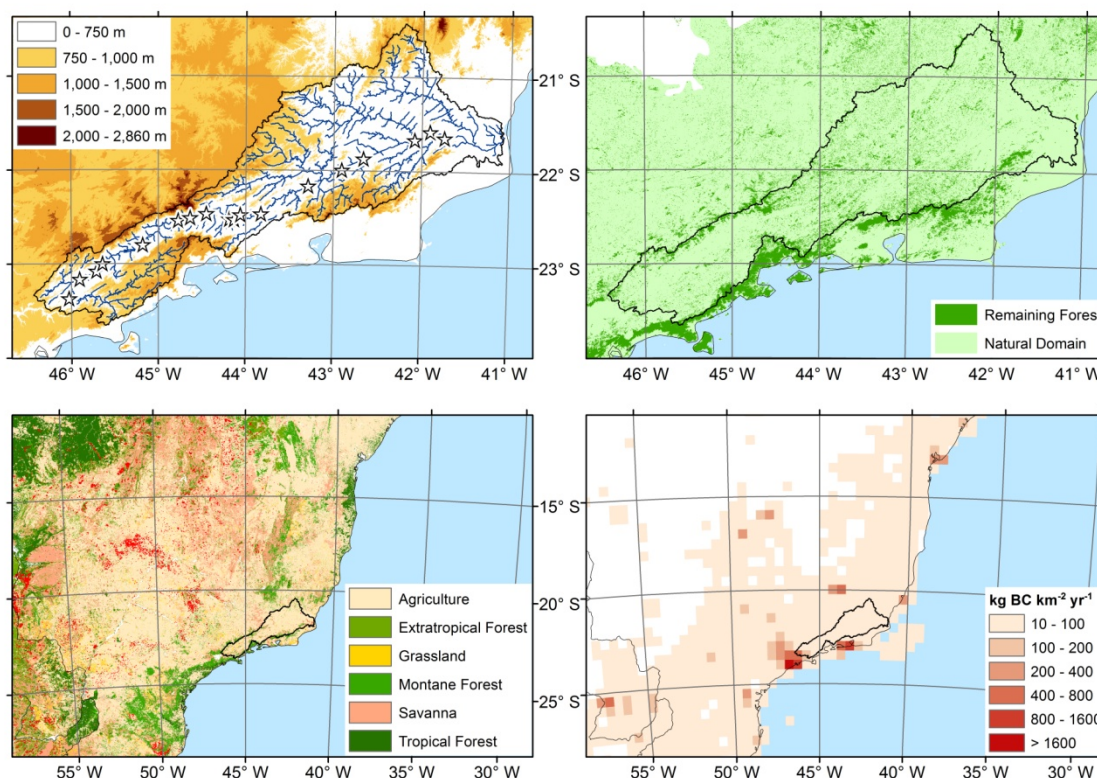


Figure 1: (Top-left panel) Sampling locations (black stars) shown overlaying a hydrological and topographical map of the Paraíba do Sul River catchment. Digital elevation model data (resolution 90 m) data is from the SRTM version 4.1 [Reuter *et al.*, 2007]. (Top-right panel) Remaining fragments of tropical Atlantic Forest [Fundação SOS Mata Atlântica/Instituto Nacional de Pesquisas Espaciais, 2013] overlaying the natural domain of the biome [IBGE, 2004]. (Bottom-left panel) Point vector data (red points) mapping burned areas recorded in the MODIS MCD45 dataset [Roy *et al.*, 2008] in the 2009 dry season (May-October) overlaying land cover information simplified from the GLC2000 land cover map of South America [Eva *et al.*, 2004]. (Bottom-right panel) Emissions of BC aerosol from fossil fuel and biofuel combustion in 2010 as observed in the GAINS 4a dataset at native resolution [Klimont *et al.*, 2013].

3 Materials and methods

3.1 Reference dataset of dissolved black carbon concentrations

Our reference dataset of observed DBC concentration measurements ($c\text{DBC}_{\text{MEAS}}$) was published previously by Dittmar *et al.* (2012; figure 2). Their work in the catchment included the collection of a time series of surface water samples between 1997 and 2008 taken near the river mouth and a spatial set of surface water samples from 20 locations along a 750 km downstream transect of the main stem of the Paraíba do Sul River in April 2010. Samples were vacuum-filtered (pore size $0.7 \mu\text{m}$) and DOM was isolated via solid phase extraction (SPE) [Dittmar *et al.*, 2008]. DBC concentrations from the spatial set of water samples formed the reference data for our modelling exercise, which sought to identify the mixtures of sources that best reproduce their observations.

For the determination of BC, various analytical methods are available. Each option utilises the resistance of BC to oxidation relative to bulk OC but is sensitive to different ranges of chemical and physical properties within the black carbon continuum [Hammes *et al.*, 2007]. Dittmar *et al.* (2012) determined dissolved BC using the benzenepolycarboxylic acid (BPCA) method [Brodowski *et al.*, 2005], on a Shimadzu 10ADvp HPLC (temporal dataset) or Waters UPLC (spatial dataset) equipped with a photodiode array light-absorbance detector. This

method isolates the condensed aromatic compounds that are uniquely associated with BC [Dittmar, 2008]. Dittmar et al. (2012) observed that the average DBC flux from the river system is $2,700 \text{ Mg BC year}^{-1}$. Regular seasonal cycles of DBC concentration were observed in the system and these correlated strongly and positively with river water discharge. Substantial downstream variation in DBC concentration was identified in the spatial dataset of samples (figure 2). For detailed methodology we refer the reader to Dittmar et al. (2012).

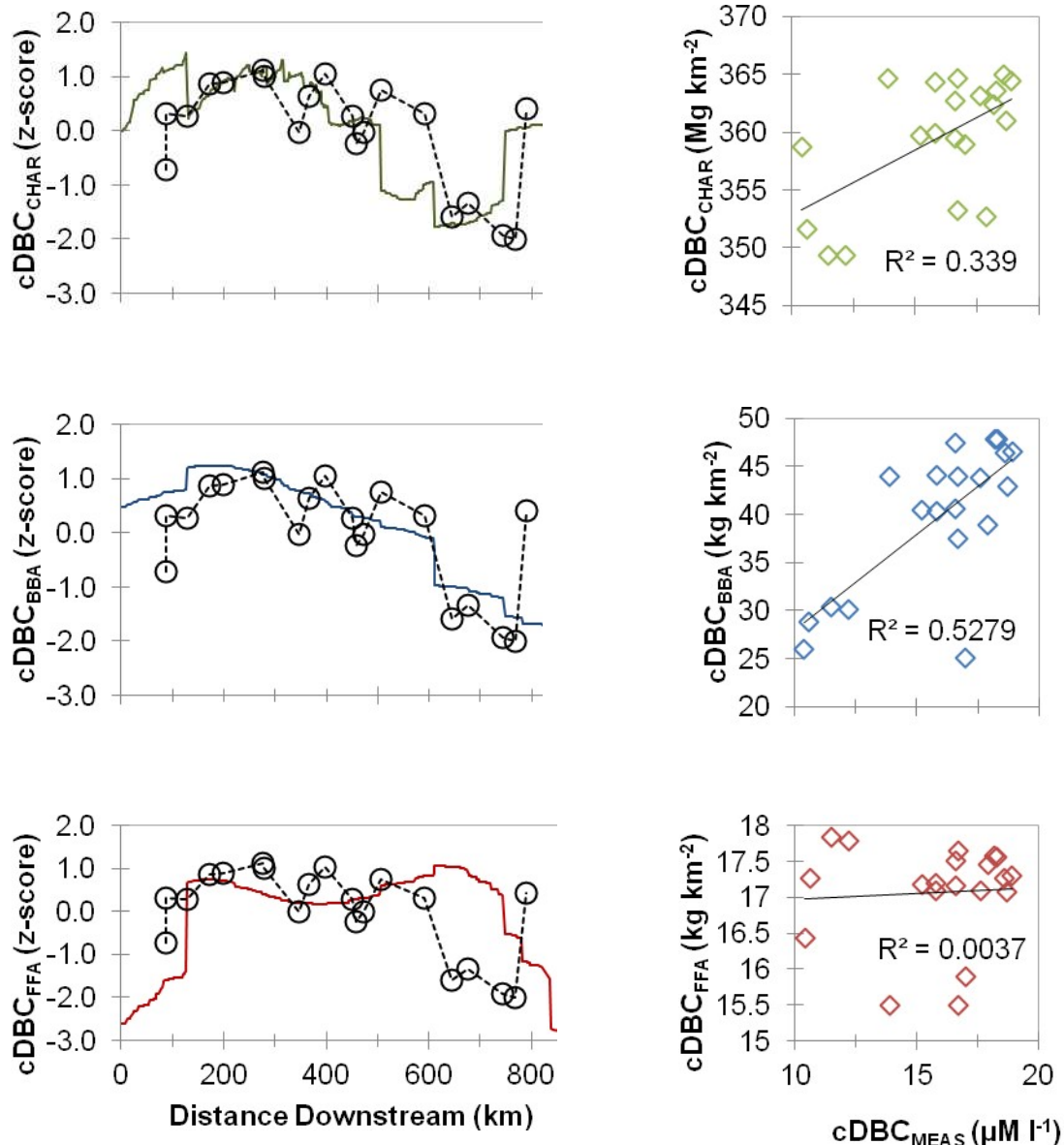


Figure 2: (Left panels) Z-scores for downstream datasets of measured DBC concentrations ($c\text{DBC}_{\text{MEAS}}$; black points and dashed line) and modelled source-specific DBC concentrations for charcoal ($c\text{DBC}_{\text{CHAR}}$; green line), biomass burning aerosol ($c\text{DBC}_{\text{BBA}}$; blue line) and fossil fuel aerosol ($c\text{DBC}_{\text{FFA}}$; red line). **(Right panels)** Scatter plots showing the modelled concentrations of BC from each source plotted against measured DBC concentrations. In this figure delivery factors (f_{CHAR} , f_{BBA} and f_{FFA}) are held at 1 for all sources, representing the hypothetical situation in which all stocks were transferred to the river in 2010; changing f affects only the magnitude of the concentrations and not the downstream pattern of concentration.

3.2 Defining the hydrological network of the catchment

The watersheds and channels of 485 tributaries (figure 1) were delineated using ArcGIS hydrology tools and a shuttle radar topography mission (SRTM) digital elevation model

(DEM) with a resolution of 90 metres. A hydrographic mesh with a scale of 1:2,500,000, produced by the Brazilian National Water Agency (ANA), was burned onto this DEM. The Paraíba do Sul River was measured to be almost 900 km in length when measured from the confluence of the Paraíba and Paraitinga Rivers to its mouth. The areas of the 485 tributary sub-catchments amounted to a total area of 58,000 km². Stocks of BC associated with each source were calculated for each sub-catchment and these formed the units of integration in our modelling exercise for fluvial DBC concentrations.

3.3 Stocks of charcoal black carbon

The BC_{CHAR} stock for each sub-catchment was defined as the product of deforested area and a conversion factor for charcoal production per unit area deforested. Deforested area was derived by subtraction of the current Atlantic Forest coverage from its natural extent mapped by satellite remote sensing [*Fundação SOS Mata Atlântica/Instituto Nacional de Pesquisas Espaciais*, 2013] (figure 1). In the absence of site-specific data for charcoal BC production per unit area burned, the published range of 160 to 420 Mg Ha⁻¹ for tropical forests [*Fearnside et al.*, 1999; *Fearnside and Maurõ*, 2001] was used in our calculations. No specific information about the rate of loss of BC from soils in this region could be found. However we verified, using a historical record of production in the catchment [*Dittmar et al.*, 2012] and a loss curve based on a global dataset of available space-for-time substitution studies of BC stock degradation in soils from various environments [*Singh et al.*, 2012], that at least 80% of the original charcoal BC stock can be expected to remain in the catchment. For the purposes of our study we used initial BC_{CHAR} stock values and did not attempt to account for uncertain losses.

3.4 Stocks of BC aerosol deposits

Stocks of BC_{BBA} and BC_{FFA} deposited in the catchment were modelled using the HYSPLIT air mass trajectory model in combination with gridded emissions datasets. Our analysis included only the BC deposited in the dry season of 2009 (May to October), which preceded the collection of our reference dataset of samples from the April 2010 (wet season) field campaign. For BC_{BBA}, the MODIS MCD45 burned area product was used as a spatially gridded record of fires in the 2009 dry season (May-October) across central South America (resolution 500 m). Published carbon stock densities and BC aerosol emission factors [*Andreae and Merlet*, 2001; *Akagi et al.*, 2010] were assigned to burned area cells according to land cover type in the GLC2000 South America land cover map [*Eva et al.*, 2004]. For BC_{FFA}, the GAINS 4a dataset for annual emissions [*Amann et al.*, 2011] was used to represent emissions in 2009 and we assumed a constant rate of emission throughout the year. We modelled the interception by a sample of air masses that arrived in the catchment of BC aerosol emitted from regional sources and applied a first-order exponential loss function to account for BC deposition in the catchment. Atmospheric back-trajectories of a sample of air masses were modelled using the NOAA Hybrid Single-Particle Lagrangian Integrated Trajectory model (HYSPLIT) [*Draxler*, 1997]. HYSPLIT was driven by 3-hourly NCEP GDAS reanalysis data over a 1° global grid with full vertical dynamics in 23 vertical levels to simulate back trajectories for the sample air masses [*National Centers for Environmental Prediction/National Weather Service/NOAA/U.S. Department of Commerce*, 2009]. The model was initialised over a 0.2° x 0.2° grid of 126 endpoints within the catchment at 6 hour intervals. An atmospheric half-residence time of 118 hours was adopted for the BC aerosol intercepted by air masses en route to the catchment, consistent with an atmospheric residence time of 7.12 days as reported on average for global aerosol models [*Textor et al.*, 2006]. In total over 90,000 air mass trajectories were generated and used as a sample from which total BC deposition to each endpoint was scaled (figure 3). Deposition from the sample air masses

was then scaled to obtain data for the entire dry season period for each endpoint, and an optimised Empirical Bayesian Kriging model was used to spatially interpolate deposition rates across the catchment area.

Our modelling exercise using HYSPLIT was able to produce high-resolution values for BC deposition in the river catchment. To assess the validity of the deposition rates modelled using HYSPLIT we also extracted lower-resolution values from the UK Met Office Hadley Centre Global Environment Model version 2 earth system model (HadGEM2-ES, resolution $1.85 \times 1.25^\circ$) [Hewitt *et al.*, 2011] for the same time period.

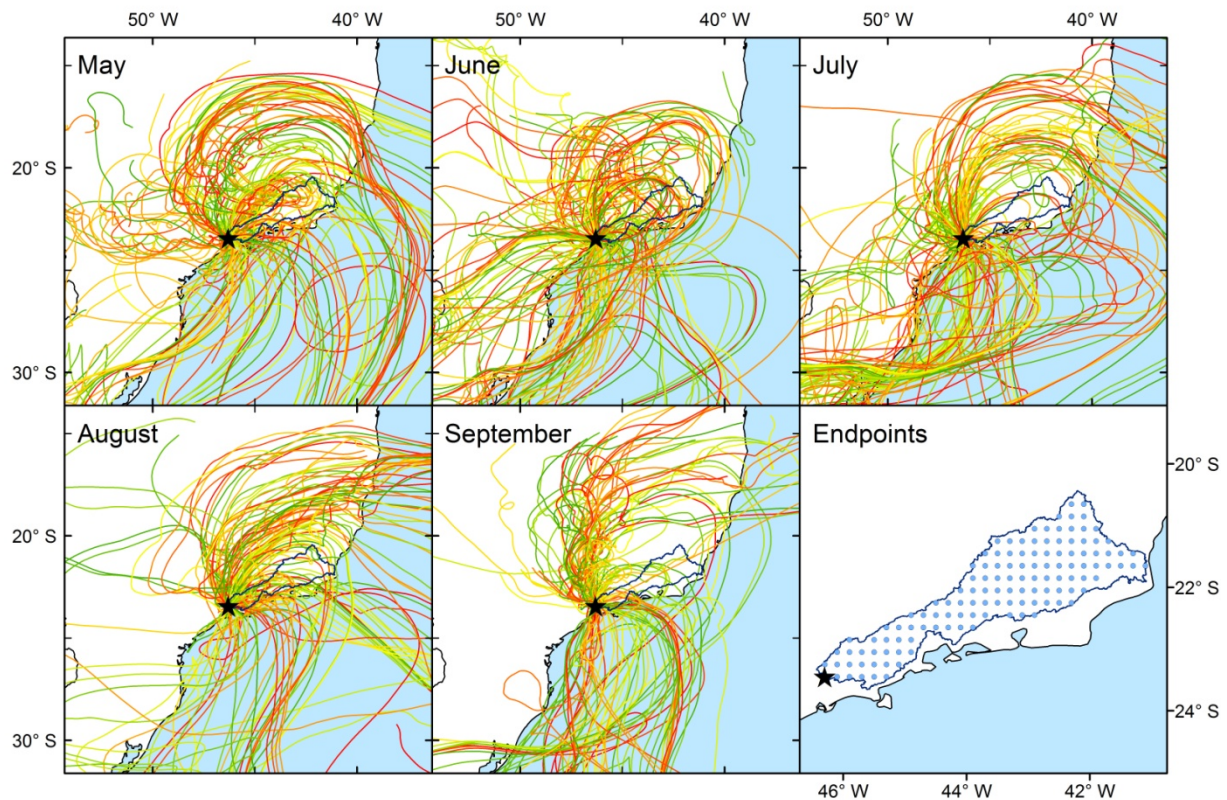


Figure 3: Monthly batches of modelled trajectories of air masses that reached one endpoint (star) in the 2009 dry season. A map of all 126 modelling endpoints (blue points) is also provided.

3.5 Modelling of fluvial dissolved black carbon concentrations

We modelled the concentrations of DBC in the Paraíba do Sul River that would be expected to result from over 35,000 mixing scenarios for source contributions to the total DBC concentration ($c\text{DBC}_{\text{MIX}}$). Scenarios were constructed by varying the delivery factors applied to the stocks associated with each source by the methods described above such that the cumulative fluxes from all sources in the catchment amounted to the 2,700 Mg BC annual flux from the system ($0 \leq f_{\text{BBA}} \leq 1 \text{ g DBC g}^{-1} \text{ BC}_{\text{BBA}}$; $0 \leq f_{\text{FFA}} \leq 1 \text{ g DBC g}^{-1} \text{ BC}_{\text{FFA}}$; $3.01 \times 10^{-5} \leq f_{\text{CHAR}} \leq 1.31 \times 10^{-4} \text{ g DBC g}^{-1} \text{ BC}_{\text{CHAR}}$). The concentration of BC associated with each source x ($c\text{DBC}_x$; equation 1) in any section of river is a function of the stock of BC in its upstream catchment area (S_x ; g BC), water discharge from its upstream catchment area (D ; Litres, L), the fraction transferred from the BC stock to DBC (f_x ; g DBC g^{-1} BC) and the fraction lost, for example by mineralisation or sorption to POM, whilst in transit (L_x ; g DBC g^{-1} DBC).

Equation 1

$$cDBC_x = \frac{S_x f_x (1 - L_x)}{D}, \quad g \text{ BC } L^{-1}$$

In the absence of discharge data for individual sub-catchments, we substitute D for the sub-catchment area (A). Discharge data from 6 discharge gauges that lie along the main stem of the Paraíba do Sul River maintained by the Agência Nacional de Águas revealed an extremely strong linear goodness-of-fit between the area of upstream catchments and the monthly discharge from upstream catchments at the time of sampling in April 2010 ($R^2 = 0.966$, $p < 0.001$). We thus consider the area of catchments to be a proxy for water discharge, specifically by assuming that the discharge of water at any point in the river system in April 2010 is proportional to the catchment area that drains to this point. We also ignored the term L_x , assuming that the time for which BC is present in the river DOC before being exported to the ocean is a small fraction of its residence time in this pool. With these considerations, we substituted equation 1 for equation 2.

Equation 2

$$cDBC_x = \frac{S_x f_x}{A}, \quad g \text{ BC } km^{-2}$$

It was assumed that, for each source, f_x does not display systematic spatial variation throughout the catchment; therefore, f_x influences only the magnitude of the DBC flux associated with each source and not the relative magnitude of fluxes from sub-catchments. The distribution of source mixture scenarios included contributions to annual fluvial DBC discharge of 0 – 47% from BC_{BBA} and 0 – 30% from BC_{FFA} . The upper limits of these ranges were defined by the stocks of aerosol deposited in the 2009 dry season, which fell below the annual export of BC from the catchment. By deduction, the scenarios included contributions of 23 – 100% from BC_{CHAR} . In each scenario the delivery factors f_{CHAR} , f_{BBA} and f_{FFA} were applied to the individual stocks of tributary sub-catchment to calculate $cDBC_{MIX}$ as the sum of $cDBC_{CHAR}$, $cDBC_{BBA}$, and $cDBC_{FFA}$ throughout the main stem of the Paraíba do Sul River. In reality, the term f_x may vary from one catchment to another owing to differences in the age of the stock (and any associated rate of stock deterioration), runoff, geometry, slope and soil porosity. While a function that includes such parameters applied to individual catchments would undoubtedly better approximate BC transfer to the river from the stocks, in the absence of data at the required resolution for these parameters we hold f_x constant throughout the catchment for each individual source.

4 Results

4.1 Stocks of BC in the catchment

We calculated that 7.8 to 20.6 Tg of BC_{CHAR} was created in the Paraíba do Sul River catchment during the deforestation of the Atlantic Forest depending on the published production factor used to calculate stocks. The distribution of these stocks throughout the catchment is complex (figure 4) but relate to the positioning of the remaining fragments of forest, which are located predominantly in the mountainous regions of the catchment away from land that is suitable for agriculture [*Fundação SOS Mata Atlântica/Instituto Nacional de Pesquisas Espaciais*, 2013]. According to our HYSPLIT modelling approach, 1,270 Mg of BC_{BBA} and 810 Mg of BC_{FFA} were deposited in the catchment in the 2009 dry season (May-October), equivalent to an average of 21.9 kg $BC_{BBA} \text{ km}^{-2}$ and 14.0 kg $BC_{FFA} \text{ km}^{-2}$ throughout

the catchment. These values equate to 47% and 30% of the total annual DBC flux from the river catchment ($2,700 \text{ Mg year}^{-1}$ [Dittmar *et al.*, 2012]), respectively. In HadGEM2-ES the average BC deposition concentrations for the 2009 dry season were $19.2 \text{ kg BC}_{\text{BBA}} \text{ km}^{-2}$ and $22.8 \text{ kg BC}_{\text{FFA}} \text{ km}^{-2}$. Thus the HYSPLIT model produces deposition intensities for BC_{BBA} and BC_{FFA} that are within 14% and 39% of HadGEM2-ES, respectively. The spatial patterns of BC deposition rates estimated using the HYSPLIT model are also comparable to those of the HadGEM2-ES model, varying predictably with proximity to noteworthy areas of emission (figure 5). For BC_{BBA} , deposition intensity falls with distance east in the catchment, reflecting an increase in distance from hotspots of fire in the northeast of São Paulo state that lie to the west of catchment (figure 1). For BC_{FFA} , deposition intensity reduced with distance from the far west and the central southern borders of the catchment associated with increasing distance from the emissions centres of São Paulo and Rio de Janeiro (figure 1).

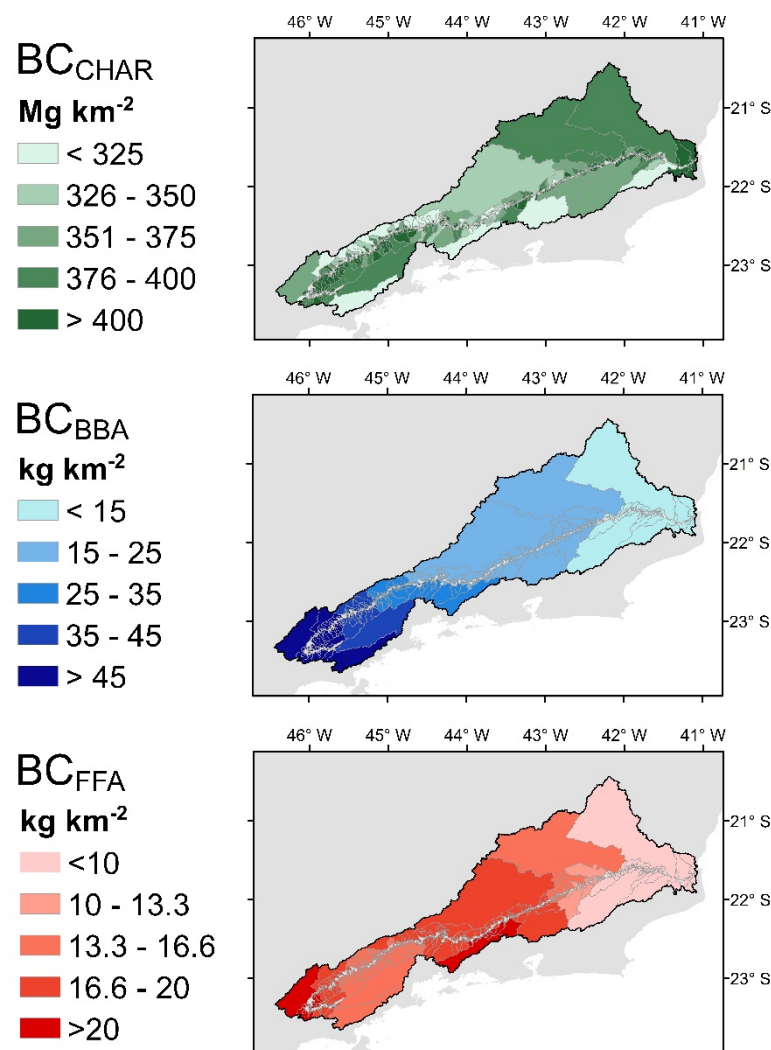


Figure 4: Spatial distribution of stocks for BC associated with charcoal (BC_{CHAR}), biomass burning aerosol (BC_{BBA}) and fossil fuel aerosol (BC_{FFA}) in the Paraíba do Sul River catchment. For BC_{CHAR} , the values plotted are based on production factor estimates at the upper limit of the observed range for tropical forests.

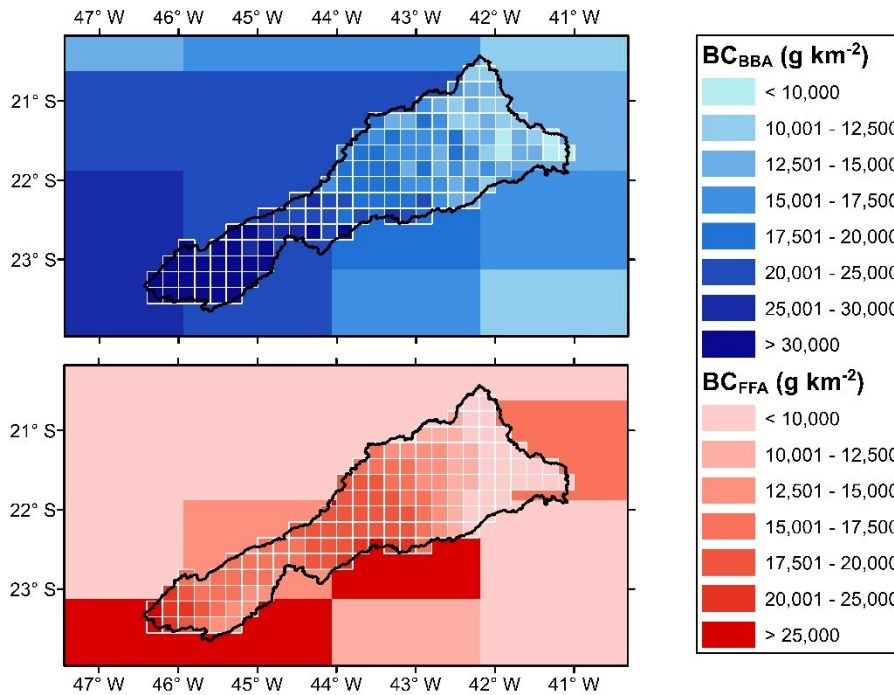


Figure 5: Gridded datasets for the deposition of BC_{BBA} and BC_{FFA} in the Paraíba do Sul River catchment (black line defines boundary) in the 2009 dry season (May-October) as derived from the HYSPLIT model endpoints (resolution 0.2° ; white boxes within catchment boundary) overlaying HadGEM2-ES model deposition rate outputs for the same time period (resolution $1.85^\circ \times 1.25^\circ$; non-bordered background tiles).

4.2 Source apportionment

The spatial distributions of BC stocks associated with each source, evident across the Paraíba do Sul River catchment in figure 4, produce distinctive downstream patterns of DBC concentrations associated with each source ($cDBC_{CHAR}$, $cDBC_{BBA}$, and $cDBC_{FFA}$; figure 2) that may each be capable of explaining portions of the observed downstream variation in concentration measured in the river ($cDBC_{MEAS}$).

Figure 6 plots the goodness-of-fit between $cDBC_{MIX}$ and $cDBC_{MEAS}$ associated with each scenario of source contribution to total fluvial DBC export. All three source components influence the goodness-of-fit, resulting in a clear structural convergence around a zone of optimal fit. R^2 values in the 90th percentile of the distribution ($R^2 > 0.536$) are observed for scenarios with contributions of 70 – 86% from BC_{CHAR} , 5 – 20% from BC_{BBA} and 4 – 16% from BC_{FFA} , while in the 99th percentile ($R^2 > 0.538$) contributions are 78 – 82%, 7 – 11% and 9 – 13%, respectively. Thus, variation in the measured concentrations of BC in the time period sampled was best reproduced by scenarios in which up to a quarter of the BC transported from the river was associated with deposits of BC aerosol from sources that were connected to the catchment by atmospheric pathways during the preceding dry season. However, the absolute range in goodness-of-fit between the 50th and 99th percentiles is not substantial (0.531 to 0.538) and so we are conservative in our suggestion that these are the most likely source contribution mixtures.

A far greater range in goodness-of-fit is observed between the 0th and 50th percentiles of the goodness-of-fit distribution ($0.279 < R^2 < 0.531$) and we therefore focus on the scenarios that explain low portions of the variation in $cDBC_{MEAS}$. Perhaps the most remarkable feature of figure 6 is the steep decline in R^2 values in scenarios with extremely low contributions from BC_{BBA} (<4%) and/or extremely high contributions from BC_{CHAR} (>90%). Indeed, all scenarios in which BC_{CHAR} provides over 94% of the total DBC flux are in the lowest decile of the R^2

value distribution. We interpret this evidence to be suggestive of a considerable aerosol component of the fluvial load of DBC in the Paraíba do Sul River during our period of study.

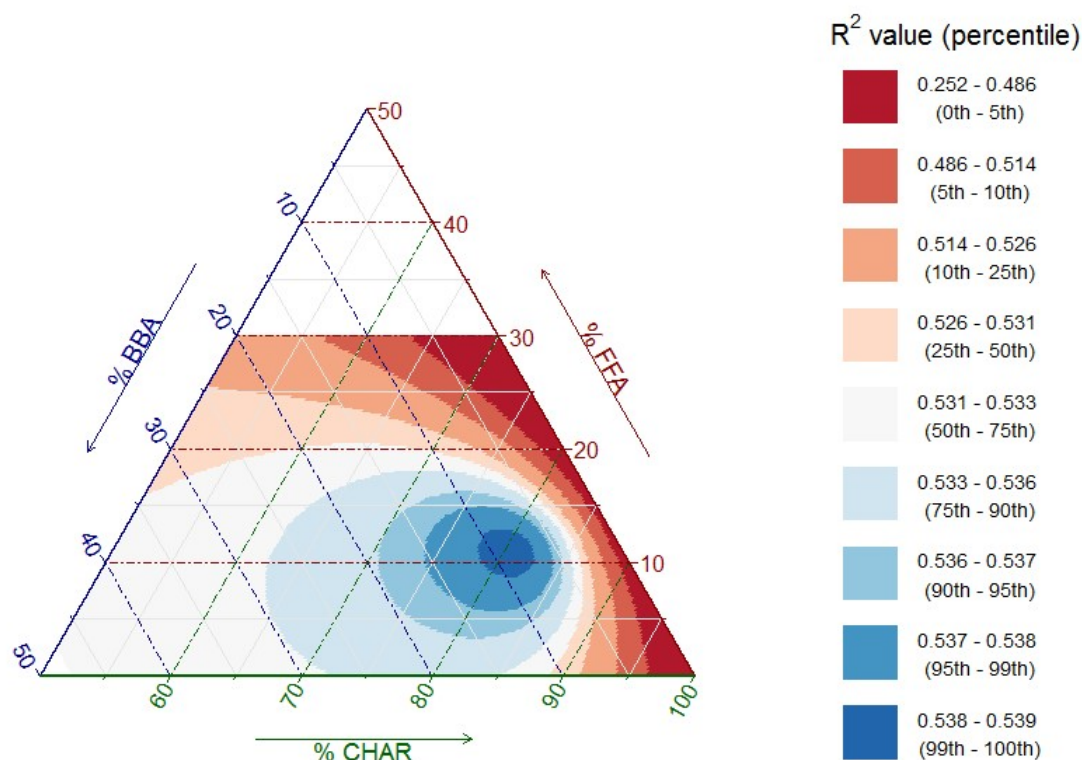


Figure 6: R² values describing the goodness of fit between modelled (cDBC_{MIX}) and measured (cDBC_{MEAS}) concentrations of DBC (as in figure 2) for plausible mixtures of source contribution to fluvial DBC.

5 Discussion

5.1 Implications

By modelling DBC concentrations in the Paraíba do Sul River as those resulting from a mixture of historical stocks of BC_{CHAR} and recent stocks of BC_{BBA} and BC_{FFA}, we show that the inclusion of a substantial aerosol BC component results in a strong improvement in the prediction of observations in our reference dataset. Scenarios in which charcoal contributed ~80% of the DBC and aerosols contributed ~20% were the best predictors of the observed concentrations, but perhaps the most striking of our findings is that scenarios in which BC_{CHAR} contributes the most towards DBC produced cDBC_{MIX} concentrations that were among the poorest predictors of cDBC_{MEAS}. This leads us to reason that aerosol BC deposits can contribute meaningfully towards the riverine export of DBC to oceans in a manner that is greatly disproportionate to the magnitude of their stock in drainage catchments.

The Paraíba do Sul River catchment is noted for its particularly large stock of BC_{CHAR}, which persists in the catchment following centuries of deforestation of tropical Atlantic Forest [Dittmar *et al.*, 2012]. Hence it is somewhat surprising that considerable fractions of the DBC exported from this river catchment are modelled to be linked with recent deposits of aerosol BC. In recent years many studies have maintained a focus on quantifying the load of BC carried by rivers rather than its sources and it is generally expected that BC derives exclusively from stocks of charcoal in catchments [Jaffé *et al.*, 2013]. However, it has previously been proposed that portions of fluvial BC can derive from aerosol [Mittra *et al.*, 2013]. Analyses of the ratios of polycyclic aromatic hydrocarbons (PAH), which are

precursor molecules for aerosol BC, in particulates and sediments from river systems have previously indicated both local and regional origins of PBC [Mitra *et al.*, 2002; Yunker *et al.*, 2002; Elmquist *et al.*, 2008]. Our study is the first to evidence that fluvial fluxes of BC in the dissolved pool can also not be assumed to derive exclusively from BC_{CHAR} without adequate consideration of the aerosol stocks in drainage catchments. Instead, a portion of the 27 Tg DBC year⁻¹ discharged globally by rivers to the oceans [Jaffé *et al.*, 2013] is likely to be explained by stocks of recently deposited aerosol BC.

5.2 Sources of aerosol BC

In contrast to the inherently local nature of BC_{CHAR} contribution to the DBC load of the Paraíba do Sul River, sources of aerosol BC are distributed throughout the Southeast region of Brazil and the patterns of deposition in the catchments reflect variation in proximity to concentrated source regions. With respect to BC_{FFA}, the spatial pattern of deposition rates is clearly framed around proximity to the two major cities in the region, São Paulo and Rio de Janeiro, whose influences on downwind concentrations are observable in global model outputs and empirical studies [Bond *et al.*, 2013]. With respect to BC_{BBA}, the decline in deposition rates with distance east in the catchment indicates a dominant influence of sources to the west of the catchment. Cropland and pasture cover 30% and 35% of the area of São Paulo state, compared to the national values of 9% and 20%, respectively, highlighting the intensive nature of agriculture to the west of the catchment [IBGE, 2009]. Over 50% of the country's sugarcane cultivation area is located in São Paulo and this cropland is concentrated in the north east of the state [Aguiar *et al.*, 2011; Martinelli and Filoso, 2014]. Elevated concentrations of BC in air and rainwater samples collected downwind of sugarcane plantations in Southeast Brazil have been highlighted in previous studies [Lara *et al.*, 2001, 2005].

We calculated that almost half of the MODIS burned area detections within one atmospheric half-residence time of the catchment boundaries occurred in municipalities of São Paulo state in which the land cover fraction associated with sugarcane cultivation exceeded 60% in 2009 (supplementary material). Further, we found that 17% of the BC_{BBA} source interceptions made by the modelled air masses were located in these municipalities, despite their collective areas equating to just 2.3% of the total land area within one half-residence time of the catchment. This evidence alone does not directly implicate sugarcane burning as the cause of burned area detections in these municipalities because the spatial patterns in sugarcane land cover observed may also reflect variation in the intensity of agricultural land use more generally. However, evidence from remote sensing studies that 50% of sugarcane croplands undergo a pre-harvest burn treatment in the region [Rudorff *et al.*, 2010] indicates that sugarcane burning is likely to be an important contributor to the total fire count in the region.

5.3 Considerations

In this study we took advantage of the one available spatial dataset of DBC concentrations for the Paraíba do Sul River from the wet season of 2010. While the dataset provides a useful downstream signature against which modelled DBC concentrations can be assessed, we emphasise that it does not represent any temporal variation in the downstream pattern of DBC. We assume, therefore, that due to the scale of the catchment (and its non-flashy nature) this dataset is representative of the downstream pattern of DBC throughout the annual cycles of discharge observed by Dittmar *et al.* 2012. Thus an underlying assumption is that the temporal variation in DBC discharge observed in the entire catchment scales down proportionally to the individual sub-catchments. We recognise that this may be a simplification; however, this is necessary in the absence of other spatial DBC concentration datasets.

The dynamic processes that might determine the transfer of BC aerosol to fluvial DBC require further investigation. The evidence provided herein suggests that a fraction of the BC aerosol stocks that accrued within the Paraíba do Sul River catchment during the 2009 dry season was rapidly transferred to fluvial DBC in the following wet season. This requires the efficient mobilisation of DBC by runoff and near-surface flows, and thus implies that a sufficient fraction of deposited BC aerosol enters short-term near-surface stores from which it can be readily remobilised. Scenarios in which BC_{BBA} contributed 5 – 20% and BC_{FFA} contributed 4 – 16% towards total fluvial DBC loads, aligning with the 90th percentile of the R^2 value distribution, require the transfer of 10-42% and 12-55% of the 2009 dry season deposits to fluvial DBC, respectively. The remaining fraction might infiltrate into soil pores and be stored for longer periods, undergo mineralisation or be transported with particulate matter. Stocks of BC aerosol in soils are likely to accrue over time, which implies increasing potential to influence DBC fluxes from the river system.

6 Conclusion

This work provides a strong indication that the fluvial DBC exported from river catchments derives from a mixture of sources that includes a substantial BC aerosol component, as evidenced in this case study of the Paraíba do Sul River despite the particularly large inherited stock of BC_{CHAR} in its catchment. The goodness-of-fit between modelled and measured concentrations was greatly improved by inclusion of the aerosol sources and scenarios in which charcoal contributed ~80% of the DBC and aerosols contributed ~20% were the best predictors of the observed concentrations. While large fluvial fluxes of DBC in river systems are often associated exclusively with stocks of charcoal in catchments, we establish that this is not the case in our study region. If our observations are representative of the regional-scale dynamics of BC in other catchments then it would appear that BC aerosol has the potential to contribute substantially towards the 27 Tg DBC year⁻¹ that is discharged globally to highly recalcitrant oceanic stores.

Intuitively, BC_{BBA} and BC_{FFA} deposition rates increased with proximity to prominent aerosol source areas in the intensive agricultural systems that lie to the west of the catchment and the densely populated cities of São Paulo and Rio de Janeiro. Our work highlights the downwind influence of these source regions on environmental concentrations of BC.

This work represents the first indication of an aerosol component in DBC fluxes. It does not provide a detailed understanding of the degradation processes that occur in the atmosphere, soils and sediments to facilitate its dissolution and export to the global oceans in the dissolved pool. Targeted geochemical analyses that seek to trace BC aerosol from drainage catchments to rivers and elucidate the key processes that determine its fate would certainly be complementary to our findings.

Acknowledgments and Data

This work was supported by the UK Natural Environmental Research Council (NERC grant number NE/L002434/1).

References

- Aguiar, D. A., B. F. T. Rudorff, W. F. Silva, M. Adami, and M. P. Mello (2011), Remote Sensing Images in Support of Environmental Protocol: Monitoring the Sugarcane Harvest in São Paulo State, Brazil, *Remote Sens.*, 3, 2682–2703, doi:10.3390/rs3122682.
- Akagi, S. K., R. J. Yokelson, C. Wiedinmyer, M. J. Alvarado, J. S. Reid, T. Karl, J. D. Crounse, and P. O. Wennberg (2010), Emission factors for open and domestic biomass burning for use in atmospheric models, *Atmos. Chem. Phys. Discuss.*, 10(11), 27523–27602, doi:10.5194/acpd-10-27523-2010.

- Amann, M. et al. (2011), Cost-effective control of air quality and greenhouse gases in Europe: Modeling and policy applications, *Environ. Model. Softw.*, 26(12), 1489–1501, doi:10.1016/j.envsoft.2011.07.012.
- Andreae, M. O., and P. Merlet (2001), Emission of trace gases and aerosols from biomass burning, *Global Biogeochem. Cycles*, 15(4), 955–966, doi:10.1029/2000GB001382.
- Bird, M. I., and P. L. Ascough (2012), Isotopes in pyrogenic carbon: A review, *Org. Geochem.*, 42(12), 1529–1539, doi:10.1016/j.orggeochem.2010.09.005.
- Bond, T. C. et al. (2013), Bounding the role of black carbon in the climate system: A scientific assessment, *J. Geophys. Res. Atmos.*, 118(11), 5380–5552, doi:10.1002/jgrd.50171.
- Brodowski, S., a. Rodionov, L. Haumaier, B. Glaser, and W. Amelung (2005), Revised black carbon assessment using benzene polycarboxylic acids, *Org. Geochem.*, 36(9), 1299–1310, doi:10.1016/j.orggeochem.2005.03.011.
- Ciais, P. et al. (2013), Carbon and Other Biogeochemical Cycles, *Clim. Chang. 2013 - Phys. Sci. Basis*, 465–570, doi:10.1017/CBO9781107415324.015.
- Coppola, A. I., L. A. Ziolkowski, C. A. Masiello, and E. R. M. Druffel (2014), Aged black carbon in marine sediments and sinking particles, , 2427–2433, doi:10.1002/2013GL059068.Received.
- Crutzen, P. J., Andreae, M. O. (1990), Biomass burning in the tropics: Impact on atmospheric chemistry and biogeochemical cycles, *Science (80-.)*, 250(4988), 1669–1678.
- Czimczik, C. I., C. M. Preston, M. W. I. Schmidt, and E.-D. Schulze (2003), How surface fire in Siberian Scots pine forests affects soil organic carbon in the forest floor: Stocks, molecular structure, and conversion to black carbon (charcoal), *Global Biogeochem. Cycles*, 17(1), 1020, doi:10.1029/2002GB001956.
- Ding, Y., Y. Yamashita, W. K. Dodds, and R. Jaffé (2012), Dissolved black carbon in grassland streams: Is there an effect of recent fire history?, *Chemosphere*, 90(10), 2557–2562, doi:10.1016/j.chemosphere.2012.10.098.
- Dittmar, T. (2008), The molecular level determination of black carbon in marine dissolved organic matter, *Org. Geochem.*, 39, 396–407, doi:10.1016/j.orggeochem.2008.01.015.
- Dittmar, T., and J. Paeng (2009), A heat-induced molecular signature in marine dissolved organic matter, *Nat. Geosci.*, 2(3), 175–179, doi:10.1038/ngeo440.
- Dittmar, T., B. Koch, N. Hertkorn, and G. Kattner (2008), A simple and efficient method for the solid-phase extraction of dissolved organic matter (SPE-DOM) from seawater, *Limnol. Oceanogr. Methods*, 6, 230–235, doi:10.4319/lom.2008.6.230.
- Dittmar, T., C. E. de Rezende, M. Manecki, J. Niggemann, A. R. C. Ovalle, A. Stubbins, and M. C. Bernardes (2012), Continuous flux of dissolved black carbon from a vanished tropical forest biome, *Nat. Geosci.*, 5(9), 618–622, doi:10.1038/ngeo1541.
- Draxler, R. R. (1997), Description of the HYSPLIT_4 modeling system. NOAA Tech. Memo. ERL ARL-224, , (August 2002).
- Elmqvist, M., I. Semiletov, L. Guo, and Ö. Gustafsson (2008), Pan-Arctic patterns in black carbon sources and fluvial discharges deduced from radiocarbon and PAH source apportionment markers in estuarine surface sediments, *Global Biogeochem. Cycles*, 22, 1–13, doi:10.1029/2007GB002994.
- Eva, H. D., A. S. Belward, E. E. De Miranda, C. M. Di Bella, V. Gond, O. Huber, S. Jones, M. Sgrenzaroli, and S. Fritz (2004), A land cover map of South America, *Glob. Chang. Biol.*, 10(5), 731–744, doi:10.1111/j.1529-8817.2003.00774.x.
- Fearnside, P. M., and P. Maurõ (2001), Burning of Amazonian rainforests : burning efficiency and charcoal formation in forest cleared for cattle pasture near Manaus , Brazil, , 146.
- Fearnside, P. M., P. Maurõ, N. Leal, Â. A. Rodrigues, J. M. Robinson, and F. Jose (1999), Tropical forest burning in Brazilian Amazonia : measurement of biomass loading ,

- burning efficiency and charcoal formation at Altamira, Para, *For. Ecol. Manage.*, *123*, 65–79, doi:10.1016/S0378-1127(99)00016-X.
- Fierce, L., N. Riemer, and T. Bond (2014), Explaining variance in black carbon's aging timescale, *Atmos. Chem. Phys. Discuss.*, *14*(13), 18703–18737, doi:10.5194/acpd-14-18703-2014.
- Flores-Cervantes, D. X., D. L. Plata, J. K. MacFarlane, C. M. Reddy, and P. M. Gschwend (2009), Black carbon in marine particulate organic carbon: Inputs and cycling of highly recalcitrant organic carbon in the Gulf of Maine, *Mar. Chem.*, *113*(3–4), 172–181, doi:10.1016/j.marchem.2009.01.012.
- Fundação SOS Mata Atlântica/Instituto Nacional de Pesquisas Espaciais (2013), ATLAS DOS REMANESCENTES FLORESTAIS DA MATA ATLÂNTICA PERÍODO 2011-2012, , 1–61. Available from: <http://mapas.sosma.org.br/> (Accessed 1 September 2012)
- Hammes, K. et al. (2007), Comparison of quantification methods to measure fire-derived (black/elemental) carbon in soils and sediments using reference materials from soil, water, sediment and the atmosphere, *Global Biogeochem. Cycles*, *21*, 1–18, doi:10.1029/2006GB002914.
- Hedges, J. I., R. G. Keil, and R. Benner (1997), What happens to terrestrial organic matter in the ocean?, *Org. Geochem.*, *27*(5/6), 195–212.
- Hewitt, H. T., D. Copley, I. D. Culverwell, C. M. Harris, R. S. R. Hill, a. B. Keen, a. J. McLaren, and E. C. Hunke (2011), Design and implementation of the infrastructure of HadGEM3: The next-generation Met Office climate modelling system, *Geosci. Model Dev.*, *4*(2), 223–253, doi:10.5194/gmd-4-223-2011.
- Hockaday, W., A. Grannas, S. Kim, and P. Hatcher (2007), The transformation and mobility of charcoal in a fire-impacted watershed, *Geochim. Cosmochim. Acta*, *71*, 3432–3445, doi:10.1016/j.gca.2007.02.023.
- IBGE (2004), *Mapa de Biomas*, Instituto Brasileiro de Geografia e Estatística, Brasília.
- IBGE (2009), *Censo Agropecuário 2006*, Rio de Janeiro.
- Jaffé, R., Y. Ding, J. Niggemann, A. V. Vähätalo, A. Stubbins, R. G. M. Spencer, J. Campbell, and T. Dittmar (2013), Global charcoal mobilization from soils via dissolution and riverine transport to the oceans., *Science*, *340*(6130), 345–7, doi:10.1126/science.1231476.
- Klimont, Z. et al. (2013), ECLIPSE V4a: Global emission data set developed with the GAINS model for the period 2005 to 2050: key features and principal data sources, *Int. Inst. Appl. Syst. Anal. (IIASA), Schlossplatz, 1*, 2361.
- Klink, C. A., and R. B. Machado (2005), Conservation of the Brazilian Cerrado, *Conserv. Biol.*, *19*, 707–713, doi:10.1111/j.1523-1739.2005.00702.x.
- Kuhlbusch, T. A. J. (1998), Enhanced : Black Carbon and the Carbon Cycle, *Science* (80-), *280*(5371).
- Kuhlbusch, T. A. J., and P. J. Crutzen (1995), Toward a global estimate of black carbon in residues of vegetation fires representing a sink of atmospheric CO₂ and a source of O₂, *Global Biogeochem. Cycles*, *9*(4).
- Lapola, D. M. et al. (2014), Pervasive transition of the Brazilian land-use system, *Nat. Clim. Chang.*, *4*(1), 27–35, doi:10.1038/nclimate2056.
- Lara, L., P. Artaxo, L. Martinelli, P. Camargo, R. Victoria, and E. Ferraz (2005), Properties of aerosols from sugar-cane burning emissions in Southeastern Brazil, *Atmos. Environ.*, *39*, 4627–4637, doi:10.1016/j.atmosenv.2005.04.026.
- Lara, L. B. L. ., P. Artaxo, L. . Martinelli, R. . Victoria, P. . Camargo, a Krusche, G. . Ayers, E. S. . Ferraz, and M. . Ballester (2001), Chemical composition of rainwater and anthropogenic influences in the Piracicaba River Basin, Southeast Brazil, *Atmos. Environ.*, *35*(29), 4937–4945, doi:10.1016/S1352-2310(01)00198-4.

- Ludwig, W., J.-L. Probst, and S. Kempe (1996), Predicting the oceanic input of organic carbon by continental erosion, *Global Biogeochem. Cycles*, *10*(1), 23–41, doi:10.1029/95GB02925.
- Mannino, A., and H. R. Harvey (2004), Black carbon in estuarine and coastal ocean dissolved organic matter, *Deep-Sea Res.*, *49*(June 1996), 735–740.
- Martinelli, L. A., and S. Filoso (2014), EXPANSION OF SUGARCANE ETHANOL PRODUCTION IN BRAZIL, *Environ. Sci. Technol.*, *18*(4), 885–898.
- Martines-filho, J., H. L. Burnquist, and C. E. F. Vian (2006), Bioenergy and the Rise of Sugarcane-Based Ethanol in Brazil, *Bioenergy*, *21*(2), 91–96.
- Masiello, C., and E. Druffel (1998), Black Carbon in Deep-Sea Sediments, *Science* (80-.), *280*, 1911–1913, doi:10.1126/science.280.5371.1911.
- McMeeking, G. R., N. Good, M. D. Petters, G. McFiggans, and H. Coe (2011), Influences on the fraction of hydrophobic and hydrophilic black carbon in the atmosphere, *Atmos. Chem. Phys.*, *11*(10), 5099–5112, doi:10.5194/acp-11-5099-2011.
- Middelburg, J. J., J. Nieuwenhuize, and P. Van Breugel (1999), Black carbon in marine sediments, *Mar. Geol.*, (September 1998).
- Mitra, S., T. S. Bianchi, B. A. McKee, and M. Sutula (2002), Black carbon from the Mississippi River: quantities, sources, and potential implications for the global carbon cycle., *Environ. Sci. Technol.*, *36*, 2296–2302.
- Mitra, S., A. R. Zimmerman, G. B. Hunsinger, and W. R. Woerner (2013), Black Carbon in Coastal and Large River Systems, in *Biogeochemical Dynamics at Major River-Coastal Interfaces: Linkages with Global Change*, edited by C. W. J. Bianchi, T. S., Allison, M. A., pp. 1–58, Oxford Publishing Company.
- National Centers for Environmental Prediction/National Weather Service/NOAA/U.S. Department of Commerce (2009), NCEP GDAS Satellite Radiance Data. Research Data Archive at the National Center for Atmospheric Research, Computational and Information Systems Laboratory., Available from: <http://rda.ucar.edu/datasets/ds735.0> (Accessed 1 September 2012)
- Ohlson, M., B. Dahlberg, T. Økland, K. J. Brown, and R. Halvorsen (2009), The charcoal carbon pool in boreal forest soils, *Nat. Geosci.*, *2*(10), 692–695, doi:10.1038/ngeo617.
- Oliveira, P. S., and R. J. Marquis (2002), *The cerrados of Brazil : ecology and natural history of a neotropical savanna*, edited by R. J. Marquis and P. S. Oliveira, Columbia University Press, New York.
- Preston, C. M., and M. W. I. Schmidt (2006), Black (pyrogenic) carbon: a synthesis of current knowledge and uncertainties with special consideration of boreal regions, *Biogeosciences*, *3*(4), 397–420, doi:10.5194/bg-3-397-2006.
- Reuter, H. I., A. Nelson, and A. Jarvis (2007), An evaluation of void-filling interpolation methods for SRTM data, *Int. J. Geogr. Inf. Sci.*, *21*(9), 983–1008, doi:10.1080/13658810601169899.
- Roy, D. P., L. Boschetti, C. O. Justice, and J. Ju (2008), The collection 5 MODIS burned area product — Global evaluation by comparison with the MODIS active fire product, *Remote Sens. Environ.*, *112*(9), 3690–3707, doi:10.1016/j.rse.2008.05.013.
- Rudorff, B. F. T., D. A. de Aguiar, W. F. da Silva, L. M. Sugawara, M. Adami, and M. A. Moreira (2010), Studies on the Rapid Expansion of Sugarcane for Ethanol Production in São Paulo State (Brazil) Using Landsat Data, *Remote Sens.*, *2*(4), 1057–1076, doi:10.3390/rs2041057.
- Santín, C., S. H. Doerr, C. M. Preston, and G. González-Rodríguez (2015a), Pyrogenic organic matter production from wildfires: a missing sink in the global carbon cycle, *Glob. Chang. Biol.*, n/a-n/a, doi:10.1111/gcb.12800.
- Santín, C., S. H. Doerr, E. S. Kane, C. a. Masiello, M. Ohlson, J. M. de la Rosa, C. M.

- Preston, and T. Dittmar (2015b), Towards a global assessment of pyrogenic carbon from vegetation fires, *Glob. Chang. Biol.*, n/a-n/a, doi:10.1111/gcb.12985.
- Schmidt, M. W. I., and A. G. Noack (2000), Black carbon in soils and sediments: Analysis, distribution, implications, and current challenges, *Global Biogeochem. Cycles*, 14(3), 777–793.
- Seitzinger, S. P., J. a. Harrison, E. Dumont, A. H. W. Beusen, and a. F. Bouwman (2005), Sources and delivery of carbon, nitrogen, and phosphorus to the coastal zone: An overview of Global Nutrient Export from Watersheds (NEWS) models and their application, *Global Biogeochem. Cycles*, 19(4), 1–11, doi:10.1029/2005GB002606.
- Singh, N., S. Abiven, M. S. Torn, and M. W. I. Schmidt (2012), Fire-derived organic carbon in soil turns over on a centennial scale, *Biogeosciences*, 9(8), 2847–2857, doi:10.5194/bg-9-2847-2012.
- Textor, C. et al. (2006), Analysis and quantification of the diversities of aerosol life cycles within AeroCom, *Atmos. Chem. Phys.*, 6, 1777–1813, doi:10.5194/acp-6-1777-2006.
- Yunker, M. B., R. W. Macdonald, R. Vingarzan, H. Mitchell, D. Goyette, and S. Sylvestre (2002), PAHs in the Fraser River basin: a critical appraisal of PAH ratios as indicators of PAH source and composition, *Org. Geochem.*, 33, 489–515, doi:10.1016/S0146-6380(02)00002-5.
- Ziolkowski, L. A., and E. R. M. Druffel (2010), Aged black carbon identified in marine dissolved organic carbon, *Geophys. Res. Lett.*, 37, 4–7, doi:10.1029/2010GL043963.

SUMMARY

Approach

Modelled concentrations of DBC under a range of source mixture scenarios were compared to measured concentrations from the Paraíba do Sul River at four time periods (wet seasons of 2010, 2013 and 2014 and the dry season of 2013) by regression analysis. The Wet 2013, Dry 2013 and Wet 2014 datasets came from Marques et al., 2017 and derive from replicate samples collected from the same positions. R^2 values obtained from the analyses were treated as a measure of the model's ability to reproduce observations from the available time periods. The sources included as contributors to the modelled concentration dataset are charcoal, BC aerosol from biomass burning and fossil fuel burning. Modelled concentrations are simulated as the estimated stocks of BC in the sub-catchments of the Paraíba do Sul basin (normalised by area) multiplied by a transfer factor (i.e. % transfer from stock X to DBC in time period t) for each individual source. Transfer factors are varied within plausible ranges for each source so as to produce different source mixtures that are capable of producing the annual flux of DBC from the PSR, and the goodness-of-fit between the modelled and the measured concentrations is used as a method through which to evaluate “well-fitting” source mixtures against those that poorly reproduce the observed concentrations of DBC in the river. Unfortunately, stocks of aerosol BC deposits are modelled only for the 2009 dry season (May-October) and so we must assume for the purposes of this work that the spatial distribution of aerosol deposition rates is representative of other years (i.e. that deposition is consistent through time).

Transfer factors are constrained by the time period t , because for example the stock of aerosol deposits from one dry season period are insufficient to produce >50% of the annual DBC flux from the river. In other words, the transfer factor cannot exceed 100% of the stock of BC in the catchment. We must assume that transfer factors do not display spatial variability in the sub-catchments, although we note that this is likely to be a simplification. This is explained in the manuscript.

Results

Clear structural convergence around regions of best fit are observed for all time periods. For Wet 2010, Wet 2013 and Dry 2013 there is evidence that a mixture of all three sources of BC influence the ability of the modelled concentrations to reproduce observations. In 2010, the optimum R^2 values ($R^2_{MAX} = 0.539$) converge around a contribution mix *Charcoal: Biomass Burning Aerosol: Fossil Fuel Aerosol* (reported consistently herein of approximately 80:10:10. For Wet 2013 and Dry 2013 the R^2 values converge around 80:<5:20 ($R^2_{MAX} = 0.385$) and 65:15:20 ($R^2_{MAX} = 0.723$), respectively. For Wet 2014, the influence of fossil fuel aerosols appears minimal as the R^2 values converge around 95:5:0 ($R^2_{MAX} = 0.419$).

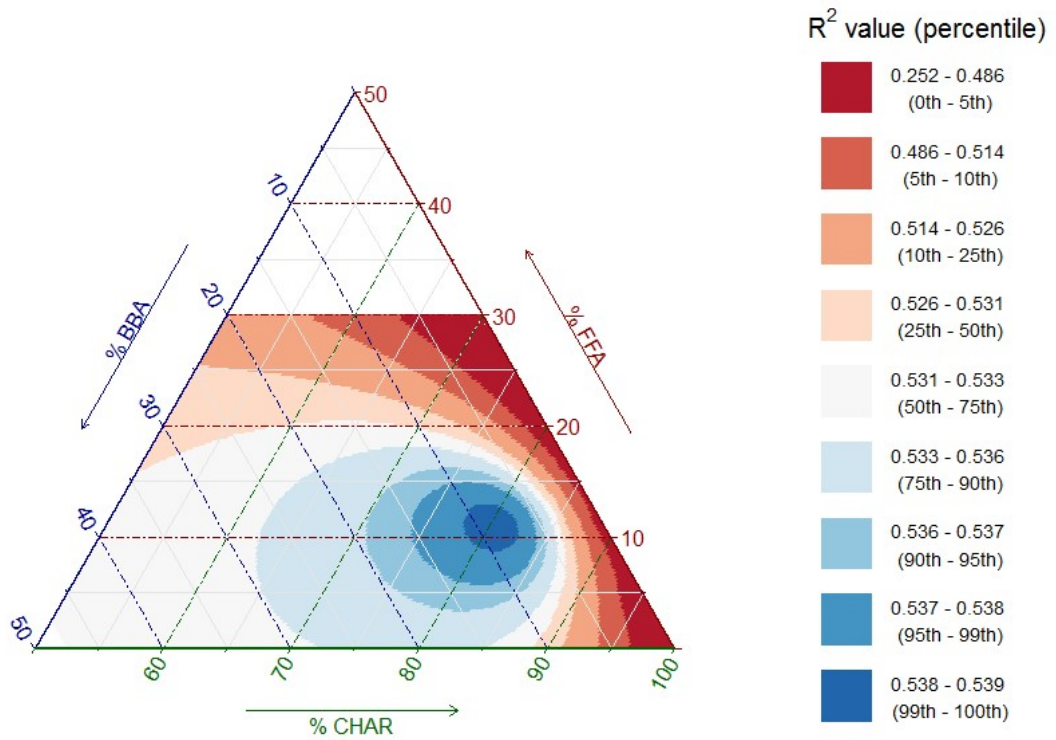
If average values for the wet season replicates (Wet 2013, Wet 2014) are compared with the modelled values, the R^2 values converge around 85:15:0 ($R^2_{MAX} = 0.595$). If average values for the 2013 replicates (Wet 2013, Dry 2013) are considered then all three sources influence the reproducibility of the results (75:5:20, $R^2_{MAX} = 0.761$). If the average of concentrations from all three of the replicate datasets are considered, R^2 values converge around 80:20:0 ($R^2_{MAX} = 0.795$), highlighting the particular influence of the Wet 2014 measurements on the overall goodness-of-fit of the model outputs.

Variation in the goodness-of-fit between the model outputs and the measurements could relate to annual variation in the spatial patterns of BC aerosol deposition in the catchment which are not captured in the model outputs (these relate to the 2009 dry season only). If fresh aerosol deposits experience fast transfer to the DOC pool then annual variation in the spatial patterns of deposition may explain parts of the temporal variation in fluvial DBC concentration observed in the catchment. This evidence points towards the need for more representative modelling of BC aerosol stocks for the time periods prior to the 2013 and 2014 field campaigns (in particular, the dry seasons when biomass burning aerosols are predominantly deposited).

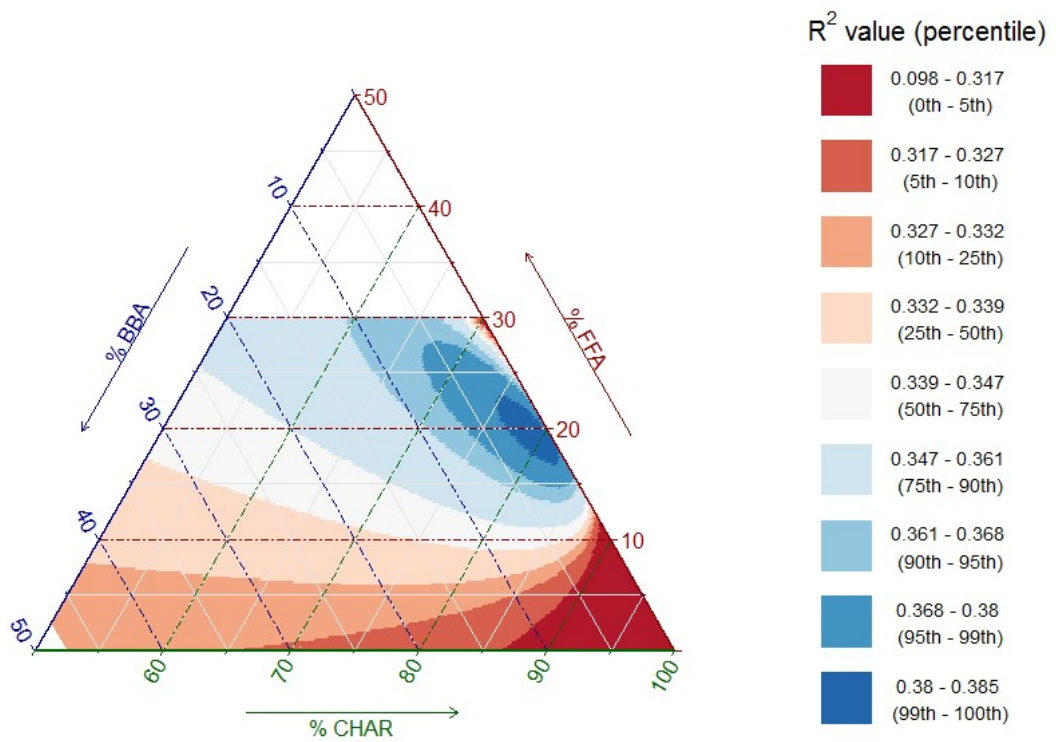
If, hypothetically, the assumptions about the consistency of fallout are correct or if the patterns of aerosol deposition have low temporal variation then these results identify a temporally variable source mixture for DBC in the Paraíba do Sul River. This further underlines the importance of verifying the assumption that BC aerosol fallout patterns have low annual variation in this catchment.

OUTPUTS

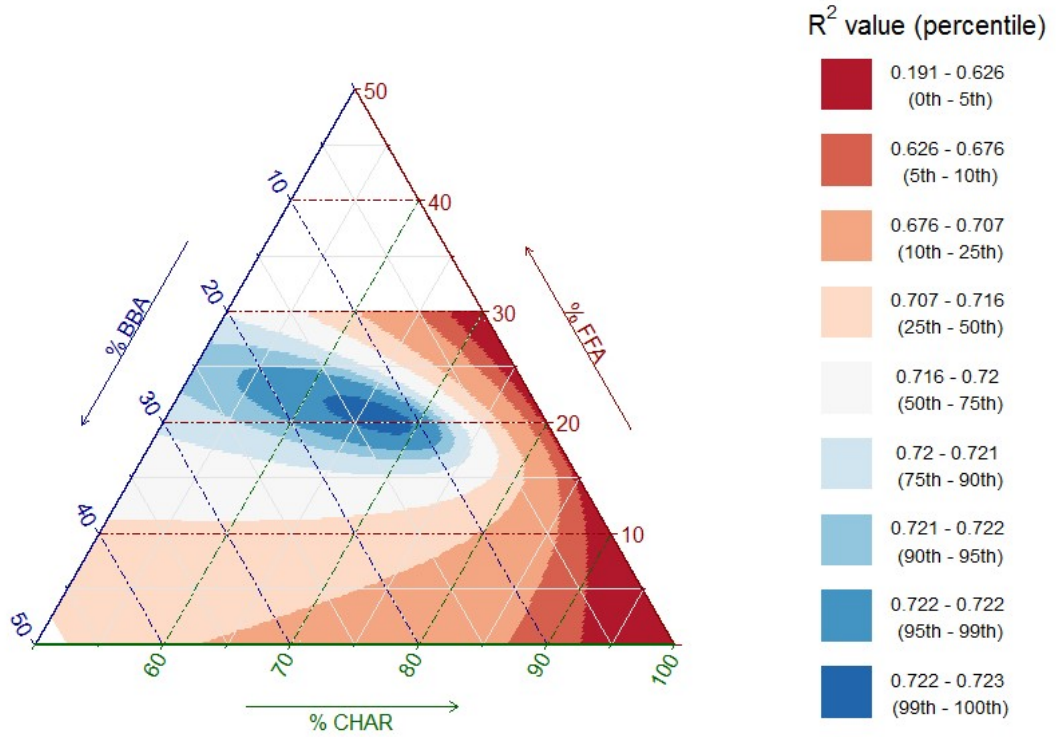
Wet 2010



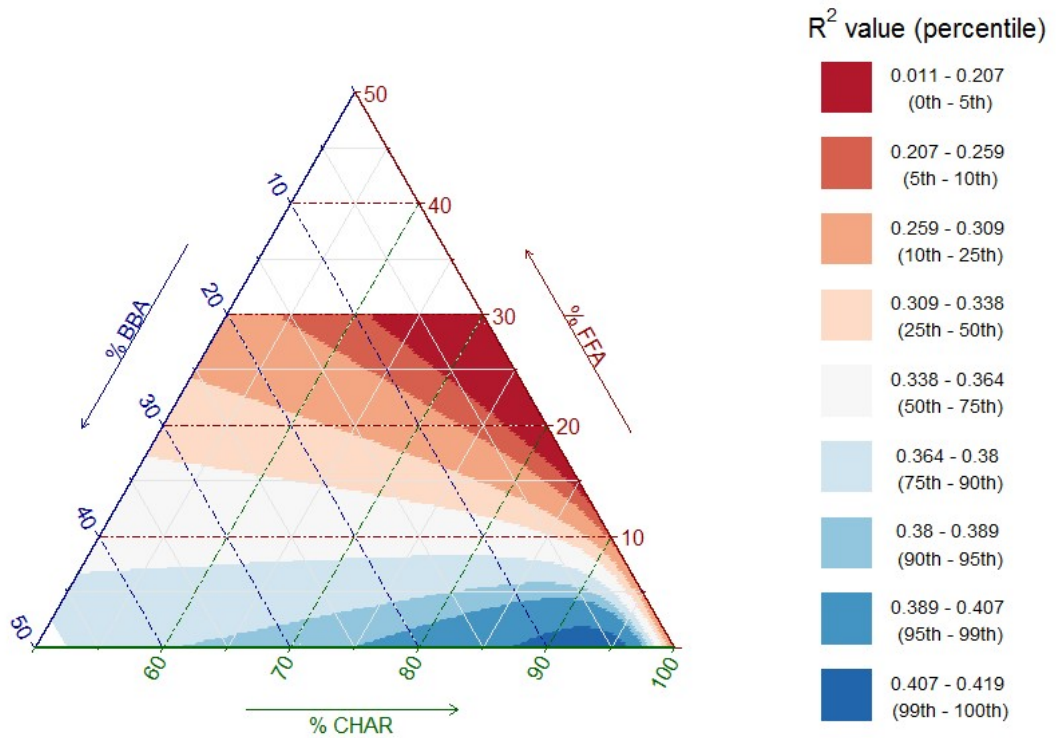
Wet 2013



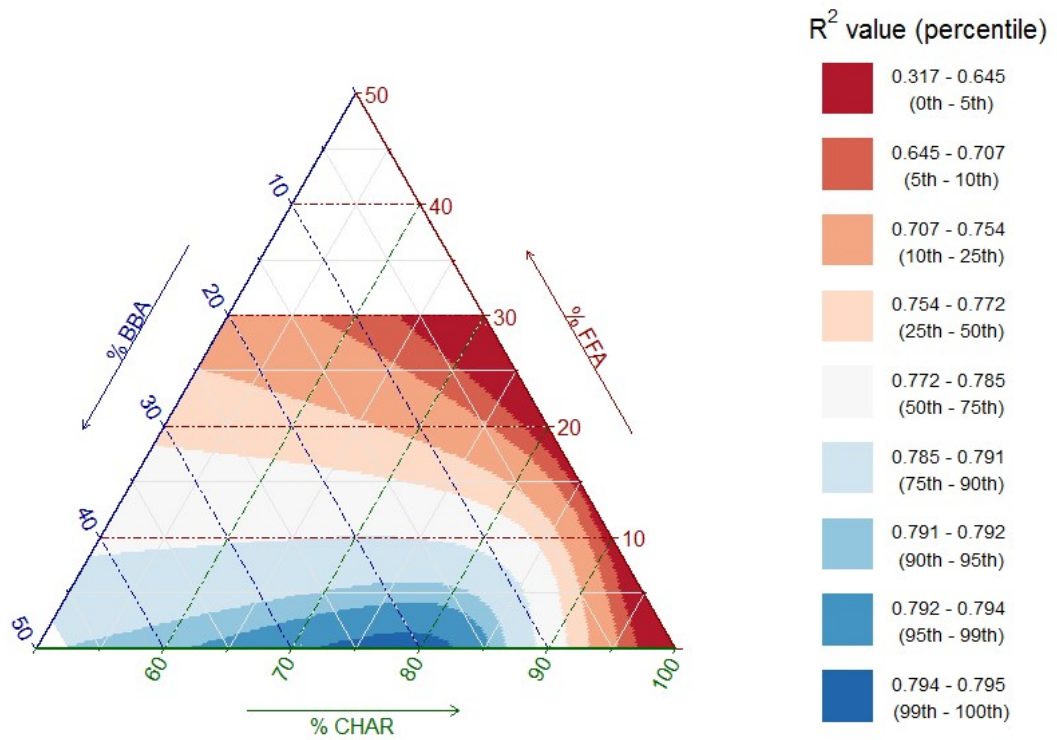
Dry 2013



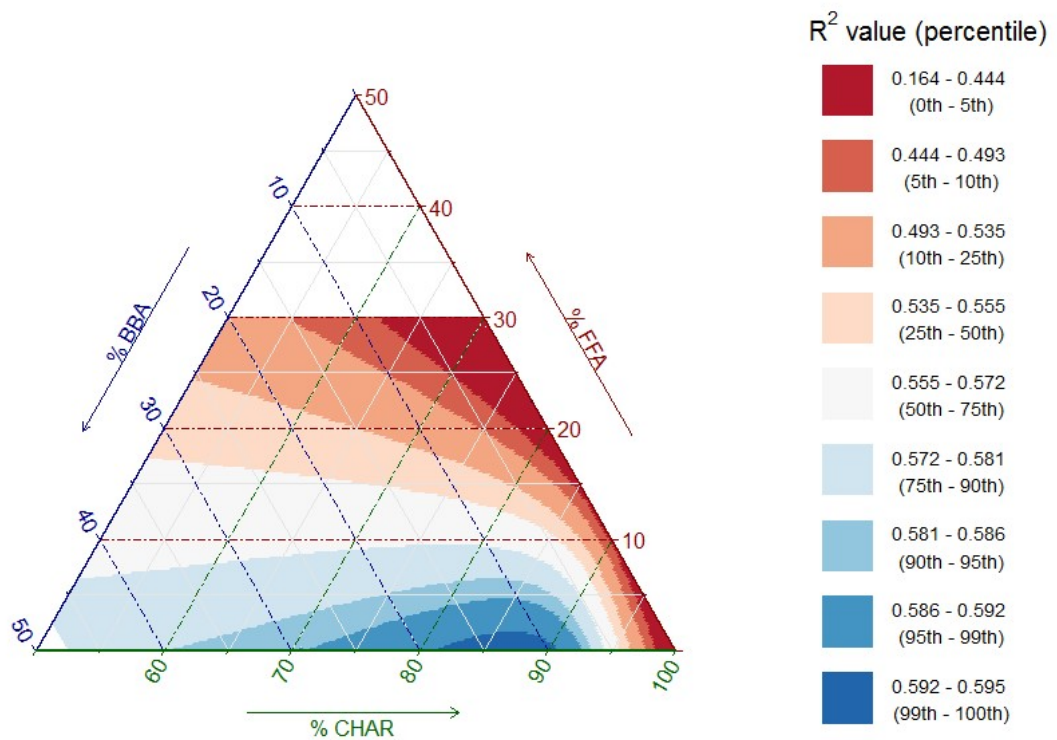
Wet 2014



Average of Replicates from Marques et al., 2017 (Wet 2013, Dry 2013, Wet 2014)



Average of Wet Season Replicates from Marques et al., 2017 (Wet 2013, Wet 2014)



Average of 2013 Replicates from Marques et al., 2017 (Wet 2013, Dry 2013)

